THE UNIVERSITY *of* EDINBURGH

Regulation and Function of miR-199-3p in Murine and Human Cytomegalovirus Infections

Nouf N. M. Laqtom
s0898296

A thesis submitted in fulfilment of requirements for the degree of Doctor of Philosophy

Division of Pathway Medicine, School of Biomedical Sciences
The University of Edinburgh

May 2013

Supervisors:

Dr. Amy Buck and Dr. Bernadette Dutia

Declaration of Authorship

I hereby declare that this thesis is of my own composition, and that it contains no material previously submitted for the award of any other degree. The work reported in this thesis has been executed by myself, except where due acknowledgement is made in the text.

Nouf N. M. Laqtom

Abstract

Human Cytomegalovirus (HCMV), the prototypic β-herpesvirus, is the most common cause of congenital infections as well as morbidity and mortality in immunocompromised patients. The anti-HCMV drugs currently available have a number of drawbacks (i.e. detrimental side-effects and/or the appearance of drug-resistant strains), which limit their clinical usefulness. Therefore, a better understanding of host-virus interactions is important to develop new, safe and effective ways to treat HCMV. HCMV has evolved various strategies to make the host cell more conducive for the replication process, many of these involve modulation of host signalling pathways through proteins or non-coding RNAs. The focus of this thesis is on the regulation of one class of non-coding RNA, microRNAs (miRNA) by HCMV as well as murine CMV (MCMV). miRNAs are short ~22 nucleotide RNA sequences, which negatively regulate the stability and translational efficiency of specific target messenger RNAs (mRNAs). It has been previously shown that three host-encoded miRNAs, miR-199-3p, miR-199-5p and miR-214, are down-regulated in both MCMV and HCMV infected cells. Despite the biological and genomic differences between the two viruses, this down-regulation occurs in both infections, suggesting a possible conserved antiviral role of the miRNAs in mouse and human cells. Consistent with this, miR-199-3p and miR-214 manifest antiviral properties against MCMV and HCMV when over-expressed *in vitro*. This thesis investigates two hypotheses: 1) CMV down-regulates the expression of these host miRNAs through a mechanism involving viral factors, 2) The down-regulation of miR-199-3p leads to the up-regulation of its targets and this influences the cell in a way that favours some aspect of the viral life cycle. The first part of this project examined the regulation of miR-199-3p, miR-199-5p, and miR-214, which derive from a single primary transcript (pri-miRNA). The down-regulation of all three miRNAs was found to occur at the transcriptional level by 4 hours post infection. The promoter of the miR-199a/214 cluster was therefore cloned into a reporter vector in order to interrogate the factors regulating transcription of pri-miRNA in infection; this was carried out in the murine model based on availability of reagents. The reduction in the pri-miRNA was found to correlate with a decrease in the transcriptional activity of miR-199a/214 promoter in infected cells. Further analysis

revealed the presence of a sequence between -421 to -273 relative to the transcription start site (TSS) that was critical for promoter activity. This sequence contains a putative serum response element (SRE), which includes two binding sites for the SRF dimer (serum response factor) and a binding site for a molecule of TCF (ternary complex factor), ELK-1. Initial knock-down studies suggest that these transcription factors are required for basal activity but it remains unknown whether they are involved in the differential expression of miR-199a/214 observed during infection. Another binding site for the transcription factor TWIST-1 was found outside this region, which is known to regulate the miR-199a/214 cluster in other cell types. Western blot analysis showed reduced expression of TWIST-1 in cells infected with HCMV and MCMV infections, by 24 and 48 hours, respectively, suggesting a role of TWIST-1 in regulating miR-199a/214 cluster during these infections. This regulation seems to be dependent on viral gene expression, as a replication deficient viral mutant fails to repress the promoter function and subsequent pri-miRNA production. Taken together, these results suggest an active viral mechanism for transcriptional repression of the miR-199a/214 promoter. To understand the antiviral function of miR-199-3p, the second part of this thesis examined whether miR-199-3p regulates host signalling pathways important for CMV replication and/or the life cycle. A microarray analysis was carried out with samples from cells transfected with miR-199-3p mimic versus inhibitor. This revealed 198 genes significantly down-regulated by the miRNA. From the 198 genes, Ingenuity pathway analysis (IPA) software identified several host pathways with a potential role in HCMV infection including: PI3K/AKT signalling, the ERK-MAPK cascade, and prostaglandin production. This thesis examined the role of miR-199-3p in regulating the PI3K/AKT pathway in HCMV infection. It was found that miR-199-3p modulates the phosphorylation of the central regulator of PI3K/AKT signalling, AKT. Transfection of miR-199-3p before the infection impedes the complete phosphorylation of AKT, which is known to be required for the immediate early viral gene expression and replication. This provides an explanation for the antiviral function of miR-199-3p, through its ability to modulate AKT phosphorylation. An open question, however, is how the natural down-regulation of miR-199-3p from 24 to 72 hours post infection naturally affects AKT phosphorylation. Several predicted targets of miR-199-3p, such as PIK3CB,

ITGA3, and ITGA6 were shown to be up-regulated at these late time points, correlating with the miR-199-3p down-regulation. The interaction of miR-199-3p with target sites in the 3′UTRs of PIK3CB and ITGA3 was validated by luciferase reporter assays and western blotting and qRT-PCR results indicated that protein and mRNA levels of ITGA6 were regulated by miR-199-3p mimic transfection. However, the knock-down of these three targets did not result in a significant decrease of the viral growth, and thus cannot alone explain the antiviral function of miR-199-3p. Overall, this study suggests that the transcriptional repression of miR-199a/214 is likely a strategy employed by CMV to support its own growth through attenuating the biological effect of miR-199-3p within the host cell.

Acknowledgements

This thesis marks the end of my journey to obtain my Ph.D. Working for the Buck lab at the University of Edinburgh has been a wonderful learning experience. It gives me great pleasure to express my heartfelt thanks to all those who have contributed in many different ways to the success of this Ph.D and made it an unforgettable experience for me.

Dr. Amy Buck – Ph.D supervisor. It cannot be argued that the most influential person throughout my graduate career has been you. I would hereby like to express my immense gratitude for giving me the opportunities to do both Master and Doctoral degrees with you and even more so for putting up with me for the past five years. Your advice and encouragement have been a great support throughout and indispensable towards my professional and personal development, be it while facing endless technical challenges in the lab, having questions regarding giving talks, making posters, writing documents or patiently revising my English. To work with you has been a real pleasure so a big THANK YOU for everything.

Dr. Bernadette Dutia– Ph.D co-supervisor. Thank you for your invaluable input, insight and support throughout the writing of this thesis.

Mama. There was no one more instrumental in helping me get through this process than you. I am blessed to have you. You were, are and always will be a continuous source of unconditional love, tremendous support and inspiration.

Mohssen Alyami – Husband. You bore alone the responsibility of our family while I worked in the lab, yet pushed, persuaded and supported me when I needed it the most. Neither did your faith in my abilities ever waver, nor your belief that this moment would arrive one day. I thank you for your love and patience, and for sharing this dream with me.

The angels of mine - Ali, Raghad and the one yet to come. I apologise to you for working late hours and weekends during my Ph.D as this stole our special moments together. I know you will understand someday that a Ph.D is a difficult task and realise that although mum was not perfect, she tried her best and that all this will be for your good one day. Please forgive me for ever having said, "I am busy, I cannot listen now". I would also like to thank you for being the smile, the hope and the greatest absolute loves of my life. I look forward to extending this love to the little baby growing inside me and kicking around. It will be a while yet before he pulls mum's thesis off the shelf and looks through it out of curiosity.

Brothers, sisters in law, nephews, and nieces. You all have had an immeasurable impact throughout my life and particularly these last five years. I have the 8 coolest nephews and nieces in the world and cannot wait to be back with them.

Dr. Tali Jowers Pechenick and Dr. Valentina Libri. I have been very privileged to get to know and work with both of you during the course of my time here. You have proven to be faithful friends over the last several years and I have learnt a lot from you about life and research. Tali, we would never forget climbing Arthur's Seat together with your family, it ended up being one of my prouder moments when I made it to the top! Valentina, "ti vo**g**lio bene ciccina."

Anna Hoy. People sometimes are fortunate to have a friend as constant and close to their hearts as you are. During our graduate careers, we did most things together. From morning coffees, working at benches, discussing our findings and experimental failures to attending talks, routine cleaning of our lab and walking to the bus stop at the end of our day. I am frustrated with the English language for not having the appropriate words to express the magnitude of Anna's friendship. She is like the sister that I never had.

Dr. Alessandro Ceroni, Divya Malik, Diwakar Santhakumar, Dr. Fabio Simbari, Gillian Coakley, Dr. Jessica Borger, Kaija Allikmets, Marissa Lear, Pairoa Praihirunkit, Pascal Miesen and Shatakshi Sood. In brief, I wish I could be here to support all of you as you have so devotedly supported and helped me throughout this journey. I am grateful to you for sharing the scientific knowledge, teaching me so much, and giving me a bunch of fun memories. I hope to keep in touch long after my Ph.D defense.

THANK YOU…GRAZIE…SHUKRIYA…ROMBA NANDRI…TÄNAN…KHOB-KHUN…DANKE SCHÖN

Special thanks to **Dr. Dominik Ruckerl, Marie Craigon, Dr. Paul Dickinson, Dr. Tara Sutherland, Dr. Tony Travis, and Dr. Kay Samuel**

I have had the pleasure of learning FACS from Dominik, microarray experiment from Marie, microarray data analysis from Paul, and the statistical analysis required for my experiments from Tara and Tony. Thank you for your kind assistance and valuable suggestions whenever I turned to you or send e-mails despite your busy schedules. I would like to thank Kay for undertaking the task of editing my thesis. I greatly appreciate the meticulous work she has done to mend the structure of my sentences and words.

I would also like to express a warm gratitude for the wonderful staff in the **IIIR** as well as **DPM** for constantly being helpful, supportive and friendly. People here are genuinely nice and willing to help each other and I am delighted to have interacted with them. I am also grateful for the generous funding support from **King Abdulaziz University** that allowed me to pursue my graduate studies.

At last, this PhD thesis is dedicated to the GREATEST woman EVER. ***'Nazeerah'*** *who dedicated her life to support my mother financially, emotionally and physically in raising us and made the most positive impact on our lives as well as encouraged us to make the most of our lives. There are no words to show you my appreciation. Love you.*

Table of contents

List of Figures

Chapter 1: General Introduction

Chapter 2: Materials and Methods

Chapter 3: Regulation of miR-199a/214 Cluster Expression in CMV Infections

Chapter 4: A Proposed Model for the Antiviral Function of miR-199-3p in CMV Infections

Chapter 5: The Antiviral Properties of miR-199-3p May Associated with Suppression of AKT Phosphorylation

List of Tables

Chapter 1: General Introduction

Chapter 2: Materials and Methods

Chapter 4: A Proposed Model for the Antiviral Function of miR-199-3p in CMV Infections

List of Appendices

Abbreviations

%	**Percentage**
~	**Approximately**
°C	**Degrees Celsius**
µ	**Micro**
µg	**Microgram**
µl	**Microliter**
µM	**Micromolar**
µmol	**Micromole**
A	**Absorbance**
AGO	**Argonaute protein family**
AKT	**V-Akt murine thymoma viral oncogene homolog**
ANOVA	**Analysis of variance**
ATP	**Adenosine triphosphate**
bp	**Base pairs**
CAGE	**Cap analysis gene expression**
Cd151	**Tetraspanin**
CD44	**Cell surface glycoprotein**
cDNA	**Complementary deoxyribonucleic acid**
Co_2	**Carbon dioxide**
ddH_2O	**Double-distilled water**
dH_2O	**Distilled water**
DMSO	**Dimethyl sulfoxide**
DNA	**deoxyribonucleic acid**
dsDNA	**Double stranded deoxyribonucleic acid**
dsRNA	**Double stranded ribonucleic acid**
ELK-1	**Member of ETS oncogene family**
Firefly	***Photinus pyralis***
g	**gravitational force or grams, depending on context**
GFP	**Green fluorescent protein**
HBV	**Hepatitis B virus**
HCMV	**Human cytomegalovirus**

HCV	**Hepatitis C virus**
HF	**High fidelity**
hpi	**hours post infection**
HSV-1	**Herpes simplex virus-1**
IE1	**Immediate early 1**
IE3	**Immediate early 3**
IPA	**Ingenuity Pathway Analysis**
ITGA3	**Integrin-alpha 3**
ITGA6	**Integrin-alpha 6**
kb	**kilo bases**
kDa	**Kilodalton**
M	**Molar**
MCMV	**Murine cytomegalovirus**
MCMVdie3	**Murine cytomegalovirus with ie3-deficient mutant**
Mg	**Milligram**
MIEP	**Major Immediate Early Promoter**
min	**Minute**
miRNA	**Micro- ribonucleic acid**
ml	**Milliliter**
mM	**millimolar**
MOI	**Multiplicity of infection**
MRC-5	**Human Lung Fibroblast Cells**
mRNA	**Messenger ribonucleic acid**
MW	**Molecular weight**
NCBI	**National Center for Biotechnology Information**
NIH-3T3	**Murine fibroblast cell line**
nM	**Nanomolar**
nm	**Nanometer**
nmole	**Nanomole**
nt	**Nucleotide**
ORF	**Open reading frame**
P	**Probability value " It is a measure of statistical significance**

pH	**Measure for the hydrogen ion concentration**
PI3K	**Phosphoinositide 3-kinase**
PIK3CB	**Phosphatidylinositol-4,5-bisphosphate 3-kinase, catalytic subunit beta**
Pre-miRNA	**Precursor microRNA**
Pri-miRNA	**Primary microRNA**
qRT-PCR	**Quantitative reverse transcriptase polymerase chain reaction**
Renilla	***Renilla reniformis***
RISC	**RNA-induced silencing complex**
RNA	**Ribonucleic acid**
rpm	**Rounds per minute**
rRNA	**Ribosomal ribonucleic acid**
SD	**Standard deviation**
siRNA	**Small interfering ribonucleic acid**
SRE	**Serum response element**
SRF	**Serum response factor**
ssDNA	**Single stranded deoxyribonucleic acid**
ssRNA	**Double stranded ribonucleic acid**
STAT3	**Signal transducer and activator of transcription 3**
TCF	**Ternary complex factor**
tRNA	**Transfer ribonucleic acid**
TSS	**Transcription start site**
TWIST1	**Twist homolog 1**
U	**Unit**
U6 snRNA	**Small nuclear RNA U6**
UK	**United kingdom**
USA	**United state of America**
UTR	**Untranslated region of mRNA**
UV	**Ultraviolet**
x	**Times**

1 General Introduction

1.1 Herpesviridae 'Family of Herpes viruses': overview

Herpesviridae are a significant cause of human diseases worldwide and are amongst the most disseminated and successful human pathogens, with specific viruses infecting more than 90% of the population (Tanaka-Taya et al. 1996). The *Herpesviridae* virus family is believed to have arisen from a common ancestral virus, at least 300 million years ago (Davison 1993). These viruses are relatively large (approximately 130-250 nm diameter), with an envelope surrounding the icosahedral capsid, enclosing a linear dsDNA genome (from 130 to 250 kb). In addition to these characteristics, *Herpesviridae* encode a group of enzymes involved in DNA replication (e.g. DNA-polymerase, DNA helicase-primase complex), nucleic acid metabolism (e.g. thymidine kinase), and protein processing and modification (e.g. protein kinases). *Herpesviridae* can also establish latent infections, enabling them to reside life-long in their hosts, during which time the virus enters a dormant phase. Its genome exists in a circular configuration within the cell nucleus and viral gene expression is almost suspended (Davison 2007). The family of *Herpesviridae* contain eight known human-pathogenic members, Herpes Simplex viruses 1 and 2 (HSV1/HHV-1 and HSV2/HHV-2), Varizella Zoster virus (VZV/HHV-3), Cytomegalovirus (CMV/HHV-5), Human Herpes virus-6 (HHV-6), Human Herpes virus-7 (HHV-7), Epstein-Barr virus (EBV/HHV-4), and Karposi Sarcoma-associated Herpes virus (KSHV/HHV-8) (Table 1.1). The current classification of *Herpesviridae* (2011) by the International Committee for the Taxonomy of Viruses (ICTV) has further divided this family into three subfamilies *Alphaherpesvirinae, Betaherpesvirinae* and *Gammaherpesvirinae* (http://www.ictvonline.org/index.asp) based on their specific biological properties, genetic content, genomic organisation and sequence alignment (Alba et al. 2001; Hannenhalli et al. 1995; Karlin et al. 1994; McGeoch et al. 1995; Montague and Iii 2000). The biological properties include the specificity of host and target cells for productive and latent infection *in vivo*, host cell tropism *in vitro*, the duration of virus replication and spread of infection (Roizman et al. 1992) (Table 1.2). The genome-wide sequence comparison between the subfamilies reveals at least 26 conserved open reading frames (ORFs) that encode

diverse genes required for replication, transcription or packaging of the viral genome, as well as those ORFs involved in the formation of virus structure, such as the nucleocapsid and glycoprotein spikes. The conserved ORFs comprise approximately a third of the identified viral proteins of Alpha and Gamma-herpes viruses, but not Beta-herpes viruses, owing to their larger genomes. This is particularly true in the case of Human Cytomegalovirus (HCMV), which encodes more than 200 ORFs (Table 1.1) (Alba et al. 2001). The *Betaherpesvirinae* HCMV belongs to the genera *Cytomegalovirus* and is the central focus of this thesis.

SubFamily	Virus	Acronyms	ORF	Length (Kb)
Alphaherpes viruses				
α1	Human herpes virus 1	HSV-1/HHV1	77	152
α1	Human herpes virus 2	HSV-2/HHV2	77	154
α2	Human herpes virus 3	VZV/HHV3	71	124
Betaherpes viruses				
β1	Human herpes virus 5	HCMV/HHV5	203	229
β2	Human herpes virus 6a	HHV6 A	121	159
β2	Human herpes virus 6B	HHV6 B	105	161
β2	Human herpes virus 7	HHV7	107	144
Gammaherpes viruses				
γ1	Human herpes virus 4	HHV-4/EBV	86	172
γ2	Human herpes virus 8	HHV8/KSHV	82	137

Table 1:1: The genomic characteristics and number of open reading frames (ORFs) of all human herpes viruses.

Alphaherpesvirinae	*Betaherpesvirinae*	*Gammaherpesvirinae*
Rapid destruction of infected cells	Enlarged infected cells	
Variable host range	Limited host range	Tend to be specific for either T or B lymphocytes
Relatively short cycle	Long cycle	Short replication cycle
Rapid spread of infection	Slow spread of infection	
Latent infection is maintained in sensory ganglia	Site of latency is myeloid progenitor cells	Site of latency is lymphoid tissue

Table 1:2: A summary of biological characteristics used to define members of the three subfamilies of herpes viruses.

1.2 Biology of Human Cytomegalovirus

Betaherpesvirinae includes two genera, *Cytomegalovirus* and *Roselovirus,* which includes HHV-6A, HHV-6B, and HHV-7. All exhibit a restricted host range and slow replication mechanism. Several species of *Cytomegalovirus* have been identified in distinct mammalian hosts, namely human, primates, and rodents. However, no cross-species infection has been identified, so a human virus cannot infect a mouse, or vice versa. The first isolation of HCMV was reported in 1956, from a dead infant with cytomegalic inclusion disease (Smith 1956). The virus was also subsequently isolated in two other laboratories, one from a patient with suspected varicella (Rowe et al. 1957) and another with suspected toxoplasmosis (Weller et al. 1957). In 1960, Weller *et al.* proposed that the virus be named '*Cytomegalovirus'* (Brennan 2001; Ho 2008).

1.2.1 Virion Structure

The structural properties of HCMV resemble that of the classic herpes viruses (Figure 1.1a,b).

1. The envelope comprises a phospholipid bilayer derived from the infected cell that is impregnated with viral glycoproteins. The HCMV envelope includes a set of glycoprotein homologues, gB, gH, gL, gM and gN. These are essential for initial virus-host attachment, virus internalisation, and cell to cell viral transmission (Navarro et al. 1993; Gicklhorn 2003; Kinzler and Compton 2005; Shimamura et al. 2006; Shen et al. 2007; Hobom et al. 2000; Keay and Baldwin 1991). Virion envelopes also contain another glycoprotein, gO. A gO gene deletion mutant of HCMV is viable but forms smaller plaques in fibroblast cells (Hobom et al. 2000). In addition, there are multiple HCMV specific glycoproteins, gp48, gpTRL10, gpTRL11, gpTRL12 and gpUL132, which are not considered essential for productive infection (Dunn et al. 2003). HCMV also encodes a number of receptors known as G-protein-coupled receptors (GPCRs) that are homologous to human chemokine receptors. These receptors (GPCRs), encoded by the ORFs, US27, US28, UL33, and UL78, are able to activate multiple cell signaling networks in a ligand-independent manner (Vischer et al. 2006). Some of these GPCRs, such

as UL78 and US27, have been shown to be important for viral entry in epithelial cells and its efficient extracellular spread, respectively (O'Connor and Shenk 2011; 2012).

2. The capsid or nucleocapsid packages and maintains the viral genomic dsDNA. It has an icosahedral geometry shape and each icosahedral lattice is composed of pentons, hexons, and triplexes arranged in a triangulation number = 16 (T=16) (Butcher et al. 1998; Chen et al. 1999).

3. The tegument is defined as the compartment between the capsid and the lipid envelope. Currently, 20 viral tegument proteins are known to assist with important functions in multiple events during the viral life cycle (Kalejta 2008). For example, pp71, ppUL35, and pUL69 transactivate viral gene expression (Liu and Stinski 1992; Winkler et al. 1994; Schierling et al. 2004), pp65 and pIRS1/pTRS1 facilitate immune evasion (Browne and Shenk 2003; Abate et al. 2004; Child et al. 2004; Marshall et al. 2009), and pp150 supports the egress of viral particles at the final envelopment stage (AuCoin et al. 2006; Tandon and Mocarski 2008). This compartment also contains a total of 71 host cellular proteins, with cytoskeletal proteins, translational protein factors, signaling transduction protein 14-3-3 and intracellular vesicular trafficking proteins (Varnum et al. 2004). Moreover, cellular and viral mRNAs appear to be incorporated within the tegument domain presumably through non-specific interactions with several viral proteins such as tegument pp28 (Terhune et al. 2004). The proportions of different host RNAs within tegument are similar to those expressed in host cells, it therefore seems to be independent of either signal-specific or sequence-specific mechanisms. A similar situation has been described for retroviruses, where RNA is packaged in virus particles and acts as a structural component promoting the integrity of the virion (Muriaux et al. 2001; Wang and Aldovini 2002).

4. The HCMV genome, which consists of one molecule of linear dsDNA, ~ 220 to ~ 240 kb in length, is the longest genome identified among animal viruses. The complete genome of nine strains of HCMV have been sequenced: 3157,

HAN13, HAN20, HAN38, JP and 3301, AD169, Towne, and Merlin (Cunningham et al. 2010; Dolan 2004; Bradley et al. 2009). The HCMV AD169 strain, isolated from a child's adenoids in 1956 (Montague and Iii 2000), is the virus strain used in this study. There are 208 ORFs in the prototypic reference strain of HCMV AD169 (Chee et al. 1990), however, extensive propagation in different laboratories over time has resulted in multiple mutations. In comparison to a low-passage strain virus, AD169 has mutation in genes TRL5A, TRL13, TRL14, UL36, UL131A, UL140, UL141, UL142, and UL144 (Skaletskaya et al. 2001; Yu et al. 2002; Akter 2003; Davison 2003; Bradley et al. 2009). One of multiple changes is a substitution in gene UL36 rendering this protein non-functional (Skaletskaya et al. 2001). Those mutations do not exist in HCMV strains that have a wider cell tropism than AD169, therefore it has been speculated that these genes are critical for determining cell tropism (Cha et al. 1996; MacCormac and Grundy 1999). ORFs in the HCMV strain AD169 have been assigned into three major classes functionally: (i) 41 essential (ii) 27 augmentative and (iii) 88 nonessential genes. This was based upon the generation of a library of ORF mutations in this strain, which were analysed for their growth properties in fibroblasts (Yu et al. 2003).

1.2.2 Genome structure of HCMV

Like many other herpes viruses, the HCMV genome is organised into two unique regions: unique long (U_L) and unique short (U_S) regions (Figure 1.1c). Each unique region is flanked by a terminal repeat component (TR_L or TR_S) at one end and an inverted repeat component (IR_L or IR_S) at the other end, which results in the overall genome arrangement TR_L–U_L–IR_L–IR_S–U_S–TR_S. These unique sequences can be inverted, giving rise to equimolar populations of four isomeric variants of the HCMV genome (Kilpatrick and Huang 1977) (Figure 1.1c). The four isomers have basically the same DNA sequences but vary in the orientation and position of the inverted ends relative to the rest of the DNA molecule (Kilpatrick and Huang 1977). It is unclear whether the organisation of the isomeric forms have an inherent biological importance in terms of the infection and propagation of HCMV as studies have shown that the circular isomeric forms of the HCMV genome in the form of bacterial

artificial chromosome (BAC) are infectious (Borst et al. 1999). The nomenclature used to designate the ORFs of HCMV depends on their position within the unique or repeat segments, with the ORF within this segment being given numbers in sequential order (Chee et al. 1990).

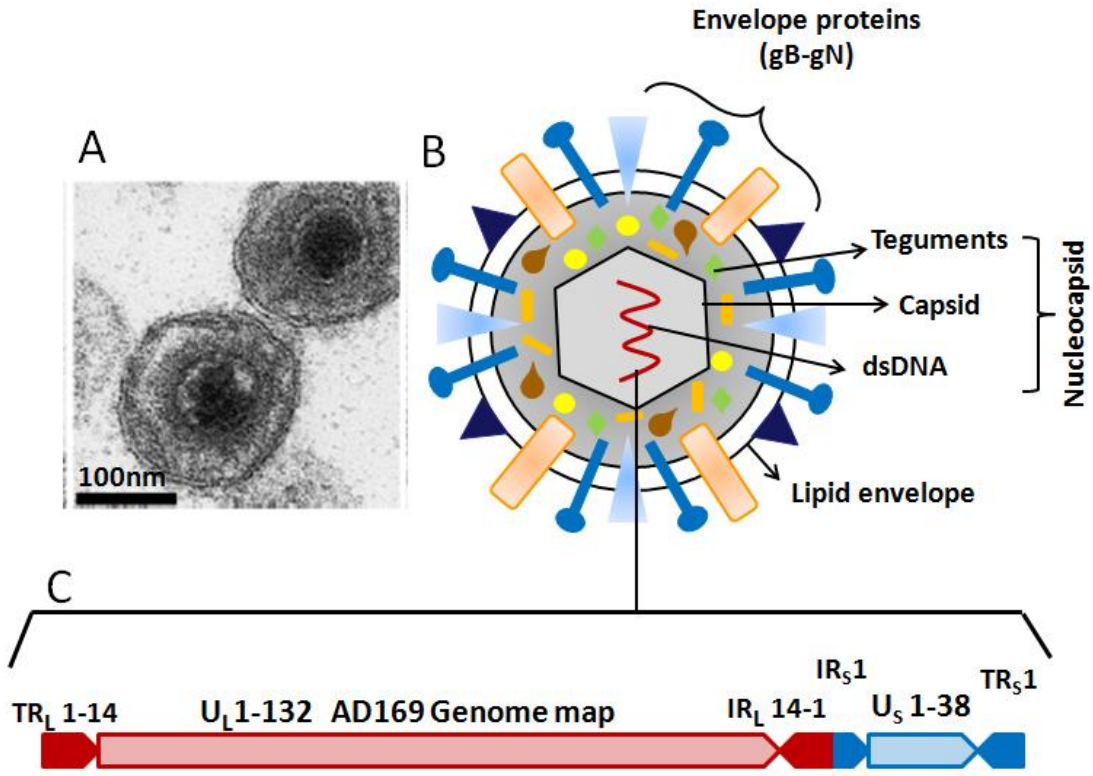

Figure 1.1: Structure of CMV virion and genome. A) electron micrograph image showing two HCMV particles (Mettenleiter et al. 2009). B) Schematic representation of a cytomegalovirus virion showing the lipid bilayer that is studded with at least 10 glycoproteins (gB-gN), linear double-stranded DNA (dsDNA) is encased by an icosahedral capsid, and tegument proteins. C) The genome of HCMV is composed of a unique long (U_L) and a unique short (U_S) sequence, bounded by inverted terminal and internal repeats (TR_L, IR_L, IR_S and TR_S).

1.2.3 HCMV life cycle

1.2.3.1 Attachment and entry

HCMV initiates infection through multi-step sequential interactions with cellular receptors. The viral envelop glycoproteins gB and gCII (gM/gN) mediate low-affinity interaction with heparan sulfate proteoglycans (HSPGs) present in the cell membrane of host cells, as treatment of cultured fibroblasts with heparin, heparinise, and other sulfated polysaccharides reduces viral attachment and plaque titer (Kari and Gehrz 1992; Neyts et al. 1992). This reduction was also seen in a CHO cell line harbouring mutations in HSPGs or all GAGs suggesting this interaction occurs via the glycosaminoglycans (GAGs) portion of the HSPGs (Figure 1.2a) (Neyts et al. 1992; Compton et al. 1993; Boyle and Compton 1998).

In the response to the initial binding of HCMV gBs with HSPGs, more stable interactions between one or more viral and cellular receptors appear to take place. Several cellular receptors have been studied in this context, but whether they are essential for virus entry has not been confirmed. For example, (i) Annexin II on the host cell membrane binds to the viral envelope protein gB, promoting virus and cell membrane fusion (Pietropaolo and Compton 1997; Raynor et al. 1999). However, treatment of cells with anti-annexin II antibody suggests that Annexin II is not required for virus entry into fibroblasts (Pietropaolo and Compton 1999). (ii) HCMV mediates the phosphorylation of host cell epidermal growth factor receptor (EGFR) briefly upon infection. The rapid phosphorylation of EGFR results in the activation of Ca^{++} fluxes and phosphorylation of the regulatory subunit of the PI3K, p85 and AKT (Wang et al. 2003). However, polyclonal antibodies directed against human EGFR or blocking its kinase activity have no effect on HCMV entry or levels of infectivity in fibroblast, epithelial, or endothelial cell lines (Isaacson et al. 2007), further EGFR is not expressed by all cells permissive to HCMV infection. (iii) HCMV infection has also been associated with host cell expression of CD13 (Aminopeptidase N). Antibodies against CD13 or compounds known to block its enzymatic properties can inhibit the binding of HCMV to susceptible cells (Söderberg et al. 1993), suggesting CD13 is essential. A more recent report has shown that CD13 antibodies interact directly with the virus and neutralise HCMV

impeding viral entry. However, HCMV has also been shown to successfully enter CD13 depleted cells (Giugni et al. 1996), suggesting it is not essential. (iv) The effect of neutralising antibodies against integrins on HCMV entry has also been assessed by Feire et al. (2004). Anti-α2β1, α6β1, and αvβ3 antibodies caused a pronounced decrease in HCMV infectivity. The integrin antibodies did not block attachment of virus to the host cells but blocked internalisation of the virus. Viral glycoprotein B disintegrin-like domain was shown to mediate interactions between the virus and integrins and HCMV gB disintegrin-like peptide inhibits CMV infection (Feire et al. 2004). However, it remains important to confirm the role of integrins as cellular co-receptors for HCMV, as well as to identify the cellular receptors essential for infection.

Upon the attachment, there are three main routes by which the virus enters into the host cells.

1- Fusion: direct pH-independent fusion was demonstrated between the HCMV envelope and host cell membrane in permissive fibroblasts (Compton et al. 1992) (Figure 1.2a).

2- Endocytosis: viral internalisation into epithelial and endothelial cells occurs through the low-pH-dependent endosomal pathway. Acidification of the endosome promotes the fusion of the viral and endosomal membranes and the subsequent release of the nucleocapsid particles (Ryckman et al. 2006) (Figure 1.2b). Most internalised viruses (AD169 and Towne laboratory strains) appear to be sequestrated and degraded within the endosomes, resulting in a low level of infection, and a delay in DNA synthesis and virus replication (Bodaghi et al. 1999). However, the epithelial and endothelial cells are permissive for replication of clinical strains of HCMV (Toledo, Merlin, and TR). It might be because the clinical isolates retain a cluster of genes located between UL128 to UL150 that are lost by natural deletion in laboratory strains (Cha et al. 1996; Murphy et al. 2003). Recent reports show that individual genes within this cluster (UL128, UL-130, UL-131) are required for HCMV replication in epithelial and endothelial cells (Hahn et al. 2004; Patrone et al. 2005; Wang and Shenk 2005).

3- Macropinocytosis: Haspot et al., (2012) reported that HCMV enters dendritic cells by promoting the formation of membrane ruffles within the cholesterol-enriched domain of the membrane of dendritic cells through an actin-driven mechanism. Viruses are then internalized into a large macropinosome-like vesicle, which has endosomeal-features, protecting the virus particles from degradation. The membranes of the macropinosome and enveloped virus fuse to release the nucleocapsid in close proximity to the nuclear envelope of the infected dendritic cells (Figure 1.2c).

4- Combined entry methods: in a study on the infection of macrophages by HCMV, it has been found that the entry of virus into M2 anti-inflammatory macrophages involves both fusion and endocytosis (Wang et al. 2009).

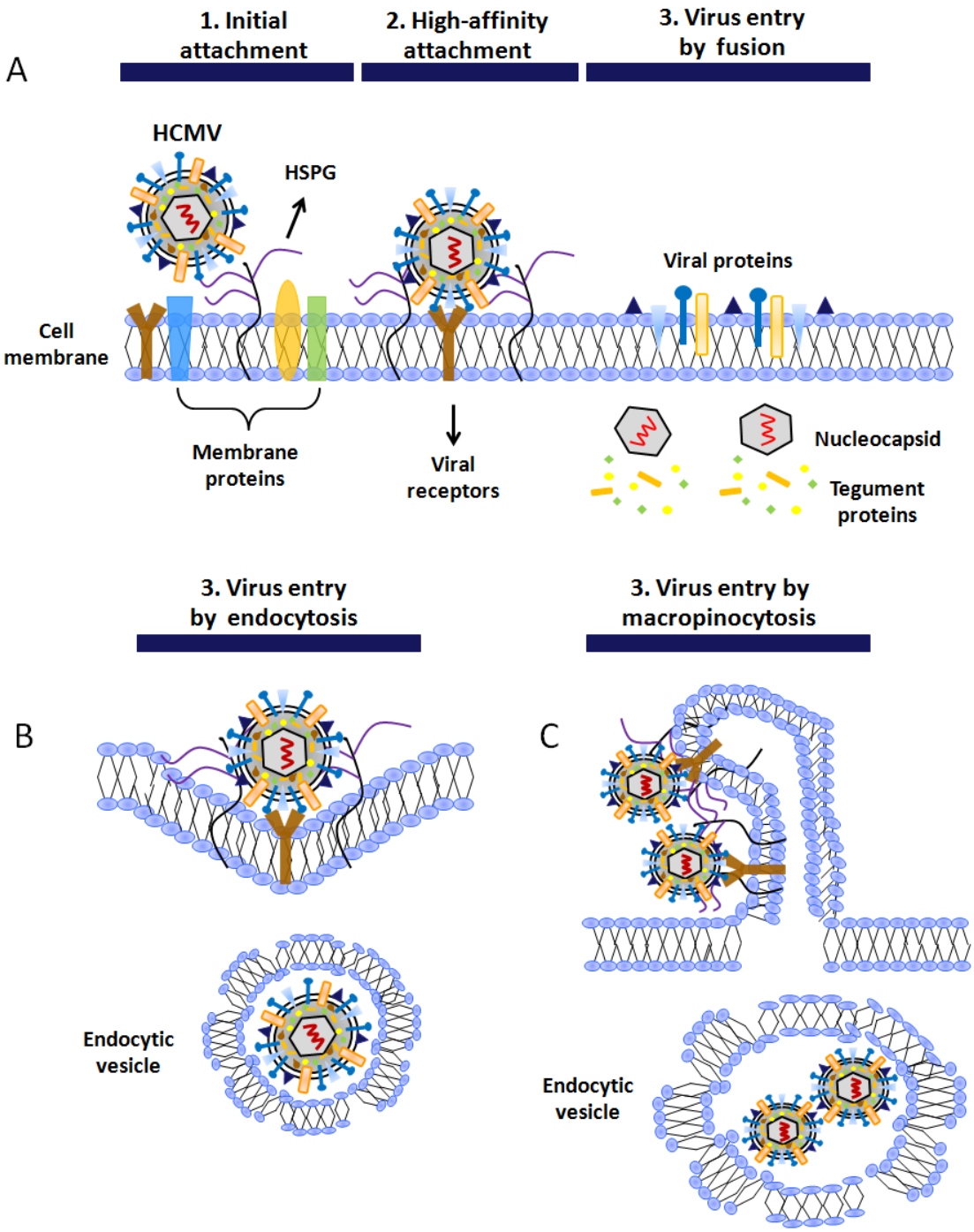

Figure 1.2: Models of the different mechanisms of HCMV entry into the host cell. HCMV is initially attached to host cells through an interaction between heparan sulfate proteoglycans (HSPGs) and virus glycoproteins. This is followed by a stable interaction with unidentified cellular receptors. One or more of these interactions induces fusion that leads to the internalization of virion nucleocapsid (A). At least one of these interactions activates the endocytosis (B) or macropinocytosis (C) that result in endocytic internalization of the virion particle. Adapted from (Compton et al. 1992)

1.2.3.2 The translocation

Interaction of the virion with cellular receptors is followed by the fusion of the virus envelope with the host cellular membrane, which results in release of the nucleocapsid into the cytoplasm of the infected cell, along with free or capsid bound tegument proteins. In case of viral entry via endocytosis and macropinocytosis, the viral envelope fuses with the endocytic vesicle and the viral nucleocapsid and tegument proteins are then released into the cytoplasm of the host cell. Some disassociated tegument proteins are sequestered in the cytoplasm, while others such as pp65 and pp71 migrate to the nucleus. The mechanisms that mediate capsid disassembly and the delivery of viral DNA into the nucleus through the nuclear pore complexes are poorly understood in herpes viruses. Tegument proteins that are associated with the nucleocapsid, such as pUL48 have been shown to mediate interactions between the nucleocapsid and cellular microtubule-associated motor proteins during intracellular transport into the nucleus, through p180, an endoplasmic reticulum protein (Figure 1.3) (Ogawa-goto et al. 2007; Irie et al. 2002). Also, a complex of tegument proteins maybe formed from interaction of pUL47 with pUL48, pUL69, and major capsid protein (MCP or pUL86) (Bechtel and Shenk 2002). A constructed mutant HCMV strain AD169 lacking pUL47 displays deficits in the protein expression of pUL48 and IE gene expression (Bechtel and Shenk 2002). Studies from HSV-1 support that the homologs of HCMV pUL47 and pUL48 (named UL37/VP1 and UL36/VP2, respectively) form a complex with the capsid (Klupp et al. 2002; Vittone et al. 2005; Coller et al. 2007) that directs the trafficking of HSV-1 nucleocapsids toward the nucleus (Luxton et al. 2005; Wolfstein et al. 2006).

1.2.3.3 Gene expression

Once the viral genome enters the host nucleus, transcription is initiated in a cascade manner. Consequently, HCMV proteins are characterised according to their temporal expression pattern, namely (i) immediate-early 'IE', (ii) early 'E', and (iii) late proteins (Wathen and Stinski 1982).

The first stage in the expression involves the transcription of IE1 (IE-72) and IE2 (IE-86). This happens within the first 3 hours of HCMV infection (Stinski et al.

1983), and utilises host cell RNA-Polymerase II together with viral tegument proteins pp71 and pUL69 (Cantrell and Bresnahan 2006; Preston and Nicholl 2006). The expression of IE genes is therefore independent of *de novo*-synthesised viral proteins. Tegument pp71 interacts directly with a death domain-associated protein (Daxx) to counteract its repressive function through the recruitment of histone deacetylase (HDAC) to the IE promoter (Hofmann et al. 2002; Cantrell and Bresnahan 2005). pp71 induces proteasome-dependent degradation of Daxx at the start of productive infection (Saffert and Kalejta 2006) (Figure 1.3). Similarly, pp71 interacts with and degrades the hypophosphorylated forms of retinoblastoma proteins (pRB, p107 and p130) in a proteasome-dependent manner (Kalejta and Shenk 2002) leading to the activation of the transcription factor E2F, which is involved in DNA replication and cell cycle progression from G0/G1 toward G1/S phase (Kalejta and Shenk 2003). However, the latter degradation is not essential for efficient HCMV replication, as HCMV has other mechanisms to control the RB-E2F pathway, such as viral UL97 (Hume et al. 2008) or IE-2 (Song and Stinski 2002). Binding of viral protein pUL69 to UAP56-URH49 regulates the export of viral mRNA and supports translation (Lischka et al. 2006; Aoyagi et al. 2010; Zielke et al. 2011). The transcription and translation of the viral immediate early gene products, IE-1 and IE-2 initiates viral gene expression. These IE proteins also play a role in suppressing cellular immune responses, for example, IE1 disrupts interferon (IFN) signaling cascades. The IE1 protein interacts directly with signal transducer and activator of transcription 2 (STAT2), inhibiting the formation of STAT1:STAT2 heterodimers which in turn impedes the formation of the STAT1:STAT2:IRF9 trimeric transcription factor complex known as interferon stimulated gene factor 3 (ISGF3). ISGF3 is able to bind to IFN-stimulated response elements (ISREs) within the promoter of ISGs and subsequently activate their transcription (Paulus et al. 2006; Krauss et al. 2009; Huh et al. 2008). IE-1 protein also has multiple inductive and repressive interactions with other host proteins (Hayhurst et al. 1995; Hwang et al. 2009; Iwamoto et al. 1990; Kline et al. 1994.; Koh et al. 2009; Lee et al. 2005; Lukac et al. 1997; Margolis et al. 1995; Murayama et al. 2000; Nevels et al. 2004; Poma et al. 1996; Stråat et al. 2009; Yurochko et al. 1997; Iwamoto and Konicek 1997). In HCMV strains where IE1 has been deleted, the expression of the late early genes

are reduced and this causes a severe growth deficiency in fibroblasts infected at low multiplicities of infection (MOI), though at high MOI, replication is normal, negating the absence of IE1 (Mocarski et al. 1996; Greaves and Mocarski 1998; Gawn and Greaves 2002). IE-2 protein is essential for productive infection. A deletion in the IE-2 gene in recombinant HCMV results in total absence of viral gene expression and the subsequent failure of DNA replication and virus production (Marchini et al. 2001; Sanders et al. 2008). IE2 is a crucial trans-activator for viral early and late genes. Activation occurs through the interaction of IE2 with specific DNA motifs (Arlt et al. 1994; Scully et al. 1995), which may include RNA polymerase II transcription initiation complexes such as TBP, TFIIB (Caswell et al. 1993; Lukac et al. 1994; Sommer et al. 1994), transcription factors such as Rb, p53, CREB (Lang et al. 1995; Bonin and McDougall 1997; Fortunato et al. 1997), and histone acetyltransferase, such as PCAF and CBP (Schwartz et al. 1996; Bryant et al. 2000).

The second stage of viral gene expression involves the early genes, whose expression is controlled by the immediate early genes (Fortunato and Spector 1999). The products of early genes include the proteins required for transcription and DNA replication, which are expressed between 3 and 36 hours following infection. DNA synthesis, which starts from the replication origin (oriLyt) (Zhu et al. 1998; Borst and Messerle 2005), occurs by the rolling circle-mechanism to generate concatemeric viral DNA of head-to-tail-linked genomes (McVoy and Adler 1994).

The final step of viral gene expression starts with the expression of viral late proteins from 36 to 72 hours. These mainly include the structural proteins such as envelope glycoproteins, teguments, and capsids.

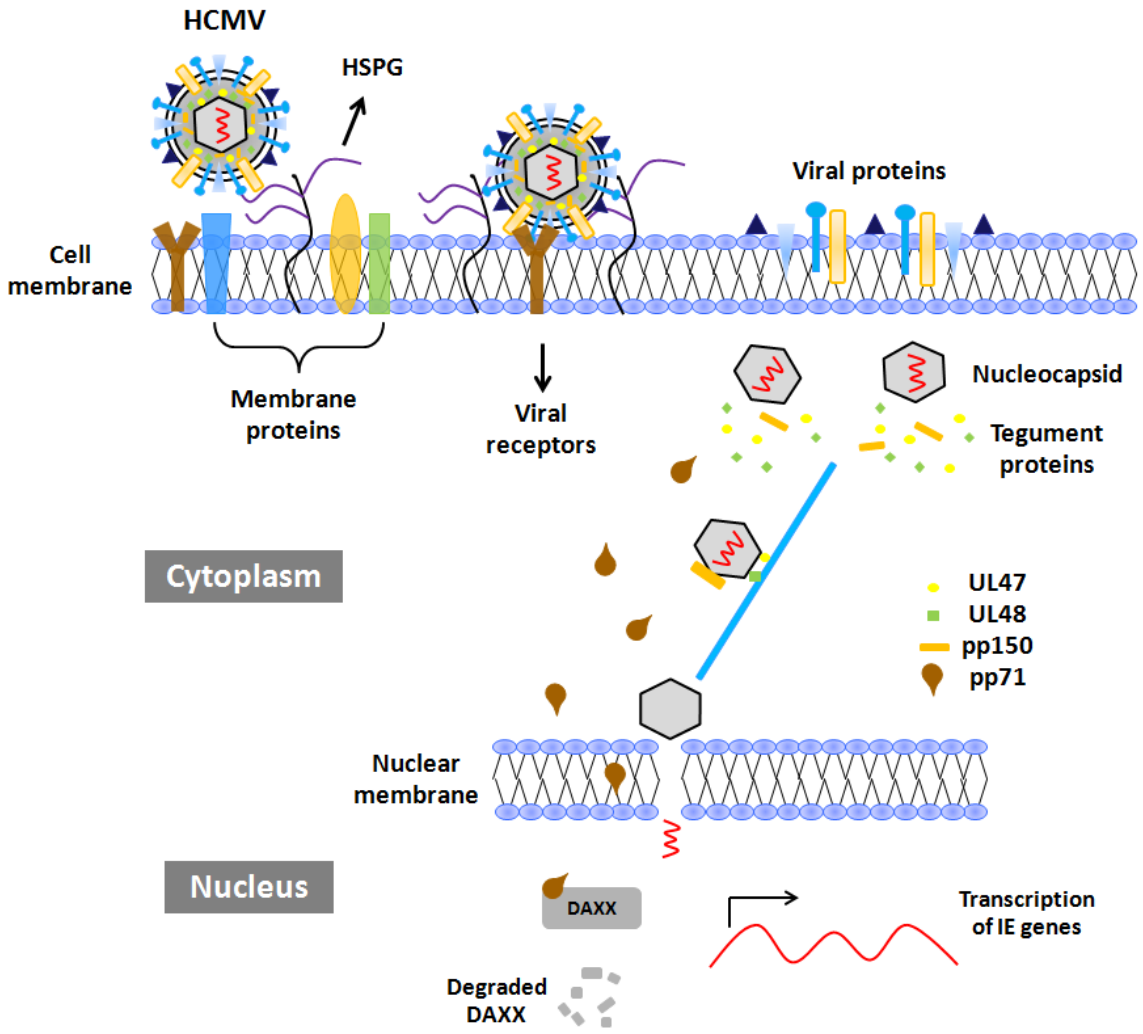

Figure 1.3: Tegument proteins aid the translocation of HCMV nucleocapsid to the nucleus upon viral entry and assist the initiation of the transcription of the immediate early viral genes. (1) Capsid-associated tegument proteins UL47 and UL48 (and possibly pp150) are involved in the trafficking of the viral nucleocapsids along the microtubule toward the nucleus. (2) Some of tegument proteins (such as pp71) are transported to the nucleus independently of capsids. (3) Capsids ultimately detach from microtubules, dock at nuclear pores, and release their DNA into the nucleus. (4) pp71 interacts with Daxx in the nucleus to induces Daxx degradation and transcription of viral IE genes, and thus starts the lytic cycle of HCMV. Adapted from (Compton et al. 1992; Kalejta 2008).

1.2.3.4 Formation of capsid and DNA packaging

The processes of HCMV capsid maturation and viral DNA genome packaging occur exclusively in the nucleus of infected cells. Capsid formation starts with the construction of a spherical procapsid in the cytoplasm through a series of interactions between MCP and the two alternatively translated gene products of UL80, scaffolding protein (preAP) and proteinase precursor (pPR) (Beaudet-Miller et al. 1996; Oien et al. 1997; Wood et al. 1997). These interactions, together with the complex of the minor capsid protein (mCP or pUL85) and its binding protein (mC-PB or UL46) (Gibson et al. 1996), are also required for nuclear translocation of the procapsid (Plafker and Gibson 1998). Simultaneously, the portal protein pUL104 is incorporated at one end to form the channels for DNA import into the capsid (Dittmer and Bogner 2005; Holzenburg et al. 2009). The complete assembled capsid includes two protein layers: structural components are located in the outer layer, and scaffold elements are located the inner layer. Before DNA can be imported, the capsid has to be matured through the cleavage of the scaffold proteins by the proteolytic activity of the pPR derived protease, PR (Welch et al. 1991; Rixon 1993). The correct formation of mature capsid is believed to be dependent on the overall time and speed of scaffold protein digestion and binding of DNA. Variations in these factors determine the final outcome of capsid formation (Welch et al. 1991; Yu et al. 2005). The accurate timing of digestion of scaffold proteins enables efflux of digested products from the capsid and DNA packaging to proceed concurrently before angularization and sealing of the capsid occurs, resulting in capsid C formation which can develop into infectious particles (Figure 1.4) (Yu et al. 2005). Two other defective forms of capsids can arise if a failure occurs during scaffold protein processing, neither of which are infectious as they fail to import DNA (Gibson and Roizman 1972): 1) Capsid A will release the digested proteins and be sealed before importation of DNA; 2) Capsid B, where sealing occurs before efflux of all digested scaffold products occurs (Yu et al. 2005). HCMV infected cells therefore not only release infectious virions (capsid C), but also non-infectious enveloped particles (NIEPs) and dense bodies (DBs) believed to be A and B capsids, respectively (Figure 1.4). The biological importance of these non-infectious particles is not well-studied, however, it has been shown that these particles can stimulate the

immune response in the absence of viral gene expression *in vivo* (Pepperl et al. 2000). The viral DNA concatamer has to be processed for entry into the capsid. Viral terminase subunits pUL56 and pUL89 recognise and bind to two specific packaging sequences of viral DNA (pac1 and pac2) (Bogner et al. 1998) and their endonuclease activity cleaves the concatemers into unit-length viral genomic DNA strands (Scheffczik et al. 2002; Thoma et al. 2006). The terminase subunits also have ATP activity producing sufficient energy for packaging through ATP-hydrolysis (Scholz 2003; Hwang and Bogner 2002). The terminase translocates the DNA through the capsid channel into the capsid (Dittmer and Bogner 2005; Welch et al. 1991).

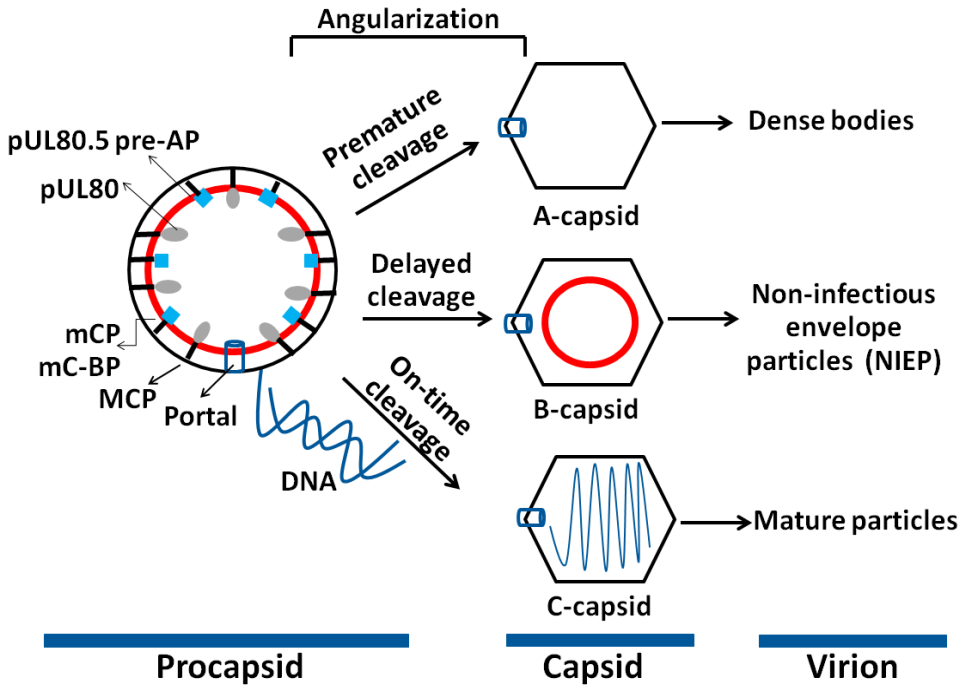

Figure 1.4: HCMV capsid assembly and maturation. HCMV capsid proteins come together into an inner circular capsid, which angularizes to generate A, B, or C capsids, depending on the packaging of DNA and timing of scaffold protein cleavage by PR. The failure of proper formation of C capsids leads to non-infectious enveloped particles (NIEPs) and dense bodies (DBs). Adapted from (Yu et al. 2004).

1.2.3.5 Egress

Once the unit-length viral genomic DNA packaging into the capsid is completed, the nucleocapsids will be exported from the host cell nucleus into the cytoplasm where the mature virions are assembled. HCMV nucleocapsids cannot simply exit though the nuclear pore as they are larger (~120nm) than the nuclear pore (~39nm) (Pante and Kann 2002). Therefore, the nucleocapsids penetrate the nuclear envelope in a process known as a perinuclear budding. The budding of nucleocapsids at the inner nuclear membrane leads to the acquisition of the first temporal envelope, which is lost in the perinuclear space when this envelope fuses with the outer nuclear membrane before leaving the nucleus (Figure 1.5) (Mettenleiter 2002; 2004; Mettenleiter et al. 2006). The inner nuclear membrane is normally stabilized by attachment to the nuclear lamina, however, in mitosis the association is disrupted by phosphorylation of the lamina by specific cellular kinases (Peter et al. 1990; Buendia et al. 2001; Otto et al. 2001). Therefore, during budding the nucleocapsid engages a complex mixture of cellular and viral proteins including, pUL50, pUL53, UL97, protein kinase C (PKC) and PKC-binding protein p32 to access and disassemble the inner nuclear membrane (Milbradt et al. 2010). It is proposed that the morphogenesis of HCMV, specifically the tegumentation and final envelopment of the infectious particle, is largely acquired within a cytoplasmic virion assembly complex (cVAC). The cVAC is a compartment adjacent to the nucleus, which contains abundant structural and nonstructural HCMV proteins (Hensel et al. 1995; Sanchez et al. 2000; Theiler and Compton 2002; Das and Pellett 2007; Seo and Britt 2008) with endoplasmic reticulum at its periphery, around which concentric arrangements of Golgi, trans-Golgi network (TGN) are formed. At the centre, the cVAC contains early endosomal vesicles (Figure 1.5) (Das and Pellett 2007; 2011; Das et al. 2007). It is believed that HCMV pp150 (pUL32) (AuCoin et al. 2006; Tandon and Mocarski 2008; Indran et al. 2010; Indran and Britt 2011) and pUL71 (Womack and Shenk 2010; Schauflinger et al. 2011) are critical for efficient trafficking of the partially tegumented nucleocapsids during the maturation in the cVAC and for egress from infected cells. The inhibition of the interaction between pp150 and the cellular protein Bicaudal D1, a trafficking protein that associates with dynein motor protein and the Rab6 GTPase, interrupts the localization of pp150 and results in a reduction

in the production of infectious virions. Whereas infection with a virus in which pUL71 is mutated causes marked accumulation of mutant virions (Womack and Shenk 2010) . Other mutations can also affect egress, infection with a virus in which UL103 ORF is deleted prevents release of enveloped virions and dense bodies (Ahlqvist and Mocarski 2011). The proposed model for the final envelopment of HCMV hypothesizes that the viral envelope is acquired from the cisternal membrane, which has features of the vesicles derived from the TGN as well as endosomes (Cepeda et al. 2010). Therefore, it appears that the endosomes are recruited to TGN in order to incorporate their endosomal proteins into the viral envelop (Cepeda et al. 2010). Upon the completion of morphogenesis, mature enveloped virions are released by exocytosis at the plasma membrane of host cells (Figure 1.5) (Mettenleiter 2004).

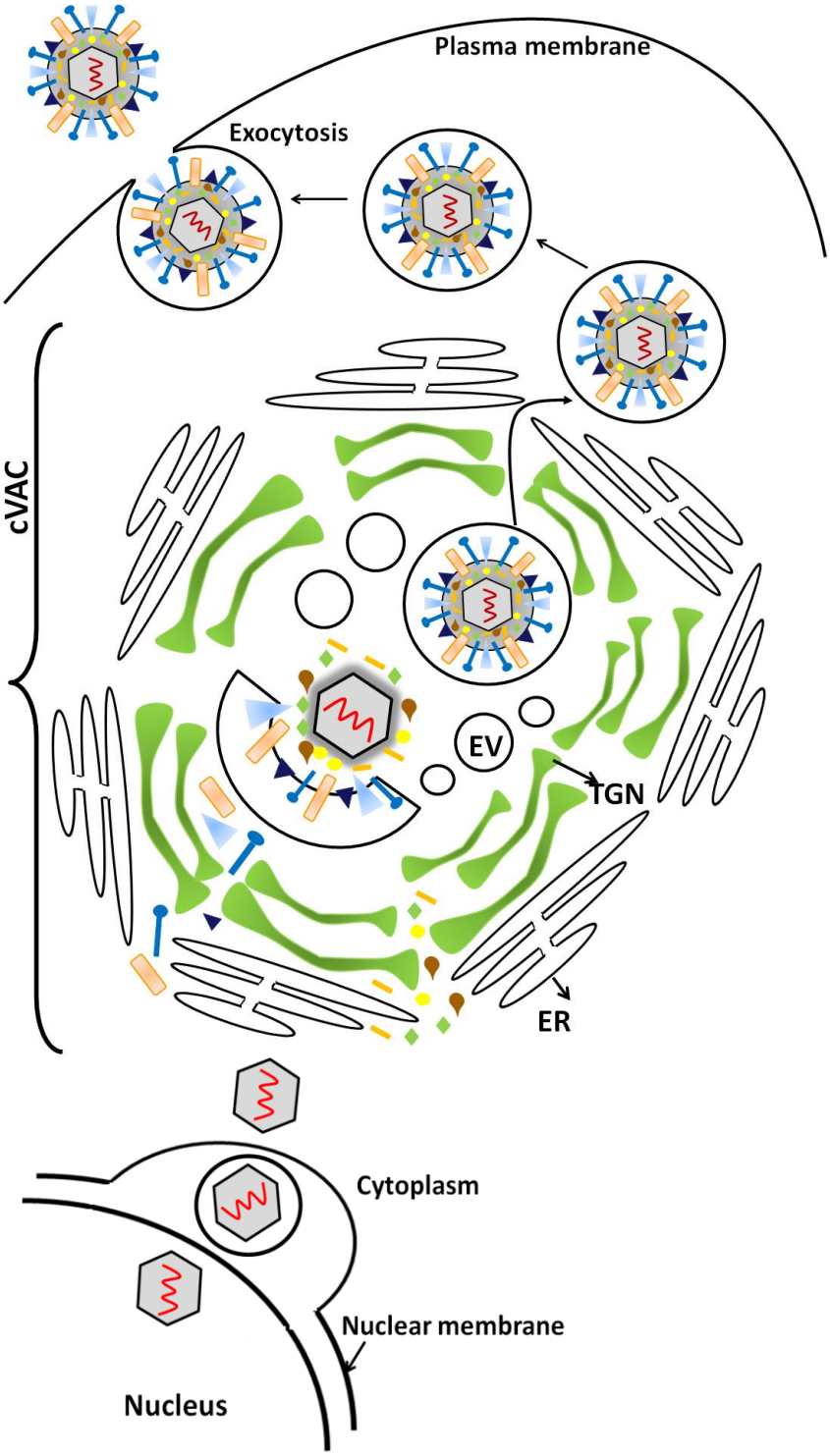

Figure 1.5: Schematic representation of HCMV envelopment and egress. The nucleocapsid is released from the nucleus through the nuclear membrane. In the cytoplasm, tegumentation and envelopment occur during migration from the periphery of cVAC {known as virion assembly complex} to the exit in a vesicle, which occur close from the plasma membrane. Virus is released from host cells by exocytosis. The cVAC is composed of endoplasmic reticulum (ER), trans-Golgi network (TGN) and endosomal vesicles (EV).

1.2.4 Mouse cytomegalovirus (MCMV) provides a model for HCMV infection

β-herpes viruses exhibit a strict host specificity, with the result that HCMV is incapable of infecting species other than humans. This fact prohibits experimental studies of HCMV infection in an animal model and limits them to *in vitro* studies using human cells. MCMV is a close relative of HCMV that provides a good *in vivo* model for the following reasons. 1) MCMV and HCMV share 80 conserved ORFs, representing ~40% of encoded ORFs in these viruses (Rawlinson et al. 1996; Brocchieri et al. 2005). 2) The pathological outcomes of MCMV infection of mice resemble those of HCMV in its host. It has been reported that infection with MCMV leads to the establishment of latent MCMV infection in immunocompetent mice (Hudson 1979), whereas the infection of immunosuppressed mice is lethal (Reddehase et al. 1985; Krmpotic et al. 2003). 3) MCMV can be reactivated from its latent phase (Anon 1977; Jordan et al. 1978; Shanley et al. 1979; Reddehase et al. 1994; Krmpotic et al. 2003) and transmitted during transplantation and blood transfusion (Hamilton and Seaworth 1985; Roback et al. 2006) 4) MCMV is also similar to HCMV in terms of the structure, kinetics of gene expression, dynamics of the replication cycle (Mocarski and Kemble 1996), and the host immune response to infection (Mocarski 2004). MCMV has been proven to be an invaluable model for the investigation of responses to potential antiviral drugs, host susceptibility to infection, and the identification of host resistance genes. This MCMV model also enables the study of MCMV-mutants in intact physiological system (Scalzo et al. 2007). However, it is important to consider that conserved modulation of host proteins performed by HCMV and MCMV could be mediated through different viral products of the two viruses as well as mechanisms.

1.3 microRNAs (miRNAs)

1.3.1 Introduction to small non-coding microRNAs (miRNAs)

The insights resulting from the sequence-profiling of the full-mammalian transcriptome have challenged the traditional view that the majority of genes code for proteins and that the more complex the organism, the greater the number of protein-coding genes. It is now quite evident that the number of protein-coding genes in human and mice are comparable to those in the nematode, *Caenorhabditis elegans* (*C. elegans*) (Carninci et al. 2005). A possible explanation is that the complexity of organism correlates with the proportion of non-protein-coding RNAs, whilst only 2% of the mammalian genome encodes mRNAs, the vast majority is transcribed as ncRNAs, some, if not many, of which have been shown to have biological functions (Taft et al. 2007; 2010).

Non-coding RNAs (ncRNAs) are defined as classes of functional regulator RNAs that do not encode protein sequences. ncRNAs can be categorised into small, mid-size and long ncRNA. The focus of this thesis is the most-studied class of small non-coding, microRNAs (miRNAs) (originally called short temporal RNAs (stRNAs)). miRNAs are single-stranded RNAs between 19 to 24 nt in length, which function to regulate protein expression at the post-transcriptional level (Bartel et al. 2004). The first miRNA, lin-4, was identified in the nematode *C. elegans* in 1993 by Ambros and Ruvkun. They observed an inverse correlation between the lin-4 gene product and the protein level of lin-14 in *C. elegans*. lin-4 was shown to produce two short non-coding RNAs of 22 nt and 60 nt, rather than a protein. These RNAs of lin-4 have complementary sequences to the 3′ untranslated region (3′UTR) of lin-14 mRNA and able to reduce the translation of lin-14 through the formation of a lin-4:lin-14 RNA duplex (Lee et al. 1993; Wightman et al. 1993). Through a similar mechanism, lin-4 also seems to repress the translation of lin-28, a cold-shock-domain protein that is involved in regulation of the developmental transition between the L2 and L3 larval stages of *C. elegans* (Moss et al. 1997). Almost seven years after these reports on lin-4, Reinhart et al. (2000) identified a second small RNA in *C. elegans* named let-7 RNA. This RNA contributes to the transition from the larval to adult stage through its interaction with the 3′UTR of lin-41 and hbl-1 (lin-57), which results in inhibition

of their translation (Slack et al. 2000; Abrahante et al. 2003; Lin et al. 2003; Vella et al. 2004). The let-7 RNA was found to be conserved in several species, including *Homo sapiens*, resulting in the assumption that more short RNA molecules were likely to exist (Pasquinelli et al. 2000). The number of miRNAs identified continues to increase, and online miRNA database was established to publish and categorise miRNA sequences (Griffiths-Jones 2004): (http://www.mirbase.org/). To date, more than 1500 miRNAs in the human genome have been annotated in the latest version of miRBase (version 19.0) (Kozomara and Griffiths-Jones 2011).

1.3.2 Biogenesis of mammalian miRNAs

Biogenesis of miRNAs involves two sequential processing reactions: pri-miRNA processing in the nucleus and subsequent pre-miRNA maturation in the cytoplasm (Figure 1.6).

1) Pri-miRNA processing in the nucleus

- Transcription of the pri-miRNA

The majority of the miRNAs are transcribed by RNA polymerase II (also called RNAP II and RNA Pol II), while RNA polymerase III mediates the transcription of a relatively small proportion (Lee et al. 2002; Cai et al. 2004; Borchert et al. 2006; Monteys et al. 2010). miRNAs are transcribed as single primary transcripts (pri-miRNA) ranging from hundreds to thousands of nucleotides in length. The pri-miRNAs that are synthesised by RNA Pol II have been shown to be capped at their 5′-ends and polyadenylated at their 3′-ends (Cai et al. 2004). Independent transcription units within introns, exons, or intergenic regions can host either monocistronic miRNA, dicistronic, or polycistronic clusters of miRNAs that are transcribed from the same promoter (Lee et al. 2002), or they can also be transcribed and regulated independently of each other (Song and Wang 2008). Pri-miRNAs contains at least one region of imperfectly paired double-stranded RNA (dsRNA) known as the stem-loop structure that is required for the expression of mature miRNAs. This stem-loop is flanked by single-stranded RNA (ssRNA) (Figure 1.6).

- pri-miRNA cleavage by the Drosha-DGCR8 microprocessor complex

The RNAse III enzyme Drosha interacts with its co-factor anchor protein, DiGeorge syndrome critical region gene 8 (DGCR8) to form the microprocessor complex, which recognises the stem-loop structure of the pri-miRNA (Lee et al. 2003; Denli et al. 2004; Gregory et al. 2004; Han et al. 2004; Landthaler et al. 2004; Zeng et al. 2005). DGCR8 guides Drosha to cleave the base of the stem-loop structure and release a precursor miRNA (pre-miRNA) of ~60 to 70nt in length having a 5′-phosphate and 3′-OH with 2nt overhang (Zeng 2003; Zeng et al. 2005; Zeng and Cullen 2005). Few miRNAs that have been found to be processed independent of Drosha-DGCR8 microprocessor complex as the two ends of their precursors reside at the splice sites of the intron. These miRNAs are known as mirtron (Figure 1.6) (Okamura et al. 2007; Ruby et al. 2007).

- Pre-miRNA export mediated by Exportin 5-RanGTP

The 3′ overhang of pre-miRNA facilitates its interaction with Exportin 5 and RanGTP molecules, producing a stabilized heterotrimer that allows efficient nuclear export to occur (Yi et al. 2003; Bohnsack 2004; Lund et al. 2004; Zhang et al. 2004; Okada et al. 2009). Once the heterotrimer arrives in the cytoplasm, the pre-miRNA is released from Exportin 5 following hydrolysis of RanGTP to RanGDP, promoted by RanGAP and other cofactors (Kehlenbach et al. 1999; Wang et al. 2011).

2) pre-miRNA maturation in the cytoplasm

pre-miRNA processing

Following export of pre-miRNA from the nucleus, RNaseIII nuclease Dicer and its cofactors, TAR DNA-binding protein (TRBP) and protein activator of PKR (PACT) form the RISC loading complex (RLC) that subsequently associates with the core component Argonaute-2 (Ago2) (Gregory et al. 2005; Haase et al. 2005; Maniataki and Mourelatos 2005; Lee et al. 2006; MacRae et al. 2008). Dicer's PAZ domain and two RNase III domains (RIIIa and RIIIb) are involved in the recognition and binding of RLC to the exported pre-miRNA (Lingel et al. 2003; Song et al. 2003; Yan et al. 2003; Ma et al. 2004; MacRae and Doudna 2007). A single RNase domain is required in order to cleave pre-miRNA at the base of the stem loop, producing an

imperfect miRNA:miRNA* duplex with a 5′ phosphate and 3′ OH with 2nt overhang (Zhang et al. 2004). While neither TRBP nor PACT is important for the pre-miRNA cleavage reaction stage, PACT facilitates the RLC formation and TRBP contributes to the stabilization of Dicer (Lee et al. 2006; Kok et al. 2007) and the recruitment of Ago2 to the RLC (Chendrimada et al. 2010). Although Dicer seems to be the predominant molecule for pre-miRNA processing, a Dicer-independent miRNA biogenesis pathway has been identified in which there is an Ago2-mediated cleavage reaction of pre-miRNA. An unusual pre-miRNA, pre-miR-451, is relatively short (~39nt) for loading into Dicer, instead Ago2 is used (Figure 1.6) (Cheloufi et al. 2010; Cifuentes et al. 2011; Yang et al. 2010).

miRNA duplex unwinding and loading

Following Dicer cleavage, the miRNA duplex is separated into the functional guide strand and the subsequently degraded passenger strand (Gregory et al. 2005). The guide strand incorporates into the RNA-induced silencing complex (RISC). The selection of the mature strand from the duplex is partially based on the thermodynamic stabilities of the two terminal base pairs. The miRNA strand with the less stable base pair at its 5' end in the duplex is incorporated into RISC and becomes the mature miRNA, whereas the miRNA strand with the more stable base pair is generally discarded (Khvorova et al. 2003; Schwarz et al. 2003).

RISC complex

The minimal efficient RISC complex includes the mature miRNA in combination with at least one Ago protein (Ago 1-4). Four Ago proteins hAgo1-4 are expressed in humans, all contain a PAZ domain required for the binding of the 3′OH of loaded miRNA (Song et al. 2003; Lingel et al. 2003; Sasaki et al. 2003; Yan et al. 2003; Ma et al. 2004), and a MID domain that has an important role in anchoring the 5′ phosphate end of the miRNA (Yuan et al. 2005). Amongst the Ago proteins, Ago2 exhibits endonuclease “slicer” activity that is capable of cleaving target mRNA strands that are perfectly complementary to the mature miRNA (Liu et al. 2004; Meister et al. 2004; Song et al. 2004). Once the mature miRNAs have become associated with the RISC complex, these miRNAs are able to bind to their target sites

through base complementarity on the 3′UTR of mRNA transcripts. Most miRNAs have their targets pair at position 2–7 or 2–8 nt of the 5′ end of the mature miRNA (called the seed site). It is possible that interactions between the 3-end of an miRNA and an mRNA could support a seed match (supplementary pairing) or compensate for mismatch in the seed region (compensatory pairing) (Doench and Sharp 2004; Kiriakidou et al. 2004; Kloosterman et al. 2004; Grimson et al. 2007). Furthermore, few miRNAs naturally have extensive interaction with their target mRNAs, examples include miR-196, which leads to repression of mouse HOXB8 through perfect complementarity with its 3′UTR sequence in myeloid differentiation of HL 60 cells (Kawasaki and Taira 2004; Yekta et al. 2004).

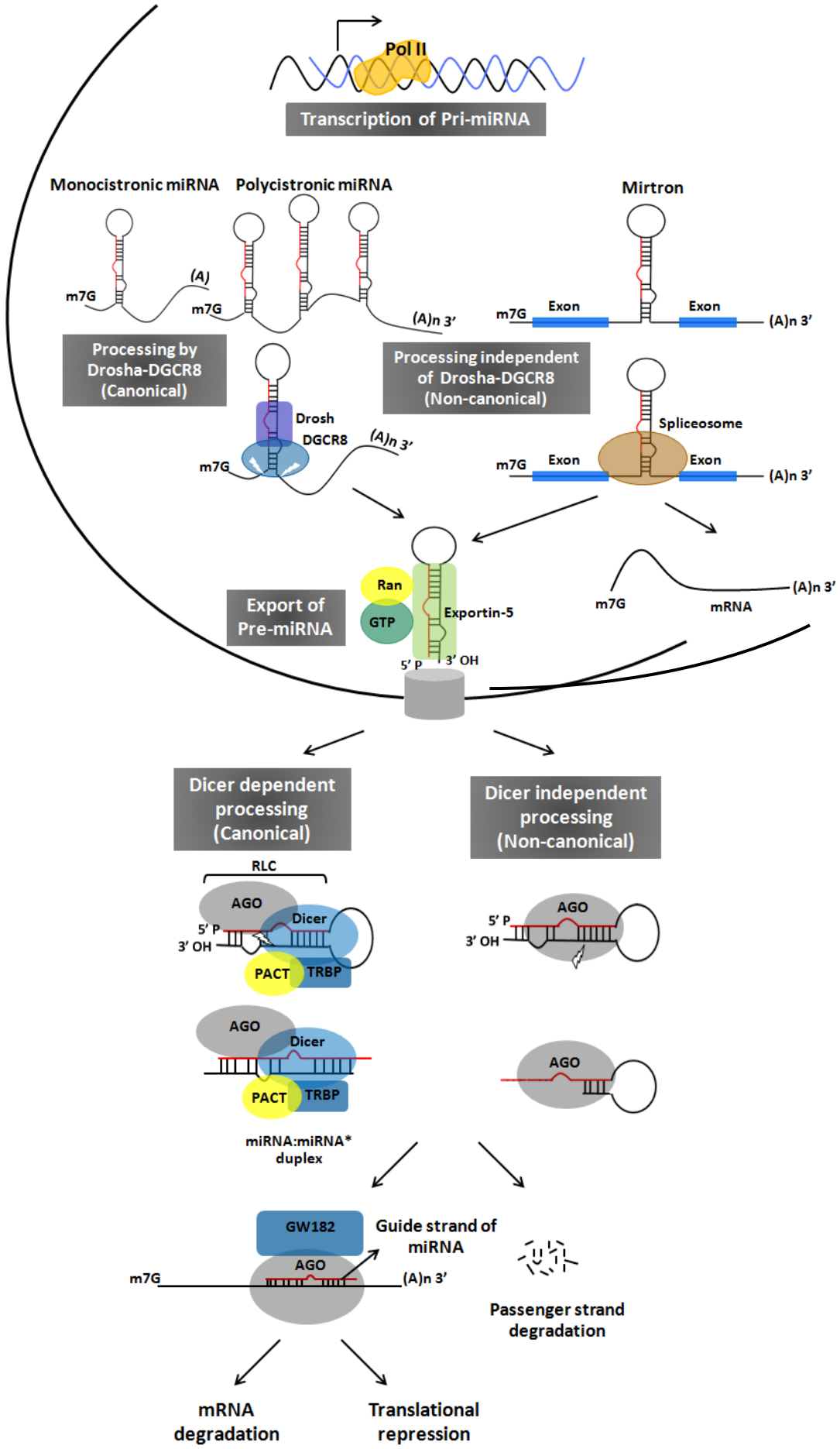
Pol II
Transcription of Pri-miRNA
Monocistronic miRNA
Polycistronic miRNA
Mirtron
m7G
(A)
(A)n 3'
Exon
Processing by Drosha-DGCR8 (Canonical)
Processing independent of Drosha-DGCR8 (Non-canonical)
Drosh
DGCR8
Spliceosome
Export of Pre-miRNA
Ran
GTP
Exportin-5
5' P
3' OH
mRNA
Dicer dependent processing (Canonical)
Dicer independent processing (Non-canonical)
RLC
AGO
Dicer
PACT
TRBP
miRNA:miRNA* duplex
GW182
Guide strand of miRNA
Passenger strand degradation
mRNA degradation
Translational repression

Figure 1.6: Schematic overview of canonical and non-canonical pathways of miRNA biogenesis and regulation in animals. The canonical miRNA biogenesis produces pri-miRNA transcripts, which are transcribed by RNA polymerase II in the nucleus. The pri-miRNA transcript is capped and polyadenylated. It can harbour either a single pre-miRNA (monocistronic) or multiple pre-miRNA (polycistronic). Splicing of short intron without the microprocessor complex, Drosha and DGCR8, produces pre-miRNA of the non-canonical mirtron pathway. Both pre-miRNAs produced by the canonical and non-canonical pathways are exported through the nuclear pore complex via Exportin-5 into cytoplasm where the stem of the precursor is cleaved by Dicer within the RISC loading complex (RLC) in the canonical pathway or by Ago in the non-canonical pathway. The miRNA/miRNA* duplex is separated and loaded into Ago protein within RLC, where one strand of the duplex is preferentially retained. This strand is associated with Ago and GW182, which mediates the gene silencing.

1.3.3 Modes of miRNA-mediated regulation of target mRNAs

Besides the cleavage of mRNA, the miRNA-associated with RISC affects the expression of target mRNA by two modes of regulation: inhibition of translation and/or destabilisation and degradation of the target transcript.

1) miRNA-mediated mRNA degradation

A) Deadenylation

The miRNAs guide the RISC complex to mRNAs bearing imperfectly complementary sequences in the 3′ UTR of target mRNAs. This requires the CCR4-CAF1-NOT1 deadenylation complex and to a lesser extent PAN2-PAN3 deadenylation complex to mediate the deadenylation of target mRNAs. GW182 protein is able to recruit both complexes, CCR4-CAF1-NOT1 complex through direct interaction with NOT1 and PAN2-PAN3 complex through direct and/or indirect interactions with PAN3 and PABP, respectively (Jakymiw et al. 2005; Yamashita et al. 2005; Behm-Ansmant et al. 2006; Eulalio et al. 2008; Fabian et al. 2009; Braun et al. 2011; Chekulaeva et al. 2011; Fabian et al. 2011). Thus, the interaction between GW182 and CCR4-CAF1-NOT1complex seems critical for the removal of the poly (A) tail, as well as for the degradation of mRNA in a 3′-to-5′ direction (Figure 1.7).

B) Decapping

The next critical step in the degradation of target mRNA is the decapping and 5′ to 3′ exonuclease activities. The 5′ terminal cap (m^7GpppG) of target mRNA is removed by the DCP1:DCP2 decapping complex catalyses and is degraded by the XRN1 5′- 3′ exonuclease (Sheth and Parker 2003; Cougot et al. 2004; Rehwinkel et al. 2005; Behm-Ansmant et al. 2006) (Figure 1.7).

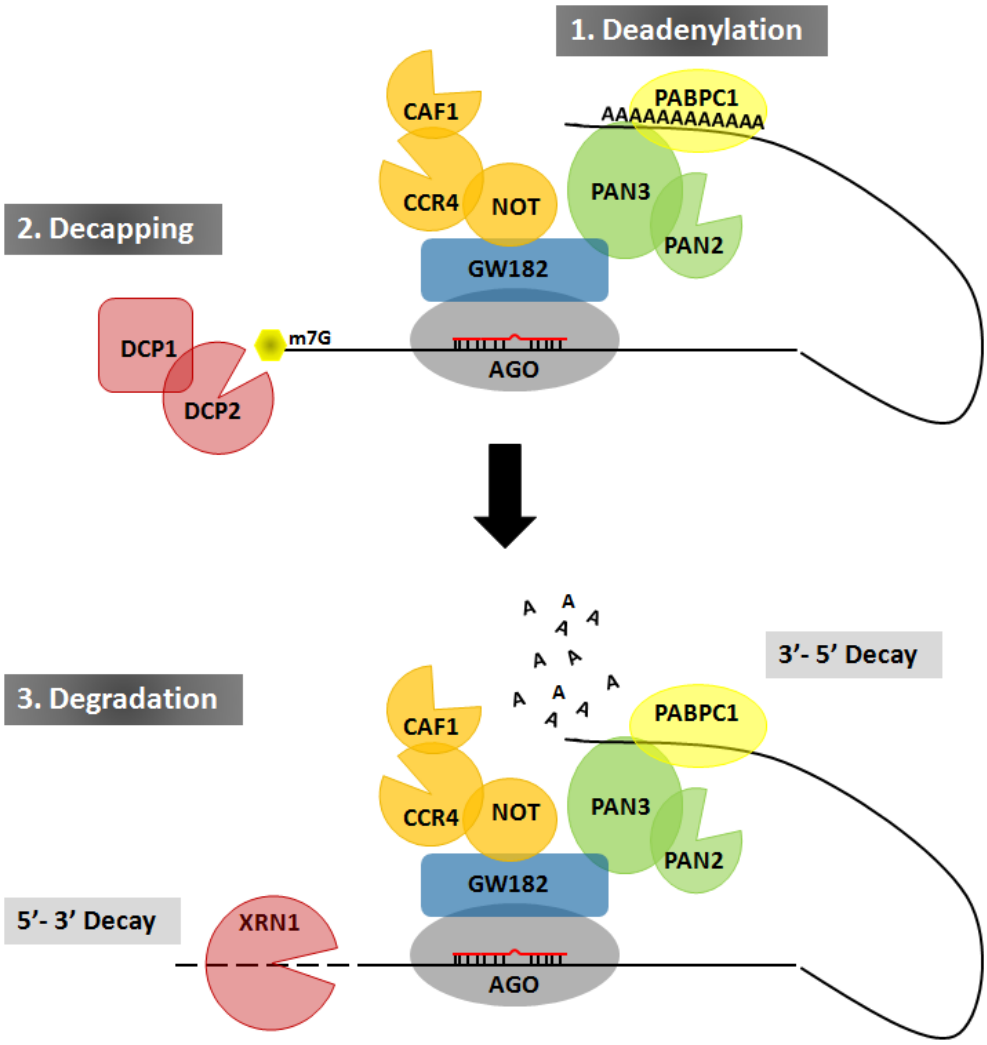

Figure 1.7: A schematic model of miRNA-mediated mRNA degradation. (1) GW182 binds Argonaute (AGO) to form the RISC. GW182 interacts with two cytoplasmic deadenylase complexes, CCR4-CAF1-NOT1 and PAN2-PAN3. These interactions lead to the deadenylation of the poly(A) tail, which is a prerequisite to 3′-5′ degradation (2) Following deadenylation, The removal of the mRNA 5′ cap structure by the decapping enzyme DCP1:DCP2 causes a rapid 5′-3′ mRNA degradation by XRN1 exonuclease.

C) miRNA-mediated translational repression

The first known miRNA in *C. elegans*, lin-4, was shown to impair the translational level of its target gene lin-14 without a corresponding reduction in its transcript level (Lee et al. 1993; Wightman et al. 1993). Following this the initial studies of miRNAs focused on the inhibition of translation, as the primary mechanism by which miRNAs regulates their target genes. The translation process is initiated by the binding of the translation initiation factor eIF4E to the cap structure of mRNAs. eIF4E and other eukaryotic initiation factors (eIFs) are involved in the recruitment of ribosome to the 5′ end of mRNA and thus initiate the translation (Reviewed in Sonenberg and Hinnebusch 2009). RISC has been shown to repress the cap-dependent translation at the initiation step by interfering with the recruitment of ribosome to the target mRNAs (Pillai et al. 2005; Chendrimada et al. 2007; Mathonnet et al. 2007; Wang et al. 2008; Ding and Grosshans 2009). RISC also could repress the translation at the post-initiation level by slowing down or inhibiting ribosome elongation (Petersen et al. 2006; Gu et al. 2009). The details of the molecular mechanisms of the translation repression, however, are still unclear.

Results from recent reports suggest that translational repression, deadenylation and decay, molecular mechanisms employed by miRNAs to mediate gene expression, are all linked processes. miRNAs were first shown to repress the translation of the target mRNA and this was followed by induction of mRNA deadenylation and finally its degradation (Bazzini et al. 2012; Béthune et al. 2012; Djuranovic et al. 2012).

D) miRNA-mediated the translational activation

A small number of miRNAs, miR-122, miR-10a, and miR-369-3 have been reported to activate rather than repress mRNA translation under certain conditions. For instance, in G1/G0 arrested cells, miR369-3p was shown to target the 3′UTR of TNFα mRNA and mediate its translational upregulation but not in proliferating cells (Vasudevan et al. 2007; Vasudevan and Steitz 2007). In response to stress or amino acid starvation, miR-10a interacts with the 5′UTR of several ribosomal protein mRNAs downstream of their 5′-TOP motif (terminal oligopyrimidine tract), showing an increase in their translation (Ørom et al. 2008). Furthermore, miR-122, a liver-

enriched miRNA was found to bind to two sites within the 5′UTR of HCV RNA in hepatic cells and to stimulate HCV RNA translation (Jopling et al. 2005; Henke et al. 2008).

E) miRNAs target the 5′UTR and coding sequence (CDS) of mRNA

Besides the reports from Jopling et al. (2005) and Ørom et al. (2008), relatively few studies have shown possible miRNA interaction sites in the 5′-UTR of target mRNAs (Lytle et al. 2007). A small number of studies have revealed functional miRNA sites located within the coding sequence of mRNAs, which mediated the translational repression. For example, the miR-148 target site in Dnmt3b1 CDS (Duursma et al. 2008), the miR-134 site in Sox2 CDS, the miR-470 site in Oct4 CDS, and two sites for miR-296 and a site for miR-470 in Nanog CDS (Tay et al. 2008). Out of these identified sites, only two have canonical miRNA seed matches (Duursma et al. 2008; Tay et al. 2008). However, the impact of miRNA regulation on transcripts containing sites within their CDS appears to be smaller than those mRNAs with sites in 3′UTRs (Fang and Rajewsky 2011). To date, no studies have addressed whether the mechanism of miRNA regulation is the same for a transcript with a functional site within the CDS as those within the 3′ UTRs.

1.3.4 Studying the biological function of miRNA

Understanding the biological functions of an miRNA relies to a large extent on the identification of their target genes. This has been addressed by the application of a combination of computational and experimental approaches.

1) In silico miRNA target prediction

A number of bioinformatic algorithms were developed to predict miRNA sites: miRanda (John et al. 2004), TargetScan (Ruby et al. 2007), Pictar (Lall et al. 2006), and PITA (Kertesz et al. 2007). These algorithms are based on well known miRNA-mRNA interaction rules. The first of these rules is the pattern of base pairing between the miRNA and its target mRNA including 1) At least 6 nucleotides of consecutive match between the seed site of a miRNA and the 3′UTR of target mRNA (2-8 nt) with a preference for an 'A' at the first position in the target site; 2) The pairing between the 3′ end of an miRNA and its target mRNA ranging from no interaction to extensive compensatory interactions; and 3) The composition of AU 30 nt up and downstream of the target site is associated with a more favourable site (Lee et al. 1993; Wightman et al. 1993; Brennecke et al. 2003; Grimson et al. 2007; Nielsen et al. 2007). The miRNA target sites in the 3′UTR are often conserved among vertebrates (Lewis et al. 2005; Friedman et al. 2009). However, some software programmes either do not include conservation as a criterion for target predication or they permit the examination of both conserved and non-conserved sites. Nonetheless, there is a concern that a significant proportion of false targets are predicted by these algorithms as the actual factors involved in making the target site accessible for miRNA binding are not fully understood (Lewis et al. 2005; Didiano and Hobert 2006). This means that relying on bioinformatic identification of miRNA targets is still problematic and requires validation through complimentary biochemical approaches.

2) Biochemical target identification

Given that miRNAs cause degradation of their mRNA targets, the inverse correlations between the expression levels of miRNAs and mRNAs can be used to further support the prediction of miRNA-target mRNA interactions (Lim et al. 2005;

Huang et al. 2007). The transcriptome experiments are based on the introduction or inhibition of a particular miRNA in cultured cells. It is expected that introduction of the miRNA leads to decreased mRNA and/or protein expression levels, while inhibition of an miRNA can result in increased levels. The set of regulated genes holding miRNA seed match sites in their transcripts are expected to be miRNA targets; however there are limitations to the application of transcriptome microarrays for the identification of miRNA targets. For example, miRNAs causing regulation at the translational levels with little or no change in the mRNA levels are undetectable using this approach. In order to overcome this condition, proteomics can be used to assess the impact of miRNA on protein levels through quantitative mass spectrometry using SILAC (Stable Isotope Labelling by Amino Acids in Cell Culture) (Baek et al. 2008). A key insight into the miRNA-mediated mRNA regulation obtained from the proteomic approach is that all proteins repressed by more than 30% also displayed down-regulation at the transcriptional levels. This strongly suggests that the effect of miRNA on gene expression involves repression at both transcript and protein levels. A drawback of quantitative mass spectrometry is that its application is limited to proteins whose solubility and abundance are sufficient for the approach to identify (Baek et al. 2008; Selbach et al. 2008). Both transcriptome and proteome-based approaches have identified targets that exhibit sites that match the miRNA seed(s) in their 3′UTRs and change in response to miRNA expression. A second limitation of these approaches is that a large number of genes that change in expression level in response to miRNA manipulation do not possess seed matches between the miRNA and the mRNAs of those genes. It is possible that regulation of these genes could result from secondary regulatory effect of miRNA overexpression or inhibition or interactions could occur through non-canonical-seed sites. Several recent studies have observed that certain miRNAs bind to non-canonical sites at the 5′ end of mRNA, with a preference for positions 3-8 or 9 nt or through the centred sites (from position 4 or 5 to position 14 or 15) instead of the canonical seed sequence (2-7 nt or 2-8 nt) (Wu and Belasco 2005; Didiano and Hobert 2006; Grimson et al. 2007; Selbach et al. 2008; Tay et al. 2008; Shin et al. 2010).

Several groups have therefore developed biochemical methods for direct identification of miRNA:mRNA target pairs. These methods are based on the co-immunoprecipitation of either mRNAs bound to a single biotin-tagged miRNA (Ørom et al. 2008) or mRNAs bound to the RISC complex through pulling down the Ago protein (Beitzinger et al. 2007; Easow et al. 2007; Karginov et al. 2007; Hendrickson et al. 2008; Chi et al. 2009). The purified target mRNAs can then be identified by means of microarray analysis or deep sequencing. The microarray study of immunoprecipitated mRNAs from biotin-tagged miR-10a revealed the interaction between miR-10a and the 5′UTR of ribosomal protein mRNAs (Ørom et al. 2008). The immunoprecipitation of a tagged Ago, which was over-expressed in cultured cells with a particular miRNA, also led to the detection of several potential target mRNAs. As an example of this, Hendrickson et al (2008) showed that the enrichment of the seed sequence within the 3′UTRs of purified target mRNAs was more than 70% for miR-1 or miR-124 targets containing a 6 nt seed match. An advance in the Ago immunoprecipitation technique termed crosslinking immunoprecipitation (CLIP or HITS-CLIP) utilises UV cross-linking and RNase treatment to detect only miRNA:mRNA complexes directly protected by Ago (Chi et al. 2009; Zisoulis et al. 2010). This improves the specificity in determining the sites of miRNA interactions within the target transcripts in both UTRs and CDS.

Combining in silico prediction with one of the experimental approaches above has identified numerous potential miRNA-regulated mRNAs. A common tool for functionally validating the direct target of miRNA is the use of a luminescent or fluorescent reporter construct expressing the potential target sequence (Zeng et al. 2002; Brennecke et al. 2003; Doench et al. 2003). The 3′UTR of an miRNA target gene is cloned and inserted downstream of a luciferase or fluorescent reporter gene. This construct is then transfected into the cultured cells, along with the miRNA of interest (or miRNA inhibitor). The degree of reporter gene expression is then measured 24 or 48 hours after transfection, in order to determine the effect of a particular miRNA on repressing the expression of reporter gene. The direct regulation of the reporter by a miRNA can be validated by mutating the sequence of the identified seed match. The mutation should abolish the interaction with the miRNA resulting in no repression.

1.4 miRNAs in host–virus interactions

Given the diverse and important function played by miRNAs in gene regulation, it is not surprising that viruses express miRNAs and utilise host miRNAs to modulate the expression of both their own genes and those of the host cells.

Pfeffer et al. (2004) discovered the first virus-encoded miRNA, which is expressed in the latent stage of EBV infected B cells. To date, about 143 viral miRNAs have been reported in the three subfamilies of human herpes viruses (α, β, and γ) (Reviewed in Kincaid and Sullivan 2012) and one or two miRNAs in each of the human retrovirus (Ouellet et al. 2008), polyomavirus (Seo et al. 2009) and adenovirus families (Andersson et al. 2005). These viral-encoded miRNAs were shown to contribute to the regulation of host cell functions, viral replication, to establishing/maintaining latency, immune evasion, or pathogenicity (Reviewed in Skalsky and Cullen, 2010; Cullen 2011).

1.4.1 Host-encoded miRNAs

In addition to the viral-encoded miRNAs, several studies have demonstrated modulation in the expression profile of host miRNAs during infection caused by viral genes or the host antiviral immune response. At the same time, host miRNAs have been directly or indirectly implicated in regulating viral gene expression, having either a positive or negative effect on virus replication and pathogenesis.

1) Direct regulation of viral genes by host miRNAs

Jopling et al. (2005) made the important discovery that the liver-specific miRNA, miR-122 interacts with the 5′ end of Hepatitis C virus genomic RNA (HCV). This interaction is required for virus replication as the inhibition of miR-122 led to a reduction in the viral RNA load and production of infectious virus *in vitro* (Randall et al. 2007). An miR-122 inhibitor was also reported to be successful in reducing the viral loads *in vivo* when administered to chimpanzees with chronic HCV infection (Lanford et al. 2010) and is presently undergoing phase II clinical trials (Broderick and Zamore 2011). Beyond the proviral effect of miR-122, many other cellular miRNAs have been reported to have antiviral effects against HCV. For example, interferon-mediates the upregulation of several miRNAs that

have imperfect complementarity to the HCV RNA genome including miR-196, miR-296, miR-351, miR-431, miR-448 (Pedersen et al. 2007). It was also shown that miR-199-3p targets both the HCV RNA genome and Hepatitis B virus (HBV) transcripts, thereby suppressing their replication (Murakami et al. 2009; Zhang et al. 2010). Further interactions have been reported between host miRNAs and human viruses from the *Flaviviridae, Hepadnaviridae, Orthomyxoviridae and Rhabdoviridae* families (Table 1.3). For example, several miRNAs in resting CD4+ T cells including miR-150, miR-125-5p, miR-28, miR-223, miR-382, were found to target the 3′ end of human immunodeficiency virus type-1 (HIV-1) RNA to maintain the latent infection in those cells (Huang et al. 2007).

Viral family / Human virus	Host miRNA	Function	Reference
Flaviviridae			
-HCV	miR-122	Proviral	(Jopling et al. 2005b)
-HCV	miR-196, miR-199a-3p, miR-296, miR-351, miR-431, miR-448	Antiviral	(Pedersen et al. 2007; Murakami et al. 2009).
Hepadnaviridae			
-HBV	miR-122, miR-125-5p, miR-199-3p, miR-210.	Antiviral	(Zhang et al. 2010; Potenza et al. 2011; Chen et al. 2011)
Orthomyxoviridae			
- H1N1	miR-323, miR-491, miR-654, Let-7c	Antiviral	(Song et al. 2010; Ma et al. 2012)
Retroviridae			
-HIV-1	miR-29, miR-32, miR-28, miR-125-5p, miR-150, miR-223, miR-382	Antiviral	(Huang et al. 2007; Ahluwalia et al. 2008; Nathans et al. 2009).
Rhabdoviridae			
-VSV	miR-24, miR-93	Antiviral	(Otsuka et al. 2007)

Table 1:3: Direct interactions between host-encoded miRNAs and viruses. Adapted from (Laqtom and Buck 2011). HCV: hepatitis C virus, HBV: hepatitis B virus, H1N1: Influenza, HIV-1: human immunodeficiency virus-1, VSV: vesicular stomatitis virus.

2) miRNAs that influences viral infection through regulation of host genes

miRNAs regulate many cellular processes (e.g. proliferation, survival, metabolism, immune response), therefore, their expression levels can affect the infection process. One of the earlier studies of miRNAs in this context demonstrated that the two cellular miRNAs, miR-17-5p and miR-20, were inhibited following HIV infection. This inhibition resulted in a corresponding increase in the target expression of p300/CBP-associated factor (PCAF), which is a cellular histone acetylase and co-factor for the viral Tat protein (Triboulet et al. 2007). Another related example is the inhibition of miR-100, miR-101 (Wang et al. 2008), and all the mature members of miR-199a/214 cluster (Santhakumar et al. 2010) following the lytic HCMV infection. The ectopic expression of miR-100, miR-101, miR-199-3p or miR-214 results in a significant inhibition of viral growth. Wang et al (2008) suggested that miR-100 and miR-101 target the mTOR signaling through direct interactions with two components within this signaling pathway, mTOR and Raptor. Similar to lytic HCMV infection, the expression of miR-92a in CD34+ haematopoietic progenitor cells is reduced during the latent infection of HCMV. A consequence of this reduction is an increase in the expression of GATA-2 and a corresponding increase in IL-10 production, supporting the maintenance of viral genomes in CD34+ cells the during latent infection (Poole et al. 2011). As the expression of anti-viral miRNAs can be inhibited, viruses also can cause significant increase in miRNAs could have proviral properties. For example, miR-132 is upregulated following KSHV infection and has a negative impact on the expression of interferon-stimulated genes through the direct regulation of P300 transcriptional co-activator, thus enhances viral replication (Lagos et al. 2010). miR-31 is also up-regulated by the expression of KSHV protein K15 to target FAT4, which is a tumor suppressor and thereby contributes to progression of malignant Kaposi sarcoma (Wu et al. 2011). An additional list of host-encoded miRNAs that manifests anti- or proviral properties by regulation of host genes is presented in Table 1.4. This thesis focuses on the regulation and function of an antiviral host miRNA, miR-199-3p, in HCMV and MCMV infections.

Viral family / Human virus	Host miRNA	Cellular target	Function	Reference
Herpesviridae				
-HCMV	miR-100, miR-101	mTOR, Raptor	Antiviral	(Wang et al. 2008)
	miR-199-3p	multiple genes (predicted)	Antiviral	(Santhakumar et al. 2010)
	miR-92	GATA-2	Proviral	(Poole et al. 2011)
-KSHV	miR-221, miR-222,	ETS-1, EST-2	Proviral	(Wu et al. 2011)
	miR-32	FAT4	Proviral	(Wu et al. 2011)
	miR-132	P300	Proviral	(Lagos et al. 2010)
-HSV-1	miR-199-3p	multiple genes (predicted)	Antiviral	(Santhakumar et al. 2010)
Hepadnaviridae				
-HBV	miR-155	SOCS1	Antiviral	(Su et al. 2011)
Picornaviridae				
-EV71	miR-141	EIF4E	Proviral	(Ho et al. 2011)
-RV1B	miR-23	VLDLR	Antiviral	(Ouda et al. 2011)
Retroviridae				
-HIV-1	miR-17-5p, miR-20	PCAF	Antiviral	(Triboulet et al. 2007)
Rhabdoviridae				
-VSV	miR-155	SOCS1	Antiviral	(Wang et al. 2010)
Papoviridae				
- HPV	miR-218	LAMB3	Proviral	(Martinez et al. 2008)
	miR-203	P63	Proviral	(Greco et al. 2011)
	miR-146	phosphorylation of p38 and ERK1/2	Proviral	(Greco et al. 2011)
Togaviridae				
-SFV	miR-199-3p	Multiple genes (predicted)	Antiviral	(Santhakumar et al. 2010)
Paramyxoviridae				
-RSV	miR-221	NGF, its receptors, TrKA and/or p75NTR	Antiviral	(Othumpangat et al. 2012)

Table 1:4: Indirect interactions between host miRNAs and host targets, which are involved in the infection process. Adapted from (Laqtom and Buck 2011). HCMV: human Cytomegalovirus, KSHV: Kaposi's Sarcoma-associated Herpes virus, HSV-1: Herpes Simplex virus-1, HBV: Hepatitis B virus, EV71: Enterovirus 71, RV1B: Rhinovirus 1B, HIV-1: human Immunodeficiency virus-1, VSV: Vesicular Stomatitis virus, HPV: Human Papillomavirus, SFV: Semliki Forest virus, RSV: Respiratory Syncytial virus.

1.5 miR-199-3p is a member of miR-199a/214 cluster

The miR-199a/214 cluster is encoded within the opposite strand of an intronic region of the dynamin 3 (DNM3) gene (GeneID: 100628315 in NCBI database, http://www.ncbi.nlm.nih.gov/pubmed/) (Figure 1.8). It comprises two miRNA precursors, miR-199a and miR-214, both of which are evolutionarily conserved among several species. The products of this cluster are number miR-199-5p, miR-199-3p, miR-214-5p, and miR-214-3p (Accession number of miR-199a: MI0000281 and miR-214: MI0000290 in miRBase, http://mirbase.org/) (Figure 1.8). Notably, the seed sequences (nucleotides 2–8) of miR-199-3p and miR-214-3p share significant similarity (Figure 1.9) and hence, presumably similar or overlapping functions. However, the seed sequence of miR-199-5p is distinct from these two miRNAs.

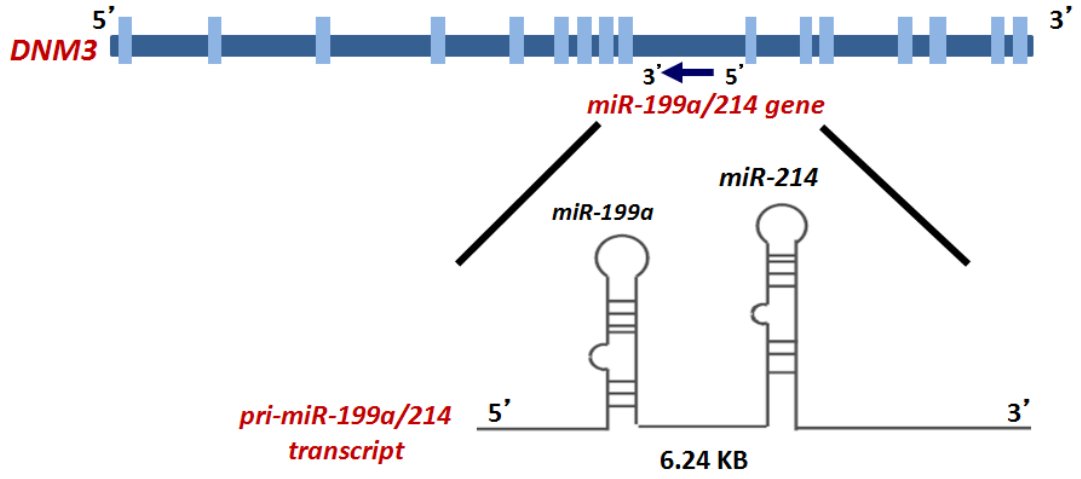

Figure 1.8: A schematic diagram of human dynamin3 (DNMIII) gene showing that miR-199a/214 gene lies within the opposite strand of its intron. The pri-miR-199a/214 transcript encodes miR-199a and miR-214 precursors.

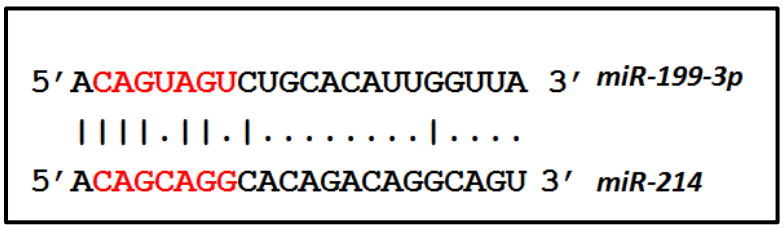

Figure 1.9: Alignment of miR-199-3p with the mature sequence of miR-214-3p. Red indicates seed sequence.

1.5.1 *Cancer*

miRNA profiling studies have shown that in various cancers, the expression pattern of one or more member of the miRNA cluster, miR-199a/214, are deregulated (Table 1.5). Although, their functional significance has not yet been elucidated in all cancers, the concurrent alteration in expression of miR-199-3p, miR-199-5p, and miR-214 indicates a possible cooperative and/or supportive role in the disease. At the same time, decrease or increase of an individual member of this cluster could point towards their specific or individual functions.

MET and mTOR signaling pathways in hepatocellular carcinoma (HCC)

It has been reported that compared to normal liver there is a simultaneous decrease of miR-199-3p, miR-199-5p, and miR-214 in hepatocellular carcinoma. The decrease in expression of miR-199-3p contributes to the increased expression of its targets, MET proto-oncogene (MET) (Fornari et al. 2010), p21-activated kinase 4 (PAK4) (Hou et al. 2011), and the cell surface glycoprotein CD44 (Henry et al. 2010). It is important to note these target genes, MET, PAK4, and CD44, are part of the MET signaling pathway, which act together to amplify the signaling cascade thereby regulating downstream effectors, such as mitogen-activated protein kinase-1 (MAPK1, Known as ERK2). Thus, decreased miR-199-3p expression can effectively enhance HCC cell proliferation and invasion. In addition to targeting MET signaling, miR-199-3p targets mTOR, the central kinase in the mammalian target of rapamycin (mTOR) signaling pathway. Therefore, attenuated level of miR-199-3p elevates mTOR signaling and enhances the survival and resistance to doxorubin-induced cell death of HCC cells (Fornari et al. 2010) (Figure 1.10).

In agreement with the tumour suppressor function of miR-199-3p, Fornari et al. (2010) observed that decreased miR-199-5p expression promoted survival of HCC by increasing expression of hypoxia inducible factor 1, alpha subunit (HIF-1α) (Fornari et al. 2010). HIF-1α is also a downstream gene of mTOR, which is a target of miR-199-3p (Land and Tee 2007). Besides HIF-1α, the discoidin domain receptor-1 (DDR1) tyrosine kinase, implicated in cell invasion-related signaling pathway, is also a target of miR-199-5p (Shen et al. 2010) (Figure 1.10).

The suppression of miR-214 expression is associated with increased β-catenin signaling, enhanced cell growth and invasion of HCC cells. β-catenin is a direct target of miR-214, its suppression therefore results in modulation of several genes downstream of β-catenin such as, c-Myc, cyclinD1, TCF-1, and LEF-1 (Wang et al. 2012; Xia et al. 2012) (Figure 1.10). These examples demonstrate that miR-199-3p, miR-199-5p, and miR-214 are important regulators of multiple signaling pathways and consequently, their functional outcomes in cancer cell proliferation, survival, and invasion. These miRNAs are able to effectively cooperate though targeting genes of the same pathway or genes of different pathways with related functions in the pathological states. This could account for their co-existence in one cluster and their simultaneous deregulation in disease states.

1.5.2 Prostaglandin signaling.

The clustered miRNAs, miR-199a-3p and miR-214 have been reported to be simultaneously decreased in the uterine myometrium of full-term pregnant humans and mice, as well as in a mouse model of pre-term labour (Williams et al. 2012). As expected, the expression of their direct target, PTGS2 (COX-2), is elevated and its associated functions such as prostaglandin production and labour are induced (Williams et al. 2012). Consistent with this, increased expression of miR-199-3p has been shown to be associated with a decrease in the level of its target PTGS2 (COX-2) in early pregnancy, during implantation (Chakrabarty et al. 2007a). The regulation of PTGS2 (COX-2) and subsequent prostaglandin production mediated by miR-199-3p has also been reported in chondrocytes in osteoarthritis (Akhtar and Haqqi 2012).

Most studies on miRNAs examine one or a few cellular targets of a miRNA. However, miRNAs can simultaneously repress the expression of hundreds of proteins (Baek et al. 2008; Selbach et al. 2008) and the regulatory impact on most of these target genes is subtle ‘fine-tuning’ (Reviewed in Bartel and Chen 2004). Therefore, elucidating how a single miRNA induces observable functional consequences with such subtle regulation is complicated. It seems likely that miRNA can exert its functions by targeting several genes of host signaling pathway and/or genes of multiple functionally-related pathways. Consequently, the subtle regulation

of several target genes could produce a cumulative effect and contribute to observable functional changes (He et al. 2010). Most studies have also focused on one or two deregulated miRNAs but not the global picture of how the miRNAs in a cell act in concert with each other and with other regulatory proteins (e.g. transcription factors) to regulate the expression of their target genes and ultimately, changes in cellular functions.

Cancer	miR-199-3p	miR-199-5p	miR-214	Reference
Ovarian cancer	U/D	U/D	U/D	(Zhang et al. 2006; Iorio et al. 2007; Dahiya et al. 2008; Yang et al. 2008; Yin et al. 2010; He et al. 2012)
Breast cancer	U	-	D	(Derfoul et al. 2011; Shatseva et al. 2011)
Hepatocellular carcinoma	D	D	D	(Murakami et al. 2006; Duan et al. 2012)
Osteosarcoma	D	-	-	(Duan et al. 2011)
Gastric cancer	U	U	-	(Song et al. 2010; Brenner et al. 2011)
Testicular cancer	D	D	-	(Cheung et al. 2011)
Colorectal cancer	U	D	-	(Wan et al. 2013; Su et al. 2012)
Biliary tract cancer	U	-	-	(Shigehara et al. 2011)
Pancreatic cancer	-	-	U	(Zhang et al. 2010)
bladder carcinoma	D	D	-	(Ichimi et al. 2009; Su et al. 2012)
Cervical cancer	-	-	D	(Peng et al. 2012)

Table 1:5: The cancers in which miRNAs of miR-199a/214 cluster are dysregulated. (U:up, D:down, U/D: up in a study and down in another).

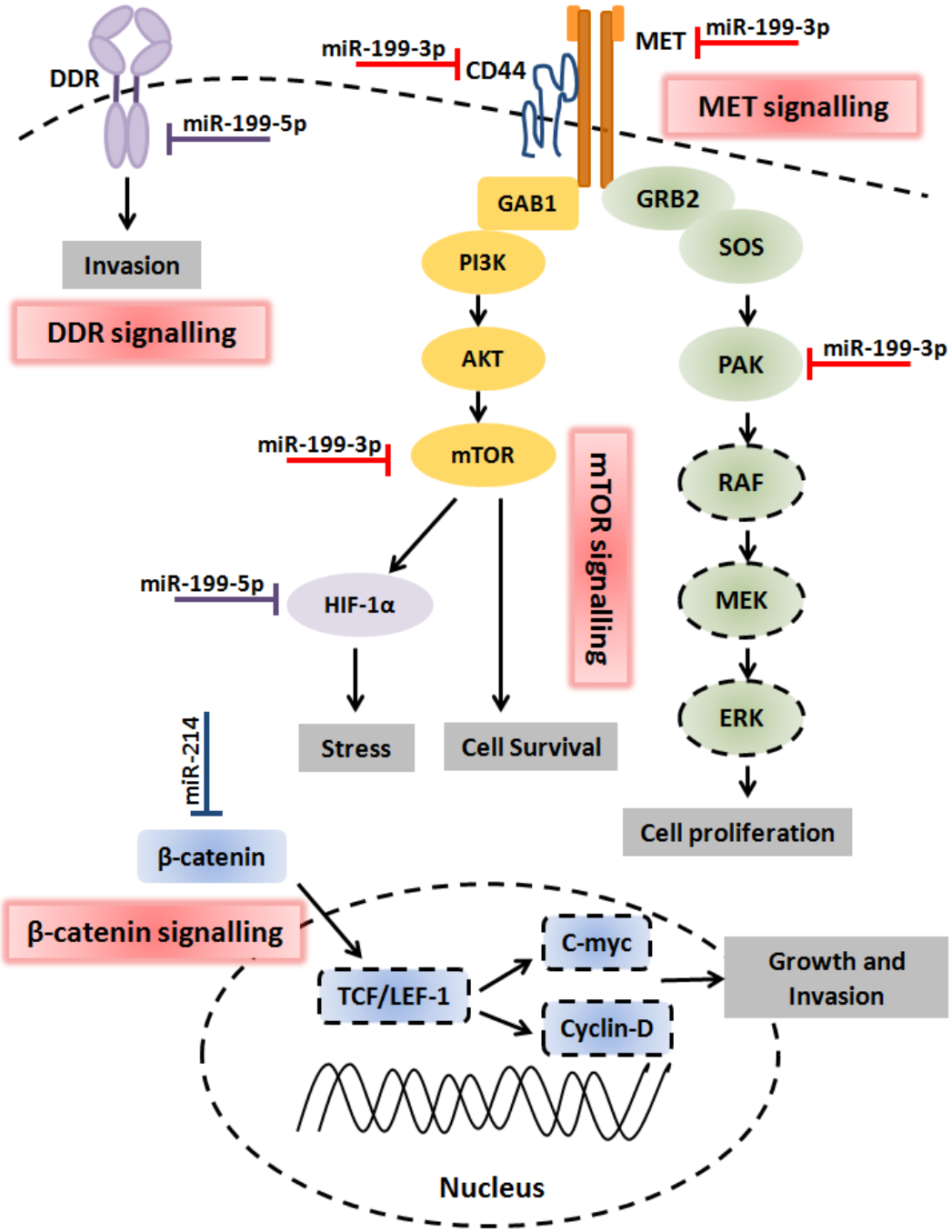

Figure 1.10: A summary diagram of the signaling pathways in hepatocellular carcinoma (HCC) modulated by miR-199a/214 cluster to regulate tumorigenicity. Pathways regulated by miR-199a/214 that are known to be important in liver cancer. Direct targets genes of miR-199-3p are shown with red arrow, miR-199-5p with purple arrow, and miR-214 with blue arrow. Circles with dashed lines represent indirect targets, which were shown to be regulated by these miRNAs through direct targeting.

1.6 Central hypothesis and objectives of the thesis

HCMV is an important virus for number reasons. Perhaps most importantly, HCMV infection is ubiquitous and affects 50% to 80% of the world's populations (Odland et al. 2001; Alanen et al. 2005; Hannachi et al. 2011). In addition, the perinatal infection of HCMV causes congenital diseases that can lead to serious complications, such as mental retardation. The virus also establishes a life-long latent infection, with a high risk of malicious reactivation whenever the immune status of an infected individual is compromised. Finally, the available anti-HCMV drugs (Ganciclovir, Cidofovir and Foscarnet) do not cure the infection and can have serious side effects that include the emergence of drug resistant virus strains (Reviewed in Lurain and Chou 2010). Therefore, a better understanding of host-virus interactions is important to be able to design new, safe and effective ways to treat HCMV infection. The recent discovery of miRNAs playing a critical role in viral replication and pathogenesis reveals a new level of host-virus interactions and that could lead to novel preventive and therapeutic strategies.

HCMV like the other viruses, modulates the profile of host-encoded miRNAs (Wang et al. 2008; Santhakumar et al. 2010) to suit its replication and other aspects of its life cycle. The host miRNA cluster, miR-199a/214 including three mature miRNAs, miR-199-3p, miR-199-5p and miR-214, are all down-regulated by both MCMV and HCMV in fibroblast cells. At least two mature members of this cluster have antiviral properties against MCMV and HCMV growth when over-expressed *in vitro* (Santhakumar et al. 2010). Interestingly, the antiviral properties of miR-199-3p extend to other herpes viruses including HSV-1 and mouse γ-herpes virus (MHV-68) as well as other unrelated viruses, such as Semliki Forest virus (SFV) (Santhakumar et al. 2010), HVB (Zhang et al. 2010) and HVC (Murakami et al. 2009).

Therefore, the study presented in this thesis was designed to test the central hypothesis that MCMV and HCMV actively repress the expression of miR-199a/214 transcript in order to evade the negative consequences of at least miR-199-3p on virus infection.

In order to test this hypothesis, 5 objectives were defined:

- To determine at what stage of biogenesis the expression of miR-199a/214 is regulated by CMV infection.
- To discover whether the observed down-regulation in miR-199a/214 expression requires viral gene expression.
- To investigate what cellular elements are involved in the down-regulation of miR-199a/214 expression.
- To ascertain which host signaling pathways are regulated by miR-199-3p which may relate to its antiviral properties.
- To identify the direct targets of miR-199-3p and to investigate their role in the infection.

2 Materials and Methods

2.1 Tissue culture

2.1.1 Cell lines

NIH-3T3 cells and P53-null MEFs cell lines were purchased from American Type Culture Collection (Manassas, VA.). NIH-3T3 cells (ATCC CRL1658) are spontaneously immortalized fibroblast cells. They are established from a NIH Swiss mouse embryo. P53-null MEFs cells (ATCC CRL2645) are mouse embryonic fibroblasts obtained from mice with a null mutation in only the p53 gene. NIH-3T3-BAM25 cells were derived by stable transfection of a plasmid bearing the MCMV IE1 and IE3 genes by Angulo et al. (2000), into NIH-3T3 cells. MRC-5 and HEF fibroblasts were also obtained from American Type Culture Collection (Manassas, VA.). MRC-5 cells (ATCC CCL-171) were derived from the normal lung tissue of a human foetus. HEF cells (ATCC SCRC-1041) are foreskin-derived human embryonic fibroblasts. All cell lines were maintained at 37°C in incubators that were supplied with 5% CO_2 and a relative humidity of 95%.

2.1.2 Cell media and tissue culture consumables

NIH-3T3and NIH-3T3-BAM25 were grown in Dulbecco's Modification of Eagle's Medium (DMEM) (Lonza, Belgium), which was supplemented with 10% heat-inactivated calf serum (HI-CS) (Sigma), 0.293 mg/ml of L-glutamine (Lonza, Belgium) and 50 U of Penicillin/Streptomycin (Lonza, Belgium) per ml. The sterilised media was stored at 4°C for up to six months. The same media was used for P53-null MEFs cells, but HI-CS was replaced with heat-inactivated fetal bovine serum (HI-FBS) (GIBCO, Invitrogen, UK). MRC-5 and HEF cells were cultured in Eagle's minimal essential medium (EMEM) (Lonza, Belgium), supplemented with 10% HI-FCS, 0.293 mg/ml of L-glutamine (Lonza, Belgium), 50 U of Penicillin/Streptomycin (Lonza, Belgium) per ml and 0.1 mM non-essential amino acids (Lonza). All tissue culture flasks were obtained from Corning, USA.

2.1.3 Passaging cell lines

When the monolayer of cells reached 70-80% confluence, culture media was discarded and the adherent cells washed once with phosphate buffered saline (PBS).

The cells were then incubated with trypsin/EDTA (Lonza, Belgium) for 5-10 min at room temperature until they detached. The cells were then collected into 3-5 ml of appropriate serum supplemented medium (to inhibit further trypsin digestion) and centrifuged at 200 g-force at room temperature for 5 min. The supernatant was discarded and the pellet resuspended in fresh medium using an appropriate volume for a split ratio between 1:2 and 1:4, according to the cell line and experimental requirements. This process was repeated up to a maximum of 10 passages. Wherever possible, low passage cells were used for the experiments.

2.1.4 Cell counts using a hemocytometer and trypan blue dye exclusion

To determine the cell count, resuspended cells were diluted (1:2 or 1:10) with trypan blue stain, 0.4% (Lonza, USA). 10µl of this dilution was then introduced into a haemocytometer (HAUSSER Scientific, USA) under a cover slip, after which the viable cells were counted in the central 16 marked squares. Counts were repeated 6 to 10 times from different replicates of the sample and an average count was then calculated. Cells per ml were calculated by means of the following equation:

*Number of viable cells per ml = Average number of counted cells * the relative area of the haemocytometer square (10^4 cm^3) * dilution factor.*

Cells were then diluted to appropriate seeding density. The seeding densities for NIH-3T3, NIH-3T3-Bam25, MRC-5, and HEF cells in different sized tissue culture plates (Costar, USA) were as follows;

- 96-well plates: $1.5x10^4$ cells in 100µl medium per well.
- 48-well plates: $4x1^4$ cells in 500µl medium per well.
- 24-well plates: $1x10^5$ cells in 1ml medium per well.
- 6-well plates: $3x10^5$ cells in 2ml medium per well.

2.1.5 Cryopreservation of cells

For the purposes of long-term preservation, cells were re-suspended after trypsinisation in a freezing medium containing 40% DMEM or EMEM, 50% CF or

FCS as appropriate, and 10% dimethyl sulfoxide (DMSO) (Sigma, UK). 1ml aliquots were placed in 2ml cryovials (SARSTEDT, Germany) containing 0.5-1x10^6 resuspended cells each. The cryovials were stored in a Nalgene Cryo 1ºC freezing container (USA) at –80°C overnight for 24 hours prior to long-term storage in a liquid nitrogen container (-170°C).

2.1.6 Thawing cells from liquid nitrogen

To effectively recover frozen cell lines from liquid nitrogen, cells should be thawed and the DMSO removed as rapidly as possible. For this reason, each vial was thawed in a 37°C water bath and the DMSO contained in the freezing medium then diluted with the addition of 5 ml of fresh growth media. Cells were then centrifuged at 200 g-force at room temperature for 5 min. The supernatant was removed and the cell pellet resuspended in 10 ml of appropriate normal pre-warmed medium and placed in a 75cm^2 tissue culture flask for propagation as previously described (2.1.2 and 2.1.3).

2.1.7 Assessing cell culture contamination

Tissue culture requires strict control measures to prevent contamination. The steps taken to avoid cell contamination were as follows:

- Penicillin and Streptomycin were used as an antibiotic mix in the growth medium to prevent bacterial infection.
- Incubators were disinfected weekly using antimicrobial agents (Aquasan from Guest Medical) and tissue culture hoods were also cleaned thoroughly with a disinfectant (Tecknon, Thermo Fisher) prior to and upon each use.
- Cells were tested for the presence of mycoplasma contamination every three months using MycoSensor^{TM} PCR assay kit (Agilent Technologies).

2.2 General methods for virology

2.2.1 Viruses

2.2.1.1 MCMV

The parental MCMV (Smith strain) was derived from bacterial artificial chromosome (BAC) clone pSM3fr (named C3X or MW97.01) which contained the complete MCMV genome, described in previous studies (Messerle et al. 1997; Wagner et al. 1999). It is important to note that recent DNA sequencing of the complete BAC genome of MCMV found four differences compared to the sequence published for MCMV Smith strain. Three point mutations and a frameshift in MCK-2 ORF resulted in prematurely truncated MCK-2 protein (Jordan et al. 2011). It was also noted that the virus stock of MCMV Smith strain contains mixtures of viruses with or without the frameshift mutation, suggesting that the mutation originated from the clonal selection process (Jordan et al. 2011). However, the sequence of MCMV BAC plasmid pSM3fr appears largely comparable to the sequence of the Smith strain.

2.2.1.2 MCMVdie3

The IE1 and IE3 mRNAs share the same first three exons which are spliced either with a fourth exon into the mature IE1 mRNA (Keil et al. 1987) or with a fifth exon into the IE3 mRNA (Messerle et al. 1992). The IE2 mRNA is transcribed in the opposite direction and spliced from three separate exons (Messerle et al. 1991). Angulo and colleagues (2000) describe the construction of MCMVdie3, in brief: almost the entire fifth exon in IE1/IE3 gene transcriptional unit was deleted from the MCMV genome of BAC plasmid pSM3fr (details of the genome map of the MCMV and MCMdie3 virus are shown in Figure 2.1). This means that the gene expression of this virus is restricted to IE1 and IE2, causing deficiency in viral growth (Angulo et al. 2000; Lacaze et al. 2011). Replication can be rescued by growing the virus on the NIH-3T3-Bam25 cell line, which expresses both IE1 and IE3.

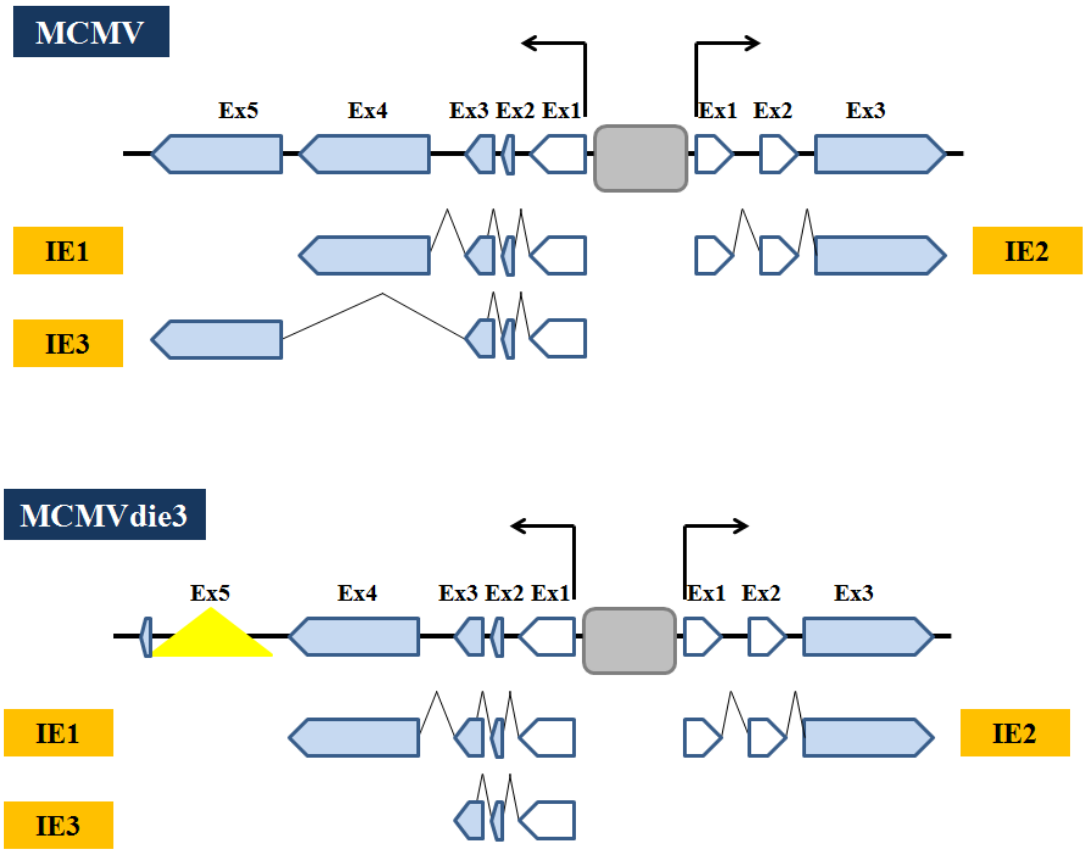

Figure 2.1: Schematic diagram of the structural organisation of the major immediate-early region (MIE) of MCMV and MCMVdie3 viruses. Coding exons are shown as blue boxes while non-coding exons are white boxes, with the arrows in these boxes indicating the direction of transcription. The gray box denotes the MCMV enhancer IE1/IE3 promoter, while the end products are shown in yellow boxes. Starting with MCMV, five exons located downstream of MCMV enhancer IE1/IE3 promoter generate two alternatively spliced major transcripts, IE1 and IE3. The IE1 transcript of MCMV is composed of exons 1 to 4, and the IE3 transcript consists of exons 1 to 3 and 5. MCMVdie3, the deletion of the fifth exon of the IE1 gene is marked by the delta (Δ).

2.2.1.3 *HCMV-eGFP*

The full-genome of the HCMV strain AD169 was cloned into BAC-pHB5 plasmid (Borst et al. 1999), which was then used to generate HCMV expressing enhanced green fluorescent protein (eGFP). AD169-derived recombinant virus additionally contain eGFP coding sequences, which was inserted as a separate ORF upstream of UL127 ORF but downstream of the UL127 promoter (Angulo et al. 2000) (The map of the HCMV and HCMV-eGFP genome are illustrated in Figure 2.2).

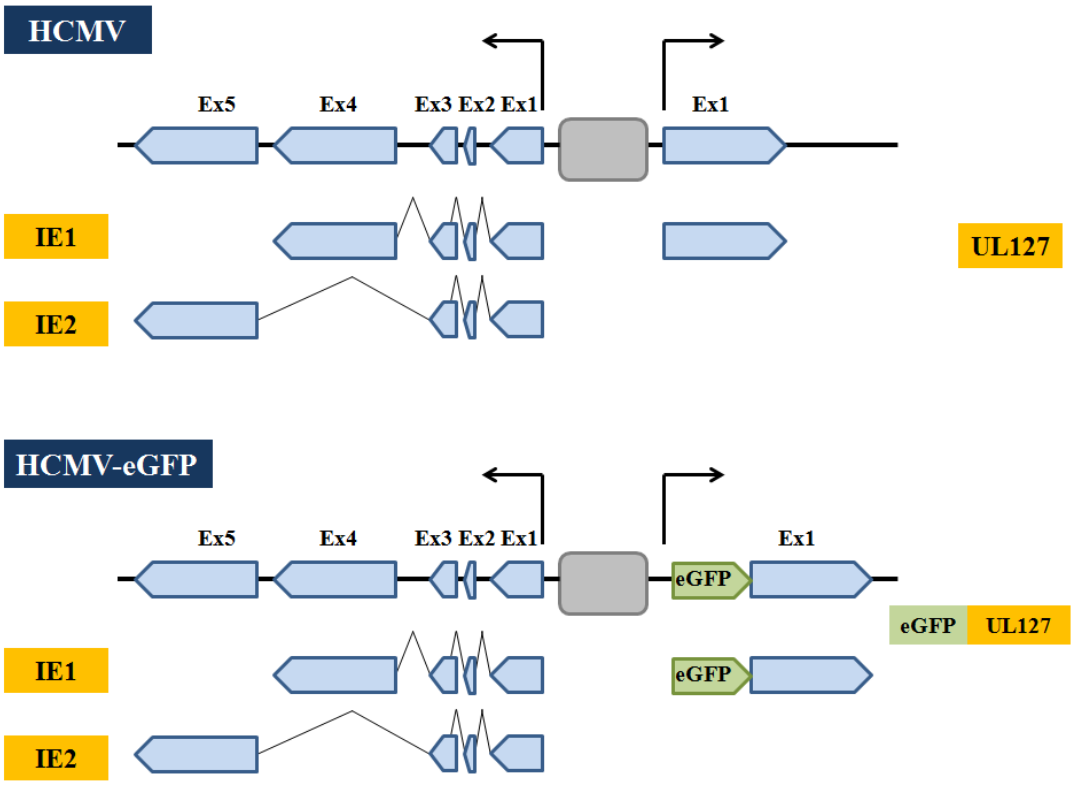

Figure 2.2: Schematic representation of the major immediate-early region of HCMV and HCMV-eGFP viruses. Coding exons are shown as blue boxes and gray box represents the enhancer elements, which are flanked by the promoters and transcription units IE1/2 and UL127. Beginning with HCMV, the region downstream from the promoter is conserved with MCMV, which gives rise to two transcripts IE1 and IE2 (known as IE3 in MCMV). Conversely, the genomic region on the other side of the regulatory elements is not conserved between MCMV and HCMV. In the recombinant HCMV-GFP virus, the coding sequence for enhanced green florescence protein (eGFP) was fused to UL127 as it is placed downstream of the UL127 promoter sequence and upstream of its coding sequence. The GFP reporter sequence is illustrated in green.

2.2.2 Viral stock propagation

In order to prepare a bulk viral stock of MCMV, confluent 150cm^2 culture flasks of NIH-3T3 cells were infected at MOI of 0.01 in 20 ml of growth medium per flask. The cells and the supernatant were collected 5-7 days after infection when cytopathic changes were observed in the infected cells. The cells and supernatant were centrifuged for 15 min at 800 g-force, collected, and the pellet from the cell debris was discarded. The cell-free supernatant was stored at -70°C in sterile in 5-10 ml aliquots. The same method was utilised to propagate MCMVdie3, grown on the complementing cell line NIH-3T3-Bam25. HCMV was grown on HEF cells using the same procedure, although in this case the infection was at MOI of 1. In order to reduce the risk of viral mutations occurring over multiple rounds of infection, a master stock was produced in a T25 flask from seed viral stock of low passage number and was stored at -70°C in aliquots of appropriate volume. These aliquots were then used to make the working viral stocks.

2.2.3 Titration of virus by plaque assay

Plaque assays are the standard method for estimating the number of infective particles in a sample. These were performed on P53-null MEF cells for MCMV, NIH-3T3-BAM25 cells for MCMVdie3, and HEFs for HCMV. The cells were seeded at a density of 4x10^4 cells in 500µl per well in 48 well plates, which were then incubated overnight in a 37°C incubator. A ten-fold serial dilution series of a virus stock was prepared in triplicate from 10^{-1} to 10^{-6}. 100µl of each dilution for each virus was added to triplicate wells. After an hour of incubation with the virus at 37°C, the cells were washed using warm growth media and then overlaid with a thick layer of a 0.25% agarose-medium mixture. This agarose-medium mixture was prepared by diluting a 2.5% agarose solution (2.5g of agarose dissolved in distilled water) 1:10 in a 3% serum supplemented medium. Agarose was used in order to prevent the spread of virus from infected cells to uninfected cells. Four to six days later, plaques were counted for each well and the viral titres were expressed as plaque forming units per ml (PFU/ml) using the following equation:

*PFU/ml = Average number of counted plaques * individual dilution factor * 10 (for case of 48 well plates)*

Based on the above calculation, the titer of a given virus stock is determined and can be used to determine the multiplicity of infection (MOI) required for experiments. The MOI corresponds to the number of PFUs delivered into each cell. For the purpose of infecting cells, the necessary quantity of virus was combined with warmed growth media in order to produce an infectious inoculum. The total volume of infecting inoculum made for different cell culture plates is presented below:

- 96-well plates - 50µl of viral inoculum
- 48-well plates - 100µl of viral inoculum
- 24-well plates - 200µl of viral inoculum.
- 6-well plates - 1ml of viral inoculum

In all experiments conducted in this study, cells were incubated with the viral inoculum for an absorption period of one hour at 37°C in the incubator. The cells were then washed twice with medium and replaced with normal growth medium. For MCMV, the hours post infection were counted starting at the end of the viral adsorption period; while in HCMV, it corresponds to the start of incubation with the virus. For mock infections the same volume of media was used but without virus. The mock infected wells were washed and the medium replenished as for the infected wells.

2.2.4 Treatment of cells with kinase inhibitors

2.2.4.1 Ly294002

Ly294002 (Cell Signalling Technology) is a potent cell-permeable inhibitor of inhibitor of phosphoinositide 3-kinases (PI3Ks). It abolishes PI3K activity without affecting other lipid or protein kinases such as PI4 kinase, PKC, PKA, MAP kinase, EGFR, and c-Src (Mahoss et al. 1994). Ly294002 was resuspended in DMSO and used at a concentration of 10 µM and 25 µM.

2.2.4.2 TGX-221

TGX-221 (Cayman Chemical) is a selective ATP-competitive inhibitor of PIK3CB (aliases PI3Kβ, p110β) at concentration of (5 ~ 50 nM). However, TGX-221 can also

inhibit other isoforms of PI3K (i.e. p110α and p110δ) at higher concentrations. TGX-221 was resuspended in DMSO and used at 50 nM.

2.2.4.3 Treatment of Cells

For investigation of the effect of kinase inhibitors on viral growth, cells were pre-treated with Ly294002 or TGX-221 inhibitors 2 hours prior to infection. Equal amount of DMSO was added to the control. The cells were washed after 2 hours of HCMV infection and the culture media replaced with normal growth media. Another aliquot of kinase inhibitors or DMSO control was added to the cultured cells.

2.3 Transfection into cells

2.3.1 DharmaFECT1 transfection

DharmaFECT1 transfection reagent (Dharmacon, Thermo Scientific) is a lipid based reagent that is an efficient means of delivering synthetic RNA (siRNA, miRNA mimic or inhibitor) into cultured cells. The lipid reagent encapsulates the small RNA molecules with cationic lipids that mediate the transfection process into the cells. The method used for the purposes of transfecting both mouse NIH-3T3 or human MRC-5 cells was a reverse transfection in which cells were simultaneously seeded and transfected. NIH-3T3 or MRC-5 cells were grown to a confluence of 70-80% or 85-90% in tissue flasks. The cells were trypsinized, counted, and diluted in antibiotic-free medium to an appropriate volume in order to ensure the desired seeding density per well, as mentioned above in 2.1.4. Cells were then incubated on ice until the transfection mixture had been prepared.

The siRNAs (SMARTpools-ON-TARGETplus modification), miRNA mimics (miRIDIAN microRNA Mimics), miRNA inhibitors (Hairpin Inhibitors), and their negative controls were purchased from Thermo Scientific Dharamcon, USA. All of these were supplied in 5 nmol powder form and were dissolved in 1x siRNA buffer (Thermo Fisher) in order to produce a concentrated stock of 20 μM. This stock was used to prepare working stocks at 500 nM. For transfection of cells, an appropriate volume of the 500 nM stock was mixed with an equal volume of opti-MEM buffer (Gibco, Invitrogen) (for volumes see Table 2.1). In parallel, the lipid mixture was prepared by mixing the DharmaFECT1 reagent with opti-MEM buffer to give concentrations of 4% for NIH-3T3 and 3% for MRC-5 transfection. The lipid-opti-MEM mixture was gently pipetted up and down, and incubated at room temperature for 5 min. The lipid-opti-MEM mixture was added to siRNA/miRNA-opti-MEM mixture and incubated for 20 min at room temperature. The appropriate volume of the transfection mix was then added into a well, followed by the addition of cells in antibiotics-free medium, see Table 2.1. The plate was then tapped every 10 min for 30 min to ensure that the miRNA/siRNA liposomes mixed fully in the cells and that the cells were equally distributed in each well. Cells were incubated at 37°C for 48

hours before samples were harvested or infected with a virus, depending on the experimental objective.

Plate format	Volume of 500 nM stock of siRNA or miRNA	Volume of Opti-MEM	Lipid-opti-MEM mixture DharmaFECT1%	Cells Count
6-well plate	50µl	50µl	100µl (4% for NIH-3T3 and 3% for MRC-5)	$3x10^5$ in 800µl
24-well plate	12.5µl	12.5µl	25µl (4% for NIH-3T3 and 3% for MRC-5)	$1x10^5$ in 450µl
96-well plate	5µl	5µl	10µl (4% for NIH-3T3 and 3% for MRC-5)	$1.5x10^4$ in 80µl

Table 2.1: Parameters for siRNA and miRNA transfection with DharmaFECT1 in various multi-well plates.

2.3.2 Lipofectamine™ 2000 transfection

Lipofectamine™ 2000 transfection reagent was used for the transfection of DNA plasmids (see Table 2.2) or for co-transfecting DNA plasmids with siRNA or miRNA into cultured cells. The number of cells, amount of DNA, and volume of transfection reagent differed according to the multi-well plate used in each experiment, as illustrated in Table 2.3 for DNA transfection and in Table 2.4 for the co-transfection of DNA and siRNA or miRNA. For each transfection reaction, DNA was diluted in opti-MEM to ensure the desired concentration in the appropriate volume. The lipofectamine-opti-MEM mixture was then prepared at 2.5% and incubated for 5 min at room temperature, after which it was added to the transfectent and incubated for 20 min at room temperature. The mixture was aliquoted into wells and cells were added, as shown in the Tables 2.3 and 2.4. The plates were then incubated at 37°C and, at 24 hours post transfection, the medium was replaced with standard culture media.

Plasmid DNA	Supplier
Firefly luciferase reporter PGL4.1 basic vector	Progema (Kind Gift of Dr. Finn Grey)
Renilla luciferase reporter PhRL-SV40	(Kind Gift of Dr. Anton Enright)
Dual luciferase reporter vector PsiCHECK-2	Progema

Table 2.2: Plasmid DNAs used in transfection.

Plate format	DNA:Opti-MEM	Lipid-Opti-MEM mixture Lipofectamine%	Cells count in media
6 well-plate	1µg of DNA in 100µl	100µl (2.5% Lipofectamine)	$3x10^5$ in 800µl
24 well-plate	250ng of DNA in 25µl	25µl (2.5% Lipofectamine)	$1x10^5$ in 450µl
96 well-plate	50ng of DNA in 10µl	10µl (2.5% Lipofectamine)	$1.5x10^4$ in 80µl

Table 2.3: Parameters for plasmid DNA transfection using Lipofectamine™ in multi-well culture plates.

Plate format	DNA:siRNA/miRNA:Opti-MEM	Lipid-opti-MEM mixture Lipofectamine%	Cells count in media
6 well-plate	1µg of DNA mixed with 50µl of 500nM miRNA/siRNA in 100µl of opti-MEM	100µl (2.5% Lipofectamine)	$3x10^5$ in 800µl
24 well-plate	250ng of DNA mixed with 12.5µl of 500nM miRNA/siRNA in 25µl of opti-MEM	25µl (2.5% Lipofectamine)	$1x10^5$ in 450µl
96 well-plate	50ng of DNA mixed with 5µl of 500nM miRNA/siRNA in 10µl of opti-MEM	10µl (2.5% Lipofectamine)	$1.5x10^4$ in 80µl

Table 2.4: Parameters for plasmid DNA and siRNA/miRNA co-transfection using Lipofectamine™ in multi-well culture plates.

2.3.3 Cell viability

The viability of cells was assessed using the cell titer-blue reagent (Promega). 20µl of the reagent was added to each well, which contained 100µl of media in a 96-well plate. The plate was tapped for 30 seconds and incubated for 2-4 hours at 37°C. Live cells will irreversibly reduce resazurin (non-fluorescent) in the blue reagent into the fluorescent molecule resorufin, whereas dead cells will have lost this capacity. The fluorescence was detected using the Varioskan Flash Multimode Reader (Thermofisher scientific) at 590nm. The cell viability was calculated by comparing the fluorescence signal from transfected cells to control cells.

2.4 RNA isolation and characterisation

2.4.1 RNA extraction

2.4.1.1 Extraction of total RNA using TRIzol

For RNA extraction, cells were washed twice with warm PBS before lysing in tissue culture plates using 200µl (24-well plates) or 400µl (6-well plates) of TRIzol reagent per well (Invitrogen, USA). The plates were gently tilted in order to ensure the equal distribution of TRIzol reagent over the cells and after 5 min RNA samples were collected into sterile 1.5 ml microcentrifuge tubes. The lysed RNA samples were stored short-term at -20ºC or long term at -70ºC. TRIzol samples were then thawed and 80µl or 40 µl chloroform was added to 400µl or 200µl samples, respectively. The tubes were then capped and inverted 5 times to ensure that they were well-mixed. TRIzol samples were incubated at room temperature for 2-3 min and then centrifuged at 12,000 g-force at 4^{o}C for 15 min, after which the clear aqueous phase harbouring the total RNA was carefully removed and transferred to a sterile 1.5 ml microcentrifuge tube, avoiding any aspiration of the white interface, which contains precipitated DNA and/or TRIzol containing cellular debris. The aqueous phase was approximately 180µl and 80µl of 400µl and 200µl RNA-TRIzol samples, respectively. The aqueous phase was then precipitated by adding 1/10 volume of 3M NaOAc (pH 5.7) (AppliChem, Germany), 0.5µl of 15 mg/ml glycogen blue (Ambion, USA), and 2x volumes of cold ethanol (100%). This was mixed by inversion, and incubated for an hour at -70^{o}C or overnight at -20^{o}C. To pellet the RNA, the samples were spun at 4^{o}C for 30 min at 12,000 g-force. Then, 100% ethanol was carefully aspirated from the edge and close from the base of each tube without touching or disrupting the RNA pellet. Each RNA pellet was washed twice with one volume 70% cold ethanol. The samples were mixed by inversion and centrifuged at 12,000 g-force at 4^{o}C for 10 min. The washed pellet was then air dried for 5-10 min and resuspended in 20-30µl of RNase/DNase free H_2O (GIBCO, Invitrogen, UK) with 0.1 mM EDTA (Promega, USA). RNA samples were placed in a water bath that was maintained at 55^{o}C for 10 min, and then transferred into ice.

2.4.1.2 Quality assessment of total RNA

The concentration and degree of contamination of the acquired RNA samples was assessed on a Nanodrop ND-1000 spectrophotometer (Thermo scientific, USA), which operates by means of locating the sample between two optical pedestals (upper and lower). The level of UV absorption was measured at wavelengths of 230, 260 and 280nm. 2µl of purified total RNA sample was used for spectrophotometry. All RNA samples in experiments have a A_{260}:A_{280} ratio of >1.8. Protein contamination is likely to have occurred if the A_{260}:A_{280} ratio is < 1.8, in which case samples were re-extracted with TRIzol. If the ratio at A_{260}:A_{230} is <1.5, phenol or chloroform contamination is possible, these samples were re-precipitated. In order to assess RNA integrity, a 12% RNA gel was prepared using the SequaGel (UreaGel System), which consists of UreaGel Concentrate, UreaGel Diluent, and UreaGel Buffer (National Diganostic). To cast 2 small gels, 4.8 ml of UreaGel Concentrate, 4.2 ml UreaGel Diluent, 1ml UreaGel Buffer, 4µl TEMED, and 80µl of APS were mixed, poured immediately into the space between the short and long slides, and the comb then fixed in place. 0.8~1µg of RNA samples were mixed with 2x RNA loading buffer and were then denatured at 95°C for 20 seconds, after which they were snap cooled on ice. This RNA samples were loaded in the UREA-TBE gel and run in 0.5x TBE at 100-120 Volt for 1-2 hours. The gel was then stained with ethidium bromide (EtBr) (Invitrogen) and visualised on a UV transilluminator (SYNGENE). Intact total RNA is characterised by three distinct bands comprising 5S, 5.8S rRNAs, and tRNAs. No smeared RNA is indication of good-quality.

2.4.1.3 Extraction of total RNA using Qiagene

The RNA samples used for microarray expression profiling were extracted using the miRNeasy Mini Kit (QIAGEN). The miRNeasy Mini Kit is designed to isolate miRNA and total RNA from tissue and cell samples using spin columns that having binding capacities for RNAs > 18 nt. Cultured cells were harvested from 6-well plates using 400µl of QIAzol lysis reagent and were transferred into sterile 1.5ml tubes and incubated at room temperature for 5 min before the addition of 80µl of chloroform to each sample. The tubes were then centrifuged at 12,000 g-force at 4°C for 15 min in order to separate the aqueous phase that contains the total RNA. The upper aqueous phase (~ 180µl) was transferred into a clean 1.5 ml tube and 1.5x

volume of 100% ethanol (270µl) was added and thoroughly mixed by pipetting up and down several times. This aqueous-ethanol mixture was transferred to a spin column in a collection tube, which was centrifuged at 12,000 g-force at room temperature for 1 min. The flow-through was discarded from the collection tube and the spin column was then washed for 1 min with 700µl of RWT buffer. Again the flow-through was discarded and the spin column was washed twice with 500µl RPE wash buffer by centrifugation at 12,000 g-force for 1 min. The flow-through and collection tube were discarded and the spin column was placed in a clean collection tube. Spin columns were then centrifuged for 1 min at 12,000 g-force to ensure that no residual RPE remained in the column, after which the columns were placed in clean 1.5 ml tubes and eluted with 30µl of 0.1 mM EDTA in RNase/DNase-free water. Purified RNA was collected in the flow through following centrifugation of the spin column in a fresh collection tube at 12,000 g-force. The 2100 Bioanalyzer (Agilent, CA, USA) was used for the assessment of the integrity of extracted RNA samples. This stage was performed by Dr. Amy Buck at the Division of Pathway Medicine, University of Edinburgh, UK. All RNA samples had RIN > 9.

2.4.2 Reverse transcription polymerase chain reaction (RT-PCR)

To determine the relative expression of miRNAs and mRNA transcripts between samples across multiple experiments, total RNA was reverse-transcribed into complementary DNA (cDNA) before being amplified and quantified by qRT-PCR. For the reverse transcription step, the miScript II RT Kit (QIAGENE) was used. The reaction components and their amounts were pipetted in a total reaction volume of 10µl, in accordance with the manufacturer's recommendations (see Table 2.5).

Component	Amount
5x miScript HiFlex Buffer	2µl
10x miScript Nucleics Mix	1µl
miScript Reverse Transcriptase Mix	1µl
Total RNA (template)	200ng
Final volume	10µl

Table 2.5: The components of the reaction mix of reverse transcription.

After the addition of 200ng of total RNA to the PCR tube (Axygen Scientific) containing the reverse-transcription master mix, the tubes were gently tapped and

centrifuged for 5 seconds using a microcentrifuge (Starlabs). The PCR tubes were kept on ice during the preparation stage. The RT reaction was carried out on a thermal cycler (BioRad) using the following thermal program:

Steps	Temperature	Time
cDNA synthesis	37ºC	60 min
Reverse transcriptase inactivation	95ºC	5 min
Cool	4ºC	For ever

The 10µl of cDNA produced in each RT reaction was diluted in RNase-free water (1:200 dilution), prior to qPCR reaction. The diluted cDNA samples were used for miRNA and mRNA quantification. For the efficiency verification of primers, 10-fold serial dilutions (1:10, 1:100, 1:1000, 1:10,000) of pooled cDNA were prepared from different samples and used to generate standard curves for each target and control RNA.

2.4.3 Quantitative real-time polymerase chain reaction (qRT-PCR)

2.4.3.1 Quantitative real-time PCR for mature miRNA

The quantification of expression levels of mature miRNA was conducted using the miScript SYBR® Green PCR Kit, which includes a universal primer (reverse primer) and SYBR Green PCR master mix. The forward primers were purchased from (QIAGENE) for each miRNA of interest. The qRT-PCR reaction mix was prepared in accordance with the manufacturer's recommendations, as shown in the Table 2.6 below.

Components	96-well plate	384-well plate
2x QuantiTect SYBR Green PCR Master Mix	4µl	2µl
10x miScript universal primer	1µl	0.5µl
RNase-free water	3µl	1.5µl
10x miScript specific primer	1µl	0.50µl
cDNA template (1:200 dilution)	1µl	0.50µl
Total volume per well	10µl	5µl

Table 2.6: The components of the reaction mix for detecting miRNAs by qRT-PCR.

The initial qRT-PCR mix was prepared from SYBR Green PCR master mix, universal primer and RNase-free water, which were mixed together gently and

thoroughly. This initial qRT-PCR mix was then aliquoted into sterile 2 ml tubes and one of the specific forward primers added. This specific qRT-PCR mix was then pipetted into 96 or 384 well plates using multichannel pipettes in order to minimise the number of pipetting steps. In the case of 384-well plates, 4.5µl of the specific qRT-PCR mix was pipetted into each well, while in 96-well plates 9µl was pipetted per well. Each diluted cDNA sample (1:200) was then added to the well (two technical replicates were carried out). The qRT-PCR plate was then carefully and tightly sealed, after which it was centrifuged at 800 g-force for 2-3 min to ensure that all the cDNA was at the bottom of well, as well as to remove bubbles. The qRT-PCR plates and seal films were purchased from Roche. The following thermal profile was used for qRT-PCR:

Steps	**Temperature**	**Time**	**Cycle**
Initial denaturation	95ºC	15 min	1 cycle
Amplification			
Denaturation	94ºC	15 seconds	45 cycle
Annealing	55ºC	30 seconds	
Extension	72ºC	30 seconds	
Cooling	40ºC	Hold	1 cycle

qRT-PCR was performed on the LightCycler® 480 Real-Time PCR instrument from Roche Applied Science and cycle threshold (C_T) values were calculated using Roche's LightCycler® 480 Software. The C_T values of the amplified products in qRT-PCR analysis are based on the detection of the fluorescent SYBR Green dye, which is specific for double-stranded DNA (dsDNA). Target miRNA levels were normalized to the non-coding small nuclear RNA, U6 snRNA and miR-16. These non-coding RNAs have been found to be abundant in the examined cells and to be stable over a range of experimental treatments.

2.4.3.2 Quantitative real-time PCR for pri-miRNA and mRNA

The LightCycler® 480 SYBR Green I Master Kit (Roche Applied Science) was also used to quantify the expression of mRNAs and pri-miRNA in samples. The specific forward and reverse primers were designed for each RNA using the online ProbeFinder software (Roche Applied Science) at (http://qRT-PCR.probefinder.com/roche3.html). Primers were produced by Invitrogen (see the

list of human primers in Table 2.8 and mouse primers in Table 2.9). Each tube containing lyophilised primer was briefly centrifuged, after which a 100 µM stock solution was made in DNase/RNase-free water and stored at –20°C. The concentrated stock solution was then further diluted to produce a working stock at a final concentration of 10 µM. The primers were also designed to have very similar melting temperatures, around 60°C, the temperature of the annealing step. All the primers were tested and experimentally validated as described below (2.4.3.3) before a qRT-PCR plate was run. As previously described (2.4.3.1), the kit components, primers, and diluted cDNAs were thawed on ice and the qRT-PCR mix was prepared in accordance with the manufacturer's instructions, as shown in the Table 2.7 below.

Components	96-well plate	384-well plate
2x SYBR Green I Master	5µl	2.5µl
RNase-free water, PCR Grade	3µl	1.5µl
Forward primer (10 µM)	0.5µl	0.25µl
Reverse primer (10 µM)	0.5µl	0.25µl
Total volume per well	9.5µl	4.5µl

Table 2.7: The components of the reaction mix for detecting mRNAs by qRT-PCR.

This mix was aliquoted into sterile tubes to which a specific set of primers was added, after which a volume of 9µl or 4.5µl of the specific mix was pipetted into the wells of 96 or 384-well plate, according to the experiment's layout. 0.5µl of cDNAs were added into the wells at the last in two repeats, the plate was sealed, centrifuged, and then run in the LightCycler® 480 Real-Time PCR instrument (Roche Applied Science). The instrument was programmed as recommended by the manufacturer.

Steps	Temperature	Time	Cycle
Initial denaturation	95ºC	5 min	1 cycle
Amplification			
Denaturation	95ºC	10 seconds	45 cycle
Annealing	60ºC	10 seconds	
Extension	72ºC	10 seconds	
Cooling	40ºC	Hold	1 cycle

Target mRNA and pri-miRNA levels were normalized to the housekeeping GAPDH mRNA, which maintains stable expression in various experimental conditions.

Human Primer	Sequence
GAPDH	
Forward primer	5′-AGCCACATCGCTCAGACAC-3′
Reverse primer	5′-GCCCAATACGACCAAATCC-3′
18S	
Forward primer	5′-GCAATTATTCCCCATGAACG-3′
Reverse primer	5′-GGGACTTAATCAACGCAAGC-3′
Pri-miR-199a/214	
Forward primer	5′-AATGAATCCCTATGGGTCCC-3′
Reverse primer	5′-TCCTGTACTTATGCCAGAGG-3′
Forward primer	5′-ACTTGCTGTGCAGAACATCC-3′
Reverse primer	5′-GGCTGCTTTCTTTCAATGGC-3′
TWIST-1	
Forward primer	5′-AAGGCATCACTATGGACTTTCTCT-3′
Reverse primer	5′-GCCAGTTTGATCCCAGTATTTT-3′
PIK3CB	
Forward primer	5′-CCCATGTGTTATCCTCTCAGAA-3′
Reverse primer	5′-TGAATCCTCACCAAATACCTTGT-3′
CD151	
Forward primer	5′-CTGCGCCTGTACTTCATCCT-3′
Reverse primer	5′-TTCTCCTTGAGCTCCGTGTT-3′
ITGA3	
Forward primer	5′-CCCTCACTCCTTCTTCATGG-3′
Reverse primer	5′-GAGCTCCCACAGCAATATCC-3′
ITGA6	
Forward primer	5′-TTTGAAGATGGGCCTTATGAA-3′
Reverse primer	5′-CCCTGAGTCCAAAGAAAAACC-3′
FGF7	
Forward primer	5′-AAGGGACCCAAGAGATGAAGA-3′
Reverse primer	5′-CCTTTGATTGCCACAATTCC-3′
CD44	
Forward primer	5′-GACACCATGGACAAGTTTTGG-3′
Reverse primer	5′-CGGCAGGTTATATTCAAATCG-3′

Table 2.8: A list of the human primers used in qRT-PCR experiment.

Mouse Primer	Sequence
GAPDH	
Forward primer	5′-AGCCACATCGCTCAGACAC-3′
Reverse primer	5′-GCCCAATACGACCAAATCC-3′
18S	
Forward primer	5′-ACATCGACCTCACCAAGAGG-3′
Reverse primer	5′-TGTACTGTCGTGGGTTCTGC-3′
Pri-miR-199-3p	
Forward primer	5′-CAGTGAAGTTGTTAAATATCTCTGCAT-3′
Reverse primer	5′-TGTTAAGTACACGAAGCAAACTGC-3′
Forward primer	5′-GGGATATCCAGCATCCTGTATCAA-3′
Reverse primer	5′-TTAAGGTGCATATAAGACAGTCAAGG-3′
TWIST-1	
Forward primer	5′-AGCTACGCCTTCTCCGTCT-3′
Reverse primer	5′-TCCTTCTCTGGAAACAATGACA-3′
STAT3	
Forward primer	5′-GGAAATAACGGTGAAGGTGCT-3′
Reverse primer	5′-CATGTCAAACGTGAGCGACT-3′
SRF	
Forward primer	5′-CCTACCAGCTTCACCCTCAT-3′
Reverse primer	5′-GTGAGGTCTGTGCTGCTGTC-3′
ELK-1	
Forward primer	5′-GCTCCCCACACATACCTTGA-3′
Reverse primer	5′-GGGTGCAATTGGACTCAGA-3′
PIK3CB	
Forward primer	5′-GAGCTCACATCGGTCAAAGAT-3′
Reverse primer	5′-AACTTCTGCTTGAACTGCTTCAG-3′
CD151	
Forward primer	5′-ACGGAACCTGTTACGCTTGTA-3′
Reverse primer	5′-TCCTTGAGCTCTGTGTTCAGC-3′
ITGA3	
Forward primer	5′-CGGCCTGTCATCAATATCCT-3′
Reverse primer	5′-AACACAGCTCCACCTGAACA-3′
ITGA6	
Forward primer	5′-GTATTCAGGAGTAGCTTGGTGGA-3′
Reverse primer	5′-TTTCTCTTGAAGAAGCCACACTT-3′
FGF7	
Forward primer	5′-TGGCTGACACCATGACTAGC-3′
Reverse primer	5′-GGCTACAGGCTGTCGTTTTT-3′

Table 2.9: A list of the mouse primers used in qRT-PCR experiment.

2.4.3.3 qRT-PCR analysis

2.4.3.3.1 Validation of qRT-PCR primers

All designed primers should meet at least two important criteria to be validated: 1) amplification efficiency is between 80 and 110% and 2) a single amplicon is produced. The traditional method for assessing amplification efficiency requires a standard curve for each primer. Therefore, 10-fold serial dilutions were prepared from pooled cDNA samples (20ng/µl, 2ng/µl, 0.2ng/µl, 0.02ng/µl, 0.002ng/µl). The reverse transcription (RT) and qRT-PCR were then performed in accordance to the protocol outlined above (2.4.2 and 2.4.3), with three technical replicates for each dilution point. The average C_T values were plotted versus the initial cDNA input (see an example in Figure 2.3) and the slope was calculated for each primer. The amplification efficiency (E value) can be determined from the slope as follows: $E=(10^{(-1/slope)}-1)*100\%$. Slopes between -3.8 and -3.1 correspond to amplification efficiencies between 80% and 110%. All primers used have shown amplification efficiency > 80 %. As for the second criterion, a default melting program was run on qRT-PCR instrument after the completion of cycling program. The melting curve analysis have shown a clean amplification of a single amplicon, which in some cases was also confirmed by a presence of a single band corresponding to the predicted length of the amplicon on the agarose gel.

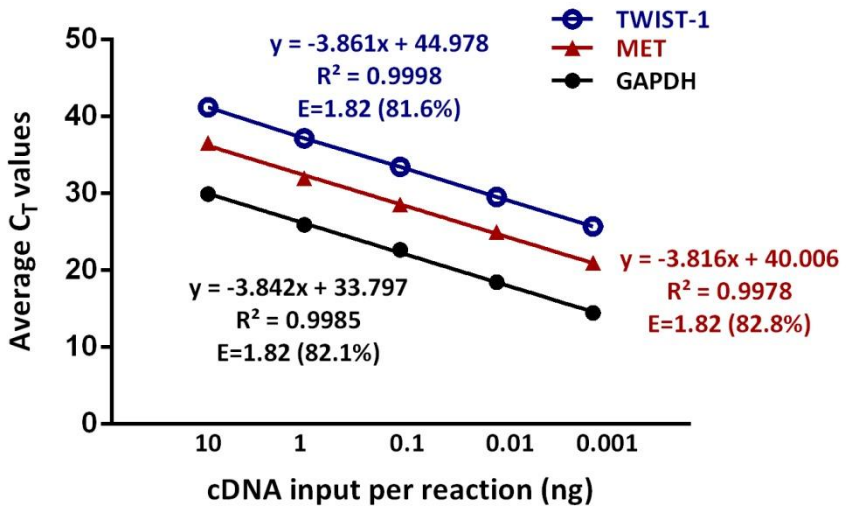

Figure 2.3: Standard curves for primer used in qRT-PCR assay.

2.4.3.3.2 qPCR quantification method

For the most reliable qPCR results, the amplification efficiencies of the target and control RNAs should be approximately equal. To calculate the changes in the miRNA or mRNA expression levels, two strategies are widely used: absolute quantification, where the absolute numbers of RNA copies in a sample is calculated (this requires the generation of the standard curve for the known quantity of RNA) and relative quantification, where a comparison of the relative expression levels of the target miRNA or mRNA is carried out between samples over a period of time or during exposure to treatment. The relative quantification for the miRNA or mRNA is performed as follows:

1. For each biological sample the C_T values of the two technical replicates are averaged.
2. The ΔC_T relative change is then calculated for each biological sample using the comparative C_T method, also known as the $2^{-\Delta Ct}$ method applying equation $\Delta C_T = C_{T(\text{Target RNA})} - C_{T(\text{Reference RNA})}$, where reference RNA stands for a control small non-coding RNA or a housekeeping gene.
3. The ΔC_T values are then compared between the samples of interest and their experimental controls (calibrators), such as untreated or mock infected in order to calculate the fold difference between the two conditions.

2.4.4 Northern blot analysis

2.4.4.1 Buffers and solutions used for Northern method

10x TBE Buffer (Tris-borate-EDTA): 109g Tris base, Boric acid 55.6g, 50 ml of 500 mM of EDTA, which is made up to 1L using ddH_2O.

15% TBE-UREA gel: 6ml concentrate reagent (SequaGel, National diagnostics), 3ml dilute reagent (Sequa gel, National diagnostics)**,** 0.5 ml 10x TBE**,** 0.5 ml ddH_2O**,** 100µl of 10% ammonium persulfate (APS) (Sigma) and 4µl Tetramethylethylenediamine (TEMED) (Sigma)

2x loading dye: 8 M urea (Sigma), 5 mM EDTA (Promega), 0.05 % bromophenol blue(Sigma), 0.05% xylene cyanol (Sigma).

Cross-linking Solution: 245µl of 12.5M 1-methylimidazole, 9ml of ddH_2O, adjust pH to 8, 0.753g EDC and then increase the volume to 25ml using ddH_2O.

Wash Buffer 1 (2x SSC, 0.1% SDS): 100 ml 20x SSC (Biosciences), 10 ml 10% SDS (Sigma), and 890 ml ddH_2O. SSC and SDS stand for sodium chloride-sodium citrate buffer and sodium dodecyl sulfate.

Wash Buffer 2 (1x SSC, 0.1% SDS): 50 ml 20x SSC (Biosciences)**,** 10 ml 10% SDS (Sigma), and 940 ml ddH_2O.

Wash Buffer 3 (0.1x SSC, 0.1% SDS): 5 ml 20x SSC (Biosciences)**,** 10 ml 10% SDS (Sigma), and 985 ml ddH_2O.

Stripping Buffer (0.1% SDS): 5 ml 10% SDS and 495 ml ddH_2O.

All the buffers were prepared with double-distilled water (ddH2O) from a Millipore system (>18 MΩ cm).

2.4.4.2 RNA gel electrophoresis

For each experimental condition, a pool of total RNA was prepared from the three technical repeats. Each pooled RNA sample (5µg in mouse/condition and 7µg in human/condition) was resuspended in a total volume of 7 or 8µl using DNase/RNase-free water. In cases where the total volume of pooled RNA exceeded

7 to 8µl, the samples were divided into approximately equal volumes and then concentrated in speedvac (Savant, USA) using a low drying rate. Following the speedvac step, RNA samples (7µl to 8µl) were mixed with an equal volume of 2x urea loading dye. The RNA samples were denatured by heating them to 95°C for 20 seconds, after which they were snap cooled on ice. The RNA samples were resolved on a denaturing 15% TBE-Urea gel, which had been made and allowed to set for >30 min. The gel was pre-run in 0.5% TBE buffer for > 30 min at 100 Volt. The wells in the gel were also cleaned with a syringe in order to remove air bubbles and urea, which collected at the bottom of each well, before loading an equal amount of the RNA samples (14µl to 16µl). At the same time, a radiolabeled RNA decade marker (10 to 150 bases) (Ambion, Applied Biosystem) was loaded to serve as a nucleotide length standard. Samples were run at 120 Volt for ~1.5-2 hours until the bromophenol blue dye reached ¾ of the overall length of the gel.

2.4.4.3 The synthesis of Northern γ-^{32}P labelled oligonucleotides probes and RNA-labelled marker

Reverse complement oligonucleotides for miR-199-3p, miR-199-5p, miR-214, miR-16, and tRNA sequences (Table 2.10) were produced by Invitrogen.

Target RNA	Oligonucleotides' sequences
miR-199-3p	5′-TAACCAATGTGCAGACTACTGT-3′
miR-199-5p	5′-GAACAGGTAGTCTGAACACTGGG-3′
miR-214	5′-GCACAGCAAGTGTAGACAGGCA-3′
miR-16	5′-CGCCAATATTTACGTGCTGCTA-3′
tRNA (Gly)	5′-GGCGAGAATTCTACCACTGAACCACCAATGC-3′

Table 2.10: Primer sequences used for Northern blot.

The radioactive labelling at the *5′*- termini was carried out using [γ-^{32}P]-dATP and T4 Kinase Kit (Invitrogen) with 20 µM of each oligonucleotide. The reaction was incubated at 37°C for 45 to 60 min in a thermocycler. The oligonucleotide probes were subsequently purified from the reaction components using microSpin™ G-25 columns (GE Healthcare). The labelled probes were then diluted in 50µl of 3 mM EDTA. The date of labelling was written on the tube and then it was stored at -20°C in a protective radioactive box.

For the decade RNA ladder, 100ng of marker RNA, 1µl 10x Kinase buffer, 1µl [γ–^{32}P]ATP, and 1µl T4 Polynucleotide Kinase were mixed in a total volume of 10 µl and incubated for one hour at 37°C. 2µl 10x cleavage reagent and 8µl of water was then added to the mixture and incubated at room temperature for 5 min. The labelled RNA marker was mixed with 20µl loading buffer and stored at -20°C. The required volume of RNA ladder was heated at 95°C for 5 min before use.

2.4.4.4 Northern blotting, cross-linking and hybridisation using γ-^{32}P labelled oligonucleotides probes

To transfer RNA from a denaturing gel, a sheet of nylon membrane (Hybond N) (GE Healthcare, Fisher Scientific) and 4-6 sheets of Whatman filter paper (Whatman Ltd, UK) of similar size to the gel were soaked in cold 0.5% TBE. The blotting sandwich of pad, filter papers, gel, nylon membrane, filter papers and pad was assembled (from negative to positive electrodes) and immersed in cold 0.5% TBE. The transfer was conducted at 80 Volt for one hour in a cold room (4°C). To cross-link the transferred RNA, the nylon membrane was placed on a pad containing EDC cross-linking solution for 2 hours at 50°C in a Techne oven. After the cross-linking stage, the membrane was immersed in 4-5 ml of Perfect Hyb Plus Hybridisation buffer (Sigma) in a 15 ml falcon tube for 30 min at 42°C in a rotary oven. 10µl of the ^{32}P-labeled probe was added to the hybridisation buffer and incubated for at least 6 hours or over-night at 42°C in a Techne hybridisation oven. The membrane was then washed successively at 42°C with increasingly stringent buffers: 1) 2x SSC, 0.1% SDS, 2) 1x SSC, 0.1% SDS, and 3) 0.1x SSC and 0.1% SDS. Following the washes, the membrane was kept in a sealed film and exposed to a phosphorimager screen (Molecular Dynamics, LabX, USA) for 24 to 48 hours. The screen was scanned using a Typhoon Trio variable mode imager (GE Healthcare) and blanked for 15 min with an imager eraser (BioSciences). The membrane was stripped to remove the radio-labelled probe to allow re-hybridisation with a new ^{32}P-labelled probe. The stripping buffer was boiled in the microwave and the membrane was placed in this buffer. The membrane left for ~ 2 hours in the stripping buffer at room temperature. The membrane was re-exposed in phosphorimager for 6 to 24 hours to ensure that no bound probe remained before re-hybridisation with another probe.

2.4.5 Primer extension analysis

2.4.5.1 Buffers and solutions used for Northern method

10x annealing buffer: 200 mM Tris-HCL (pH 8.0), 300 mM KCl, 5 mM EDTA (pH 8.0)

6x reverse transcriptase buffer: 300 mM Tris-HCL (pH 8.0), 300 mM KCl, 5 mM EDTA (pH 8.0), 60 mM $MgCl_2$, 60 mM DTT, 3 mM EDTA.

2.4.5.2 Primer extension

The primer extension technique was used to determine the transcription start site of the pri-miRNA. Two primers that have complementary sequences to different regions close to the 5′ end of the RNA transcript were designed and ^{32}P-labelled (as described in 2.4.4.3). 20µg of total RNA from mouse liver and 0.5 pmol of each primer were mixed with annealing buffer in a total volume of 4µl. The primer was annealed to RNA by incubating tubes at 90°C for 2 min, then placing them at room temperature. During the incubation period, the reverse transcriptase mix was prepared (1.5µl of 6x RT buffer, 1.8µl dNTPs (2.5 mM), 0.2µl reverse transcriptase, 0.2µl RNA inhibitor, 1.3µl DNase/RNase-free water per reaction). Following the cooling of annealed RNA primer, 5µl of the reverse transcriptase mix was added into each reaction tube to make 9µl. The reaction tubes were then incubated at 42°C for 40min, after which 9µl of 2x loading dye was added to stop the reaction. Samples and radiolabeled RNA decade markers were loaded onto a TBE-UREA gel and run at 120 Volt until the bromophenol blue dye reached ¾ of the gel. The top gel slide was carefully removed and the gel was wrapped in cling film. The wrapped gel was then exposed in the phosphorimger for 24 hours at 4^{o}C, after which the screen was scanned in the Typhoon Trio variable mode imager (GE Healthcare).

2.5 DNA purification and cloning

2.5.1 Buffers and solutions used for DNA techniques

Lysis buffer: 100 mM Tris-Hcl (pH=8), 5 mM EDTA (pH=8), 200 mM NaCl, 0.2% SDS, 250 µg/ml of proteinase K.

2.5.2 The extraction of genomic DNA

In order to isolate genomic DNA from cultured NIH-3T3 cells, the cells were trypsinised and centrifuged for 10 min at 200 g-force. The supernatant was discarded and the pellet resuspended in 1ml of 1x PBS. After the pellet had been washed, it was lysed using 1 ml of lysis buffer (for $1x10^6$ cells) for 3-4 hours at 50°C. Phenol–chloroform extraction was then used for purification of the DNA sample. An equal volume of phenol–chloroform was added to the cell lysates and then vortexed at room temperature for 15 seconds. The sample was centrifuged at 12,000 g-force for 20 min. The aqueous phase was collected and phenol–chloroform step repeated twice more. The DNA in aqueous phase was precipitated using 60µl of 5M NaCl and 2.5x volume ice cold 70% ethanol at -70°C for an hour, then centrifuged at 12,000 g-force for 10 min. The supernatant was removed and the pellet washed twice with 70% ethanol, dried for 5min and finally resuspended in 50µl of DNase/RNase free water.

2.5.3 Cloning the promoter into basic PGL4.10 vector

2.5.3.1 The amplification of the pri-miRNA promoter sequences

The mouse promoter sequence was obtained from Gene2Promoter, which is included in the Genomatix package (http://www.genomatix.de/). The basic PGL4.10 vector was kindly provided by Dr. Finn Grey (The Roslin Institute, University of Edinburgh, Edinburgh). Primers were manually designed with the help of oligonucleotide properties calculator software (http://eu.idtdna.com/analyzer/applications/oligoanalyzer/default.aspx). The annealing temperature and GC content (40 to 60%) for each pair of primer were similar. The forward and reverse primers contain restriction sites, for either XhoI or HindIII to allow cloning into the PGL4.10 vector as well as 3 nt (CCG) to act as a loading pad for the restriction enzyme (listed in Table 2.11). The primers were purchased from Invitrogen and resuspended at find concentration of 10 pmol/µl, as

described above (2.4.3.2). The PCR reactions were performed as described below (Table 2.12) using Phusion® high-fidelity DNA polymerase (Finnzymes, New England Biolabs, UK). The PCR reactions were mixed gently and thoroughly, after which the following PCR-program was used for amplification.

Steps	**Temperature**	**Time**	**Cycle**
Initial denaturation	98ºC	2 min	1 cycle
Amplification			
Denaturation	98ºC	10 seconds	25 cycle
Annealing (see Table 2.11)	60, 63 or 65ºC	30 seconds	
Extension	72ºC	30 seconds	
Final extension	72ºC	7 min	1 cycle
Cooling	4ºC	Hold	1 cycle

Primer	**Sequence**	**Melting Temp**
Forward primer Full-length (-596,+100)	5′-*CCG*CTCGAGAAAAGAAAGGGGGGAGC -3′	59.1°C
Reverse primer	5′-*CCG*AAGCTTAGAGCCTGTCTTCCTGC -3′	60.6°C
Forward primer (-421,+100)	5′-*CCG*CTCGAGAGCCCAGATCAGGCAACAAATTTG-3′	65.9°C
Reverse primer	5′-*CCG*AAGCTT AGAGCCTGTCTTCCTGCACC -3′	65.7°C
Forward primer (-273,+100)	5′- *CCG*CTCGAG CTGCCCAGTTGAGGGAAAAAATCTG-3′	65.7°C
Reverse primer	5′-*CCG*AAGCTT AGAGCCTGTCTTCCTGCACC -3′	65.7°C
Forward primer (-128,+100)	5′- *CCG*CTCGAGCCCCAGGGTGACATCATCC -3′	63.6°C
Reverse primer	5′-*CCG*AAGCTTAGAGCCTGTCTTCCTGCAC-3′	63.6°C
Forward primer (-1000,+100)	5′-*CCG*CTCGAGTAAACTTTTTAACATTTCC-3′	63.8°C
Forward primer For sequencing	5′-AGGCTGTCCC CAGTGCAAGT-3′	
Reverse primer For sequencing	5′- AATGGCGCTGGGCCCTTCTT -3′	

Table 2.11: A list of the primer sets used in amplification of the promoter sequence. Restriction sites are underlined and flanking cushion sequences are italic.

Components	Volumes	Final concentration
5x Phusion HF Buffer	5µl	1X
10mM dNTPs (Invitrogen)	1µl	200µM
Forward primer 10pmole/µl	2.5µl	0.5pmole/µl
Reverse primer 10pmole/µl	2.5µl	0.5pmole/µl
DNA template (50ng/ µl)	1µl	1ng/ µl
Phusion DNA Polymerase (2U/µl)	0.5µl	0.02 U/µl
DNase/RNase free-water	37.5µl	
Total volume	50µl	

Table 2.12: The components of the PCR reaction mix for the amplification of 3′UTRs or promoter.

2.5.3.2 Purification of PCR product

To check whether amplified DNA was the correct size, a sample of 5µl of PCR product was run in 2.5% TAE agarose gel electrophoresis and visualised in the UV transilluminator (described in more detail below). The remaining 45µl of the PCR product was purified using QIAquick PCR Purification Kit from QIAGENE, in accordance with the protocol stipulated by the manufacturer.

2.5.3.3 Restriction digestion of the PCR products and PGL4.10 basic vector

Restriction endonuclease reactions were conducted on all of the PCR products and PGL4.10, in compliance with the manufacturer's recommendations. Briefly, 1.5µg of DNA plasmid or PCR products was digested for 2 hours with the appropriate buffer (defined by BioLabs) and temperature for XhoI and HindIII (BioLabs) using 10-20 U of the enzymes. Upon completion of the restriction digestion, the QIAquick PCR Purification Kit (QIAGENE) was used to clean up the digested DNA or vector.

2.5.3.4 Cloning the promoter sequences into PGL4.10 basic vector

The amplified product (insert) was mixed with digested vector at a molar ratio of 3:1 insert to vector, based on the following equation:

Length of insert (Kb) / Length of vector (Kb) x *ng of vector = ng of insert required for a 1:1 ratio*

Ligation reactions were carried out in 10µl volume comprising 5µl 2x Quick ligation buffer (BioLabs), and 1µl 5 U T4 DNA ligase (BioLabs), which was added to the mixture of insert and vector. The reaction tubes were mixed thoroughly and briefly centrifuged. After 15-30 min incubation at room temperature, 2µl of the ligation reaction was added directly to 50µl of pre-thawed chemically competent bacteria DHα5 (Invitrogen) and then incubated on ice for 30 min. The competent cells were heat shocked for 45 seconds in a 42°C water bath and then placed on ice for 2 min. 450µl of pre-warmed S.O.C. medium (Invitrogen) was added to the transformed competent cells. After shaking for 1 hour at 225 rpm (37°C) in an orbital incubator, 50-200µl of the transformed cells was spread on LB agar plates (Agar from Sigma and plates from Corning, USA) containing 100 µg/ml ampicillin (Sigma) and incubated overnight at 37°C (LTE laboratory incubator). A negative control ligation (ligation reaction without insert), was used to estimate the 'background'. Background colonies are a consequence of the presence of undigested or re-ligated vector. Ideally the results of this test should be few or no colonies in the control and tens to hundreds in the ligation. 5 to 10 single bacterial colonies were selected from each LB plate and transferred to 3 ml of LB broth (Sigma) with ampicillin. The cultures were incubated overnight at 37°C, with constant shaking in an orbital incubator (New Brunswick Scientific Co. INC, USA).

2.5.3.5 Purification of the DNA plasmid

P1 buffer: 50 mM Tris·HCl (pH 8.0), 10 mM EDTA 100 µg/ml RNase A (stored at 4°C).

P2 buffer: 0.2N NaOH, 1% SDS

P3 buffer: 3M CH_3CO_2K

1 ml of the incubated broth was centrifuged at 12,000 g-force for 2 min. The supernatant was then discarded and the pelleted bacteria resuspended in 200µl of buffer P1. An equal volume of Buffer P2 was added, mixed by gentle inversion (4-6 times), and incubated at room temperature for 5 min. 200µl of ice cold buffer P3 was added, inverted 4 times to mix, and incubated on ice for 10 min. The mix was then centrifuged for 10 min at maximum speed in order to pellet the debris. Following centrifugation, the supernatant was transferred to a fresh tube and 500µl of isopropanol was added. The supernatant-isopropanol mix was then cooled in ice for at least an hour and then centrifuged at maximum speed for 30 min to pellet the plasmid DNA. The DNA was then washed with chilled ethanol (70%) and centrifuged for 10 min. Finally, the supernatant was removed and the pellet was air-dried for 5-10 min and resuspended in 50µl of DNase/RNase-free water.

2.5.3.6 Agarose gel electrophoresis

Agarose (electrophoresis grade, Invitrogen) was dissolved in 1x TAE buffer (Tris-Acetate-EDTA) (Fisher BioReagent) to the desired concentration based on the length of DNA fragments (1 to 2.5%) by boiling in a microwave oven. When the agarose-TAE mixture cooled to approximately 60-70°C, ethidium bromide (Etbr) was added to a final concentration of 0.5µg/ml. The agarose mixture was then poured into a gel chamber (BioRad). After solidification, 0.8-1µg of digested DNA sample was mixed with 6x DNA loading dye at a ratio of 6:1 (Biolabs) and loaded. The gels were run in 1x TAE buffer at 120 Volt and visualized on a UV transilluminator. Bands of the correct size were then sequenced.

2.5.3.7 Sequencing of the inserted sequences

Sequencing of the inserts was carried out commercially by GenePool (University of Edinburgh, Edinburgh, UK), using forward and reverse primers for the basic

PGL4.10 vector listed above. The raw sequencing files were uploaded into a freely available sequence analysis program (BioEdit Sequence Alignment Editor) (Hall., 1999). The pairwise sequence alignment was performed in BioEdit software between the sequencing results and retrieved sequences from NCBI. This program was also utilised to view chromatograms of the GenePool sequencing results.

2.5.3.8 Midi plasmid preparation

To maintain stocks of plasmid DNA, the purification was conducted using the QIAprep Midiprep Kit in accordance with the manufacturer's instructions (QIAGENE).

2.5.3.9 Preparation of glycerol stocks

For maintenance of the correct DNA plasmids with the correct sequence, overnight LB broth bacterial cultures were mixed 1:1 with sterile 50 % glycerol (Sigma) and stored in 0.5 ml aliquots at –70°C. The bacteria were recovered by thawing the 0.5ml glycerol stock of bacterial cells and adding them into 150-200 ml LB overnight at 37°C in an incubator with constant shaking.

2.5.4 Cloning a miR-199-3p sensor and the 3′UTRs of target mRNAs into psi-CHECK2

2.5.4.1 The amplification of the 3′UTR sequences

The mouse 3′UTR sequences for PIK3CB, CD151, ITGA3, and ITGA6 mRNAs were obtained from NCBI (http://www.ncbi.nlm.nih.gov/) with ID numbers NM_029094, NM_001111049, NM_013565, and NM_008397, respectively. Although CD151 has three alternative spliced mRNA transcripts, the 3′UTRs are identical. The length of 3′UTR of PIK3CB and ITGA3 are ~1.3 kb, CD151 3′UTR is ~0.7 kb and ITGA6 3′UTR is ~0.9 kb. The psiCHECK-2 plasmid DNA was purchased from Promega. Primers for cloning and sequencing the various 3′UTRs were designed (Table 2.13), ordered from Invitrogen and resuspended at a final concentration of 10 pmol/µl (as described in 2.4.3.2 and 2.5.3.1).

Primer	Sequence	Melting Temp
PIK3CB 3′UTR		
Forward primer	5′-*CTTTA*CTCGAGCGTCCGCCCTACTCTGCC-3′	57°C
Reverse primer	5′-*CTTTA*GCGGCCGCCCCCAAACAGATGAAACCAC-3′	
CD151 3′UTR		
Forward primer	5′-*CTTTA*CTCGAGGAACACTACTGACCACGATGA-3′	62°C
Reverse primer	5′*CTTTA*GCGGCCGCCGAGTGCTTATACATTTACATTTATTG-3′	
ITGA3 3′UTR		
Forward primer	5′-*CTTTA*CTCGAGTCCCCGACAAACCTTCCGGC-3′	68.2°C
Reverse primer	5′-*CTTTA*GCGGCCGCACAAAGAAGGCACAGGATCG-3′	
ITGA6 3′UTR		
Forward primer	5′-*CTTTA*CTCGAGCTTTAAGCGCTCTAGGTACG-3′	65°C
Reverse primer	5′-*CTTTA*GCGGCCGCCGCCAACAACAACAAGACCTCCC-3′	
miR-199-3p sensor		
Forward primer	5′- *TCGAG*TAACCAATGTGCAGACTACTGT*GC*-3′	
Reverse primer	5′-*GGCCGC*ACAGTAGTCTGCACATTGGTTA*C*-3′	
PsiCHECK-2		
Forward primer	5′-AAGTACATCAAGAGCTTCGTGGAG-3′	
Reverse primer	5′-GAAGACTCATTTAGATCCTCACAC-3′	
Sequencing PIK3CB		
Forward primer	5′-CGCTGAGAATCTATTGGTGG-3′	
Reverse primer	5′-AGAGAAACCGCATTCATGGC-3′	
Sequencing CD151	5′-GACAGAAGTGCCTCTTATGC-3′	
Forward primer	5′-CAAGCAGATCTGAGAGTTCC-3′	
Reverse primer		
Sequencing ITGA3		
Forward primer	5′-CCTTGAGCCATTTGTCAATGG-3′	
Reverse primer	5′-TGGGTAGCCTTTAGTGTAGC-3′	
Sequencing ITGA6		
Forward primer	5′-TGCTAACAGAGTGGCTATCC-3′	
Reverse primer	5′-ATCCATTGGCAGTCTTGAGC-3′	

Table 2.13: A list of the primer sets used in amplification and sequencing of the 3′UTR sequence. Restriction sites are underlined and flanking cushion sequences are italic.

The PCR reactions were performed using 5ng of cDNA as a template and Phusion® high-fidelity DNA polymerase from Thermoscientific and amplified according to the thermal profile below.

Steps	Temperature	Time	Cycle
Initial denaturation	98ºC	2 min	1 cycle
Amplification			
Denaturtion	98ºC	10 seconds	25 cycle
Annealing			
-PIK3CB	57ºC	30 seconds	
-CD151	62ºC	30 seconds	
-ITGA3	68ºC	30 seconds	
-ITGA6	65ºC	30 seconds	
Extension			
-PIK3CB	72ºC	2 min	
-CD151	72ºC	45 seconds	
-ITGA3	72ºC	2 min	
-ITGA6	72ºC	1 min	
Final extension	72ºC	7 min	1 cycle
Cooling	4ºC	Hold	1 cycle

The amplified products were then subjected to the same steps described previously (2.5.3.2 to 2.5.3.9) in order to obtain the final cloned plasmids.

2.5.4.2 *The mutatgensis of the miR-199-3p binding sites in the PIK3CB 3′UTR*

The plasmid psiCHECK-2 containing PIK3CB 3′UTR was subjected to mutagenesis using the QuikChange lightning site-directed mutagenesis kit (Aglient Technologies, UK Ltd). Three bases were chosen for substitution within the miR-199-3p binding sites in the PIK3CB 3′UTR. These mutants occur within nucleotides 2–4 of each mature miR-199-3p target site. The primers containing the desired mutation, flanked with intact nucleotide sequence, were designed using the QuikChange® Primer Design Program available online (https://www.genomics.agilent.com/CollectionSubpage.aspx?PageType=ToolandSubPageType=ToolQCPDandPageID=2295), as illustrated in Table 2.14.

Primer	Sequence	Melting Temp
Mutation 1		
Forward primer	5′-AGTGGTGTTAGCATGTGCAATAGGAACTTGAGGTTTGCTGTGTAAATG-3′	78.27°C
Mutation 2		
Forward primer	5′-ATGGATGTCAGGATCCAGCAAAACTTGAGCTTTCTTCTCCAAAGAC-3′	78.13°C

Table 2.14: A list of the primer sets used for the mutation of the miR-199-3p site in the 3′UTR of PIK3CB.

The PCR reaction contained 5µl of 10x reaction buffer, 100ng of psiCHECK-PIK3CB 3′UTR template, 125ng of forward primer, 125ng of reverse primer, 1µl of dNTP mix, 1.5µl of QuikSolution reagent, 1µl of QuikChange lightning enzyme, and RNase/Dnase free water. The reaction was mixed thoroughly and amplified using the thermocycler profile as shown below.

Steps	Temperature	Time	Cycle
Initial denaturation	95ºC	2 min	1 cycle
Amplification			
Denaturation	95ºC	20 seconds	25 cycle
Annealing	78ºC	10 seconds	
Extension	68ºC	4 min	
Final extension	68ºC	5 min	1 cycle

To ensure digestion of the parental strands, 2µl of the Dpn I restriction enzyme was then added after the amplification, centrifuged for 1 min, and incubated for 5 min at 37°C. 2µl of the Dpn I treated DNA was then transformed into ultracompetent cells supplied with the kit and plated in LB agar overnight. Colonies were inoculated into LB broth medium overnight, DNA extracted by mini-prep, and sequenced.

2.5.5 Dual luciferase reporter assay

The dual luciferase system (Promega, UK) was used to measure reporter gene expression. This system relies on the use of a plasmid like psiCHECK-2 that contains two luciferase reporters: the Firefly reporter (*Photinus pyralis*) and *Renilla* gene (*Renilla reniformis).* Firefly represents the normalizing transfection control for *Renilla*, which harbours the cloned 3′UTR sequence downstream of its coding sequence. In the case of the PGL4.10 plasmid, which only carries the firefly gene, a second *Renilla* construct was included to serve as a transfection control. Dual luciferase reporter assays were performed as follows. Fibroblast cells were plated into 96 well plates at a density of $1.5x10^4$ cells per well for 48 hours, the plates were swiftly turned and flicked twice to remove the culture medium. The cells were then lysed by the addition of 50µl of 1x passive lysis buffer, after which the plates were incubated for 20 min to ensure efficient lysis of the cells. 15µl of the total cell lysates were transferred into white opaque-walled 96 well-plates, which measure the output signal (NUNC, Denmark). Detection of luminescence was performed using a Varioskan Flash Multimode Reader (Thermofisher scientific). The two automatic dispensers of the instrument were cleaned with ethanol and then ddH_2o each time prior to use. The first dispenser was primed with firefly reagent, while the second was primed with Stop and Glo reagent. Both dispensers were set to dispense 50µl per well. The plate was then shaken for 2 seconds and the luminescence measured twice at the wavelength 450–700 nm. Following this measurement, 50µl from the second dispenser primed with Stop and Glo reagent was injected into the same well to quench the firefly luciferase activity within 2 seconds. The *Renilla* luciferase signal was then read twice at wavelength area 400–600 nm. The background luciferase signal generated by the untreated cells was subtracted from the luciferase signal obtained either from the firefly or *Renilla* reporter. Relative luciferase activity was calculated by normalising the firefly luciferase value to that of the *Renilla* luciferase when PGL4.10 was used. For instances where psi-CHECK-2 vector was used, the relative luciferase activity was calculated by normalising the *Renilla* luciferase value to that of the firefly luciferase. In order to standardise the luciferase activity of samples within the same experiment set, the normalised luciferase values were divided by the value of the appropriate control sample.

2.6 Western blot analysis

2.6.1 Buffers and solutions used for protein techniques

NP-40 lysis buffer: 50 mM Tris-Cl (pH 7.5), 100 mM NaCl, 1% NP40 (IGEPAL) (Sigma). Before use, the required amount of lysis buffer was supplemented with protease inhibitors (Roche, UK) and phosphatase inhibitors (Roche, UK).

4x SDS-PAGE sample loading buffer: 50 mM Tris-Cl (pH 6.8), 12.5mM EDTA, 2% SDS, 10% glycerol, 1% β-mercaptoethanol, 0.02% bromophenol blue.

Tris-buffered saline-Tween (TBS-T): 10 mM Tris-HCl, 100 mM NaCl, 0.2% Tween-20.

10% Ammonium Persulfate (APS): 1g of APS dissolved into 10 ml ddH_2O, aliquoted and stored at -20°C.

Laemmli running buffer (10x): 30.3g Tris, 144.2g Glycine, 10g SDS dissolved in 1L ddH_2O and pH was adjusted to 8.3.

Transfer buffer (10x): 29g Tris, 144g Glycine, 3.7g SDS dissolved in 1L ddH_2O. In order to make the transfer buffer (1x), 100ml of 10x transfer buffer was added to 200ml Methanol and 700ml ddH_2O.

Blocking buffer (5%): 5g of skimmed milk powder (Cell Signaling Technology, USA) was dissolved in 100ml TBS-T solution. This was made fresh before use.

1 M Tris-HCl pH 6.8: 120g Tris dissolved in 800 ml of ddH_2O, the pH was then adjusted with HCl and the total volume made up to 1L using ddH_2O.

1.5 M Tris- HCl pH 8.8: 181g of Tris dissolved in 800 ml of ddH_2O, the pH was then adjusted with HCl and the total volume made up to 1L litre with ddH_2O.

2.6.2 Materials and supplements used in protein techniques

2.6.2.1 Primary and secondary antibodies used:

Antibody	Host	Dilution	Incubation time	Supplier
Anti B-actin (mAb)	Rabbit	1:2000	2 hours at room temperature	Cell Signaling Technology (#4967)
Anti Gapdh (mAb)	Rabbit	1:2000	2 hours at room temperature	Cell Signaling Technology (#2118)
TWIST-1 (mAb)	Mouse	1:500	4°C overnight	Abcam (ab50887)
PIK3CB (mAb)	Rabbit	1:1000	4°C overnight	Cell Signaling Technology (#3011)
ITGA6	Rabbit	1:1000	4°C overnight	Cell Signaling Technology (#3750)
AKT	Rabbit	1:1000	4°C overnight	Cell Signaling Technology (#9272)
Phospho-Akt (Ser473)	Rabbit	1:1000	4°C overnight	Cell Signaling Technology (#9271)
Phospho-Akt (Thr308)	Rabbit	1:1000	4°C overnight	Cell Signaling Technology (#9275)
Phospho-p44/41 MAPK (Erk1/2) (Thr202/Try204)	Rabbit	1:1000	4°C overnight	Cell Signaling Technology (#9101)
Anti-rabbit IgG, HRP-linked antibody	-	1:2000	2 hours at room temperature	Cell Signaling Technology (#7074)
Anti-mouse IgG, HRP-linked antibody	-	1:3000	2 hours at room temperature	Cell Signaling Technology (#7076)

Table 2.15: Primary and secondary antibodies used for Western blot analysis.

2.6.2.2 Ladder

SeeBlue® Plus2 Pre-Stained Standard, ranging in molecular weight from ~3 to 198 kDa, was purchased from Invitrogen. This was used to estimate the molecular weight of the bands of interest. Ladder was loaded at 4µl or 8µl into the small or large gels respectively.

2.6.2.3 BCA protein assay reagent

The BCA protein quantification kit was purchased from Thermo Scientific and carried out according to manufacturer's recommendations.

2.6.3 Preparation of protein extracts for western blot analysis

The cells were washed once with cold PBS before addition of cold lysis buffer containing protease and phosphatase inhibitors (100µl/well in a 6 well plate). The plates were incubated on ice and shaken for 10min before scraping and transferring contents into a sterile tube. Samples were then incubated on ice for 30 min, after which the cell lysates were cleared by centrifugation at 12,000g for 15 min at 4ºC. Supernatants were transferred to a fresh tube and kept at -20°C. The protein concentration was determined by means of a BCA (BicinChoninic Acid) protein assay kit (Thermo Scientific) that uses a plate-reader on the absorbance setting from 540-590 nm. In order to calculate the protein concentration per sample, 10µl of each cell lysate was mixed with the working reagent in a 96-well plate according to the protocols stipulated by the manufacturer. Each sample was then examined in duplicate. A set of BSA standard solutions ranging from 0 to 2000 ng/µl were set up within the same plate to generate a standard calibration curve (see an example Figure 2.4). This calibration curve was in turn used to calculate the protein concentrations of samples. The absorbance value of the negative control (the lysis buffer without cells) was subtracted from the absorbance value acquired for each protein sample. Equal volume of samples containing the desired concentration of protein (typically 10-25µg) were then resuspended in 4x SDS loading buffer and boiled at 99ºC for 5min, after which they were loaded into the prepared SDS-PAGE gel.

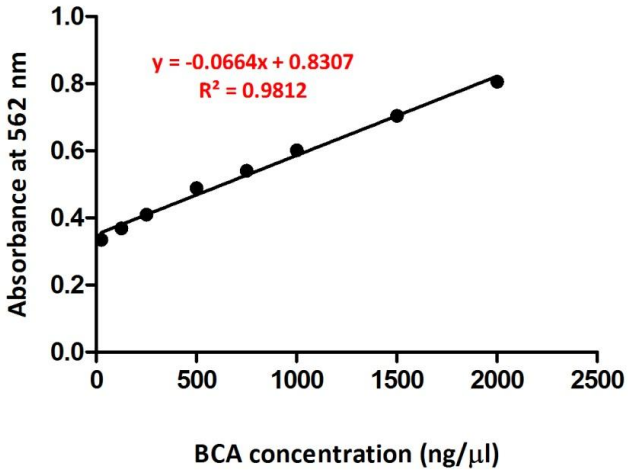

Figure 2.4: Determination of protein concentration using a BCA standard curve. Measurement of the absorbance of samples with a known concentration of diluted BSA (2000 to 125 ng/µl) was used to create the standard curve for the assessment of the protein concentration of unknown samples. In the equation, 'x' is the absorbance of the sample and y is the protein concentration.

2.6.4 Sodium dodecyl sulfate polyacrylamide gel electrophoresis (SDS-PAGE)

Gel electrophoresis was conducted on large gels using a twin vertical electrophoresis system (Galileo, Bioscience). The resolving gel (8%, 10%, 12%) was prepared with 9.9 ml H_2O, 12.0 ml 30% Acrylamide, 7.5 ml 1.5 M Tris (pH8.8), with the addition of 300µl 10% SDS, 300µl of 10% APS and 12µl of TEMED. Once the resolving gel was poured into the glass plates, it was covered with isopropanol. After polymerisation, the isopropanol was then discarded and 5% stacking gels were prepared with 6.8 ml H_2O, 1.7 ml 30% Acrylamide mix, 1.25 ml 1.0M Tris (pH 6.8), with 100µl 10% SDS, 300µl 10% APS and 10µl TEMED. The stacking gel was laid over the resolving gel and a comb was placed within the stacking gel. After polymerisation, the protein ladder and samples were loaded on the gel and electrophoresis then performed at 100-120 Volt for 2-3 hours.

2.6.5 Western blot

The resolved proteins were transferred to PVDF membranes (Millipore), using a wet transfer apparatus (Bio-Rad, UK). A PVDF membrane was soaked with methanol for 30 seconds and then equilibrated in cold transfer buffer together with the gel. Four pieces of filter paper (Whatman Ltd, UK) and two pads were also immersed in the transfer buffer, after which they were packed in the 'transfer sandwich', making sure to remove of air bubbles. The gel cassettes were placed in the apparatus and the transfer was performed at 100 Volt for 2-4 hours at 4°C. The blotted membrane was then incubated in a 5% milk blocking buffer at room temperature for 1-2 hours followed by incubation with the primary antibody (5-15 ml of 2% skimmed milk dissolved in TBS-T buffer). For antibody dilution and time of incubation, see Table 2.16). The membrane was then washed twice for 5 min each with TBS-T buffer to remove excess unbound antibodies. Incubation with the secondary HRP-conjugated antibodies took place over 2 hours, diluted in 2% skimmed milk dissolved TBS-T buffer. The membranes were washed 3 times with TBS-T buffer for 15min.

2.6.6 Enhanced Chemiluminescence (ECL) based detection

The blotted proteins were detected using the ECL Western blotting detection system (GE Healthcare, UK), according to the manufacturer's instructions. Equal volumes of the two chemiluminescent substrates were mixed together and then incubated with the blot, which has bound HRP-conjugated secondary antibodies. The chemiluminescence is based on horseradish peroxidise (HRP) catalyzing the oxidation of luminol by peroxide, resulting in light emission. The membranes were exposed to Fuji Medical X-Ray film (Fujifilm Europe GmbH) for different time periods and the films were then developed using XoGraph Compact x2 Film Processor.

2.7 Bioinformatics analysis

2.7.1 Microarray experiment and data analysis

For the microarray experiment reported in this thesis, Marie Craigon (Division of Pathway Medicine (University of Edinburgh, UK)) processed the RNA samples following a standard Affymetrix protocol and then hybridised the cDNAs to 14 GeneChip® Mouse Gene 1.0 ST Arrays. The hybridised chips produced raw probe-level data saved in CEL files. The CEL files were imported into the Partek Genomics Suite (MO, USA), where the data (background subtraction, log2 transformation, normalisation, and summarisation) was processed using of the Robust Multiarray Average (RMA) algorithms. The gene or transcript-level summarization was performed using the mean of all probes within the probeset to produce the gene or transcript level expression data for 28,853 mouse genes. In addition to the 28,853 interrogation probeset, the chip includes 6702 control probes, (5222 negative and 1480 positive). The expression data were then exported into Excel to apply a further cut-off based on the value of the median + 2*median average deviation (MAD) generated from the 5222 negative probes within each Chip. Those genes passing the cut-off criterion were re-imported into the Partek Genomics Suite software to calculate the mean values across the technical replicates (3 GeneChips for each untreated and miR-199-3p mimic samples and 4 Genechips for each RISC-free and miR-199-3p inhibitor transfected samples). The differential expression across two biological conditions was performed in Partek software using the ANOVA model and false discovery rate (FDR) multiple test correction. Annotation data for the genes were automatically obtained from Partek, which provides links to the NetAffx database (http://www.affymetrix.com/analysis/index.affy). The final expression data were exported in Excel format containing the mean normalised expression value, fold changes, corrected P values, and gene annotation. The data quality was also assessed for non-normalised and normalized expression data in Partek and Madmax. The data was visualized using boxplots, Principle Component Analysis (PCA) and sample histograms. The Partek software analysis was performed at the Division of Pathway Medicine (University of Edinburgh, UK), while the subscription to Madmax was supplied by Dr. Philip De Groot.

2.7.2 Ingenuity Pathway Analysis (IPA)

The Ingenuity Pathway Analysis program (IPA version 8.0, Ingenuity Systems Inc, California, USA. www.ingenuity.com) was utilised in order to obtain a deeper understanding of the significantly altered canonical pathways and biological functions associated with the miR-199-3p dysregulated genes that had been produced by the microarray experiment. IPA also creates networks where the uploaded differential regulated genes can be connected in either direct or indirect interactions, based on published interactions. This approach offers the advantage of highlighting unknown relationships that do not exist in the classical canonical pathways. The significance of the association between the miR-199-3p regulated genes and canonical pathways was assessed based on two measures: 1) a ratio of the number of genes from the list that are involved in a given canonical pathway divided by the total number of the genes present in this pathway; and 2) A P-value demonstrating the likelihood that the assembly of the genes in the dataset within the canonical pathway could be interpreted by random chance alone, based on right-tailed Fisher's exact test. The Fisher's exact test was also used by IPA to determine the significance of each biological function assigned to that dataset.

2.7.3 Genomatix Software Suite

2.7.3.1 Gene2Promoter

Gene2Promoter is a bioinformatic program within the Genomatix Package (http://www.genomatix.de/) that accesses or predicts the promoter sequences of all genes, as well as comparing promoter sequences across various species from flies to humans. Two characteristic features are used by Gene2Promoter to determine the putative proximal promoter regions: the detection of *over*-represented transcription factor binding sites within the sequence and the potential protein–protein interaction between these transcription factors; as well as an experimentally mapped transcriptional start region (TSR) that refers to the transcriptional start sites (TSSs) of each transcript. The experimental evidence of TSR was derived from a combination of the sequencing of the 5′ termini of the full-length cDNAs and the count of Cap Analysis Gene Expression (CAGE) tags for each individual transcript. CAGE is a technique used to profile the transcriptional starting sites by means of sequencing all

the 5′ termini of capped RNA, which are provided in CAGE Basic Databases (http://fantom3.gsc.riken.jp/) (Kawaji et al. 2006). The program then assigns a confidence level to each transcript based on the counts of CAGE tags having a minimum of 3 CAGE tags in a distance up to 3bp around the TSS (upstream or downstream). The analysis was applied using the genomatix optimised length for promoter sequence (500bp upstream from the first TSS and 100bp downstream of the last TSS).

2.7.3.2 MatInspector

Genomatix MatInspector is a program that employs a library of matrix descriptions for transcription factor binding sites in order to identify potential matches in the promoter sequences (Quandt et al. 1995; Cartharius et al. 2005). The MatInspector prediction search is based on a number of parameters by which candidate protein-binding sites can be recognised. Examples of these parameters include the default optimized matrix threshold for individual binding factor and a user-defined core and matrix similarities. The quantified values of the 'core and matrix' similarities are computed within the program based on the nucleotide weight matrices (NWM) of TF binding sites and the matches identified in the promoter sequence. The NMM designates all the possible nucleotide distributions for each individual position within the binding motif, thereby enabling the proportional quantification of the similarities. These weight matrices are present within the current MatInspector's library (Version 8.4, June 2011), which has been built using the best available research knowledge.

2.7.4 SylArray

SylArray is a computational method that can be applied to genome-wide expression data in order to determine the effect of miRNA through the search for the over- or under-represented target sequences in a sorted gene list (http://www.ebi.ac.uk/enright/sylarray) (Bartonicek and Enright 2010). SylArray uses Sylamer algorithms to assess the significance of an enriched or depleted target sequence for a given miRNA in 3′UTR sequences (Dongen et al. 2009), in addition to having a curated database for 3′UTRs in a large number of species.

2.7.5 Quantification of chemiluminescent and radioactive signals from Western and Northern blots.

GEL files produced by Phosphorimager, Typhoon and X-ray films were converted into16-bit PNG image files. These files were then imported into TotalLab Quant Software v11.4 for further analysis. First, lanes were created for all bands within a gel. Second, the average intensity of an area where no band is present on the gel is taken as the background intensity. The background subtraction method was then applied simultaneously to all bands of a gel. Third, the software quantifies the intensity of each band in the gel. Fourth, the intensity value of the target was normalised to the intensity of the loading control.

2.7.6 Statistical analysis

Standard calculations (background subtraction and normalisation) were performed in MS Excel 2007. GraphPad Prism software was used to assess statistical significances, as well as to plot the graphs (Version6; GraphPad Prism software In).

3 Regulation of miR-199a/214 Cluster Expression in CMV Infections

3.1 Introduction

3.1.1 miRNA genes

Genes that encode for miRNAs can exist within the introns or exons of annotated genes or can reside in the intergenic regions of the DNA with both sense and antisense orientations. It is believed that the sense-oriented intronic miRNAs are transcribed in parallel with the precursor messenger RNA (pre-mRNA) of their parent genes, with the result that the intronic miRNAs depend on parent gene promoters for their transcription (Bartel 2004). Consistent with this, a high degree of correlation was found between the expression profiles of miRNAs and their parent mRNAs (Baskerville and Bartel 2005). However, certain studies have also shown instances of poor correlation between intronic miRNAs and their parent gene (Baskerville and Bartel, 2005; Liang, 2007; Mi et al., 2007). Although transcript stabilities and post-transcriptional regulation may explain this poor correlation, promoter prediction studies suggest that some intronic miRNAs may be transcribed from independent promoters (Ozsolak et al., 2008; Wang et al., 2009; Monteys et al., 2010). In contrast, the antisense-oriented miRNAs and intergenic miRNAs are believed to be transcribed independent of the parent gene.

3.1.2 miR-199a/214 cluster

The miR-199a/214 cluster is an antisense-oriented miRNA cluster. Two precursor miRNAs, miR-199a-2 and miR-214 reside in a dicistronic cluster on the opposite strand of an intron (intron-14 in mouse and intron-7 in human) of the Dynamin-III (DNMIII) gene (Figure 3.1). The dicistronic cluster therefore transcribes in the opposite orientation (3′ to 5′) with respect to the DNMIII gene, which is microtubule-binding GTPase and important regulator of clathrin-mediated endocytosis (Reviewed in Hinshaw, 2000). This transcription results in a long primary transcript harbouring the two precursors, miR-199a-2 and miR-214. This primary transcript is processed into four mature miRNAs, miR-199a-3p, miR-199a-5p, miR-214-5p and miR-214-3p. miR-214-5p is expressed at a low level hence it was not studied in this work.

However, detailed analysis of the expression properties of primary transcript miR-199a/214 and its parent DNMIII gene across embryo and adult tissues showed that they were not completely identical (Loebel et al. 2005). It is also important to note that two other miR-199 isoforms, miR-199b and miR-199a-1 are encoded within the antisense strand opposite to introns of DNMI and DNMII genes, respectively. This means that miR-199 is transcribed from three different genes. At least in the human genome, miR-3154 is clustered with miR-199b in DNMI. In addition, other miRNAs are embedded within the sense strand of these genes such as the intronic miR-3120 present within DNMIII and transcribed with its parent-gene precursor mRNA (Scott et al. 2012). Also, miR-638 exists within the first intronic region of DNMII while miR-4748 is in its fifth intron. As described in the introduction, RNA Pol II transcribes most miRNA genes, suggesting the same elements directing the Pol II transcription of protein coding genes also regulate miRNA transcription (Woods et al, 2007). Furthermore, pri-miRNA transcripts have the characteristic properties of mRNAs, with 5′caps and poly(A) tails (Lee et al. 2004).

3.1.3 The transcriptional regulation of miR-199a/214 cluster

The dysregulation of miR-199a/214 expression has been shown to be associated with various biological processes and diseases (discussed below in 4.1.2). Therefore, several studies have been focused on the transcriptional regulation of this cluster. First study on the regulation of this cluster reported a correlation between the expression of the pri-miR-199a/214 transcript and the basic helix-loop-helix transcription factor TWIST-1 during mouse development (Loebel, et al. 2005). Lee et al. (2009) predicted the miR-199a/214 promoter sequence, isolated it from mouse genomic DNA, and generated a wild type and a deletion mutant promoter that lacked TWIST-1 E-box motif, which displayed a decrease in its promoter activity in fibroblast cells. The deletion was not limited to the E-box motif but was also extended to the flanking sequences (~275bp), which disrupt the interaction of other transcription factors with their sites in the promoter sequence. Knocking down TWIST-1 in mouse embryonic fibroblasts or human epithelial ovarian cancer stem cells, resulted in a reduction in the expression of miR-199-5p, miR-199-3p and miR-214 (Lee et al., 2009; Yin et al., 2010). However, a detailed comparison of expression of TWIST-1 and the pri-miR-199a/214 transcript in the mouse embryo

suggests that TWIST-1 is unlikely to be the sole regulator of expression of this primary transcript (Loebel et al. 2005). Zinc finger E-box-binding homeobox 1 (ZEB1) is another transcription factor that induce expression of miR-199a/214 cluster through a direct interaction with the E-box motif in the uterus of pregnant mice (Williams et al. 2012). As ZEB1 and TWIST-1 both bind to E-boxes and have several overlapping functions (Peinado et al. 2007), Williams et al. (2012) proposed that ZEB1 might co-ordinately induce miR-199a/214 expression (Figure 3.1). Early growth response factor-1 (EGR-1), another transcription factor, was also shown to drive the transcription of miR-199a/214 through a direct binding to its promoter in cancer cell lines (Figure 3.1) (Sakurai et al. 2011). Altered miRNA expression profile in smooth muscle cells in which the transcription factor, serum response element (SRF), is knocked down showed a decrease in the expression of miR-199-3p, miR-199-5p, and miR-214 (Park et al. 2011). In consistent with this, Zhang et al. (2011) utilised two distinct transgenic mouse models with cardiac-specific overexpression or inhibition of SRF in order to demonstrate its regulatory role over the cardiac miRNA expression. They observed that SRF regulates the expression of pri-miR-199a/214 transcript and thereby affecting its mature products (Figure 3.1). Another miRNA expression profile in signal transducer and activator of transcription 3 (STAT3)-knockout mice identified cardiac upregulation of the primary transcript and mature miR-199-5p, however, no difference in the expression of mature miR-199-3p and miR-214 were detected in these cardiomyocytes (Figure 3.1) (Haghikia et al. 2011). Recent work linked expression of miR-199a/214 cluster with the stress response. For example, the increased expression of the whole cluster was demonstrated in response to the cardiac stress (Rooij et al. 2006). One interpretation for this increase is the transcription factor SRF, which is a positive regulator of cardiac growth and failure as well as miR-199a/214 expression (Park et al. 2011; Zhang et al. 2011). Another speculation made by the authors is the existence of nuclear factor of activated T-cells (NFAT) or myocyte enhancer factor-2 or (MEF2) response elements within the promoter region of this cluster (Rooij et al. 2006). NFAT and MEFs have been shown to be involved in the transcription of several cardiac genes in response to stress stimuli (Molkentin et al. 1998; Zhang et al. 2002). In agreement with this, the work in this thesis identified five potential sites for NFAT and one site for MEF2

within the promoter sequence of miR-199a/214 based on the bioinformatic prediction of the potential transcription factor binding sites (TFBS) (3.2.5 and Appendix 4). The low expression of miR-199a/214 cluster was found to be associated with the endoplasmic reticulum (ER) stress in hepatocellular carcinoma cells and the transcription factor NF-κB contributed to the regulation of this cluster in response to ER stress (Figure 3.1) (Duan et al. 2012). In addition to the role of transcription factors in regulating the expression of miR-199a/214, the promoter of miR-199a/214 can be epigenetically modulated leading to transcriptional down-regulation or shut off. An important example of the epigenetic regulation is hypermethylation of miR-199a/214 promoter, which was demonstrated in several cancer cells (Kim et al. 2008; Cheung et al. 2011). This hypermethylation results in the transcriptional silencing of miRNA-199a/214. In ovarian cancer, reactive oxygen species (ROS), was shown to inhibit miR-199-5p repression through increasing its promoter methylation by DNA methyltransferase 1 (DNMT1) (He et al. 2012). However, He et al. (2012) has focused on miR-199-5p and has not claimed a similar inhibition in the expression of miR-199-3p and miR-214. Based on the previous data, the transcriptional regulation of miR-199a/214 is not only controlled by the expression of the transcription factors such as TWIST-1, ZEB1, EGR-1, SRF, and NF-κB, but is also subjected to modulation by epigenetic mechanisms specifically, DNA methylation,

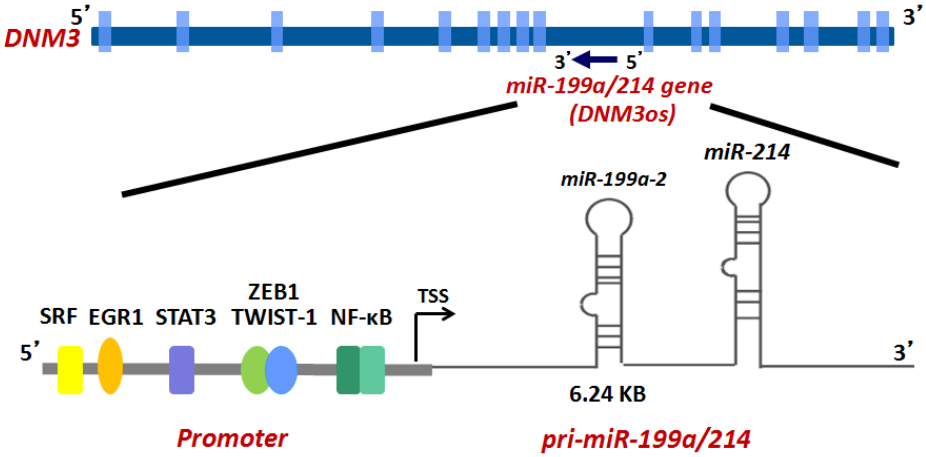

Figure 3.1: A schematic diagram of human DNM3 gene showing the complementary strand within its intron encodes a pri-miR-199a/214 transcript (DNM3os gene). The inset figure shows the pri-miR-199a/214 transcript encodes miR-199a-2 and miR-214 and those transcription factors known to regulate its promoter and drive the transcription.

3.1.4 Background and rational for studying the regulation of miR-199a/214 cluster in CMV infections

A recent report presented a global miRNA profiling of murine and human fibroblasts infected with MCMV and HCMV, respectively (Santhakumar et al. 2010). This study showed that all the mature members of the miR-199a/214 cluster (miR-199-3p, miR-199-5p, and miR-214) displayed a reduction in expression in both CMV infections at 24 hours. A functional screen of MCMV and HCMV infected cells identified two mature members of the cluster, miR-199-3p and miR-214 that exhibit antiviral properties upon the over-expression of these miRNAs in fibroblast cells. The antiviral properties of miR-199-3p reported in CMV (β-herpes viruses) extend to the other two herpes viruses subfamilies (α and γ-herpes viruses), whereas miR-214 was only shown to have antiviral properties in one subfamily (γ-herpes viruses) (Santhakumar et al. 2010). For this reason, miR-199-3p seems to have the broadest antiviral activity.

3.1.5 Aims

The work reported in this chapter investigates the molecular mechanisms involved in the down-regulation of all the mature members of the miR-199a/214 cluster during CMV infection *in vitro*. The kinetics of the down-regulation of mature miRNAs over the course of CMV infections were first examined. The expression of the pri-miRNA transcript was then measured to indicate whether the mechanism involved in the repression of mature miRNA expression during infection is transcriptional or post-transcriptional. There was also an attempt to explore cellular regulatory elements responsible for miR-199a/214 suppression during infection. The requirement of viral gene expression was also addressed with regards to regulation of the expression of the cluster.

3.2 Results

3.2.1 Kinetics of expression of the primary miR-199a/214 transcript and the mature miRNAs during MCMV infection

The expression levels of the miRNAs derived from the miR-199a/214 cluster have previously been shown to be down regulated by 24 hours post infection of cells with MCMV (Santhakumar et al. 2010). The regulation of these miRNAs during viral infection could be exerted at different levels, including transcriptional regulation, pri- or pre-miRNA processing and mature miRNA stability/turnover. Given that all mature members derived from the miR-199a/214 cluster are down-regulated, it seems likely that the regulation occurs at the primary transcript level, rather than a downstream processing step. It was therefore hypothesised that the miR-199a/214 cluster is transcriptionally regulated during infection, and this then leads to the observed reduction in mature miRNAs.

In order to test this hypothesis, the expression kinetics of both the pri-miR-199a/214 transcript and its processed mature products were examined over a time course of MCMV infection in the NIH-3T3 cell line. This cell line was used based on the following considerations: these are fibroblasts, a cell type infected *in vivo* by MCMV, they are fully permissive to MCMV infection, and miR-199-5p, miR-199-3p, and miR-214 are abundantly expressed. NIH-3T3 fibroblasts were mock infected or infected with MCMV at an MOI of 5 and total RNA was harvested at 4, 8, 12, 16, 24, 36, 48 hours post infection (hpi). The expression levels of the pri-miR-199a/214 and its mature miRNAs, miR-199-3p, miR-199-5p and miR-214, were quantified by qRT-PCR and expression levels were normalised to endogenous miR-16, as its expression is unchanged between mock infected and infected cells. The non-coding RNA U6 was also used as an additional control (Santhakumar et al. 2010). As expected, no difference was observed in miR-16 or U6 expression between uninfected or infected cells. As shown in Figure 3.2a, the levels of mature miR-199-5p, miR-199-3p, and miR-214 were reduced by 1.4 fold at 16 hpi and 3.4 fold at 48 hpi, with a steady decline in expression between these time points. For confirmation, the expression levels of the mature miR-199 and miR-214 were also examined using Northern blot analysis. The results indicated a decrease in the mature miRNAs by 16

hpi, in agreement with the results of qRT-PCR analysis (Figure 3.2b). It is important to note that the decrease in all three miRNAs showed similar kinetics, consistent with the hypothesis that viral regulation of mature miR-199a/214 is likely to be dependent on the down-regulation of the pri-miRNA transcript. In order to address this hypothesis the expression level of the pri-miRNA transcript was examined by qRT-PCR from the same samples described above. The housekeeping genes GAPDH and 18S ribosomal RNA were used as internal controls. Neither GAPDH mRNA nor 18S rRNA expression levels changed during infection. Whereas infection resulted in a 2 fold decrease in pri-miR-199a/214 expression within 4 hpi, which remained until approximately 16 hpi and further declined to give a 7 and 12 fold decrease at 24 and 48 hpi, respectively (Figure 3.2c).

In conclusion, MCMV infection causes a significant reduction in the pri-miR-199a/214 transcript, which happens earlier than the reduction in the mature miRNAs. It seems possible, therefore, that the decrease of mature miRNA occurs in response to the repression of pri-miR-199a/214 transcript. This repression in the primary transcript may result from a decrease in the rate of transcription and/or transcript degradation. To investigate the first possibility, an in silico examination of the promoter of miR-199a/214 transcript was carried out to identify transcription factors that might be involved in controlling its transcription.

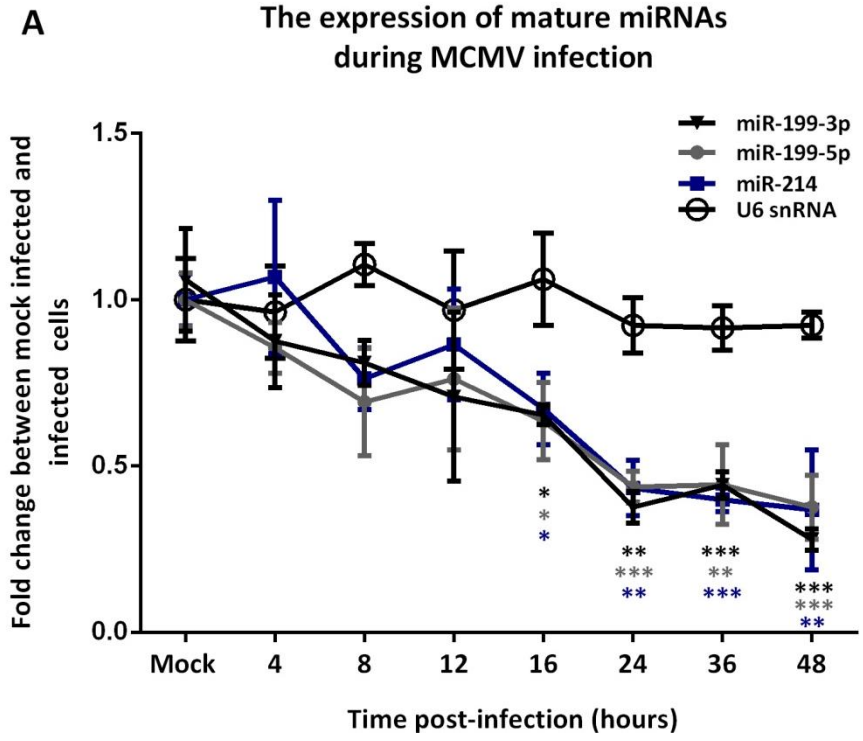
A
The expression of mature miRNAs
during MCMV infection
miR-199-3p
miR-199-5p
miR-214
U6 snRNA
Fold change between mock infected and infected cells
1.5
1.0
0.5
0.0
Mock
4
8
12
16
24
36
48
Time post-infection (hours)

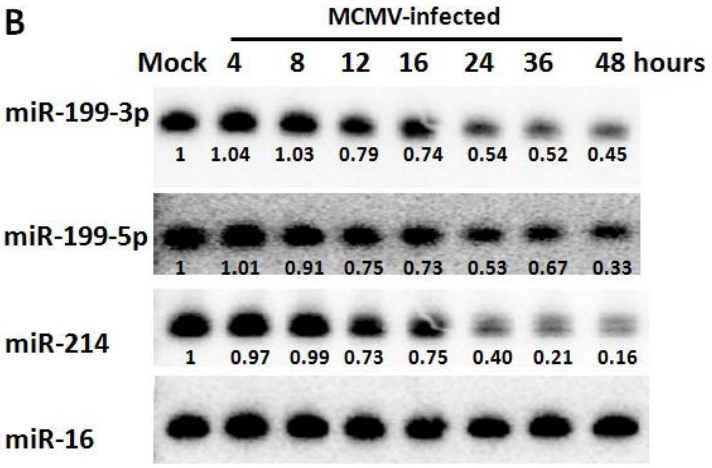
B
MCMV-infected
Mock 4 8 12 16 24 36 48 hours
miR-199-3p
1 1.04 1.03 0.79 0.74 0.54 0.52 0.45
miR-199-5p
1 1.01 0.91 0.75 0.73 0.53 0.67 0.33
miR-214
1 0.97 0.99 0.73 0.75 0.40 0.21 0.16
miR-16

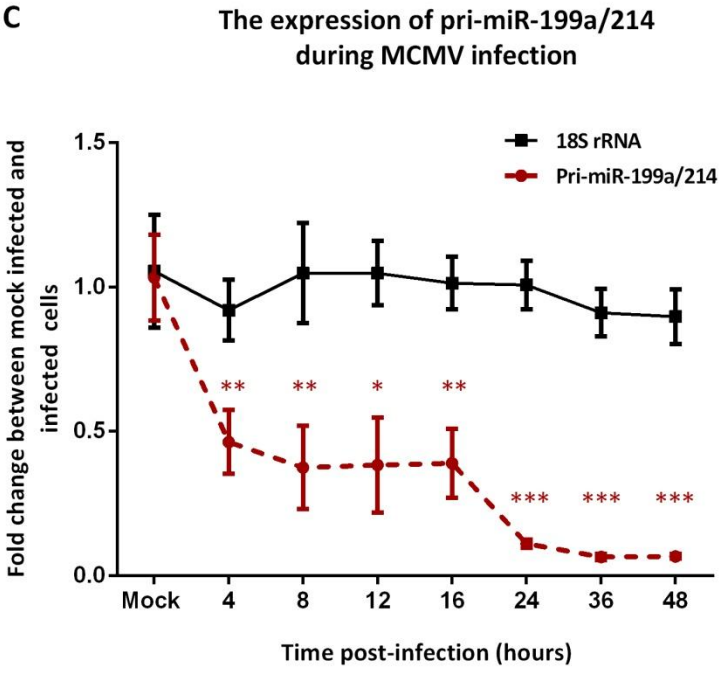
C
The expression of pri-miR-199a/214
during MCMV infection
18S rRNA
Pri-miR-199a/214
Fold change between mock infected and infected cells
1.5
1.0
0.5
0.0
Mock
4
8
12
16
24
36
48
Time post-infection (hours)

Figure 3.2: The expression kinetics of pri-miR-199a/214 and its mature miRNAs over the time course of MCMV infection. A) Down-regulation of mature miR-199-3p, miR-199-5p, and miR-214 expression in MCMV infected cells by 16 hours compared to mock infected cells. NIH-3T3 cells were mock infected or infected with MCMV at an MOI=5 for the indicated times. The expression levels of mature miRNAs were quantified by qRT-PCR and normalised to miR-16. U6 snRNA was included as a negative control. Mock infected cells from the different time points (0, 24 and 48 hours) were averaged and compared to infected cells at each time point. Data presented are the mean fold change ± S.D. of two independent experiments (n=6). *P<0.05, **P<0.01, and ***P<0.001 compared to mock infected cells as determined by a repeated measures one-way ANOVA with Sidak's post-test for multiple comparisons. B) Northern blot analysis of mature miRNAs during MCMV infection. Total RNA was harvested from NIH-3T3 cells mock infected or infected as in A. 5µg of RNA was loaded per lane and membrane was hybridised with ^{32}P-labeled probes. miR-16 probe was used as a loading control (lower panel), followed by densitometric analysis. The densitometric value for the mock infected was set as 1 and values for other time points post infection were expressed relative to the mock value. C) Down-regulation of pri-miR-199a/214 expression in MCMV infected cells by 4 hours compared to mock infected cells. Total RNA was quantified by qRT-PCR and normalized to GAPDH level. 18S rRNA was included as a negative control. Mock infected cells from the different time points were averaged and compared to infected cells at each time point. Data presented are the mean fold change ± S.D. of two independent experiments (n=6). *P<0.05, **P<0.01, and ***P<0.001 compared to mock infected cells as determined by a repeated measures one-way ANOVA with Sidak's post-test for multiple comparisons.

3.2.2 In silico sequence analysis of DNM3os proximal promoter

The results presented in the section above suggested that the expression of miR-199a/214 during MCMV infection is modulated at the transcriptional level. It is anticipated that the miR-199a/214 cluster might therefore be subject to differential regulation by specific transcription factors during infection. To identify the transcription factors potentially involved in the regulation of miR-199a/214 promoter, three lines of investigation were carried out: 1) in silico analysis for the prediction of TFs in the miR-199a/214 promoter sequence; 2) functional characterisation of the predicted promoter; and 3) examination of the promoter activity in cells infected with MCMV.

Two reports have previously documented the 5′-flanking DNA sequence upstream of the human or mouse miR-199a/214 gene (known as dynamin 3, opposite strand (DNM3os) in the National Center for Biotechnology Information (NCBI)) and considered these sequences to be bona fide promoters (Kim et al. 2008; Lee et al. 2009). However, to date, no reports have provided a detailed characterisation of either the mouse or human miR-199a/214 promoter sequence nor have they shown the minimal promoter sequence required for basal expression, transcription start site(s), conservation among species or the full set of potential transcription factor binding sites. Therefore, in order to further characterize the promoter sequence, a combination of bioinformatic and experimental strategies were used.

3.2.2.1 The murine DNM3os gene promoters

There are 8 transcripts for murine DNM3os gene annotated by Ensembl (Transcript IDs: ENSMUST00000104989, ENSMUST00000104988) and NCBI (Transcript IDs: NR_002870, AK020051, AK134411, AK053654, AK164873, AK051872) (For more details see Appendix 1). Three of these transcripts contain one or both precursor sequences of miR-199a-2 and miR-214: 1) one pri-miRNA transcript includes both pre-miR-199a and pre-miR-214; 2) two transcripts contain either pre-miR-199a or pre-miR-214; 3) an additional five distinct transcripts contain neither pre-miR-199a nor pre-miR-214 (Figure 3.3).

In order to extract the promoter sequence of DNM3os, the GeneID in NCBI (474332) was uploaded to Gene2Promoter Release 5.3 (April 2012) in the

Genomatix package, with the analysis utilising the Genomatix optimised length for promoter sequences (500bp upstream from the first TSS and 100bp downstream of the last TSS). As outlined in Appendix 1 and shown in Figure 3.3, this analysis identified four specific promoters: one upstream of the DNM3os gene and the remaining three embedded within the DNM3os genomic sequence. As the DNM3os encodes 8 distinct transcripts, promoters were designated relative to the experimentally verified TSSs of the corresponding transcripts. The evidence for these promoters was derived from a combination of existing data on 5′ termini of full-length cDNAs and the count of cap analysis gene expression tags (CAGE) (described in 2.7.3.1). The upstream promoter sequence of pri-miR-199a/214 was therefore predicted to span 696 bp, from -596 nt upstream of the first TSS to +100 nt downstream of the last of TSS. The primary transcript appears to have two alternative TSSs, each of which are supported by 2 CAGE tags. However, Genomatix states that 2 CAGE tags are insufficient to confirm the 5′ end of the transcript and the TSS(s), a crucial component in the prediction of the promoter. Therefore TSS or TSSs remain to be verified for the pri-miR-199a/214 transcript.

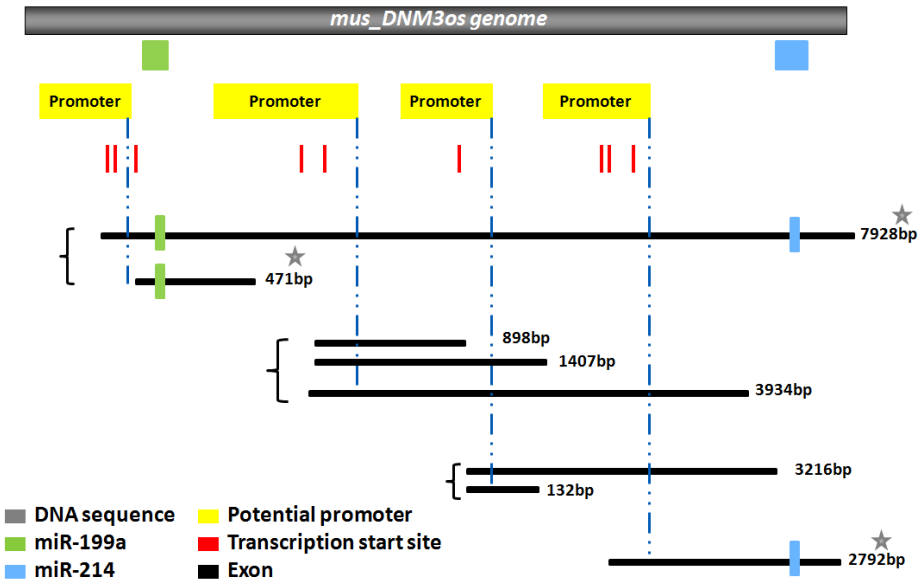

Figure 3.3: Schematic diagram of potential promoter sites for DNM3os gene. Four promoters can potentially drive the expression of eight different DNM3os transcripts (shown as yellow boxes). Each promoter was predicted relevant to the TSSs for the annotated transcripts. TSS represents the potential starts of the mapped transcripts (shown as red lines). A blue dotted line was drawn from the end of the promoter to the start of the transcripts. Only three transcripts hold both or either miR-199a and miR-214 sequence (labelled with gray stars). Adapted from http://www.genomatix.de/.

3.2.2.2 Determination of the transcription start site of the pri-miR-199a/214 transcript

In order to experimentally determine the TSS(s) of the primary transcript, primer extension analysis was used with total RNA isolated from mouse liver. Two extension primers were used; the first was 35bp downstream of the first TSS and the second oligonucleotide was 148bp and 99bp downstream of the first and second TSS, respectively. Therefore, two bands of 55bp and 168bp were expected for the first TSS and a single band of 119bp for the second TSS. Two extension products were observed: a minor product was sized at ~50 bp with the first primer and a major product at ~160bp using the second oligonucleotide primer (see Figure 3.4). These results reveal the presence of a single TSS of pri-miR-199a/214, starting from 5′-TGCAAATGTG-------3′. While the data presented herein are preliminary and therefore still require reproduction, they nevertheless support the first predicted TSS and lend confidence to the prediction of the promoter sequence.

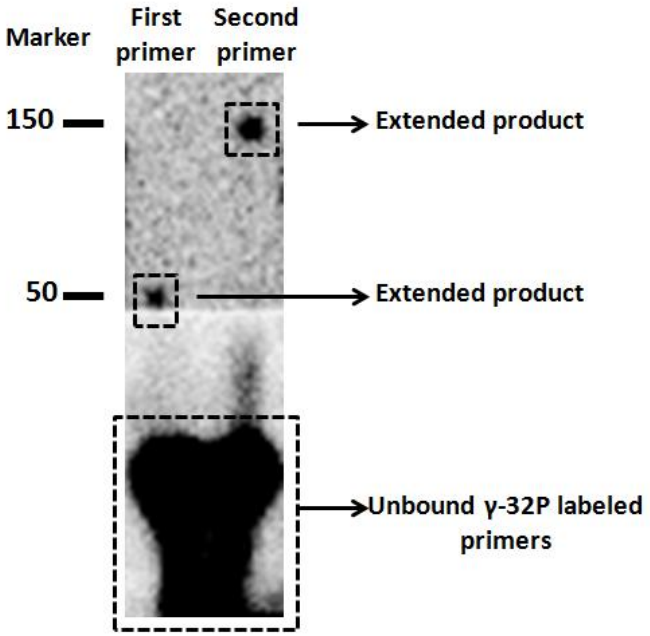

Figure 3.4: Primer extension analysis of the transcription start sites for pri-miR-199a/214 yields >50nt and >150nt long extension products. Approximately 20µg of total RNA isolated from mouse liver samples was used. Primer extension was performed using two different [γ-32P] ATP 5′-end-labeled oligonucleotides. The products were analyzed on a 15% UREA-TBE gel.

3.2.2.3 Comparative analysis of the promoter of pri-miR-199a/214 in human and mouse.

The mature miR-199-3p, miR-199-5p and miR-214 sequences are 100% conserved between mouse and human, with this cluster exhibiting the same down-modulation upon CMV infection in both species (see below 3.2.9). It seems likely that the mechanisms surrounding the transcriptional regulation of these miRNAs are also conserved. For this reason, the promoter region(s) for human DNM3os was also predicted and compared to the mouse sequence to explore conserved sites and regulatory elements.

3.2.2.3.1 In silico prediction of human DNM3os promoters

In contrast to the mouse DNM3os gene, the human DNM3os gene is annotated to encode three transcripts: 1) one transcript that contains both miR-199a-2 and miR-214 (NCBI transcript ID: NR_038397); 2) another transcript that contains only miR-199a-2 (Ensembl transcript ID ENST00000417354); and 3) a third transcript has neither miR-199 nor miR-214 (NCBI transcript ID: AK021543) (For more details see Appendix 2). As the pri-miR-199a/214 transcript is unavailable in the human genome database in the Genomatix Suite, the program will not predict its promoter sequence. Despite this, analysis was conducted on the other two transcripts of human DNM3os because the 5′ end of pri-miR-199a-2 transcript and pri-miR-199a/214 are located 5nt apart, suggesting that both transcripts may share the same promoter sequence. The predicted promoter is 601bp in length, spanning -501 to +100 relative to the TSSs, as shown in Appendix 2 and represented schematically in Figure 3.5.

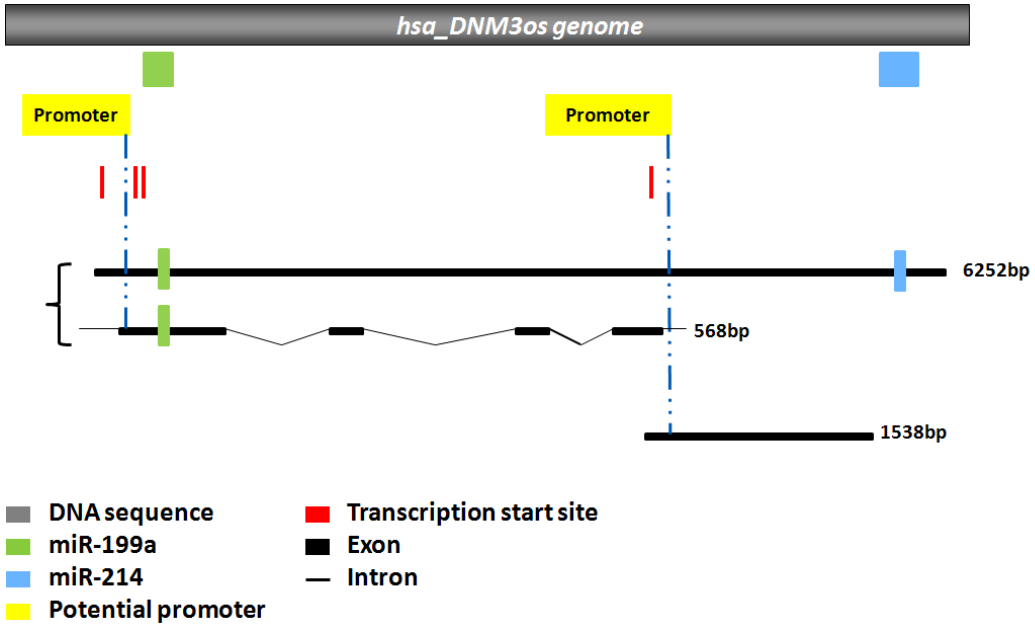

Figure 3.5: Schematic diagram of the two putative promoters of the human DNM3os gene. The promoters schematised in the figure can produce three different transcripts: one transcript includes both miR-199a and miR-214 precursors, another spliced transcript has only miR-199, and another has neither miR-199a nor miR-214. Adapted from http://www.genomatix.de/

3.2.2.3.2 Conservation of the mouse and human promoter sequences.

The predicted promoter sequences for pri-miR-199a/214 revealed a high degree of conservation between mouse and human. Nucleotide sequence from mouse: 40-591 (552 bps) and human: 5-549 (545 bps) were conserved, with 89.67% matches (495/552), 8.51% mismatches (47/552), and 1.81% gapped nucleotides (Figure 3.6 and Appendix 3).

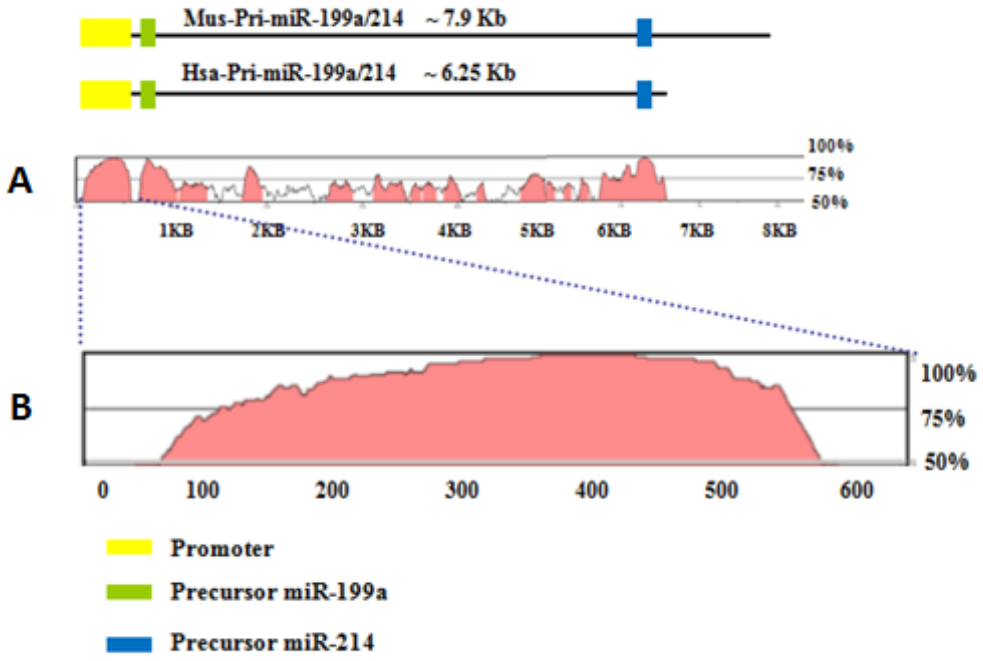

Figure 3.6: Alignment of mouse and human DNM3os gene promoter. The online software mVISTA was used to compare sequences in the mouse and human promoters. VISTA plot in A represents comparison between human and mouse DNM3os promoter and gene. The promoter region is zoomed in B to display the 600bp promoter region. The Y axis shows the percent identity ranging from 50 to 100% across the DNA genomic sequence. The X axis represents the genomic sequence. Regions having greater than 75% conservation over a minimum of 100bp are shaded.

3.2.3 Functional characterization of the murine proximal promoter of the pri-miR-199a/214 transcript

Following the in silico prediction of mouse promoter sequence (section 3.2.2), the full-length promoter sequence, consisting of a 696bp fragments, was cloned into a reporter plasmid, pGL4.10-basic to enable functional studies. This vector lacks promoter and enhancer sequences upstream of its reporter luciferase gene. In addition, several other constructs were made in parallel for comparison: one having 1000bp upstream of TSS and three deletion constructs where sequences from -421 to +100, -272, +100 and -128 to +100 were cloned.

Each reporter plasmid was co-transfected with a vector that expresses *Renilla* luciferase into NIH-3T3 cells, to enable normalisation of transfection efficiency. Cell viability post-transfection was also assessed in order to control for toxicity of the transfection procedure (in all experiments, cells were found to be >80% viable, see Figure 3.7a).

The construct containing the full-length predicted promoter (696bp) resulted in a ~15-fold increase in luciferase expression when transfected into NIH-3T3 cells, in comparison to the promoter-less vector (Figure 3.7b). Increasing the length of the promoter sequence to 1000 nucleotides upstream of the TSS did not increase the luciferase expression, which suggests that the sequence upstream of position + 596 does not contribute to the promoter activity in this cell line. The construct containing a deletion in the region −596 to -422 showed a 15.9% reduction in promoter activity compared to full-length promoter, while the construct missing the region -596 to -273 gave a 70.7% decrease in the transcriptional activity of the promoter. The shortest construct (−128/+100) showed no significant luciferase expression over the background.

These results suggest that the region spanning −596 to +100 contains the minimal promoter sequence of the pri-miR-199a/214 transcript and that the fragment (-421 to -273) is critical for the promoter activity.

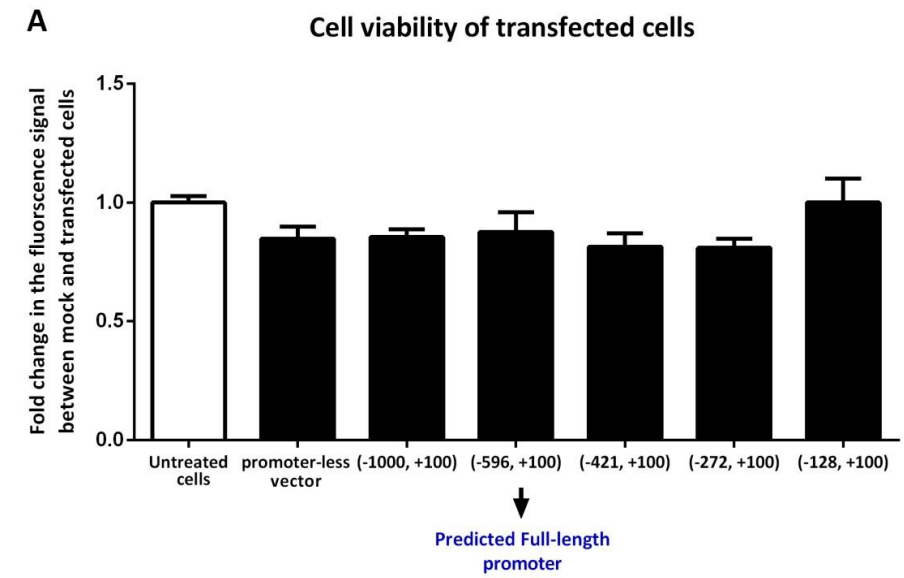
A
Cell viability of transfected cells
Fold change in the fluorscence signal between mock and transfected cells
1.5
1.0
0.5
0.0
Untreated cells
promoter-less vector
(-1000, +100)
(-596, +100)
(-421, +100)
(-272, +100)
(-128, +100)
Predicted Full-length promoter

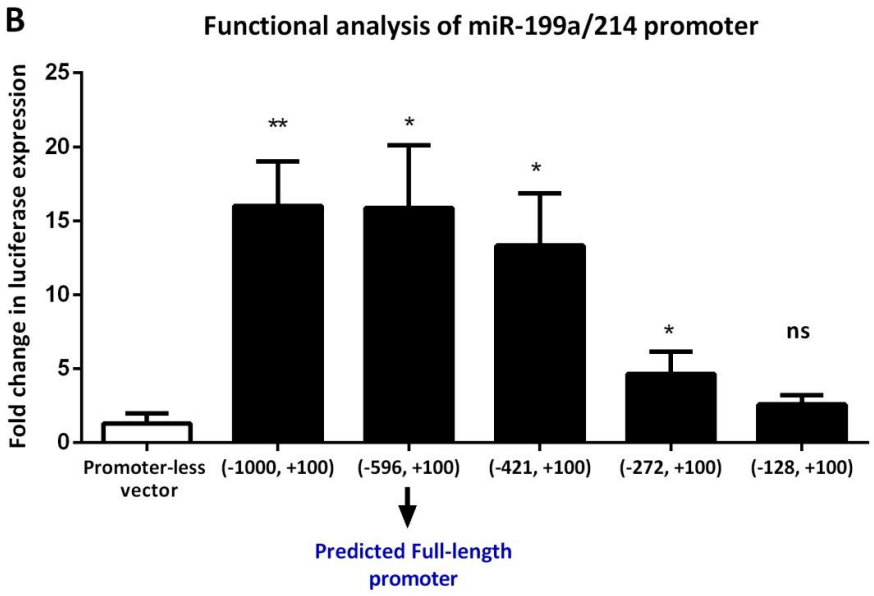
B
Functional analysis of miR-199a/214 promoter
Fold change in luciferase expression
25
20
15
10
5
0
**
*
*
*
ns
Promoter-less vector
(-1000, +100)
(-596, +100)
(-421, +100)
(-272, +100)
(-128, +100)
Predicted Full-length promoter

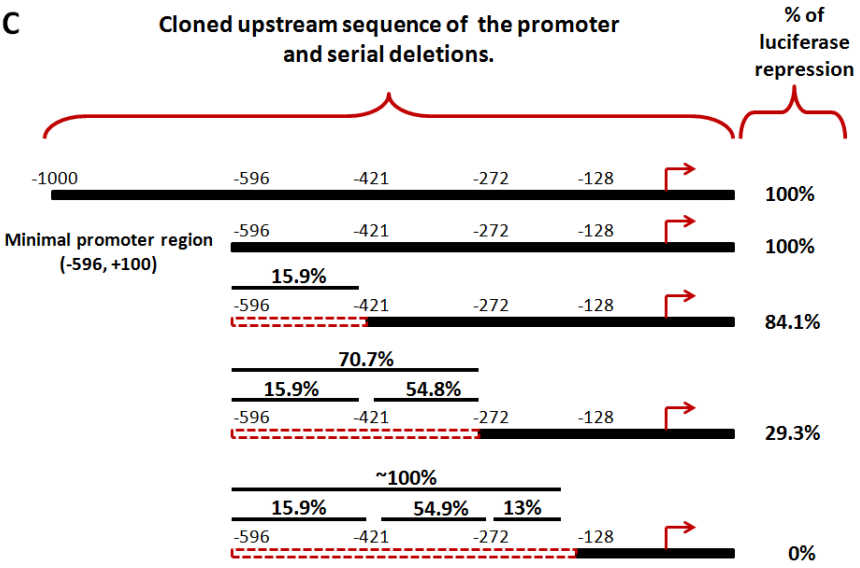
C
Cloned upstream sequence of the promoter and serial deletions.
% of luciferase repression
-1000
-596
-421
-272
-128
100%
Minimal promoter region (-596, +100)
100%
15.9%
84.1%
70.7%
15.9%
54.8%
29.3%
~100%
15.9%
54.9%
13%
0%

Figure 3.7: Effect of serial 5′-deletions of the mouse pri-miR-199a/214 promoter on its transcriptional activity. A) Effect of transfection on NIH-3T3 cell viability. NIH-3T3 cells were transfected with 1100bp, 696 (full length), or 3 sequential deletions of the pri-miR-199a/214 promoter sequence for 48 hours. Cell viability was determined based on the cell titre blue assay. The background fluorescence of the culture medium was subtracted from the fluorescence values of the untreated and transfected cells. Data presented are the mean fold change ± S.D. of two independent experiments (n=8). No significance compared to untreated cells as determined by unpaired Student's *t* test. B) The functional analysis of miR-199a/214 promoter. The promoter constructs was transfected as in A. The promoter activity was measured as the firefly luciferase values, which were normalised to *Renilla* luciferase from the co-transfected vector. The firefly/*Renilla* ratio for promoter constructs was compared to the promoter-less vector ratio. Data presented are the mean fold change ± S.D. of three independent experiments (n=12). *P<0.05 and **P<0.01 compared to promoter-less vector as determined by unpaired Student's *t* test. C) Schematic diagram of the promoter sequence with quantification of the contribution of different fragments to promoter activity. The full-length promoter (-596, +100) was set to 100%. The red-dashed bars show the deleted sequence from the promoter. The percentage of contribution was evaluated based on the data obtained from B.

3.2.4 MCMV infection suppresses the transcriptional activity of the miR-199a/214 promoter in fibroblasts.

Based on the inhibition of pri-miR-199a/214 expression upon MCMV infection (results in section 3.2.1), it was anticipated that MCMV may inhibit transcription of the pri-miR-199a/214. In silico analysis and functional characterisation of the miR-199a/214 promoter as described above (3.2.2 and 3.2.3) identified the minimal promoter sequence and a fragment critical for promoter activity. It was therefore important to test the effect of MCMV infection on the promoter construct.

NIH-3T3 cells were transfected with the luciferase reporter vector that contains the full length promoter sequence (-596, + 100) of miR-199a/214 (described above). Cells were either mock infected or infected with MCMV at an MOI of 5. At the indicated time points post infection the cells were lysed and luminescence measured. As shown in Figure 3.8, a significant down-regulation of promoter activity occurred by 4 hours post infection, which then steadily decreased until 48 hours post infection (~15 fold repression).

To summarise, these data provide evidence that MCMV infection reduces miR-199a/214 proximal promoter activity, which correlates with the down regulation of the pri-miR-199a/214 transcript.

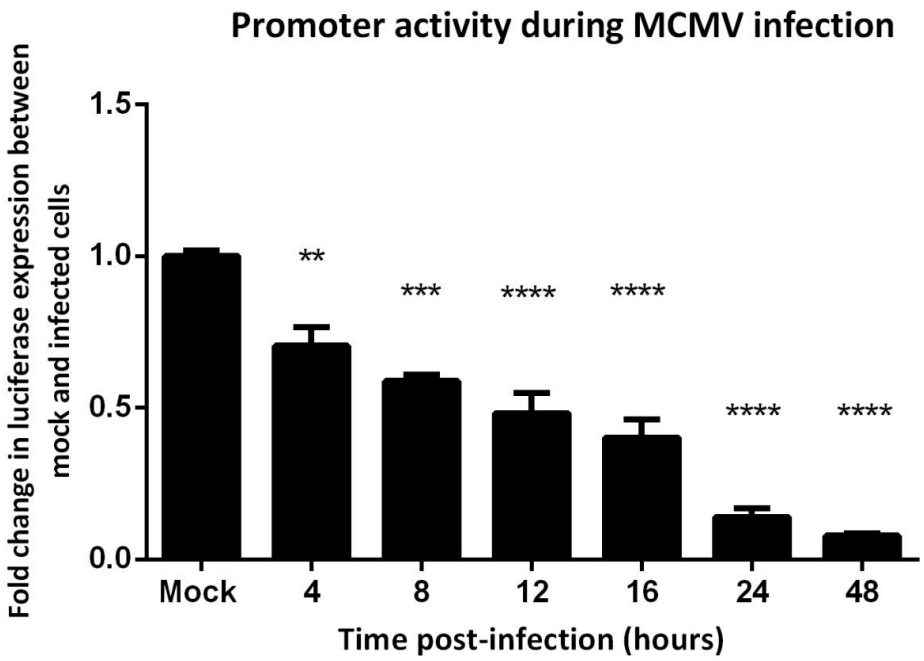

Figure 3.8: Effect of MCMV on the promoter activity of miR-199a/214. NIH-3T3 cells were transfected with full-length promoter construct (-596, +100) for 48 hours. Cells were mock infected or infected with MCMV at an MOI=5 for the indicated times. The promoter activity was measured as the firefly luciferase values, which were normalised to *Renilla* luciferase from the co-transfected vector. The firefly/*Renilla* ratio for promoter constructs was compared to the promoter-less vector ratio. Data presented are the mean fold change ± S.D. (n=5) and are representative of three independent experiments. **P<0.01, ***P<0.001, and ****P<0.0001 compared to mock infected ratios in each time point as determined by a repeated measures two-way ANOVA with Sidak's post-test for multiple comparisons.

3.2.5 Analysis of conserved regulatory elements in the proximal promoter of miR-199a/214.

Results presented in the previous section (3.2.4) demonstrated that MCMV infection suppresses the promoter activity of the pri-miR-199a/214 transcript. To examine whether this regulation occurs via specific cellular transcription factors a bioinformatic approach was used. 'Genomatix MatInspector' software was applied to define the potential transcription factor binding sites within the murine miR-199a/214 promoter. The MatInspector similarity parameters were set to >0.90 for the core and >0.85 for the matrix, whereas the optimized matrix threshold was left at the default level (the parameters are described in 2.7.3.2).

A total of 95 putative binding sites were predicted that corresponded to 59 families of transcription factors in either strand of the miR-199a/214 promoter sequence (Appendix 4), most transcription factor binding sites can occur in both orientations in a promoter or enhancer sequence. Conservation between mouse and human sequences was applied as a further filter criterion to the murine transcription-factor binding sites. Of the 95 putative sites, 53 were conserved between mouse and human miR-199a/214 promoters (Appendix 5). Given that the previous analysis of deletion constructs (3.2.3) had demonstrated the sequence from -421 to -273 as being critically important for miR-199a/214 promoter function, it was expected that the crucial transcription sites would be localised within this fragment. A total of 11 conserved sites assigned to 9 families of transcription factors (NFAT, SRF, ETS, FKHD, CIZF, RUSH, PLZF, OCT1, and HOMF) were found between nucleotides -421 and -273. Four of these families, RUSH, PLZF, OCT1 and HOMF were excluded as their expression was not detected in the microarray analysis of global gene expression in murine NIH-3T3 cells (described in Chapter 4 section 4.2). The remaining five conserved transcription factor families were predicted to bind to seven sites within -421 to -273 promoter sequence, which denote two sites for both NFAT and SRF, with a single site for each of ETS, FKHD, and CIZF.

As discussed above in 3.1.3, the knockdown of TWIST-1 and SRF have been shown to suppress the pri-miR-199a/214 and subsequent production of miR-199a/214 cluster. The data presented here identifying conserved sites for some of these TF

within the apparently critical fragment of 421 to -273 of the full-length promoter appears to be in agreement with these reports.

3.2.5.1 Identification of Putative SRE within the miR-199a/214 promoter

As illustrated in Figure 3.9, two SRF recognition sites (CArG boxes) and a DNA-binding ETS-domain (5'-GGAA-3′) were identified between -322 and -288 of the miR-199a/214 promoter. Serum response element (SRE) is defined as containing two sites for SRF, in addition to a site for a transcription factor from the ETS family, specifically the ternary complex factors (TCF) subclass. SRF is known to interact with TCFs, which include three main ETS-transcription factors: ELK-1, ELK-3 (NET/ERP/ SAP-2), and ELK-4 (SAP-1). Thus, the promoter sequence that confers the highest transcriptional activity (-421, -273) contains a potential SRE element, that includes ELK and SRF sites.

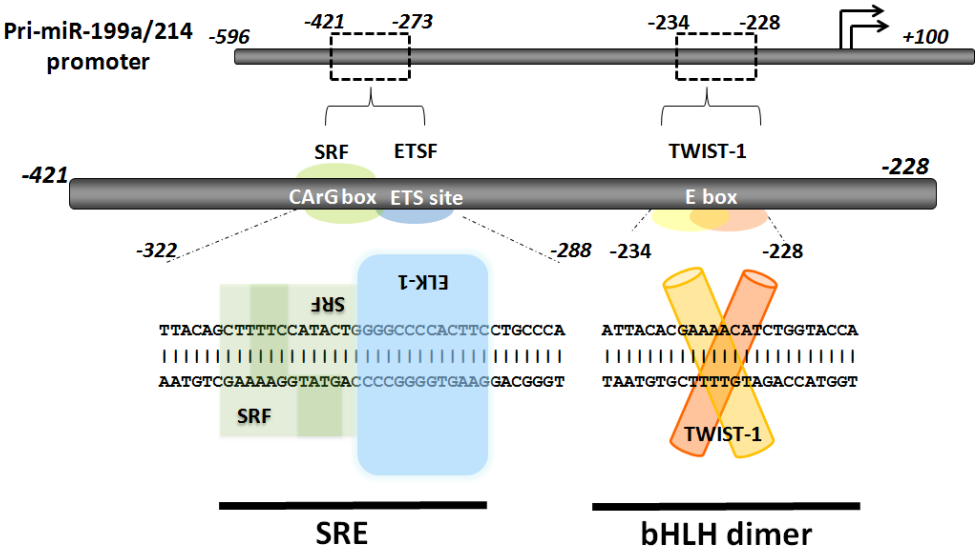

Figure 3.9: Schematic diagram of the serum response element (SRE) and TWIST-1 transcription factor located at -421 to -273 and -234 to -228, respectively, relative to the transcription start site. Conserved transcription factor sites, SRF, ETSF, and TWIST-1 were predicted by MatInspector. Zoomed view of -322 to -288 shows the potential serum response element (SRE), which is composed of two overlapping CArG motifs for SRF and a site for Ets protein. A site for SRF at -316 and another for ETS at -300 are within the opposite strand, where the primary transcript encoded. Zoomed view of -234 to -228 shows the TWIST-1-family basic helix-loop-helix (bHLH) transcription factors.

The detailed analysis of the miR-199a/214 promoter suggests that the region spanning nucleotides from -421 to -273 from the TSS is important for the regulation of this miRNA cluster. Analysis of the sequence in this region revealed potential SRF and ELK-1 sites. To examine whether these TFs regulate miR-199a/214, the promoter activity of the miR-199a/214 locus and expression levels of the mature miRNAs were examined in cells in which SRF and ELK-1 were knocked-down using specific siRNAs. TWIST-1 and STAT3 were included as controls in these experiments, as TWIST-1 siRNA has been shown to down-modulate pri-miR-199a/214 expression and STAT3 siRNA has been reported to up-regulate the promoter of miR-199a (Haghikia et al. 2011; Lee et al. 2009).

3.2.5.2 SRF and ELK-1 siRNAs interfere with the transcriptional regulation of miR-199a/214 promoter

To investigate whether knocking down SRF or ELK-1 affects the promoter activity of miR-199a/214, it was important to first assess the silencing efficiencies of the siRNAs in these experiments. NIH-3T3 cells were transfected with negative control siRNA (RISC-free siRNA), TWIST-1, STAT3, SRF, or ELK-1 siRNAs for 48 hours. Total RNA was then isolated from the transfected cells to measure the expression level of each target mRNA using qRT-PCR analysis. The expression levels of TWIST-1, STAT3, SRF, and ELK-1 were normalised to GAPDH expression and the quantification of knockdown was based on comparison to cells transfected with the control siRNA.

The data showed 65%, 53%, 63%, and 57% silencing efficiency at the mRNA level for TWIST-1, STAT3, SRF, and ELK-1 mRNA, respectively. In addition, no obvious change was observed in the expression of these mRNAs between RISC-free siRNA treated samples and untreated samples, indicating that any observed difference was specific to the siRNA rather than the transfection procedure (Figure 3.10a).

After confirming knockdown of these genes, the miR-199a/214 promoter activity was measured in cells in which TWIST-1, STAT3, SRF, or ELK-1 were knocked down. NIH-3T3 cells were co-transfected with a specific-target siRNA or control siRNA and one of the following: 1) the promoter-less vector; 2) the full-length

promoter (-596,+100) vector; or 3) the truncated promoter vector (-128,+100). The truncated promoter construct was used as a control to ensure that the results were not due to sequences present in the backbone of the plasmid. In addition, the viability of NIH-3T3 cells was monitored at 48 hours post transfection (>80% of cells were viable under all conditions) (Figure 3.10b). There was 12 fold induction of luciferase expression driven by the full-length promoter of miR-199a/214 in cells transfected with control siRNA (Figure 3.10c). The luciferase expression was used as a baseline (100% activity) for comparison of the promoter activities in cells where each transcription factor was knocked down. As shown in Figure 3.10c, knock-down of TWIST-1 resulted in a 55% repression in promoter activity. There was no observed change in the luciferase expression in cells where STAT3 was knocked down, in contrast to prior observations reporting upregulation (Haghikia et al. 2011). Luciferase expression in cells transfected with SRF or ELK-1 siRNAs showed significant 2.3 and 4 fold decreases, respectively.

Furthermore, the short promoter construct (-128, +100) showed the least expression of luciferase signal (~2 fold) in cells transfected with control siRNA and no significant change in this construct was observed across all the samples treated with TWIST-1, STAT3, SRF, or ELK-1 siRNAs. This suggests that the observed reduction in promoter activity when knocking down SRF and ELK-1 involves elements in the region between -596 and -129 upstream the start site.

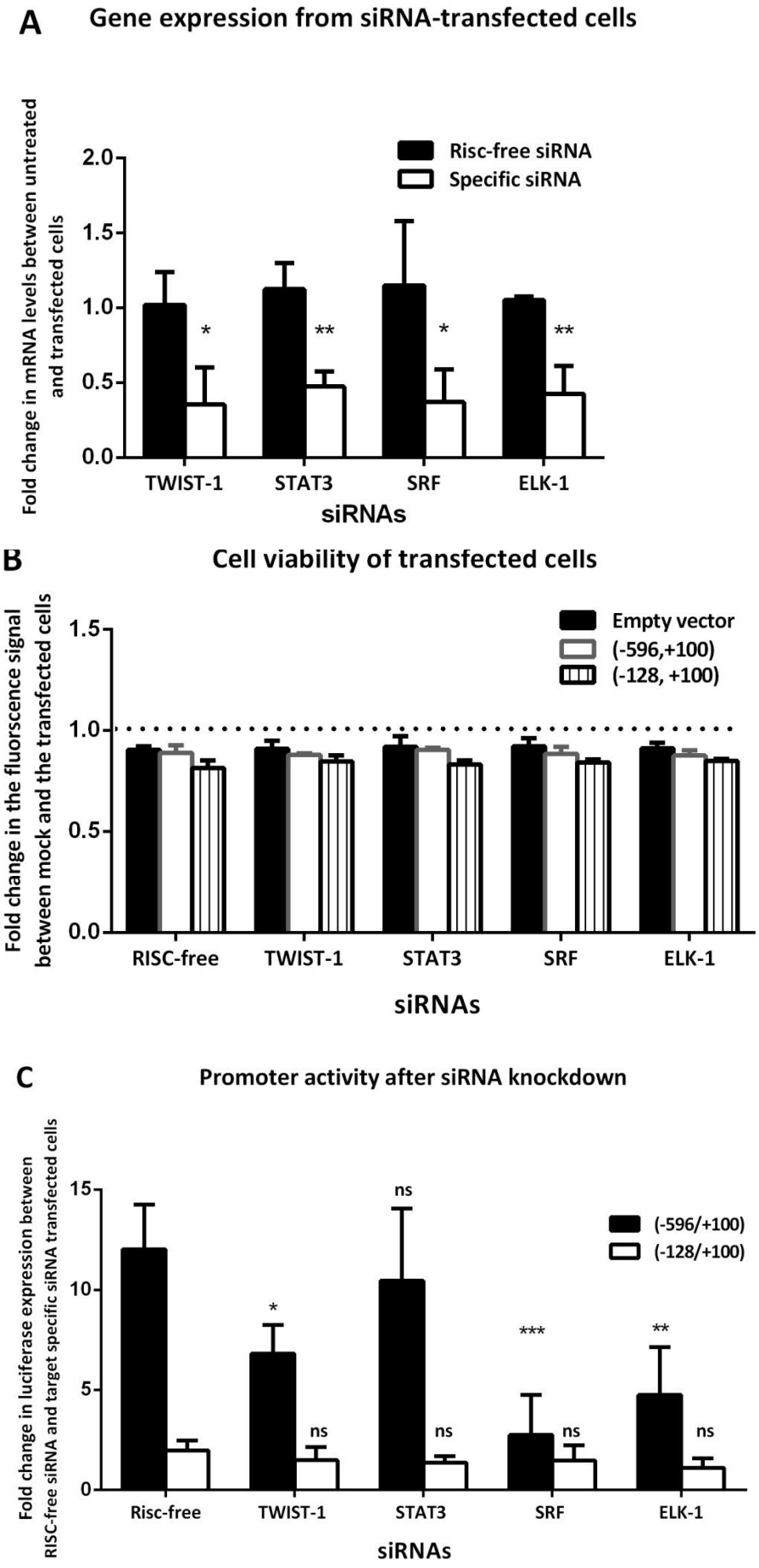
A
Gene expression from siRNA-transfected cells
Fold change in mRNA levels between untreated and transfected cells
Risc-free siRNA
Specific siRNA
2.0
1.5
1.0
0.5
0.0
*
**
*
**
TWIST-1
STAT3
SRF
ELK-1
siRNAs
B
Cell viability of transfected cells
Fold change in the fluorscence signal between mock and the transfected cells
Empty vector
(-596,+100)
(-128, +100)
1.5
1.0
0.5
0.0
RISC-free
TWIST-1
STAT3
SRF
ELK-1
siRNAs
C
Promoter activity after siRNA knockdown
Fold change in luciferase expression between RISC-free siRNA and target specific siRNA transfected cells
(-596/+100)
(-128/+100)
15
10
5
0
ns
*
***
**
ns
ns
ns
ns
Risc-free
TWIST-1
STAT3
SRF
ELK-1
siRNAs

Figure 3.10: TWIST-1, SRF and ELK-1 regulate miR-199a/214 promoter activity. A) The silencing efficiency of TWIST-1, STAT3, SRF, and ELK-1 siRNAs. NIH-3T3 cells were untreated or transfected with 25nM of each siRNA and control RISC-free siRNA for 48 hours. The expression levels of TWIST-1, STAT3, SRF, and ELK-1 were quantified by qRT-PCR and normalised to GAPDH. Data presented are the mean fold change ± S.D. (n=3) and are representative of two independent experiments. *P<0.05 and **P<0.01 compared to untreated cells as determined by two-tailed Student's t test. B) Effect of transfection on NIH-3T3 cell viability. NIH-3T3 cells were transfected with control RISC-free siRNA or specific siRNA along with one of promoter constructs, full-length promoter (-596, +100) and the deletion construct (-128, +100) for 48 hours. Cell viability was determined based on the cell titre blue assay. The background fluorescence of the culture medium was subtracted from the fluorescence values of the untreated and transfected cells. Data presented are the mean fold change ± S.D. of two independent experiments (n=8). No significance compared to untreated cells as determined by unpaired Student's *t* test. C) Reduction in the miR-199a/214 promoter activity in cells transfected with SRF, ELK-1, and TWIST-1 siRNA. The cells were transfected as in B. The promoter activity was measured as the firefly luciferase values, which were normalised to *Renilla* luciferase from the co-transfected vector. The firefly/*Renilla* ratio for promoter constructs was compared to the promoter-less vector ratio. Data presented are the mean fold change ± S.D. (n=4) and are representative of 3 independent experiments. *P<0.05, **P<0.01, and ***P<0.001 compared to RISC-free siRNA transfected cells as determined by two-tailed Student's *t* test.

3.2.5.3 Inhibition of miR-199a and miR-214 expression by SRF and ELK-1 siRNAs

The next step was to examine whether the silencing of SRF and ELK-1 could decrease the expression of mature miRNAs. Expression levels of miR-199-5p, miR-199-3p and miR-214 were determined by northern blot and qRT-PCR using samples collected under knock-down conditions. For all three members of the miR-199a/214 cluster, a significant reduction in expression level (~2.5 fold) was observed in the SRF or ELK-1 siRNA treated samples (Figure 3.11a).

It was previously reported that knockdown of TWIST-1 suppresses miR-199-5p, miR-199-3p and miR-214 expression levels (Lee et al. 2009) and the results presented here are consistent with this (Figure 3.11a). In this experiment, knockdown of STAT3 had no significant effect on the expression levels of miR-199-3p or miR-214 and did not affect the promoter activity of the primary transcript. This is in contrast to a previous report, which showed induction in promoter activity and miR-199-5p expression (Haghikia et al. 2011). The northern blot results corroborate the qRT-PCR data for TWIST-1, STAT3 and SRF, however, knockdown of ELK-1 did not result in a significant change in the miRNA expression levels in northern blots, whereas a 2.5 fold reduction was observed by qRT-PCR. However, these results should be repeated as it noted that the loading of the RNA assessed by the control probe, miR-16 was not consistent in northern blots (Figure 3.11b).

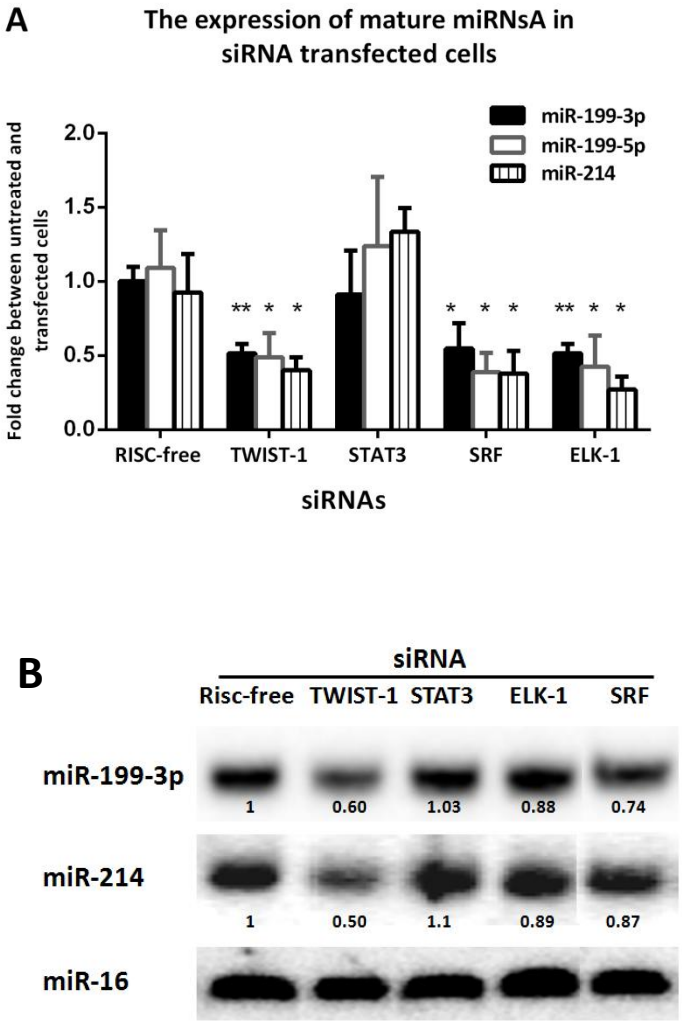

Figure 3.11: Regulation of mature miRNAs, miR-199-3p, miR-199-5p, and miR-214 by TWIST-1, SRF, and ELK-1. A) NIH-3T3 cells were transfected with either RISC-free control, TWIST-1, STAT3, SRF, or ELK-1 for 48 hours. The expression level of mature miRNAs was quantified by qRT-PCR and normalised to miR-16. Data presented are the mean fold change ± S.D. (n=3) and are a representative experiment (out of two independent experiments). *P<0.05 and **P<0.01 compared to untreated cells as determined by two-tailed Student's *t* test. B) Northern blot analysis of miR-199-3p and miR-214 in cells transfected with TWIST-1, STAT3, SRF, ELK-1 or RISC-free siRNA. Total RNA was harvested from transfected cells as in A. 5µg of RNA was loaded per lane and membrane was hybridised with ^{32}P-labeled probes. miR-16 probe was used as a loading control (lower panel), followed by densitometric analysis. The densitometric value for the RISC-free transfected cells was set as 1 and values for other transfected cells were expressed relative to the mock value.

3.2.6 TWIST-1 regulates miR-199a/214 expression and is reduced in MCMV infection

3.2.6.1 TWIST-1 mRNA and protein are down-regulated upon MCMV infection

The data presented above suggests that TWIST-1, SRF, and ELK-1 regulate miR-199a/214 expression by controlling its promoter activity. To determine whether the down-regulation of miR-199a/214 caused by MCMV involves TWIST-1, its expression was examined in uninfected and infected cells.

NIH-3T3 cells were mock infected or infected with MCMV at a MOI of 5. RNA was then harvested at various time points post infection and qRT-PCR used to determine the kinetics of TWIST-1 mRNA expression over the time-course of MCMV infection.

As shown in Figure 3.12a, there is no significant change in the expression of TWIST-1 mRNA up to 16 hpi. However, by 24 and 48 hpi, there is a 2 fold and 3.5 fold decreases in the mRNA level. In comparison to the level of TWIST-1 mRNA in infected cells at 24 hours, a significant 3 fold increase in the TWIST-1 level was noted in the mock infected cells at 48 hours. This correlated with 2 fold increase in the expression levels of primary transcript and mature miR-199-5p, miR-199-3p, and miR-214 at 48 hours, supporting the assertion that miR-199a/214 responds to the expression of TWIST-1 (Figure 3.12b). The protein level of TWIST-1 was then examined at 24, 48, and 72 hpi under the same conditions. Based on western blot analysis, a decrease in TWIST-1 protein in infected cells was observed at 48 and 72 hpi, while no decrease was detected at 24 hpi (Figure. 3.13a). In mock infected cells, a substantial increase was observed in the protein level of TWIST-1 at 48 and 72 hours by comparison with that seen at 24 hours.

To determine whether the observed increase in TWIST-1 in mock infected cells over time is a natural phenomenon of cultured cells it was important to test certain conditions, including cell densities and the effect of serum in the media. Cells were seeded in media supplemented with the same concentration of serum at various densities ($3x10^5$, $2x10^5$, $1x10^5$, and $0.5x10^5$) per well in 6-well plates and allowed to

grow to higher densities for 24 and 48 hours. As can be seen in Figure 3.13b, TWIST-1 expression is reduced at lower seeding densities. No difference in TWIST-1 expression was detected in NIH-3T3 cultured in media with or without 10% calf serum. TWIST-1 expression also increases from 24 to 48 hours post seeding, as NIH-3T3 cells became more confluent. This was clear in wells seeded with $2x10^5$ and $1x10^5$ cells/well, but was not clear at $3x10^5$ cells/well possibly due to the saturation of TWIST-1 signal on the blot film.

In conclusion, the level of TWIST-1 mRNA decreases by 24 hpi with MCMV infection, while its protein level remains unaffected at 24 hpi but is reduced at 48 hpi. Initial studies on the relationship between TWIST-1 and cell confluency suggests that TWIST-1 expression, and thereby miR-199a/214 expression, may be linked to proliferation, cell-cell contact or contact of cells with extracellular matrix.

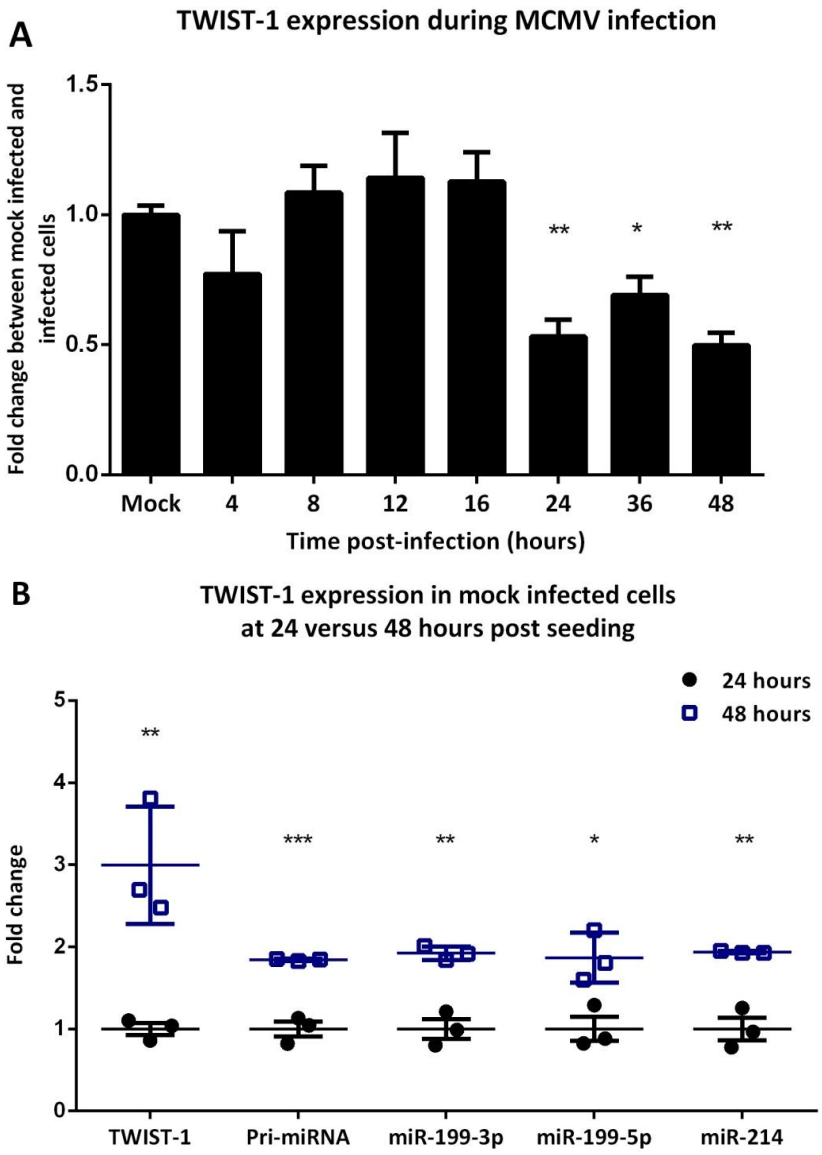

Figure 3.12: The expression of TWIST-1 mRNA during MCMV infection. A) Down-regulation of TWIST-1 expression in MCMV infected cells by 24 hours compared to mock infected cells. NIH-3T3 cells were mock infected or infected with MCMV at an MOI=5 for the indicated times. The expression level of TWIST-1 mRNA was quantified by qRT-PCR and normalised to GAPDH. Mock infected cells from the different time points were averaged and compared to infected cells at each time point. Data presented are the mean fold change ± S.D. of two independent experiments (n=6). *P<0.05 and **P<0.01 compared to mock infected cells as determined by a repeated measures one-way ANOVA with Sidak's post-test for multiple comparisons. B) The correlation between the expression of TWIST-1 mRNA and the pri-miRNA transcript and mature miR-199-3p, miR-199-5p, and miR-214, in mock infected cells at 48 hours versus 24 hours. The expression levels were quantified by qRT-PCR and normalised to GAPDH (in case of TWIST-1 and pri-miR-199a/214) or miR-16 (in case of mature miRNAs). Data presented are the mean fold change ± S.D. and are representative of two independent experiments.*$p < 0.05$, **$p < 0.01$ and ***, $p < 0.001$ compared to cells at 24 hours as determined by two-tailed Student's *t* test.

.

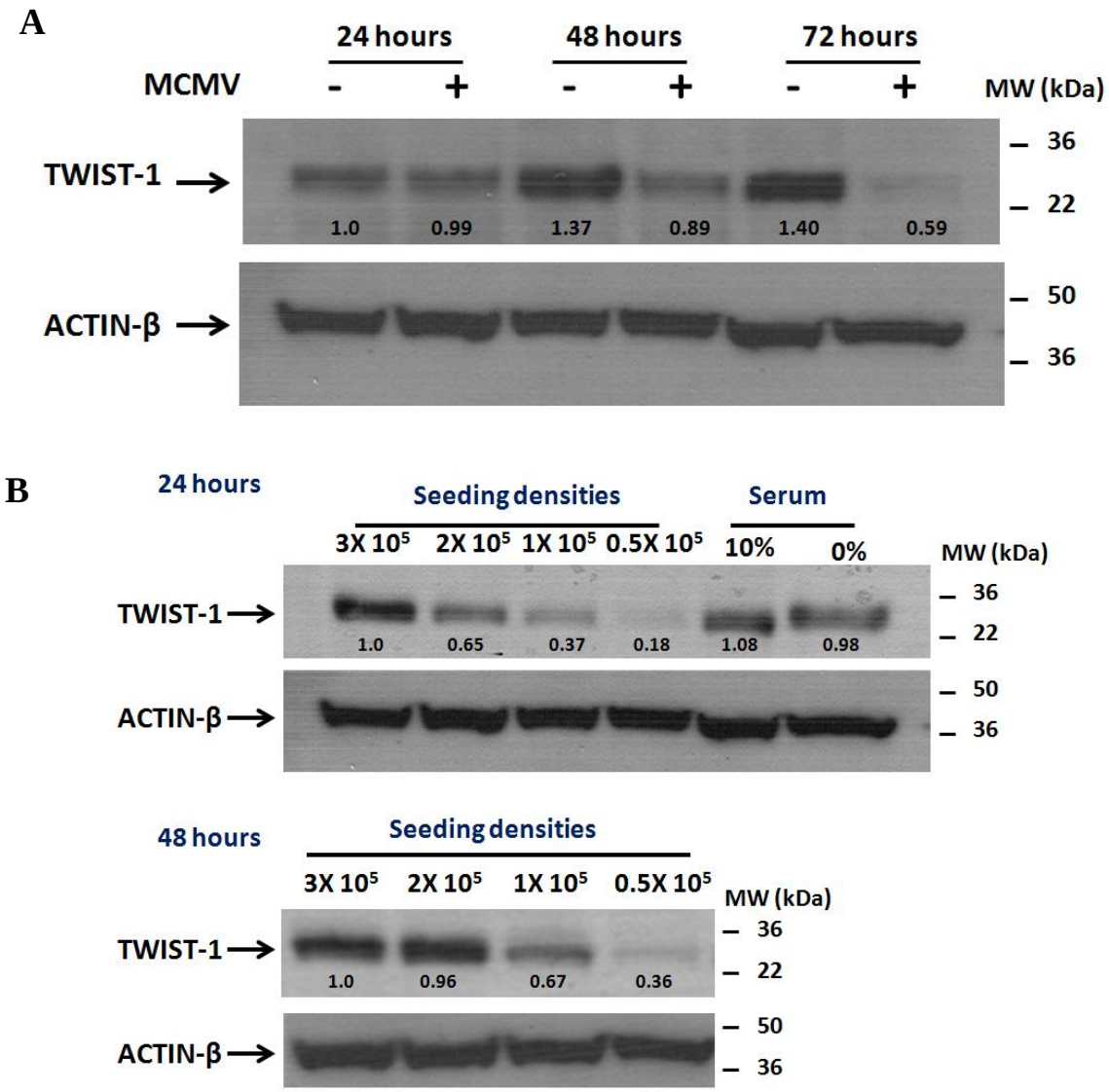

Figure 3.13: The expression of TWIST-1 protein in MCMV infected cells. A) Western blot showing reduction in TWIST-1 at 48 and 72 hours post MCMV infection. Whole cell lysates were harvested from NIH-3T3 cells mock infected or infected with MCMV at an MOI of 5 for the indicated times. 20µg of protein was loaded per lane and membrane was immunoblotted with primary antibodies against either TWIST-1 or β-ACTIN as a loading control. Blots were then quantified by densitometry and normalized to the corresponding β-ACTIN. The mock infected at 24 hours was set as 1 and values for other time points were expressed relative to this mock value. B) Western blot showing the expression of TWIST-1 in different densities or in serum-free medium. Cells were seeded either in various densities for 24 and 48 hours or in 10% serum and serum-free media. 20µg of cell lysates was loaded per lane and membrane was immunoblotted with primary antibodies against either TWIST-1 or β-ACTIN as a loading control. Blots were then quantified by densitometry and normalized to the corresponding β-ACTIN. Cells at density of $3x10^5$ were set as 1 and values for cells with other densities or those grown in 10% serum or serum-free media were expressed relative to $3x10^5$ value.

3.2.6.2 MCMV infection may regulate the expression of miR-199a/214 through TWIST-1 at 24 hours

While the data presented above demonstrates the novel link between MCMV infection and TWIST-1 expression, the down-regulation of TWIST-1 expression at 48 hours does not correlate with the down-regulation of the primary transcript that occurs much earlier by 4 hpi. This could suggest another transcription factor(s) is involved. However, it is possible that TWIST-1 is still involved, but its activity, rather than expression level, is regulated. For example, it is known that efficient binding of TWIST-1 to DNA requires phosphorylation and dimerisation with another basic helix-loop-helix (bHLH) transcription factor. A rapid disruption in TWIST-1 activity could occur upon infection and thereby affecting the transcription of miR-199a/214, even though its expression level does not change until 48 hpi.

To examine this in more depth, TWIST-1 was knockdown and mature miR-199-5p, miR-199-5p, and miR-214 expression levels compared in uninfected and infected cell. This was expected to show whether TWIST-1 knockdown recapitulates the reduction in miR-199a/214 transcript levels observed during infection, or whether there are additional effects of the virus that are independent of TWIST-1. NIH-3T3 cells were mock or transfected with RISC-free and TWIST-1 siRNA for 48 hours. Cells were then infected with MCMV at MOI of 5 for 24 and 48 hours. Total RNA and cell lysates were prepared and analysed by qRT-PCR and Western blotting. NIH-3T3 cells were mock or transfected with RISC-free and TWIST-1 siRNA for 48 hours post transfection. Cells were then infected with MCMV at MOI of 5 for 24 and 48 hours. Total RNA and cell lysates were prepared and analysed by qRT-PCR and Western blotting.

Western blot analysis confirmed that the expression of TWIST-1 protein in mock cells is unchanged at 24 hpi (see Figure 3.14a) and that TWIST-1 protein was knocked down by the siRNA in both mock infected and infected cells. Consistent with the previous results, the expression level of the miR-199a/214 transcript was reduced in infected compared to uninfected cells at 24 hpi (Figure 3.14b), even though TWIST-1 protein expression was unchanged at this time point. A significant decrease was detected in the level of the miR-199a/214 transcript in both uninfected

and infected cells in which TWIST-1 was knocked down in these cells. As the decrease was comparable regardless of infection status, it would appear that at 24 hpi, MCMV has no capacity to further down-regulate the cluster expression in TWIST-1 silenced cells.

As seen in Figure 3.14d, a reduction in miR-199a/214 comparable to that at 24 hours was found in cells in which TWIST-1 was knocked down and infected cell with MCMV for 48 hours. Interestingly, MCMV infection resulted in an significant additional inhibitory effect on the cluster expression in cells knocked down for TWIST-1 compared to mock infected cells. However, at 48 hpi the effect of TWIST-1 siRNA appeared to decline in mock infected cells, as compared to 24 hours. Such a decline was not obvious in the infected cells, suggesting that MCMV infection has down-regulated TWIST-1 protein by 48 hours. It is possible that the reduced effect of siRNA in uninfected cells is due to transient transfection, whereas in infected cells infected MCMV knocks down TWIST-1 (Figure 3.14c).

Taken together, these results show that, TWIST-1 may largely be involved in the regulation of miR-199a/214 at 24 hpi, but its protein expression is unchanged, by the virus siRNA knock down. Therefore, the effect of MCMV infection on TWIST-1 phosphorylation should be examined at early times of infection prior to 24 hours.

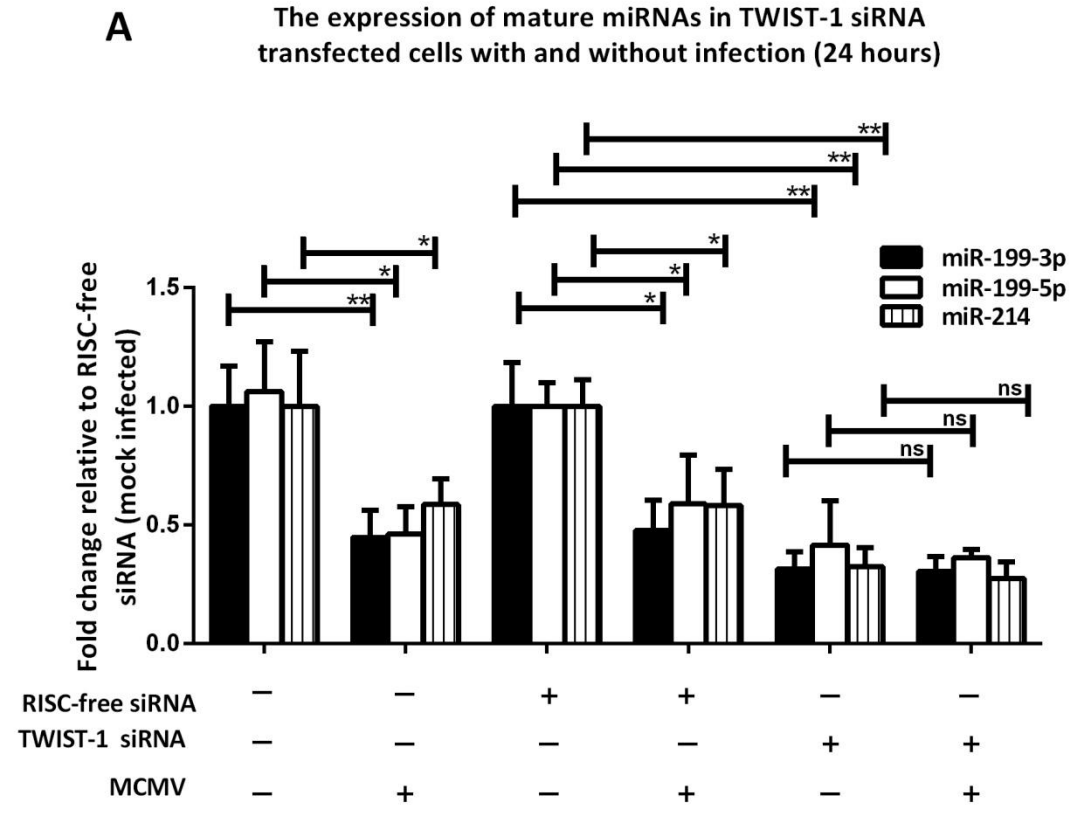
A
The expression of mature miRNAs in TWIST-1 siRNA transfected cells with and without infection (24 hours)
Fold change relative to RISC-free siRNA (mock infected)
1.5
1.0
0.5
0.0
miR-199-3p
miR-199-5p
miR-214
**
**
**
*
*
*
*
*
*
ns
ns
ns
RISC-free siRNA
TWIST-1 siRNA
MCMV
– – + + – –
– – – – + +
– + – + – +

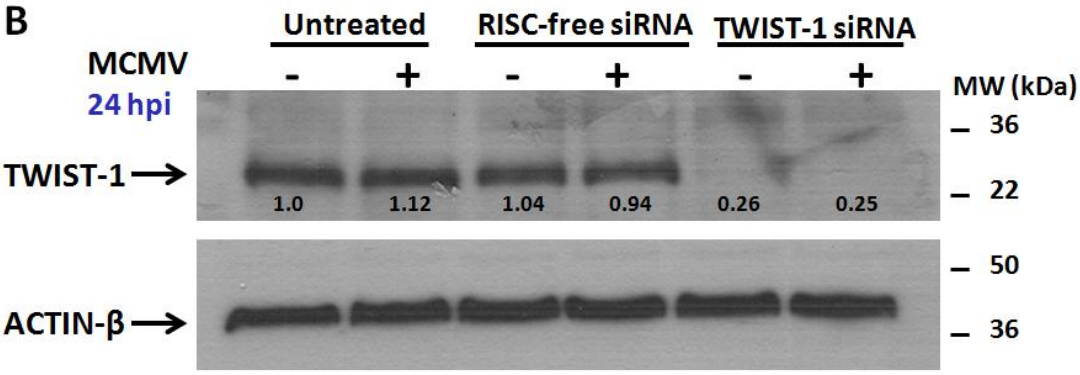
B
Untreated
RISC-free siRNA
TWIST-1 siRNA
MCMV
24 hpi
- + - + - +
MW (kDa)
TWIST-1
1.0
1.12
1.04
0.94
0.26
0.25
36
22
ACTIN-β
50
36

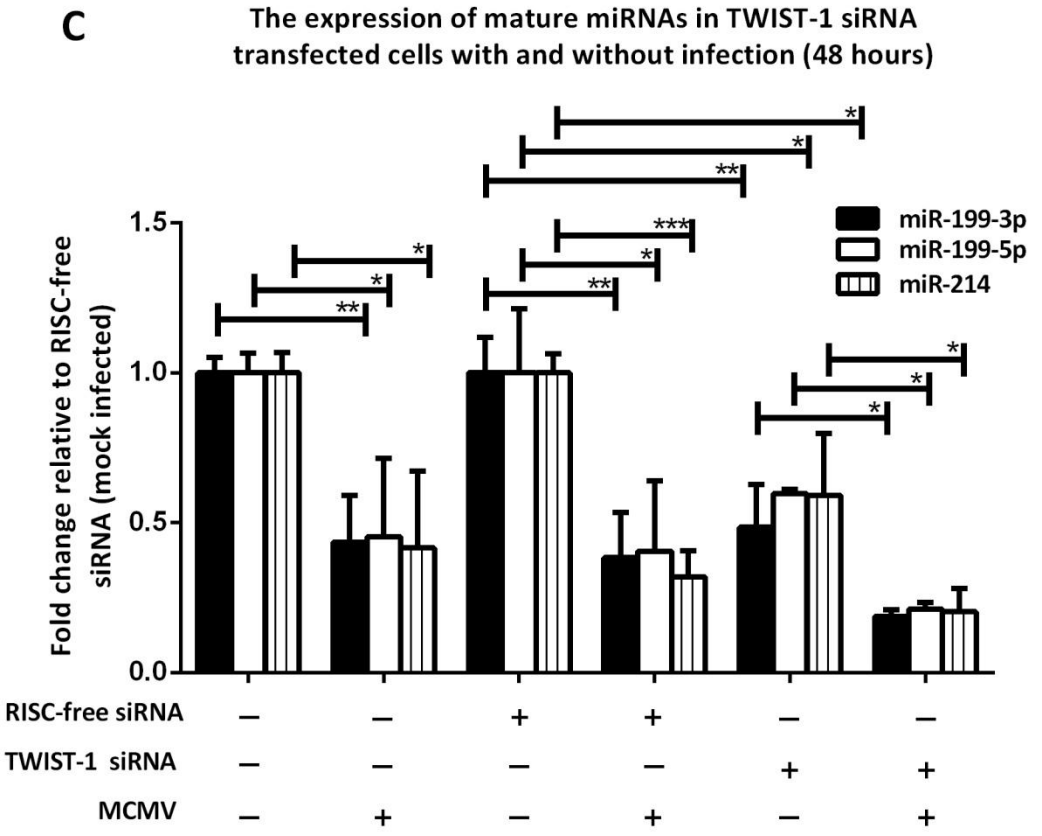
C
The expression of mature miRNAs in TWIST-1 siRNA transfected cells with and without infection (48 hours)
Fold change relative to RISC-free siRNA (mock infected)
1.5
1.0
0.5
0.0
miR-199-3p
miR-199-5p
miR-214
RISC-free siRNA
TWIST-1 siRNA
MCMV

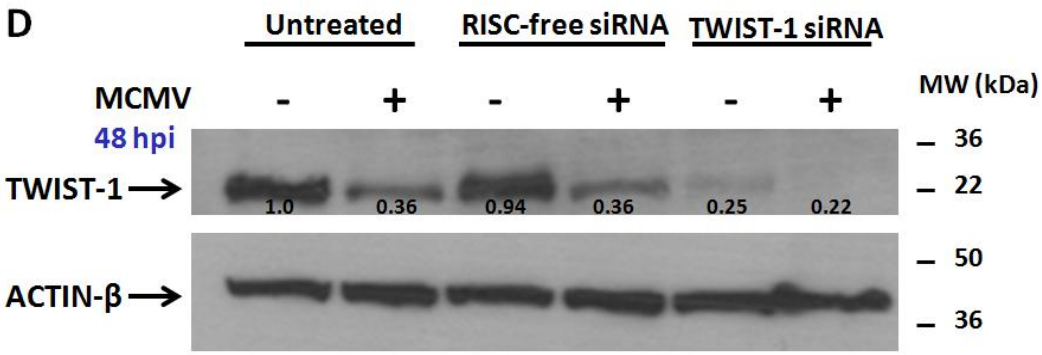
D
Untreated
RISC-free siRNA
TWIST-1 siRNA
MCMV
MW (kDa)
48 hpi
TWIST-1
1.0
0.36
0.94
0.36
0.25
0.22
ACTIN-β
36
22
50
36

Figure 3.14: MCMV induces more robust inhibition of miR-199a/214 expression than observed for TWIST-1 knockdown at 48 but not 24 hpi. A and C) NIH-3T3 cells were untreated or transfected with either control RISC-free or TWIST-1 siRNA for 48 hours. Cells were then mock infected or infected with MCMV an MOI=5 for 24 hours (A) and 48 hours (c). The expression levels of mature miRNAs was quantified by qRT-PCR and normalised to miR-16. Data presented are the mean fold change ± S.D. and are representative of two independent experiments.*$p < 0.05$, **$p < 0.01$, ***, $p < 0.001$ and ****$P<0.0001$ compared to RISC-free siRNA transfected cells at 24 hours or 48 hours as determined by a repeated measures two-way ANOVA with Sidak's post-test for multiple comparisons. B and D) Western blot confirming the knockdown of TWIST-1 and MCMV effect on its protein expression at 24 hours (B) and 48 hours (D). Whole cell lysates were harvested from cells transfected and then infected as in A and C. 20µg of cell lysates was loaded per lane and membrane was immunoblotted with primary antibodies against either TWIST-1 or β-ACTIN as a loading control. Blots were then quantified by densitometry and normalized to the corresponding β-ACTIN. The untreated (mock infected) was set as 1 and values for other conditions were expressed relative to this untreated value.

.

3.2.7 Immediate early gene 3 (IE3) and de novo viral gene expression are essential for the transcriptional suppression of pri-miR-199a/214 in MCMV-infected NIH-3T3 cells

As shown previously, MCMV infection results in a decrease in the promoter activity of miR-199a/214. In order to examine whether this requires de-novo viral gene expression, the IE3 deletion mutant virus (MCMVdie3), which lacks the fifth exon region of the IE1/IE3 gene, was used (see Figure 2.1 for genomic map). This virus can enter cells but viral gene expression is restricted to IE1 and IE2 genes and the virus cannot replicate. Replication of this mutant can be rescued by growing the virus on a complementary stable cell line (NIH-3T3-Bam25) expressing both IE1 and IE3.

3.2.7.1 Infection of cells with IE3 deletion mutant virus does not cause a reduction in expression of the pri-miR-199a/214 transcript or mature miRNAs

The expression of pri-miR-199a/214 transcript was examined in cells infected with MCMV and MCMVdie3. NIH-3T3 cells were mock infected or infected with either MCMV or MCMVdie3 at MOI of 5. Total RNA was harvested at several time points during infection, and qRT-PCR was used to measure the expression level of primary transcript, which was normalised to GAPDH, which maintains constitutive expression during MCMV and MCMVdie3 infection. 18S rRNA was used as an additional control.

As previously shown, MCMV infection leads to a significant decrease in the expression of pri-miR-199a/214 transcript, by 2 fold and 15 fold at 4 and 48 hpi, respectively (Figure 3.2). However, infection with MCMVdie3, did not significantly altered the level of pri-miR-199a/214 transcript at 2, 4, 8, or 24 hpi, though a 1.5 fold decrease was observed at 48 hpi. These results demonstrate a clear difference in the ability of MCMV and MCMVdie3 viruses to down-regulate the pri-miR-199a/214 transcript (Figure 3.15a). To determine whether this translated to differences in expression levels of mature miRNAs, a comparison of mature miR-199-5p, miR-199-3p, and miR-214 expression in cells infected with MCMV and MCMVdie3 was carried out using Northern blot analysis. As shown in Figure 3.15b, the expression levels of the mature miRNAs were down-regulated in NIH-3T3 cells infected with

MCMV, although no change was seen in MCMVdie3 infected cells relative to mock infected cells.

To investigate whether the differences observed between MCMV and MCMVdie3 mutant virus are specifically due to IE1/IE3 genes, experiments were also carried out in the complementary cell line, NIH-3T3-BAM25, which expresses IE1/IE3. NIH-3T3-BAM25 cells were infected with MCMVdie3 at MOI of 5 for 24 hours. NIH-3T3 cells also were infected in parallel with MCMV and MCMVdie3 with MOI of 5. While the infection of NIH-3T3 cells with MCMVdie3 resulted in no change in the primary transcript at 24 hpi, the infection of NIH-3T3-Bam25 cells yielded a 2.5-fold reduction in the primary transcript expression. However, this reduction was not as significant as the reduction observed with MCMV at 24 hpi (Figure 3.15c).

Taken together these results suggest that primary transcript and miR-199a/214 expression is inhibited in MCMV infected cells, and this is at least partly dependent on the activity of IE3, which is required for inducing viral gene expression and replication but also is known to interact with the promoter sequences of endogenous genes.

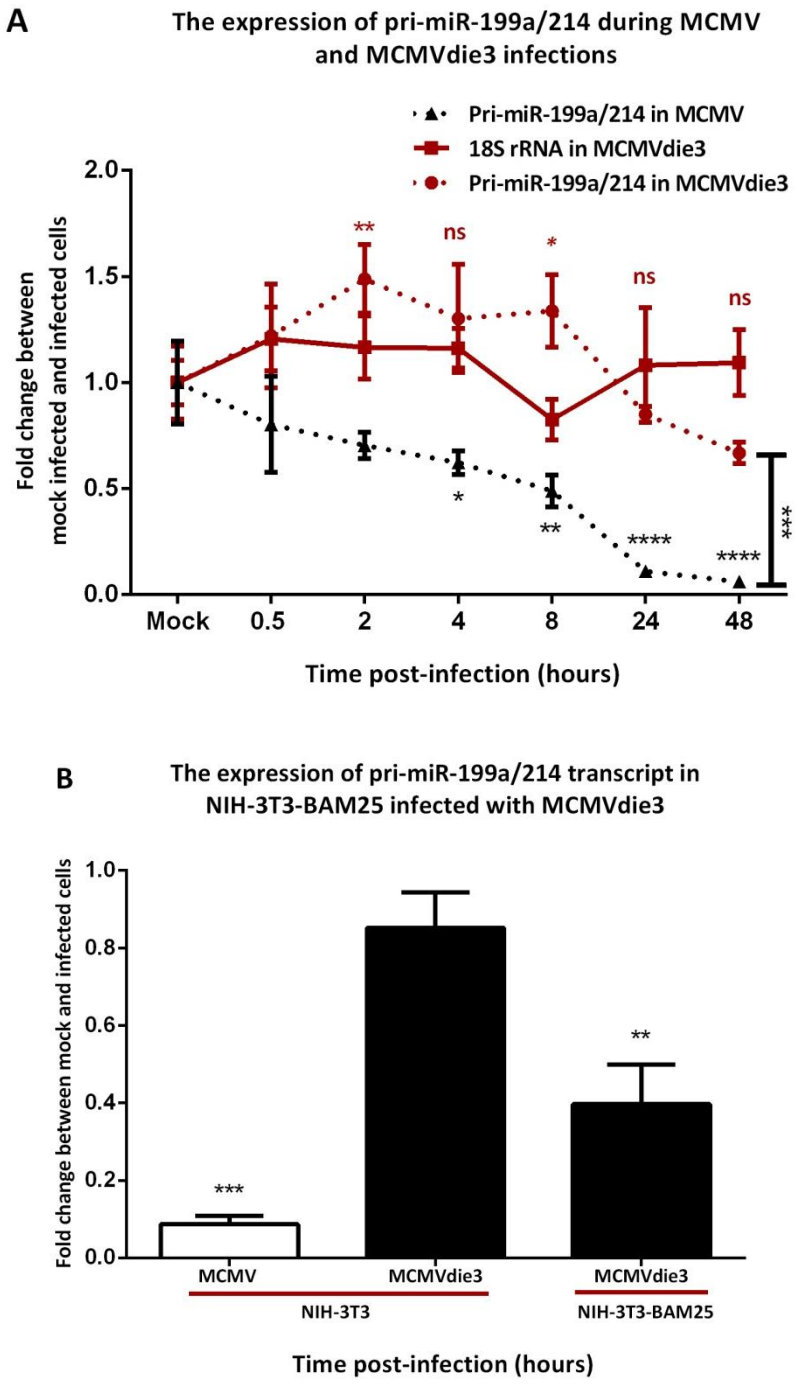
A
The expression of pri-miR-199a/214 during MCMV and MCMVdie3 infections
Pri-miR-199a/214 in MCMV
18S rRNA in MCMVdie3
Pri-miR-199a/214 in MCMVdie3
Fold change between mock infected and infected cells
2.0
1.5
1.0
0.5
0.0
**
ns
*
ns
ns
*
**
****
****
***
Mock
0.5
2
4
8
24
48
Time post-infection (hours)
B
The expression of pri-miR-199a/214 transcript in NIH-3T3-BAM25 infected with MCMVdie3
Fold change between mock and infected cells
1.0
0.8
0.6
0.4
0.2
0.0
***
**
MCMV
MCMVdie3
MCMVdie3
NIH-3T3
NIH-3T3-BAM25
Time post-infection (hours)
C
NIH-3T3
NIH-3T3-BAM25
MCMVdie3 - - + - +
MCMV - + - - -
miR-199-3p
1 0.51 1.08 1.08 0.70
miR-199-5p
1 0.60 0.96 0.98 0.64
miR-214
1 0.58 0.83 0.98 0.46
miR-16

Figure 3.15: MCMVdie3 does not inhibit the pri-miR-199a/214 and mature miRNA. A) pri-miR-199a/214 expression in MCMV versus MCMVdie3 infected cells compared to mock infected cells. NIH-3T3 cells were mock infected or infected with either MCMV or MCMVdie3 at an MOI=5 for the indicated times. The expression level of pri-miRNA was quantified by qRT-PCR and normalised to GAPDH. 18S rRNA was included as a negative control. Mock infected cells from the different time points (0hr, 24hr and 48hr) were averaged and compared to infected cells at each time point. Data presented are the mean fold change ± S.D. of two independent experiments (n=6). *P<0.05, **P<0.01, ***P<0.001, and ****P<0.0001 compared to mock infected cells as determined by a repeated measures one-way ANOVA with Sidak's post-test for multiple comparisons. B) MCMVdie3 inhibits pri-miR-199a/214 expression in NIH-3T3-BAM25 cells. NIH-3T3 cells were mock infected or infected with either MCMV or MCMVdie3 at an MOI=5 for 24 hours. Whereas, NIH-3T3-BAM25 cells were also mock infected or infected with only MCMVdie3 at an MOI=5 for 24 hours. The expression level of pri-miRNA was quantified by qRT-PCR and normalised to GAPDH. Data presented are the mean fold change ± S.D. of two independent experiments (n=6). **$p < 0.01$ and ***, $p < 0.001$ compared to mock infected cells as determined by two-tailed Student's *t* test. C) Northern blot analysis of mature miR-199-5p, miR-199-3p, and miR-214 from mock infected and infected cells at B. 5µg of RNA was loaded per lane and membrane was hybridised with ^{32}P-labeled probes. miR-16 probe was used as a loading control (lower panel), followed by densitometric analysis. The densitometric value for the NIH-3T3 mock infected was set as 1 and values for other infected cells were expressed relative to the mock value.

3.2.7.2 Pri-miR-199a/214 expression is regulated in NIH-3T3-BAM25 cells expressing both IE1 and IE3 genes

It was demonstrated that IE1 and/or IE3 are required for the down-regulation of miR-199a/214 expression. To examine the possibility that immediate early genes IE1/IE-3 are involved in the regulation of miR-199a/214, the expression of primary transcript was measured in NIH-3T3-BAM25 cells (a NIH-3T3 cell line in which IE1/IE3 locus is constitutively expressed). Total RNA was harvested from NIH-3T3-BAM25 and NIH-3T3 cells for qRT-PCR analysis. The expression of pri-miR-199a/214 was reduced 2-fold in NIH-3T3-Bam25 compared to NIH-3T3 cells whereas the 18S rRNA expressed at the same levels in both cell lines (Figure 3.16). This indicates that the expression of IE3 gene product has a direct or indirect effect on the transcription of the primary transcript.

As IE1 expression was detected in MCMVdie3 infected cells to equivalent levels to MCMV infected cells (Angulo et al. 2000) and MCMVdie3 is incapable of repressing the expression of the pri-transcript. Therefore, it is unlikely that IE1 expression in NIH-3T3-Bam25 complementing cell line is involved in the down-regulation of pri-miR-199a/214 compared to NIH-3T3 cells. Based on these findings, the expression of immediate early viral protein (IE3) is required for the down-regulation of miR-199a/214 that occurs upon infection. The mechanism by which this viral protein influences the expression of these miRNAs remains to be determined.

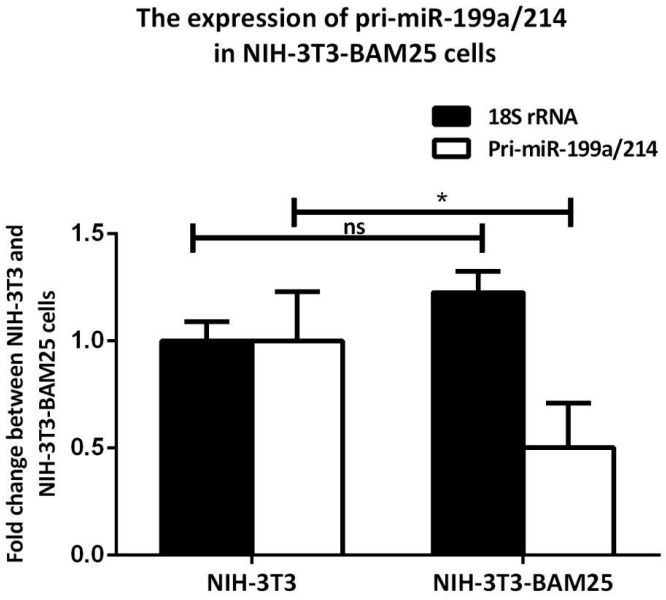

Figure 3.16: The expression of IE1 and/or IE3 down-regulates the pri-miR-199a/214 expression in NIH-3T3-Bam25 cells compared to NIH-3T3 cells. Total RNA was harvested from untreated NIH-3T3 and NIH-3T3-BAM25 cell lines. The expression level of pri-miRNA was quantified by qRT-PCR and normalised to GAPDH. 18S rRNA was included as a negative control. Data presented are the mean fold change ± S.D. of two independent experiments (n=6). *$p < 0.05$ compared to NIH-3T3 untreated cells as determined by two-tailed Student's *t* test.

3.2.7.3 MCMVdie3 regulates the activity of the miR-199a/214 promoter in infected fibroblasts.

In order to further examine whether the transcriptional regulation of pri-miR-199a/214 requires IE1/IE3 gene expression, miR-199a/214 promoter activity was measured in MCMVdie3 versus MCMV infected cells.

Cells were co-transfected with *Renilla* plasmid for normalisation and the full-length promoter construct for 48 hours prior to infection with MCMV or MCMVdie3 at MOI of 5. Cells were harvested and lysed at 30min, 2, 4, 8, 24, 48 hpi and bioluminescence readings were measured. Consistent with previous results, the luciferase expression controlled by the miR-199a/214 promoter decreased steadily in MCMV infected cells from 2 to 48 hpi (Figure 3.17). In contrast, higher levels of luciferase expression were observed upon infection with the MCMVdie3 virus from 2 to 8 hpi. However, a 1.3 and 1.7 fold decrease was detected in the luciferase signals by 24 and 48 hpi, respectively (Figure 3.17). These results nicely correlate with effects of MCMV and MCMVdie3 on pri-miR-199a/214 levels (Figure 3.15a,b). Taken together, these results further confirm that immediate early gene expression is required for the transcriptional regulation of miR-199a/214.

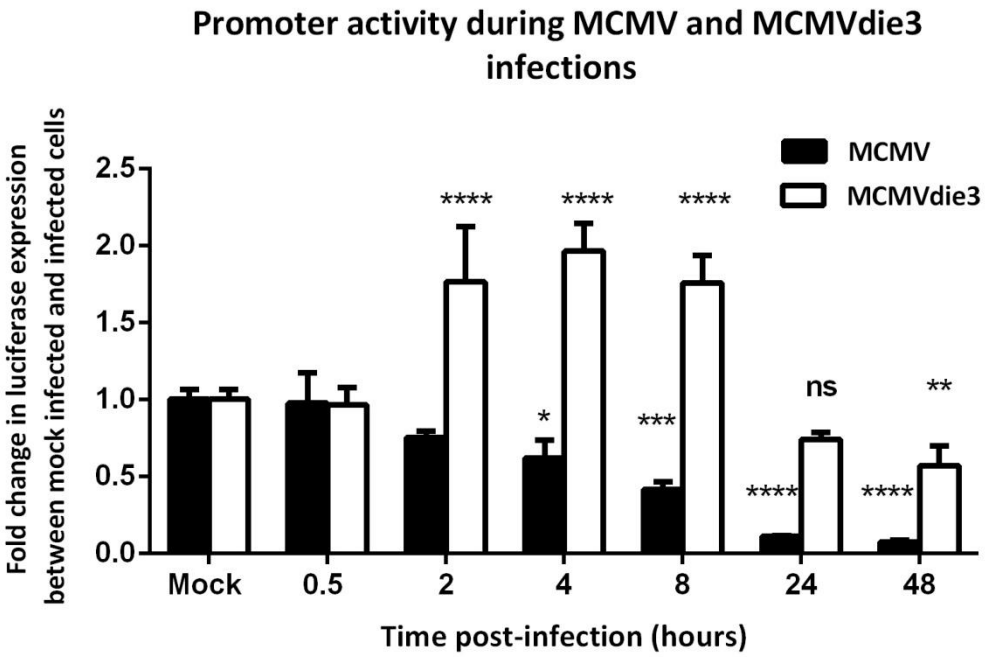

Figure 3.17: The effect of MCMVdie3 on the promoter activity of miR-199a/214. NIH-3T3 cells were transfected with the full-length promoter construct (-596, +100) for 48 hours. Cells were then mock infected or infected with either MCMV or MVMVdie3 at MOI=5 for the indicated times. The activity of promoter constructs was measured as the firefly luciferase values, which were normalised to *Renilla* luciferase from the co-transfected vector. The firefly/*Renilla* ratio for promoter constructs was compared to the promoter-less vector ratio. Data presented are the mean fold change ± S.D. (n=5) and are representative of two independent experiments. *P<0.05, **P<0.01, ***P<0.001, and ****P<0.0001 compared to mock infected ratios in each time point as determined by a repeated measures two-way ANOVA with Sidak's post-test for multiple comparisons.

3.2.8 The regulation of pri-miR-199a/214 and the mature miRNAs during HCMV infection.

MCMV and HCMV infection share roughly half of their encoded open-reading frames (ORFs) (Brocchieri et al. 2005; Rawlinson et al. 1996). As a result, there are similarities between MCMV and HCMV infections related to events during acute, latent, reactivation phase (Adler and Sinzger 2009). However, other conserved viral events for modulation of host responses are mediated through different underlying mechanisms (Mocarski 2004). We have reported a conserved down-modulation of miR-199-5p, miR-199-3p, and miR-214 in HCMV and MCMV infection (Santhakumar et al. 2010), it was therefore important to determine whether this occurred through similar mechanism. Therefore experiments similar to those described for MCMV were carried out using human CMV. Specifically, three questions were examined: 1) Does HCMV regulate the pri-miR-199a/214 and its mature products? 2) Does this regulation occur at the promoter level? and 3) Is TWIST-1 involved in miR-199a/214 regulation in HCMV infection?

3.2.8.1 Down-regulation of the miR-199a/214 primary transcript and mature miRNAs during HCMV infection

The kinetics of primary transcription and mature miR-199a/214 expression were examined in HCMV infected cells. The human lung fibroblast (MRC-5) cell line was mock infected or infected with HCMV at MOI of 5. Total RNA and cell lysates were harvested at various time points post infection and subjected to qRT-PCR and Northern blot analysis.

As with MCMV, no significant change was observed in the expression of mature miR-199-5p, miR-199-3p and miR-214 at early time points, up to 16hpi (Figure 3.18a). However, a gradual down-regulation occurred between 24 – 72 hpi (1.8 fold at 24 hpi to 4 fold at 72 hpi). Consistent with these results, Northern blot analysis confirmed the reduction in the mature miR-199-3p, miR-199-5p, and miR-214 at 24, 48, and 72 hpi; tRNA and miR-16 were measured in parallel as loading controls (Figure 3.18b).

To examine whether the reduction in mature miRNAs resulted from a decrease in pri-miR-199a/214 transcript level, the expression of primary transcript was measured

in the same time course experiment. As observed in MCMV infection, the expression of the pri-miR-199a/214 transcript decreased 1.5 fold within 4 hpi, with a continued gradual decrease to 12 fold at 72hpi. The 18S rRNA control showed no change in expression at the different time points post HCMV infection (Figure 3.18c).

Therefore, both MCMV and HCMV reduce the expression of pri-miR-199a/214 transcript by 4 hpi.

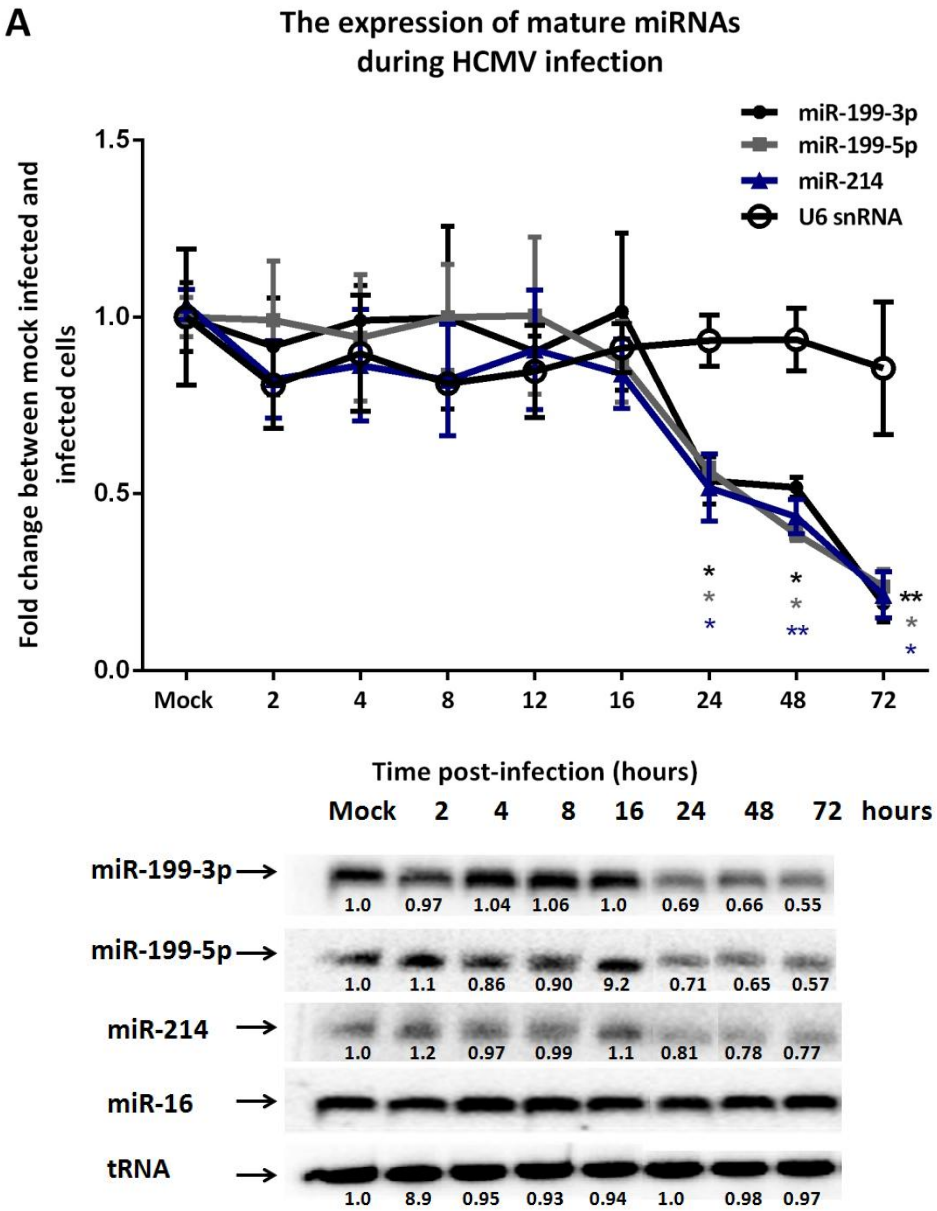
A
The expression of mature miRNAs during HCMV infection
miR-199-3p
miR-199-5p
miR-214
U6 snRNA
Fold change between mock infected and infected cells
1.5
1.0
0.5
0.0
Mock 2 4 8 12 16 24 48 72
Time post-infection (hours)
Mock 2 4 8 16 24 48 72 hours
miR-199-3p
1.0 0.97 1.04 1.06 1.0 0.69 0.66 0.55
miR-199-5p
1.0 1.1 0.86 0.90 9.2 0.71 0.65 0.57
miR-214
1.0 1.2 0.97 0.99 1.1 0.81 0.78 0.77
miR-16
tRNA
1.0 8.9 0.95 0.93 0.94 1.0 0.98 0.97

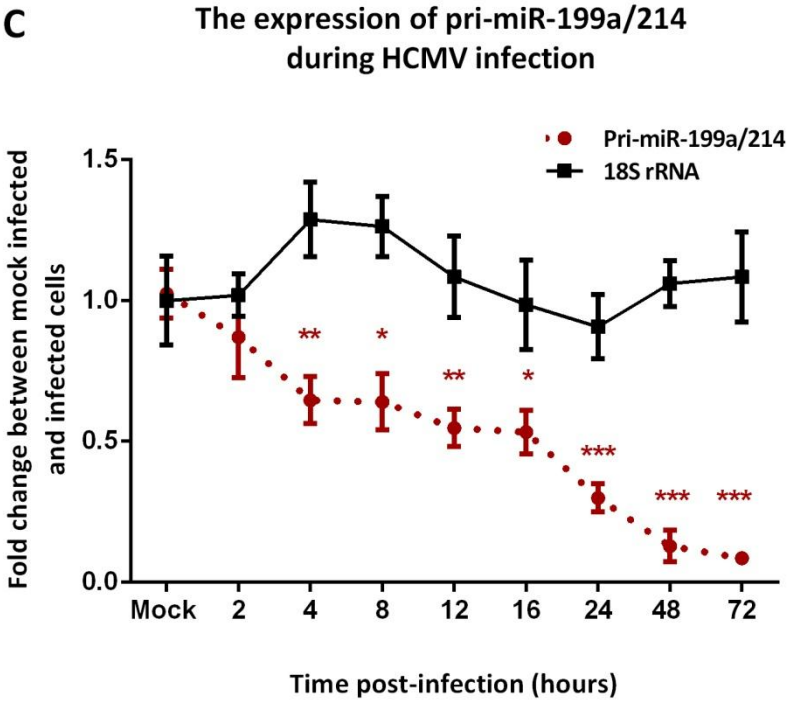
C
The expression of pri-miR-199a/214 during HCMV infection
Pri-miR-199a/214
18S rRNA
Fold change between mock infected and infected cells
1.5
1.0
0.5
0.0
Mock 2 4 8 12 16 24 48 72
Time post-infection (hours)

Figure 3.18: The expression kinetics of pri-miR-199a/214 and its mature miRNAs over the time course of HCMV infection. A) Down-regulation of mature miR-199-3p, miR-199-5p, and miR-214 expression in HCMV infected cells by 24 hours compared to mock infected cells. MRC-5 cells were mock infected or infected with HCMV at an MOI=5 for the indicated times. The expression levels of mature miRNAs were quantified by qRT-PCR and normalised to miR-16. U6 snRNA was included as a negative control. Mock infected cells from the different time points (0, 24, 48, 72 hours) were averaged and compared to infected cells at each time point. Data presented are the mean fold change ± S.D. of two independent experiments (n=6). *P<0.05 and **P<0.01 compared to mock infected cells as determined by a repeated measures one-way ANOVA with Sidak's post-test for multiple comparisons. B) Northern blot analysis of mature miRNAs during HCMV infection. Total RNA was harvested from MRC-5 cells mock infected or infected as in A. 5µg of RNA was loaded per lane and membrane was hybridised with ^{32}P-labeled probes. miR-16 and tRNA (Gly) probes were used as a loading control (lower panels), followed by densitometric analysis. The densitometric value for the mock infected was set as 1 and values for other time points post infection were expressed relative to the mock value. C) Down-regulation of pri-miR-199a/214 expression in HCMV infected cells by 4 hours compared to mock infected cells. Total RNA from A was quantified by qRT-PCR and normalized to GAPDH level. 18S rRNA was included as a negative control. Mock infected cells from the different time points were averaged and compared to infected cells at each time point. Data presented are the mean fold change ± S.D. of two independent experiments (n=6). *P<0.05, **P<0.01, and ***P<0.001 compared to mock infected cells as determined by a repeated measures one-way ANOVA with Sidak's post-test for multiple comparisons.

3.2.8.2 HCMV regulates the murine miR-199a/214 promoter in infected cells.

As shown previously (3.2.2.3), there is a high degree of sequence conservation between the mouse and human promoters of miR-199a/214. Therefore, the mouse promoter construct described above was used to examine whether HCMV affects promoter activity.

The luciferase reporter containing the full-length mouse promoter (-596, +100) was co-transfected into MRC-5 cells with a *Renilla* vector (used for normalisation). 48 hours after, the cells were then either mock infected or infected with HCMV at MOI of 5 for 24 hours. All cells were then lysed and luminescence measured.

As illustrated in Figure 3.19, the mouse promoter is functional in human cells and able to significantly drive luciferase expression by more than 16 fold, relative to the promoter-less control construct. This promoter activity in MRC-5 cells was comparable to that observed in mouse NIH-3T3 cells. The luciferase expression decreased 9-fold in cells infected with HCMV (24 hpi), suggesting that HCMV, like MCMV, regulates the pri-miR-199a/214 at the promoter level.

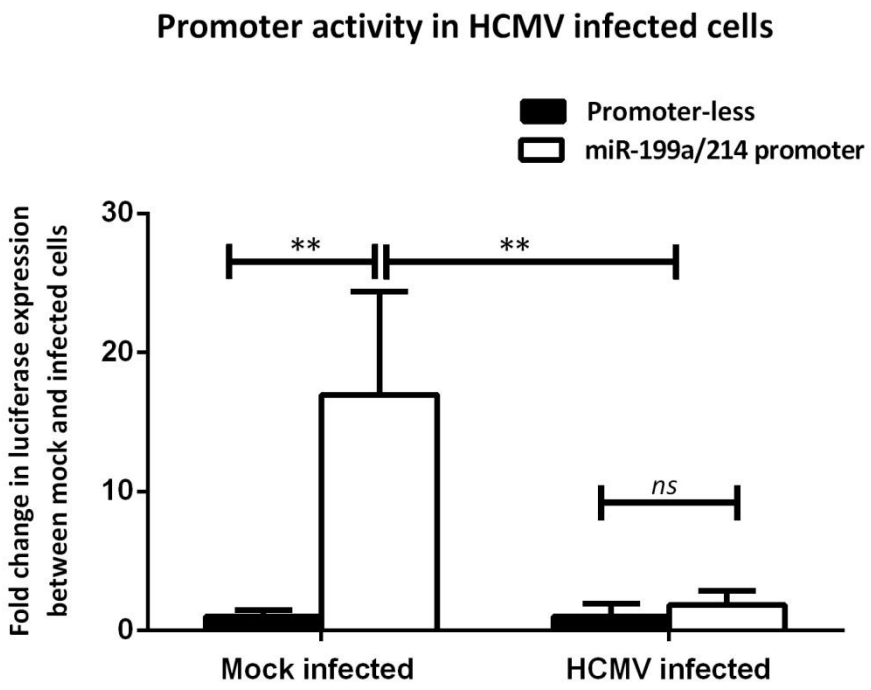

Figure 3.19: Effect of HCMV on the promoter activity of miR-199a/214. MRC-5 cells were transfected with murine full-length promoter construct (-596, +100) for 48 hours. Cells were mock infected or infected with HCMV at an MOI=5 for 24 hours. The promoter activity was measured as the firefly luciferase values, which were normalised to *Renilla* luciferase from the co-transfected vector. The firefly/*Renilla* ratio for promoter constructs was compared to the promoter-less vector ratio. Data presented are the mean fold change ± S.D. of two independent experiments (n=8). **P<0.01, compared to mock infected promoter as determined by two-tailed Student's *t* test.

3.2.8.3 HCMV down-regulates the expression of TWIST-1 mRNA and protein

The results presented in section 3.2.7, showed that TWIST-1 is downregulated in MCMV infection, which at least partially regulates the transcription of miR-199a/214. Therefore, the effect of HCMV infection on TWIST-1 expression was examined. TWIST-1 mRNA levels were measured using qRT-PCR with total RNA isolated from cells mock infected or HCMV infected at MOI of 5. As shown in Figure 3.20a, HCMV significantly suppressed the expression of TWIST-1 mRNA (from 1.5 fold at 8 hours to a 5 fold decrease by day 3 of infection).

To further examine whether the regulation occurred at the protein level, cell lysates from mock infected and infected cells at 24 and 48 hours were analysed using Western blotting. A significant reduction was observed in TWIST-1 protein expression was observed at 24 and 48 hours post HCMV infection (Figure 3.20b).

In conclusion, human TWIST-1 mRNA and protein were downregulated in HCMV infection by 8 and 24 hpi, respectively. It should be noted that down-regulation at the TWIST-1 protein level in both HCMV and MCMV is not significant until 24 or 48 hours in HCMV or MCMV infection, respectively. Therefore, the early effect(s) of the virus (by 4 hours) on the miR-199a/214 promoter is not explained by changes in TWIST-1 protein expression upon infection.

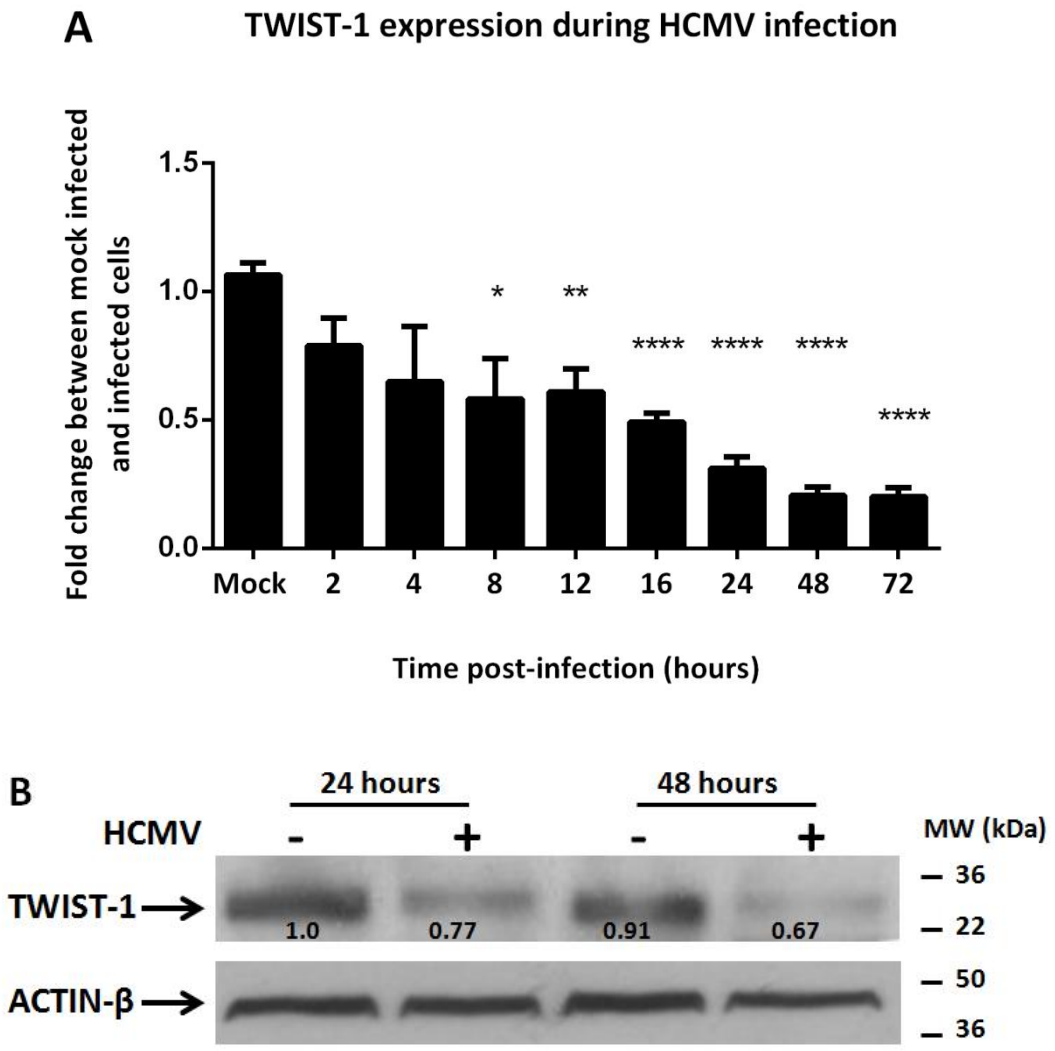

Figure 3.20: The expression of TWIST-1 mRNA and protein in HCMV infected cells. A) Down-regulation of TWIST-1 mRNA in HCMV infected cells by 2 hours compared to mock infected cells. MRC-5 cells were mock infected or infected with HCMV at an MOI=5 for the indicated times. The expression level of TWIST-1 was quantified by qRT-PCR and normalised to GAPDH. Mock infected cells from the different time points (0, 24, 48, 72 hours) were averaged and compared to infected cells at each time point. Data presented are the mean fold change ± S.D. of two independent experiments (n=6). *P<0.05, **P<0.01, ****P<0.0001 compared to mock infected cells as determined by a repeated measures one-way ANOVA with Sidak's post-test for multiple comparisons. B) Western blot showing reduction in TWIST-1 at 24 and 48 hours post HCMV infection. Whole cell lysates were harvested from MRC-5 cells mock infected or infected with HCMV at an MOI of 5 for 24 and 48 hours. 20µg of protein was loaded per lane and membrane was immunoblotted with primary antibodies against either TWIST-1 or β-ACTIN as a loading control. Blots were then quantified by densitometry and normalized to the corresponding β-ACTIN. The mock infected at 24 hours was set as 1 and values for other time points were expressed relative to the mock value.

3.2.8.4 TWIST-1 regulates miR-199-5p, miR-199-3p and miR-214

The effect of TWIST-1 knock down on the expression of miR-199a/214 was examined in MRC-5 cells either mock infected or infected with HCMV. Cells were transfected with TWIST-1 siRNA or control siRNA (RISC-free siRNA) for 48 hours prior to infection for 24 hours, after which total RNA was harvested and subjected to qRT-PCR and Northern blot analyses.

Transfection of the TWIST-1 siRNA reduced the expression of TWIST-1 mRNA in MRC-5 cells by 90%. The knock down of TWIST-1 significantly decreased the expression of the mature members of miR-199a/214 cluster by 1.5 fold. HCMV infection of cells in which TWIST-1 was knocked down caused a further 2.5 to 3 fold reduction of the expression of miR-199-5p, miR-199-3p, and miR-214 (Figure 3.21a). Northern blot analysis of mature members of miR-199a/214 cluster confirmed the down-regulation of the mature cluster in cells in which TWIST-1 siRNA was knocked down as well as a more pronounced down-regulation of these miRNAs in infected cells (Figure 3.21b).

To summarise, the human TWIST-1 is involved in the down-regulation of miR-199a/214 cluster during HCMV infection. However, since the protein is not regulated as early as the pri-miR-199a/214, clearly other factors are involved.

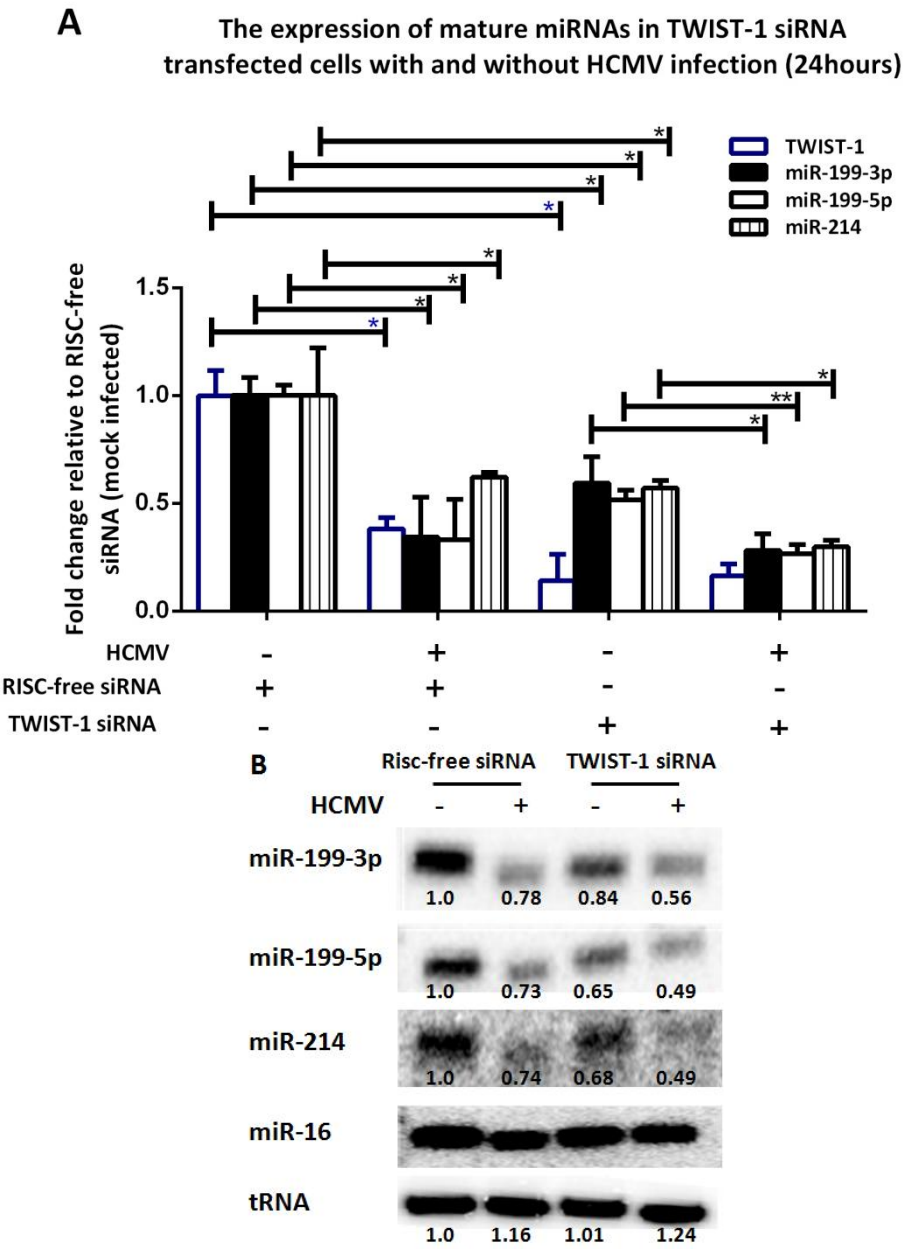

Figure 3.21: HCMV induces more robust inhibition of miR-199a/214 expression than observed for TWIST-1 knockdown at 24 hpi. A) MRC-5 cells were transfected with either control RISC-free or TWIST-1 siRNA for 48 hours. Cells were then mock infected or infected with HCMV of an MOI=5 for 24 hours. The expression level of TWIST-1 and mature miRNAs were quantified by qRT-PCR, normalised to GAPDH and U6 snRNA, respectively. Data presented are the mean fold change ± S.D. (n=3) and are representative of two independent experiments. *P<0.05 and **P<0.01 compared to mock infected cells as determined by a repeated measures two-way ANOVA with Sidak's post-test for multiple comparisons. B) Northern blot analysis of mature miRNAs from experiment A. 5µg of RNA was loaded per lane and membrane was hybridised with ^{32}P-labeled probes. miR-16 and tRNA (Gly) probes were used as a loading control (lower panels), followed by densitometric analysis. The densitometric value for the RISC-free siRNA (mock infected) was set as 1 and values for other conditions were expressed relative to the mock value.

3.4 Discussion

Increasing evidence suggests that the regulation of cellular miRNA can influence the outcome of a viral infection. miRNA expression can be regulated at the level of transcription, processing of the pri- or pre-miRNA, and/or degradation of the mature miRNA. To date, only one mechanism of cellular miRNA regulation by MCMV has been reported: the degradation of cellular miR-27a and miR-27b through the expression of a viral transcript, which acts as specific inhibitor of the mature miR-27. The mechanism for inhibiting miR-27 expression does not seem to be conserved in HCMV infection (Santhakumar et al. 2010; Libri et al. 2012; Marcinowski et al. 2012). However, three cellular miRNAs derived from the pri-miR-199a/214, are down-regulated in both MCMV and HCMV acute infections (Santhakumar et al. 2010). The mechanism(s) underlying the regulation of miR-199a/214 expression in murine and human CMV infections were previously unknown. The work presented in this chapter addresses four questions regarding the down-regulation of miR-199-5p, miR-199-3p, and miR-214 levels during MCMV infection: 1) During which stage of miRNA biogenesis, can the expression of these mature miRNAs be regulated in infection?; 2) are cellular factors involved in the regulation of these miRNAs during infection?; 3) is the down-regulation of miR-199a/214 cluster dependent on viral gene expression?; and 4) is the mechanism by which MCMV and HCMV regulate the expression of miR-199a/214 conserved?

3.4.1 Regulation of miR-199a/214 transcription during MCMV infection

The data presented in sections 3.2.1 and 3.2.4 demonstrates that MCMV infection inhibits the transcriptional regulation of the miR-199a/214 cluster, thereby revealing another mode of MCMV interference with miRNA biogenesis. The expression of the primary transcript of miR-199a/214 cluster is reduced by 4 hpi in MCMV, which is earlier than the reduction of mature miRNAs observed at 24 hpi. It is expected that the difference in timing of pri-miRNA versus mature miRNA reduction relates to the fact that these mature miRNAs are relatively stable (data not shown). There are two levels of regulation for pri-miRNA transcript: one at the transcriptional level involving promoter regulation and another at the processing level. An example of regulation at the processing level would be the editing of pri-miR-142 resulting in

inhibition of its processing and reduction of its stability, followed by its degradation (Yang et al. 2006). Therefore, the first step was to examine whether or not the transcription of pri-miR-199a/214 was altered in MCMV-infected cells.

Interestingly, the promoter activity of miR-199a/214 decreased with similar kinetics to the expression of the primary transcript during MCMV infection, strongly indicating that the down-regulation of miR-199a/214 occurs at the transcriptional level. This correlates with the short half-life pri-miR-199a/214 transcript (Data not shown). Nonetheless, this does not rule out the possibility that additional post-transcriptional mechanisms also contribute to the down-regulation of these miRNAs during infection. In addition to the primary transcript of miR-199a/214, two additional transcripts have been found to be produced from the same gene that include the precursor sequence of either miR-199a or miR-214, but are expected to be under the control of different promoters (Figure 3.3). The expression and regulation of these transcripts, pri-miR-199a and pri-miR-214, were not examined in infected cells, however, their regulation can contribute to the mature miRNA levels.

The suppression of miR-199a/214 promoter in uninfected and infected cells could be mediated through various mechanisms, including cellular or viral transcription elements and epigenetic factors such as DNA methylation and histone modifications. Kim et al (2008) previously showed that miR-199a/214 expression is silenced in several human cancer cell lines (e.g. A549 and Hela) and epithelial cells (MCF10A and PWR-1E) due to heavy methylation of the miR-199a/214 promoter. He et al. (2012) reported that reactive oxygen species (ROS) induced DNMT1 activity to mediate miR-199a/214 promoter hypermethylation in ovarian cancer. It was reported that HCMV is able to induce the generation of ROS within minutes of infection as these ROS are critical for the transactivation of MIEP (Speir et al. 1996). It would therefore be useful to examine whether the methylation status in the promoter region of miR-199a/214 is altered upon infection with MCMV. However, this was beyond the scope of this investigation.

3.4.2 The regulation of miR-199a/214 expression by TWIST-1, SRF, and ELK-1 but not by STAT3 in fibroblasts

The results presented provide some characterisation of the mouse miR-199a/214 promoter, which shows ~89.7% conservation with the human promoter. A single transcriptional start site was identified in pri-miR-199a/214 transcript using primer extension analysis. To determine the minimal promoter sequence, several reporter constructs were constructed within the pri-miR-199a/214 promoter, which span from -596 to +100 of the relative TSS. The experiment identified a specific region (-596,+100) as the minimal promoter sequence required for basal promoter activity and localized the most functional region (-421,-273) for promoter activity, which seems to contain positive regulatory element(s). Three conserved transcription factor sites were found within the critical region (-421,-273): the SRF dimer and ELK-1. Based on gene-knockdown experiments, these transcription factors were found to regulate the basal expression of miR-199-5p, miR-199-3p, and miR-214 under normal conditions (uninfected) (Figure 3.11). In accordance with these results, a previous report showed that overexpression or inhibition of SRF in transgenic mice altered the expression of a number of miRNAs, including miR-199-3p, miR-199-5p, miR-214 and the primary transcript (Zhang et al. 2011). It has been reported that HCMV stimulates the formation of a complex containing the phosphorylated ELK-1 and SRF protein shortly after infection (Caposio et al. 2010). SRF and ELK-1 are required to mediate the activation of HCMV major immediate early promoter (MIEP), and that mutagenesis in SRF and/or ELK-1 binding sites in the MIEP impairs the efficient transcription of viral IE genes and replication of recombinant HCMV in fibroblasts (Chan et al. 1996; Caposio et al. 2010). Given that the competition of viral promoters and enhancers for cellular transcription factors is a possible scenario during infection, for example, Wu et al (1998) showed that the HCMV IE2 protein can alter the DNA binding activity of a cellular transcription factor SP1, thereby activating the expression of genes associated with HCMV productive infection such as viral DNA polymerase gene promoter. Therefore, the down-regulation of miR-199a/214 promoter may be due to the competitive binding of ELK-1 and SRF to the viral promoter(s) rather than cellular promoters including miR-199a/214 promoter. Another possible scenario is that SRF and/or ELK-1 are not

involved in the down-regulation of miR-199a/214 transcription during infection. However, the role of SRF-ELK-1 complex was studied in HCMV and it is not clear if this complex is regulated in the same way during MCMV infection. Indeed, modulation of miR-199a/214 by both CMV viruses may be mediated by different proteins.

In agreement with previous studies (Yin et al. 2010; Lee et al. 2009), it was shown here that TWIST-1 regulates the transcription of miR-199a/214 cluster expression. In contrast, STAT3 was not found to regulate the miR-199a-2 promoter or miR-199-5p expression in this work (Figure 3.11), which contradicts published data showing an increase in miR-199-5p level in heart tissue from STAT3-KO mice and an increase in miR-199a-2 promoter activity in neonatal rat cardiomyocyte transduced with anti-STAT3-shRNA (Haghikia et al. 2011). This may be due to the inherent differences in cell types or organisms.

3.4.3 The transcriptional regulation of miR-199a/214 cluster involves TWIST-1

Infection of cells with MCMV led to a significant decrease in the level of TWIST-1 mRNA at 24 hours, whereas its protein level was only reduced at 48 hours. The delayed reduction in TWIST-1 protein level may be due to the half-life of this protein and suggests that the regulation of pri-miR-199a/214 transcript at 4, 8, 12, 16, 24 hpi cannot be attributed to the reduction in TWIST-1. Therefore, TWIST-1 inhibition seems to contribute to the decrease in pri-miR-199a/214 transcript at 48 hours post MCMV infection but this does not explain the early reduction of the pri-miRNA between 4 and 24 hpi. It is possible that the activity, rather than expression, of TWIST-1 might be altered earlier in infection. There are several mechanisms by which the activity of TWIST-1 can be regulated, either through phosphorylation state or dimerization with a partner to form bHLH complex (Vichalkovski et al. 2010; Firulli and Conway 2008; Firulli et al. 2008). MCMV could post-translationally regulate TWIST-1 dimerization with bHLH factor and/or its phosphorylation, thereby resulting in decreasing the transcription of pri-miR-199a/214 transcript at early time points during infection. It is tempting to speculate that in order to achieve a rapid down-regulation in pri-miR-199a/214 transcript in

host cells, MCMV deactivates the biological function of the existing TWIST-1 protein. However, to create a prolonged down-regulation of the pri-miRNA transcript, TWIST-1 expression is regulated at the levels of both transcription and translation. Further work should be conducted in order to determine whether infection affects the activity of TWIST-1 by phosphorylation or its ability to dimerize with bHLH factor, which could explain the down-regulation of the pri-miR-199a/214 transcript between 4 to 24 hours post MCMV infection. The observed findings (shown in Figure 3.14a) illustrate that the MCMV infection of cells in which TWIST-1 was knocked down was incapable of causing further reduction of miR-199-5p, miR-199-3p and miR-214 expression at 24 hpi. These results may suggest that the reduction of miR-199-5p, miR-199-3p, and miR-214 expression is largely dependent on TWIST-1 at 24 hours.

3.4.4 The expression of immediate early viral gene (IE3) is required for significant down-regulation of mature miR-199-5p, miR-199-3p, miR-214 and their primary transcript.

The most commonly used procedure to examine the importance of viral products on infection processes is the comparison of active and UV-inactivated virus. UV-inactivation damages viral DNA, making viruses incapable of gene expression and replication. Another tool in the case of MCMV is the use of IE3 mutant strains (MCMVdie3), which does not express IE3 gene product. IE3 gene encodes the transcriptional transactivator IE3 protein whose expression is essential for the expression of early genes and virus replication. The use of the MCMVdie3 mutant virus instead of UV-inactivation offers the advantage of a phenotype reversal as the replication cycle of the MCMVdie3 mutant can be restored in NIH-3T3-BAM25 cells, which express the viral IE1 and IE3 genes (Angulo et al. 2000). The data presented shows that in fibroblasts infected with MCMVdie3 the expression of miR-199a/214 is not down-regulated. There was an observable trend towards increasing the pri-miR-199a/214 level at 2, 4, and 8, as well as a small reduction at 48 hours following MCMVdie3 infection, which was markedly less than that seen in MCMV infected cells at 48 hpi (Figure 3.15). These changes may result from the ability of the MCMVdie3 mutant virus to trigger cellular cascades during the initial attachment to host cells, the release of different tegument proteins during entry, and/or the

expression of considerably attenuated levels of viral gene expression downstream of IE1/IE2 (Angulo et al. 2000; Lacaze et al. 2011). More importantly, the replicative capacity of the MCMVdie3 mutant is restored by the complementary host cell line NIH-3T3-BAM25 cells, and as expected the pri-miR-199a/214 is down-regulated under these conditions. The inhibition of the primary transcript in MCMVdie3 infected NIH-3T3-BAM25 cells (~2.5-fold) was not as drastic as that seen in wild type MCMV infection of NIH-3T3 cells (~15-fold). This reduced effect could a result from attenuated restoration of viral replication in NIH-3T3-BAM25 cells in contrast, with the MCMV (Angulo et al. 2000). More interestingly, the level of primary transcript in NIH-3T3-Bam25 where IE3 is expressed was inhibited in comparison to the parental NIH-3T3 cell line (Figure 3.16). This suggests that IE3 may play a direct role in the transcriptional regulation of miR-199a/214 or that it may play an indirect role through a cellular transcription factor. Further experiments are required to explore this hypothesis.

3.4.5 HCMV uses a conserved mechanism to regulate miR-199a/214 expression

In spite of the similarities between MCMV and HCMV (described in section 1.2.4), differences still exist between the viruses and must be considered. These viruses only share ~80 homologous ORFs, about 40% of the estimated number of ORFs encoded by these viruses (Rawlinson et al. 1996; Brocchieri et al. 2005). There are also functional differences between homologous MCMV and HCMV proteins, such as the HCMV IE1 protein, shown to bind chromatin, whereas this is not the case for the MCMV IE1 homolog (Maul and Negorev 2008). Therefore, the viruses have evolved different mechanisms for targeting the same signaling pathways in host cells.

While the overall reduction in mature miR-199-5p, miR-199-3p and miR-214 expression occurs in both infections, this does not necessarily indicate that similar mechanisms are involved. As shown in Figure 3.18, HCMV infection resulted in a clear reduction of the pri-miR-199a/214 by 4 hpi that occurred at the promoter level (Figure 3.19). TWIST-1 protein was also found to play a part in this regulation, at least by 24 hpi (Figure 3.20). The reduction of the human TWIST-1 mRNA and protein by HCMV occurs faster than for MCMV infection, either indicating the

involvement of different viral factors or differences in the cell lines used. As found with MCMV, HCMV infection of cells in which TWIST-1 was knocked down, resulted in an additive effect on the suppression of miR-199-5p, miR-199-3p and miR-214 (Figure 3.21), implying the involvement of other factors or mechanisms besides TWIST-1 in this regulation.

Overall, the results presented in this chapter demonstrate that the down-regulation of the primary transcript encoding miR-199a-2 and miR-214 in MCMV and HCMV infected fibroblast cells occurs at the transcriptional level. Additionally, this down-regulation occurs at early times post infection starting at 4 hours and seems to be dependent on the expression of IE3 and/or *de novo* viral gene expression. It was further shown that SRF and ELK-1 regulate the basal transcription level of miR-199a/214 cluster in uninfected cells and that TWIST-1 has a role in regulating the expression of miR-199a/214 and is down-regulated in both infections. Finally, the characterisation of the miR-199a/214 promoter described in this work is likely to be a useful tool for further studies that examine the transcription factors responsible for the regulation of miR-199-5p, miR-199-3p, and miR-214 expression in response to different physiological and pathogenic stimuli.

4 A proposed Model for the Antiviral Function of miR-199-3p in CMV Infections

4.1 Introduction

It has previously been shown that MCMV and HCMV mediate down-regulation in expression of the miRNA cluster miR-199/214 that encodes miR-199-5p, miR-199-3p and miR-214. *In vitro* overexpression of miR-199-3p and miR-214 can significantly inhibit the growth of these viruses. The antiviral properties of miR-199-3p also extend to other herpesviruses belonging to different subfamilies such as HSV-1 (*Alphaherpesvirinae*) and mouse γ-herpes virus (*Gammaherpesvirinae*) (Santhakumar et al. 2010). Therefore, the work presented in this chapter focuses on miR-199-3p since it harbours the broadest antiviral properties against herpes viruses. This chapter addresses the question of whether miR-199-3p is able to regulate host signaling pathways by targeting multiple transcripts, and if these regulated pathways are known to play an important role during the CMV life cycle.

4.1.1 Functions of miR-199-3p in cells

So far, a role for miR-199-3p has been implicated in several cancers, viral infections, as well as a wide range of biological processes.

- **Cancer**

Dysregulation of miR-199-3p has been found to be associated with several human cancers (Table 1.5). However, its significance has only been studied in some of these. Expression of miR-199-3p has been shown to be downregulated in hepatocellular carcinoma, epithelial ovarian cancer and osteocarcinoma cells, whereas it is upregulated in ovarian and breast cancers. The overexpression of miR-199-3p attenuates cell proliferation, survival and invasiveness in hepatocellular carcinoma as well as osteocarcinoma cells (Fornari et al. 2010; Henry et al. 2010; Yin et al. 2010; Duan et al. 2011; Hou et al. 2011; Cheng et al. 2012). In contrast, it induces the same biological processes in the case of breast cancer (Shatseva et al. 2011). A number of validated targets of miR-199-3p are associated with its above

mentioned role in cancer cells (Table 4.1). These are mainly involved in MET and mTOR signaling.

- **Cardiac proliferation and regeneration**

Functional screening identifies miR-199-3p as a proliferative miRNA in cardiomyocytes. The overexpression of miR-199-3p in neonatal and adult cardiomyocytes results in increased levels of cyclin genes that correlate with enhanced proliferative capacity of these cells *in vivo*. The exogenous administration of miR-199-3p into the infarcted heart also has a positive effect on minimising the infarct mass and improving cardiac function, consistent with the impact of promoting the proliferation of cardiomyocytes. miR-199-3p regulates cardiomyocyte proliferation via targeting its calcium signaling (Eulalio et al. 2012) (Table 4.1).

- **Chondrogenesis**

A bone morphogenic protein 2 (BMP2), which triggers chondrogenesis, was reported to inhibit the expression of miR-199-3p. miR-199-3p was found to repress the chondrogenesis via direct targeting of the SMAD1 transcription factor. The overexpression of miR-199-3p reduces expression of marker genes for chondrogenesis such as cartilage oligomeric matrix protein (COMP), type II collagen, and Sox9 (Lin et al. 2009) (Table 4.1).

- **Inflammation**

miR-199-3p was reported to be involved in the mechanism regulating the implantation and quiescence of the myometrium during pregnancy as well as its transition into a contractile state during labour (Chakrabarty et al. 2007; Williams et al. 2012). miR-199-3p was up-regulated in pregnant mouse myometrium and down-regulated during labour, thereby correlating with the differential regulation of the inflammatory gene PTGS2 (COX-2) and the production of prostaglandin and TNF-α Down-regulation of miR-199-3p also contributes to inflammation of joints in patients with osteoarthritis via PTGS2 (COX-2) and prostaglandin production (Akhtar and Haqqi 2012) (Table 4.1).

- **Viral infection**

miR-199-3p has been reported to significantly inhibit viral function in a range of virus families (*Flaviviridae* "HCV", *Hepadnavirus* "HBV", *Togaviridae* "SFV", and *Herpesviridae* "CMV – HSV-1 – MHV-68") (Murakami et al. 2009; Santhakumar et al. 2010; Zhang et al. 2010). Although these viruses have distinct replication processes, it is possible that they employ similar host proteins or signaling to support their life cycle. Therefore, it is possible that miR-199-3p targets factor(s) or signaling cascades that are shared amongst all these viruses and are crucial for their respective life cycle. However, miR-199-3p was shown to target the HCV and HBV RNAs during infections (Murakami et al. 2009; Zhang et al. 2010) (Table 4.1).

Function of miRNA	Regulated pathway and validated target genes	Cells	Reference
anti-inflammatory	-***Prostaglandin signaling*** -PTGS2 (COX-2)	Uterus and chondrocytes	(Chakrabarty et al. 2007; Akhtar and Haqqi 2012; Williams et al. 2012)
Negative regulator of Proliferation, invasion, and survival of cancer cells	-***MET signaling*** -MET -CD44 -PAK4 -STAT3 ***-mTOR signaling*** -mTOR	Hepatocellular, ovarian carcinoma, and osteosarcoma cell lines	(Fornari et al. 2010; Henry et al. 2010; Yin et al. 2010; Duan et al. 2011; Hou et al. 2011; Cheng et al. 2012)
Positive regulator of proliferation	-CAV-2	Breast cancer and hair follicle	(Shatseva et al. 2011)
	-Calcium signaling -HOMER1 -HOPX	Cardiomyocytes	(Eulalio et al. 2012)
Epigenetic regulation	-BRM	Cancer cell lines	(Sakurai et al. 2011)
Negative regulator of chondrogenesis	***-BMP-2 signaling*** -SMAD1	Chondrocytes	(Lin et al. 2009)

Antiviral function	Hepatitis B surface antigen (HBsAg) transcript.	Hepatic cell infected with HBV	(Zhang et al. 2010)
	HCV RNA	Hepatic cells infected with HCV	(Murakami et al. 2009)
	Unknown	Fibroblast cells infected with either HCMV, HSV-1, or SFV	(Santhakumar et al. 2010)

Table 4.1: List of miR-199-3p-regulated functions and target genes.

4.1.2 Aims

Given that miR-199-3p has antiviral properties in a range of viruses, this may relate to targeting host genes, rather than to direct interactions with viral factors. For this reason, work in this chapter is aimed at understanding the role of miR-199-3p in host cells during infection. In order to address this, expression profiling was carried out comparing cells transfected with miR-199-3p mimics versus inhibitors. Following analysis of transcriptoma profile, the targets of miR-199-3p were selected on the basis of genes that were regulated by the expression of miR-199-3p and contained seed match sites in their 3′UTRs. The modulated biological functions and signaling pathways associated with these potential targets were then inferred using the Ingenuity Pathway Analysis (IPA). Literature studies were then used to determine the pathways implicated in the modulation of viral infection.

4.2 Results

4.2.1 Experimental design of whole genome gene expression study

For investigation into the cellular targets of miR-199-3p, the mRNA profile was examined in NIH-3T3 fibroblasts in which miR-199-3p was over-expressed by mimics or knocked down by inhibitors. The mRNA expression was analysed using transcriptome microarrays from Affymetrix as miRNA are believed to primarily transcriptionally suppress the target and lead to mRNA degradation.

Cells were untreated or transfected with miR-199-3p mimic, inhibitor, or control siRNA (RISC-free siRNA) for 72 hours. RISC-free siRNA is RNA duplex that is chemically modified to impede the incorporation into RISC complex, however, it is used to control for non-specific effects of transfection. miRNA mimics are chemically modified double-stranded RNAs that mimic endogenous mature miRNAs, in here one strand is preferentially incorporated into RISC. miRNA inhibitors are chemically modified single-stranded RNAs that act as a 'fake' target and inhibit the endogenous miRNA. Total RNA was harvested from 3 replicates of untreated or miR-199-3p mimic transfected cells as well as from 4 samples of control siRNA or miR-199-3p inhibitor transfected cells. Prior to the microarray experiment, the transfection efficiency and RNA integrity were assessed. All 14 RNA samples had a RIN (RNA Integrity Number) value of ≥ 9.10, which meets the required RNA integrity for microarray analysis (Jones et al. 2006). The extent of over-expression or inhibition of miR-199-3p in these samples was assessed by qRT-PCR. Transfection of miR-199-3p inhibitor into NIH-3T3 cells resulted in at least a 2 fold knockdown whereas transfection with an miR-199-3p mimic gave a 22.8 fold increase relative to control RISC-free siRNA or untreated samples (Figure 4.1). These RNA samples were then subjected to the experimental preparation according to manufacturer's protocol and hybridized onto GeneChip Mouse Gene 1.0 ST Array (Affymetrix), which was performed by Marie Craigon at the Division of Pathway Medicine, The University of Edinburgh, UK.

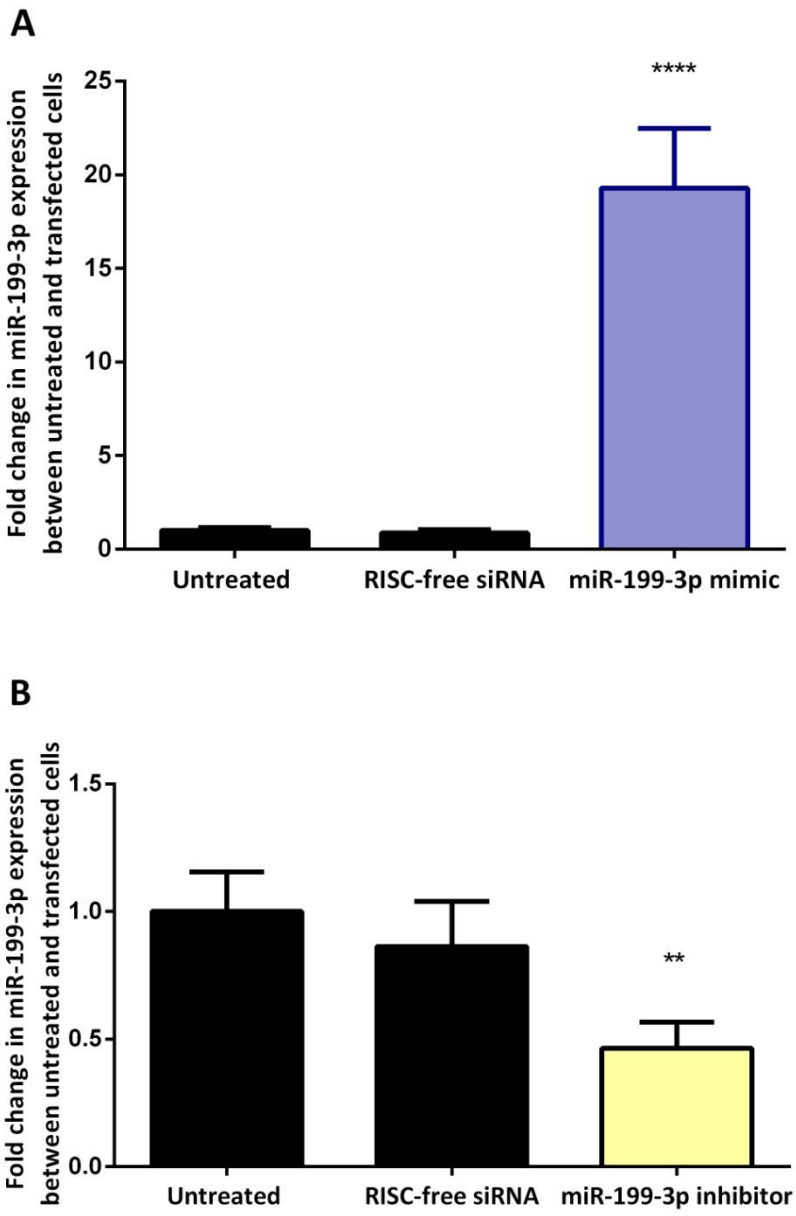

Figure 4.1: The quantification of miR-199-3p levels following transfection of its mimic and inhibitor. Up-regulation of miR-199-3p in cells transfected with miR-199-3p mimic (A) and inhibition in miR-199-3p in cells transfected with miR-199-3p inhibitor (B) compared to untreated cells. NIH-3T3 cells were untreated or transfected with 25nM control RISC-free siRNA, miR-199-3p mimic (A) or miR-199-3p inhibitor (B) for 72 hours. The expression level of miR-199-3p was quantified by qRT-PCR and normalised to miR-16. Data presented are the mean fold change ± S.D (n=5). **$p < 0.01$ and ****, $p < 0.0001$ compared to untreated cells determined by two-tailed Student's *t* test.

4.2.2 Array quality control (QC) metrics

Several statistical methods were used to determine the quality of the array experiment, including both platform specific and sample specific controls, as outlined below.

4.2.2.1 Affymetrix GeneChip Built in Controls

The GeneChip mouse Gene 1.0 ST ArrayChip has four built-in controls designed to assess the quality of the array experiment including cDNA preparation, labelling, hybridisation, and resultant signal intensities.

1- 5,222 probe sets were defined as negative controls to estimate the background signal.
2- 1,324 probe sets were used as positive controls to indicate the overall quality of the cDNA sample.
3- 4 spike-in hybridisation controls of increasing concentrations were selected to examine the hybridisation efficiency.
4- 4 spike-in Poly-A controls were used to assess the success of the cDNA preparation, in particular the reverse transcription step.

1 and 2) Negative and positive controls

The signal obtained from the negative probes of each GeneChip is expected to be an artefact of the imaging system background, non-specific binding or cross-hybridisation. The median signal that was produced from these negative probes defined the background (~ 3.35 arbitrary unit (a.u.)) whereas the median deviation (MAD) of the probes determined the noise in the array (~0.88 a.u.) as illustrated in Table 4.2. These values were then used to establish the limits of detection within the array, so that genes with expression values below the negative could be discarded. The median intensity values obtained from the positive control on the GeneChips was ~6.4 compared to the median of the intensities of the negative probes. However, the median values of the expression intensities of negative and positive probe sets within each array chip were comparable between chips. The intensity values for positive probe sets were also found to be stronger relative to the negatives, which reflects the background level (see Figure 4.2a).

3) PolyA unlabeled spikes: in order to monitor the quality of experimental preparation of the samples, four polyA-mRNAs of *Bacillus subtilis* (lys, phe, thr, and dap) were spiked into each RNA sample at various concentrations (1, 2, 4, and 15 fgrams (fg)) respectively, in accordance with the manufacturer's instructions. As can be seen in Figure 4.2b, the lowest signal intensities for all the 14 chips were for lys mRNA, which subtly increased in phe and thr. The strongest intensity values were found in the dap transcript, as it was spiked at a higher concentration of 15fg. This suggests that the processed samples were of sufficient quality to produce informative results.

4) Hybridisation labelled spikes: BioB, BioC, BioD and CreX transcripts were biotinylated and spiked into the hybridization buffer in various concentrations by the manufacturer. These transcripts served as controls for the efficiency of hybridization. As illustrated by Figure 4.2c, the biotin-labelled spike in transcripts exhibited a similar pattern of signal intensities among all 14 GeneChips. The increase in the intensities of the control transcripts was found to correlate with the concentration of biotinylated transcripts, which is an indication of successful and uniform hybridisation, staining and washing.

The GeneChips	Median of Negative control intensities (a.u)	Median absolute deviation (MAD)	Background Signal (a.u)
Untreated _1	3.39498	0.9078	4.30278
Untreated_2	3.36119	0.89486	4. 25605
Untreated_3	3.34638	0.88528	4.23166
RISC-free siRNA transfected_1	3.38342	0.89364	4. 27706
RISC-free siRNA transfected_2	3.3185	0.8567	4.27706
RISC-free siRNA transfected_3	3.38534	0.88864	4.27398
RISC-free siRNA transfected_4	3.36806	0.8987	4. .26676
miR-199-3p mimic transfected_1	3.35568	0.8848	4. 24048
miR-199-3p mimic transfected_2	3.33461	0.87006	4. 20467
miR-199-3p mimic transfected_3	3.33031	0.8828	4. 21311
miR-199-3p inhibitor transfected_1	3.38186	0.88278	4. 26464
miR-199-3p inhibitor transfected_2	3.33506	0.8691	4. 20416
miR-199-3p inhibitor transfected_3	3.28884	0.8312	4. 12004
miR-199-3p inhibitor transfected_4	3.34047	0.85412	4. 19459

Table 4.2: The background signal of each GeneChip. The intensity values of 5,222 probe sets, acting as negative built-in controls, were used to estimate the background signal of each GeneChip. The obtained background value was calculated for each chip based on the median value of the negative intensities and the median absolute deviation. The median absolute deviation (MAD) was computed by StatPlus statistical tool pack software (AnalystSoft).

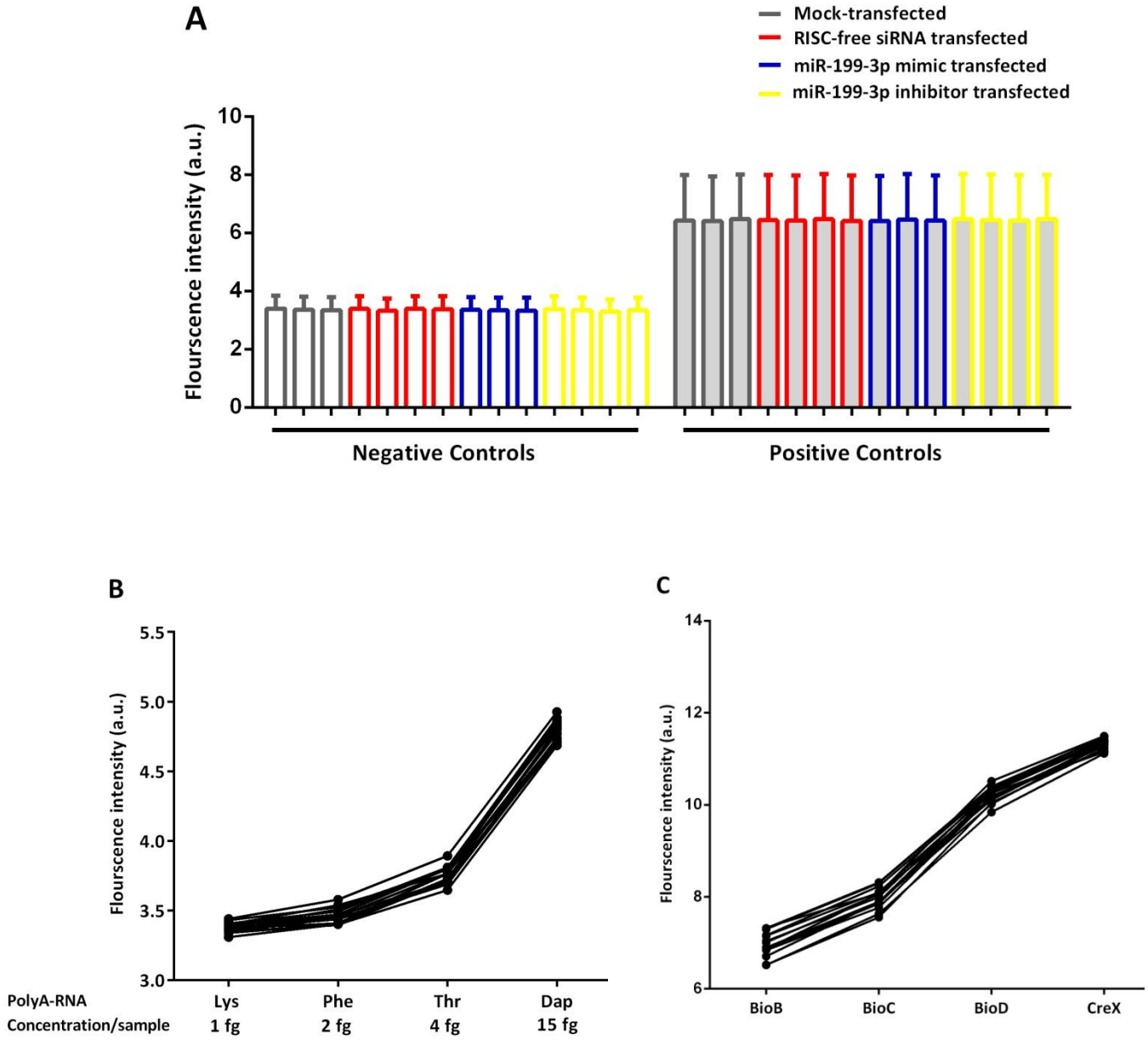

Figure 4.2: Summary of Affymetrix microarray quality control data. A) The median of the negative and positive controls for each GeneChip. B) Four poly-A RNA controls were added to the RNA samples in different concentrations in order to assess the labelling efficiency and processing of RNA samples. C) Four hybridisation controls are spiked into the hybridisation buffer used in this experiment at increasing concentrations (1.5 pM BioB, 5 pM Bio C, 25 pM BioD, and 100 pM Cre).

4.2.3 Pre-processing of data

Pre-processing is a preliminary step applied to the unprocessed raw data prior to the differential expression analysis. This process involves three steps: 1) produce background corrected and log-2 transformed values for probe intensities, 2) normalise probe intensities between the different GeneChips by means of quantile normalisation, and 3) summarise all the related probes into a signal expression value. The pre-processing steps were conducted using a robust multi-array average (RMA) within the Partek program and Madmax pipeline https://madmax.bioinformatics.nl.

Box plot of log2 intensities

The box plots of the log2 intensity distribution are plotted for the 14 GeneChips (Figure 4.3a). The distributions of raw log-intensities do not show dramatic differences between the chips, however these differences in log-intensities were corrected by RMA to make the distributions most comparable.

Principle component analysis (PCA)

PCA is a statistical method used to summarise complex datasets into a compact principle components. This method was performed on RMA pre-processed values for all the GeneChips and the results plotted in Figure 4.3b. An obvious correlation can be seen between the expression profiles of the biological replicates in miR-199-3p mimic, inhibitor and untreated cells, as these replicates clustered closely to each other. The biological replicates in the RISC-free treated samples do not seem to cluster together and this is an indication of variability within the expression profile in these samples, which warrants caution in using them as controls.

Clustering analysis

Clustering analysis is a mathematical approach that assigns GeneChips into groups based on the similarity/dissimilarity of the expression profiles of these samples. This data was then analysed using Partek's default measures, Elucidean distance and average linkage and plotted as a hierarchical tree (dendrogram). GeneChips were closely clustered to the corresponding biological treatment, except that two of four RISC-free samples were clustered with different groups, either untreated or miR-

199-3p inhibitor (Figure 4.3c). Irrespective of the results of the PCA and clustering technique, all four chips of RISC-free siRNA were included in the subsequent analysis.

Overall, these primary quality control measures and pre-processing methods showed that the GeneChips used were of satisfactory standard, allowing for the differential expression analysis.

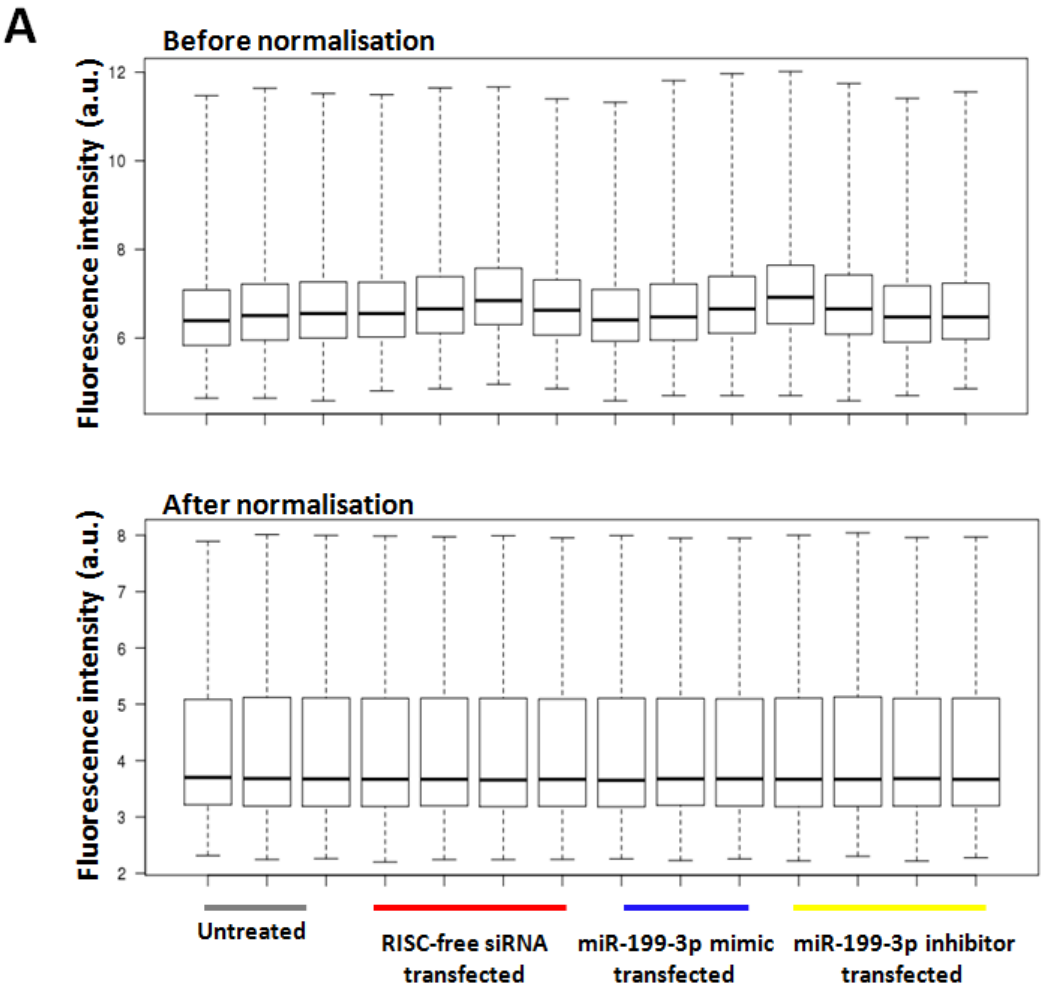

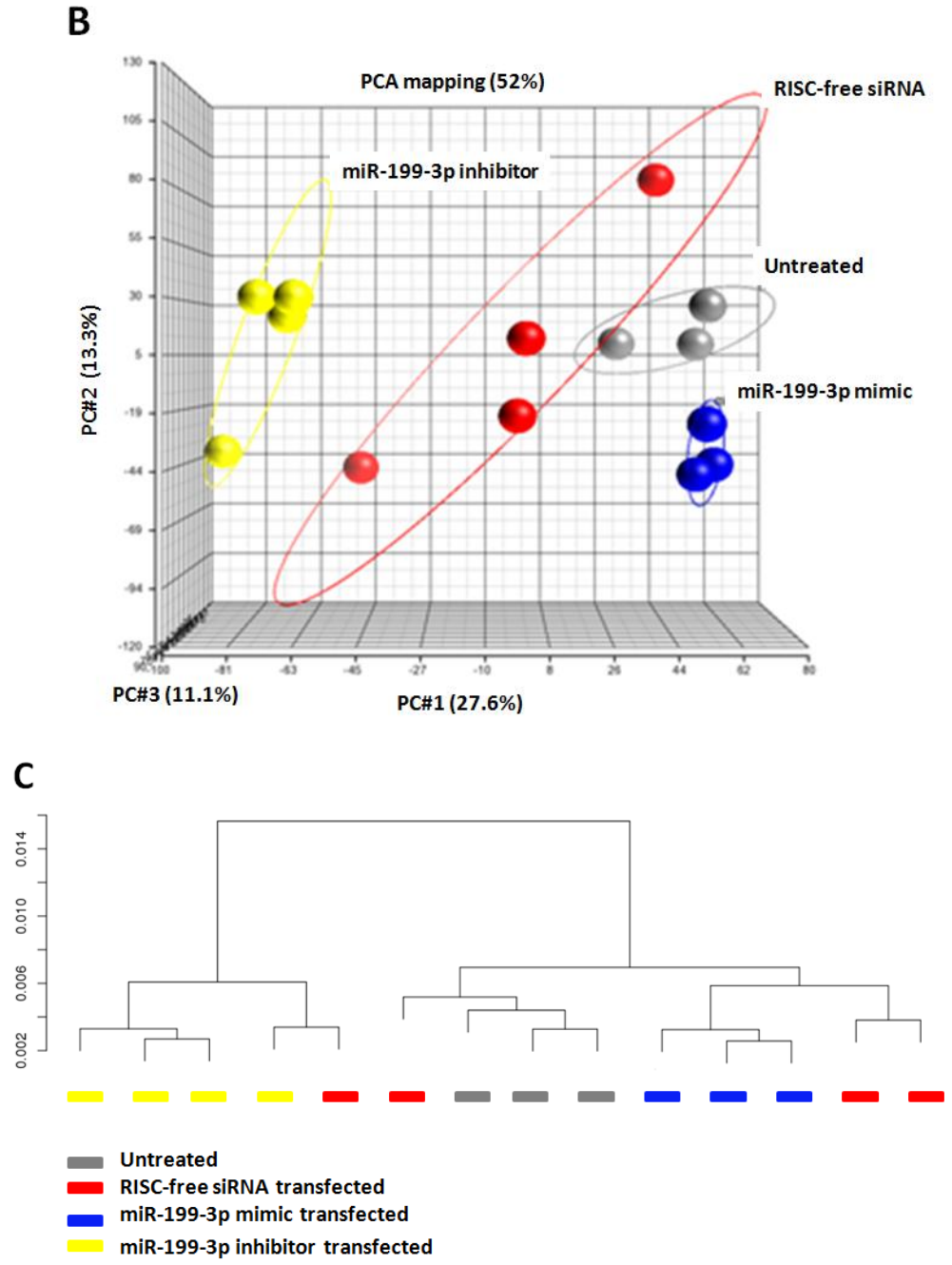

Figure 4.3: Normalisation and comparisons of the expression data between GeneChips. A) Box plots representation of log-intensity distributions of raw and normalised data, which was corrected using RMA method. B) A principle component analysis (PCA) was performed on the expression data of all the 14 array chips. The points represent the different chips and are coloured based on the biological treatment and ellipsoid (circle) are drawn around the biological replicates of each biological treatment. PCA shows a variance of 52%. C) A hierarchical cluster analysis based on the similar expression profile between the various samples. The Y-axis represents the distance between any two samples measured by the correlation distance method (Elucidean). The distance between the samples was computed using the average linkage method and then plotted in Madmax pipeline.

4.2.4 Identification of differentially expressed transcripts in miR-199-3p mimic versus inhibitor transfected NIH-3T3 cells

The next step involved the identification of the differentially regulated genes in response to miR-199-3p mimic and miR-199-3p inhibitor at the genome-wide level. The data were filtered in two steps: the first discarded the probeset intensities that were not expressed above the background; the second selected only the transcripts with differential expression levels.

The background signal of each GeneChip was produced from the background and noise measurements, which were calculated from the signal intensities generated from the built-in negative controls (5,222 probe sets), as previously demonstrated in Table 4.2. The signal intensities that were equal to or lower than the background signals were discarded. As a result, of 28,853 transcript clusters, only 12,207 transcripts, corresponding to 10,652 genes, were expressed over background and therefore included in the analysis.

In the next filtering step, the list of 12,207 transcript intensities were imported into Partek's analysis program in order to calculate the differential expression between the mean values of two different treatments, as well as the statistical significance (p-values) using ANOVA. Several comparisons were conducted for the detection of differentially expressed transcripts: 1) the data from miR-199-3p mimic or inhibitor were compared to RISC-free siRNA; 2) the data from miR-199-3p inhibitor were compared to miR-199-3p mimic; and 3) the data of untreated samples was compared to RISC-free siRNA. A fold change of ≤ 1.2 down in miR-199-3p mimic or ≥ 1.2 up in miR-199-3p inhibitor relative to RISC-free siRNA treatment and FDR p-value below 0.05 were used as cut offs. The fold change and FDR p-value cut offs resulted in 190 down-regulated genes in response to miR-199-3p mimic and 198 up-regulated genes for inhibitor transfection (Appendix 6). 12 genes were found to be intersected between the down and upregulated gene lists. Another method for determining differential expression of genes in response to miR-199-3p was direct comparison of the miR-199-3p mimic versus inhibitor data. The fold change and significance cut-offs were set at ≤ 1.4 and FDR p-value < 0.05, which identified 198 down-regulated genes by miR-199-3p mimic versus miR-199-3p inhibitor. In order to ensure that the

differential expression was not based on transfection, RISC-free siRNA and untreated cells were subjected to the above analysis. A total of 28 up-regulated and 16 down-regulated genes were found, with a fold difference of (≥,≤) 1.2 and FDR p-value < 0.05. Since these genes change as a result of the transfection protocol, their differential expression in miR-199-3p transfected cells was considered as a false positive. However, the transfection procedure and RISC-free siRNA did not affect the gene expression profile of most of the genes indicating it is reliable system.

4.2.5 SylArray analysis for the enrichment of miR-199-3p seed site across the 3'UTRs of miR-199-3p regulated genes

For the purpose of assessing whether differences in gene expression data could result from direct regulation of genes by miR-199-3p, a computational analysis was performed using SylArray. The list of 12207 transcripts was ranked based on the differential expression in mimic samples compared with inhibitor samples (from the most down-regulated to most up-regulated transcripts) regardless of the statistical significance and then uploaded to SylArray program. The 3′UTR sequences were retrieved from the SylArray database and submitted to the ranked list. The SylArray analysis identified a significant overrepresentation of the conserved miR-199-3p seed words [the first 2–7 followed by an 'A' or 2–8 nucleotides of miR-199-3p] across the ranked list of 3′UTRs. The other miRNA seed sequences were not enriched in the 3’UTRs changing in this dataset. The enrichment curve of miR-199-3p peaks in the left of the plot, which indicates a direct effect of miR-199-3p, as more targets are present within the most down-regulated part of this plot (Figure 4.4). This was also the case when evaluating mimic dataset individually, relative to the RISC-free siRNA control. Figure 4.4 also shows an unexpected depletion of miR-29a seed sequences across the most up-regulated transcripts in the miR-199-3p ranked list, which has not been examined.

It can be concluded that the changes in gene expression observed in response to miR-199-3p are at least partly mediated by direct interaction with elements in the 3′UTRs of host genes.

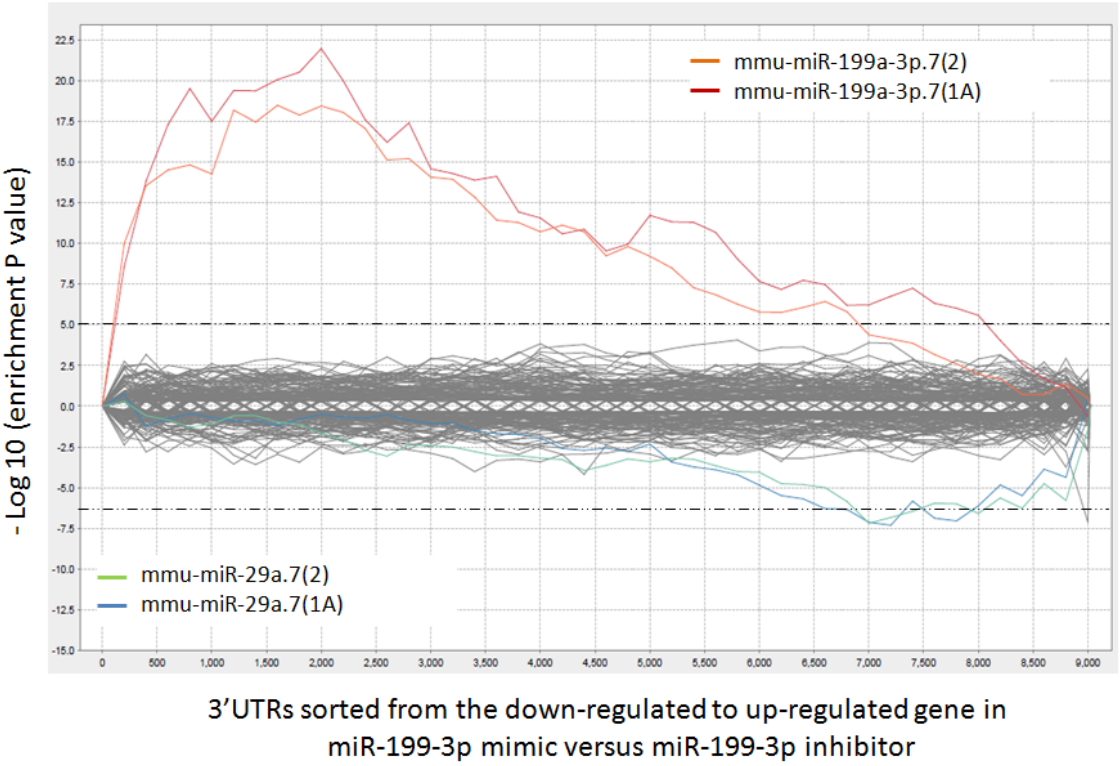

Figure 4.4: SylArray plot analysis for the seed-match for miR-199-3p in the expression profile of cells transfected with miR-199-3p mimic versus inhibitor. The X-axis denotes all the annotated 3′UTR sequences in the ranked list of genes downregulated in cells treated with miR-199a-3p mimic versus upregulated in cells treated with miR-199-3p inhibitor (left to right). The Y-axis represents $\log_{10}$-transformed P values for enrichment of seed site. The dotted black line denotes the Bonferroni-corrected P value significance cut-off of 0.01. This figure illustrates the words of length 7mer for miR-199-3p, 7-mer(1A)=CTACTGA and 7-mer(2)=ACTACTG, which are highlighted in red and orange. Also, 7-mer(1A)=GGTGCTA and 7-mer(2)=TGGTGCT for miR-29a are coloured in blue and green, respectively.

4.2.6 The prediction of miR-199-3p targets using TargetScan

The expression profile of down-regulated genes in miR-199-3p mimic transfected samples compared to miR-199-3p inhibitor could be a result of both direct and indirect regulation of gene expression by this miRNA. As shown by the SylArray plot, there is clearly a global enrichment for miR-199-3p seed sites in the genes that are down-regulated. To more specifically examine these sites, TargetScan algorithms were applied. A list of candidates of direct miR-199-3p targets was produced: out of the 198 down-regulated genes, 30 putative targets conserved between human and mouse were predicted using TargetScan, based on the requirement that their 3′ UTRs have at least one seed target site for miR-199-3p (Table 4.3). Another 20 down-regulated genes were predicted to be targets of miR-199-3p in only the mouse genome while seven other genes were only predicted in the human genome. Three of the down-regulated genes, PTGS2, CD44, and MET are previously validated targets of miR-199-3p, (Chakrabarty et al. 2007; Kim et al. 2008; Henry et al 2010), supporting the validity of our approach.

Target gene	Target sites in mouse 3′UTR	Target sites in human 3′UTR	Fold-Change
ANKRD13C	3 sites	1 site	-1.94
CD151	4 sites	1 site	-4.9757
CD2AP	1 site	2 sites	-1.41428
CD44	1 site	1 site	-1.734
CEP55	1 site	1 site	-1.52784
CNOT7	2 sites	1 site	-1.41417
CYB5B	1 site	1 site	-1.76464
DUSP5	1 site	1 site	-1.75294
FAM60A	1 site	1 site	-1.51947
FGF7	1 site	1 site	-1.96465
FKTN	3 sites	1 site	-1.42653
G3BP2	1 site	1 site	-1.67028
GALNT7	3 sites	3 sites	-1.64384
GNPTAB	1 site	1 site	-1.4333
ITGA3	1 site	1 site	-2.61409
ITGA6	1 site	1 site	-1.56552
MAPRE1	1 site	1 site	-1.53862
MSN	1 site	1 site	-1.40409
NET1	1 site	1 site	-1.67275

NUTF2	1 site	1 site	-1.50017
OSTM1	1 site	1 site	-1.49464
OTUD6B	2 sites	1 site	-1.99201
PIK3CB	2 sites	2 sites	-1.6513
PLEKHA3	1 site	1 site	-1.57282
PON2	1 site	1 site	-1.84996
PPP2R5E	2 sites	2 sites	-1.47809
SLC39A10	1 site	1 site	-1.54734
TMSB4X	1 site	1 site	-1.54004
VAMP3	2 sites	2 sites	-2.12268
YWHAE	1 site	1 site	-1.48533

Table 4.3: TargetScan identified 30 targets conserved between mouse and human in the genes regulated by miR-199-3p. Prediction of miR-199 direct targets among 198 genes found to be down regulated in miR-199-3p mimic transfected cells versus miR-199-3p inhibitor cells. The list of genes were analysed using TargetScan (http://www.targetscan.org/) to search for the genes harbouring at least a site for the miR-199-3p seed sequence in the 3′UTR sequence of each gene. 8mer (ACTACTGA), 7-mer(1A)=CTACTGA, 7mer-8m=ACTACTG, and 3′compensatory interaction. The table also contained the official gene symbols for these conserved targets of miR-199-3p between human and mouse.

4.2.7 Pathway and functional analysis of miR-199-3p regulated genes

In order to understand the signaling pathways and functions of miR-199-3p regulated genes, functional and pathway analyses on the 198 genes down-regulated in miR-199-3p mimic transfected versus inhibitor transfected cells, was carried out in Ingenuity pathway analysis programme (IPA) (http://www.ingenuity.com/).

4.2.7.1 The analysis of canonical pathways

A canonical pathway is defined as "a core pathway established for a given molecule in the cell, in which molecular interactions occur in a linear and stepwise manner"(Chung et al. 2011). The IPA library of canonical pathways identified statistically significant enriched canonical pathways associated with the 198 genes regulated by miR-199-3p. Ten canonical pathways met the p-value cut off of ($P < 0.001$). This analysis suggests that miR-199-3p may modulate a number of cellular pathways, which are associated with eicosanoid synthesis, PI3k-AKT signaling, MAP Kinase cascade, and IGF response. Various cancer-related pathways were also present, such as the role of tissue factor in cancer glioma and ovarian cancer (Table 4.4).

4.2.7.2 Functional analysis of miR-199-3p regulated genes

Further analysis was also conducted in IPA to understand the enriched and significant biological functions of genes identified in this dataset. A total of 21 significantly enriched molecular/cellular functions were identified by means of this analysis, using a p-value threshold of 0.001. Among them, the p-value significance was shown to be higher for functions associated with cellular movement, survival, cellular growth, development and proliferation (Table 4.5). These top functions appear to be linked with cancer, which was supported by the presence of canonical cancer pathways and cancer-related pathways, such as impairment in PI3K-AKT functions, IGF signaling, and MAP-kinase activation (Zhu et al. 2011).

Ingenuity Canonical Pathways	P value	Ratio	Molecules
Glioma Invasiveness Signaling	3.08E-06	0.117	RRAS2, F2R, TIMP1, **CD44**, PLAUR, **PIK3CB**, PLAU
Role of Tissue Factor in Cancer	3.46E-06	0.0789	CTGF, RRAS2, **ITGA6**, PLAUR, HBEGF, **PIK3CB**, **ITGA3**, CYR61, EIF4E
PI3K/AKT Signaling	5.13E-05	0.0576	RRAS2,**YWHAE, PIK3CB,** PTGS2, **PPP2R5E**, **ITGA3**, CCND1, EIF4E
Eicosanoid Signaling	5.27E-05	0.0759	PLA2G4A, PTGFR, PTGS1, PTGS2, PLA2G7, **PRDX6**
ERK/MAPK Signaling	2.18E-04	0.0441	PLA2G4A, RRAS2, DUSP1, **DUSP6, PIK3CB, PPP2R5E, ITGA3**, PPP1R14B, EIF4E
Oncostatin M Signaling	5.28E-04	0.114	RRAS2, MT2A, PLAU, CHI3L1
Coagulation System	5.91E-04	0.105	F2R, PLAUR, PLAU, SERPINE1
Ovarian Cancer Signaling	6.83E-04	0.0493	GJA1, RRAS2, PTGS1, **CD44**, **PIK3CB**, PTGS2, CCND1
Role of MAPK Signaling in the Pathogenesis of Influenza	7.37E-04	0.0735	PLA2G4A, RRAS2, PTGS2, PLA2G7, **PRDX6**
IGF-1 Signaling	7.83E-04	0.0566	CTGF, RRAS2, **YWHAE**, SOCS6, **PIK3CB**, CYR61

Table 4.4: The top ranked miR-199-3p regulated canonical pathways based on Ingenuity Pathway Analysis (IPA). P value for inclusion here is ≤ .001. P-value is calculated using Fischer's exact test indicates the probability of the involvement of the genes in the dataset in a given pathway. Ratios represent the number of molecules in the dataset that are found in a given pathway, divided by total number of molecules that make up that pathway. Molecules are shown in the dataset (≥1.4 decrease and $p \leq 0.05$), Potential target genes of miR-199-3p seed (targetscan.org) are shown in bold.

Molecular/Cellular functions	Number of molecules	P value
Cellular Movement	68	6.05E-15-3.87E-04
Cellular Growth and Proliferation	92	1.11E-12-3.48E-04
Cell Death	83	4.87E-12-3.56E-04
Cellular Development	76	4.12E-11-3.48E-04
Carbohydrate Metabolism	41	3.00E-10-3.67E-04
DNA Replication, Recombination, and Repair	22	3.13E-09-3.13E-04
Cell-To-Cell Signaling and Interaction	52	8.01E-09-3.87E-04
Cell Morphology	58	1.84E-08-3.90E-04
Antigen Presentation	37	4.10E-08-2.46E-04
Lipid Metabolism	30	6.24E-08-3.66E-04
Molecular Transport	44	6.24E-08-2.66E-04
Small Molecule Biochemistry	47	6.24E-08-3.87E-04
Cellular Assembly and Organization	41	8.76E-08-2.82E-04
Cellular Function and Maintenance	70	8.76E-08-2.82E-04
Cell Cycle	32	2.42E-06-1.53E-04
Energy production	3	5.36E-06-3.66E-04
Protein synthesis	20	6.39E-06-2.66E-04
Free Radical Scavenging	17	1.29E-05-2.88E-04
Cell Signaling	24	4.88E-05-2.50E-04
Vitamin and Mineral Metabolism	16	4.88E-05-4.88E-04
Cellular Compromise	2	1.23E-05-1.23E-04

Table 4.5: Enrichment of biological functions in the miR-199-3p disregulated genes from Ingenuity Pathway Analysis (IPA). A p-value of inclusion is ≤ .001.

4.2.8 The interpretation of the miR-199-3p data in the context of viral infection pathways

To understand the antiviral role of miR-199-3p in HCMV virus infection, a study of the current literature was conducted in order to determine whether any of the miR-199-3p regulated pathways and candidates targets are already known to be important for CMV infection. Below is a list of putative miR-199-3p targets with links to infection.1) ITGA6, a cellular integrin α-subunit was identified to be down-regulated in miR-199-3p dataset. It has been shown that HCMV utilizes ITGA6 and other integrins as coreceptors during the entry pathway to host cells, most probably at the viral internalisation step. It was also suggested that the activation of integrins trigger the focal adhesion kinase (FAK) and the cytoskeletal rearrangement in HCMV infected fibroblasts (Feire et al. 2004) that is important for cellular signaling events associated with HCMV infection. 2) PIK3CB was found to be down regulated by miR-199-3p. Interestingly, PIK3CB is a lipid kinase having a critical role in initiating the PI3K signaling cascade, which starts from the phosphorylation of phosphatidylinositol 4,5-bisphosphate (PIP2) to the recruitment and phosphorylation of AKT, which has a number of downstream substrates that contribute to proliferation, survival, growth, cellular metabolism, angiogenesis, migration, and cross talk with other signaling pathways, (reviewed by Manning and Cantley 2007). Importantly, PI3K-AKT signaling is known to have an important role in different stages of HCMV infection, from replication to viral spread and persistence (Yu and Alwine 2002; Johnson et al. 2001b; Smith et al. 2007). Moreover, previous studies have shown that a PI3K inhibitor caused reduction in both viral titers and DNA replication in HCMV infection of fibroblast cells (Yu and Alwine 2002; Johnson et al. 2001b; Smith et al. 2007). 3) MAP kinase and its downstream regulated kinase (ERK1/2) is another signaling pathway regulated by miR-199-3p. It has been shown previously that MAPK/ERK kinase can be activated at immediate early times of infection via the binding of the HCMV envelope glycoprotein gB to host cell receptors. The use of U0126, a selective inhibitor of MAPK/ERK kinase had a significantly inhibitory effect on the early viral protein products UL44 and UL84 and the late protein UL94. In addition the phosphorylation of IE1 and IE2 was reduced. Thus, MAPK/ERK kinase is required for viral DNA replication (Johnson et al.

2001a; Boyle et al. 1999). 4) PTGS2 (COX-2) is reported to be a direct miR-199-3p target in human and mouse cells (Chakrabarty et al. 2007; Williams et al. 2012).This gene was found in the microarray study (Results 4.2.4) to be regulated by miR-199-3p expression. The eicosanoid pathway is responsible for prostaglandin production induced upon HCMV infection through the increase in PTGS2 (COX-2). Importantly PTGS2 inhibitors interfere with the accumulation of IE2 and reduce viral replication in cultured fibroblasts (Zhu et al. 2002). In addition, drugs which antagonise prostaglandin synthesis through its receptors and PTGS2 (COX-2) can also block the direct spread of HCMV from cell to cell (Schröer and Shenk 2008). Collectively, the attenuation of infection induced signaling cascades such as integrin coreceptor, PI3K-AKT, ERK-MAP kinase and prostaglandin synthesis (any or all) is expected to impact the infection process (Figure 4.5). These pathways appear to be regulated through direct miR-199-3p target genes. It should be noted that these targets are only those already linked to infection, but it is expected that additional miR-199-3p targets could also be important in this context.

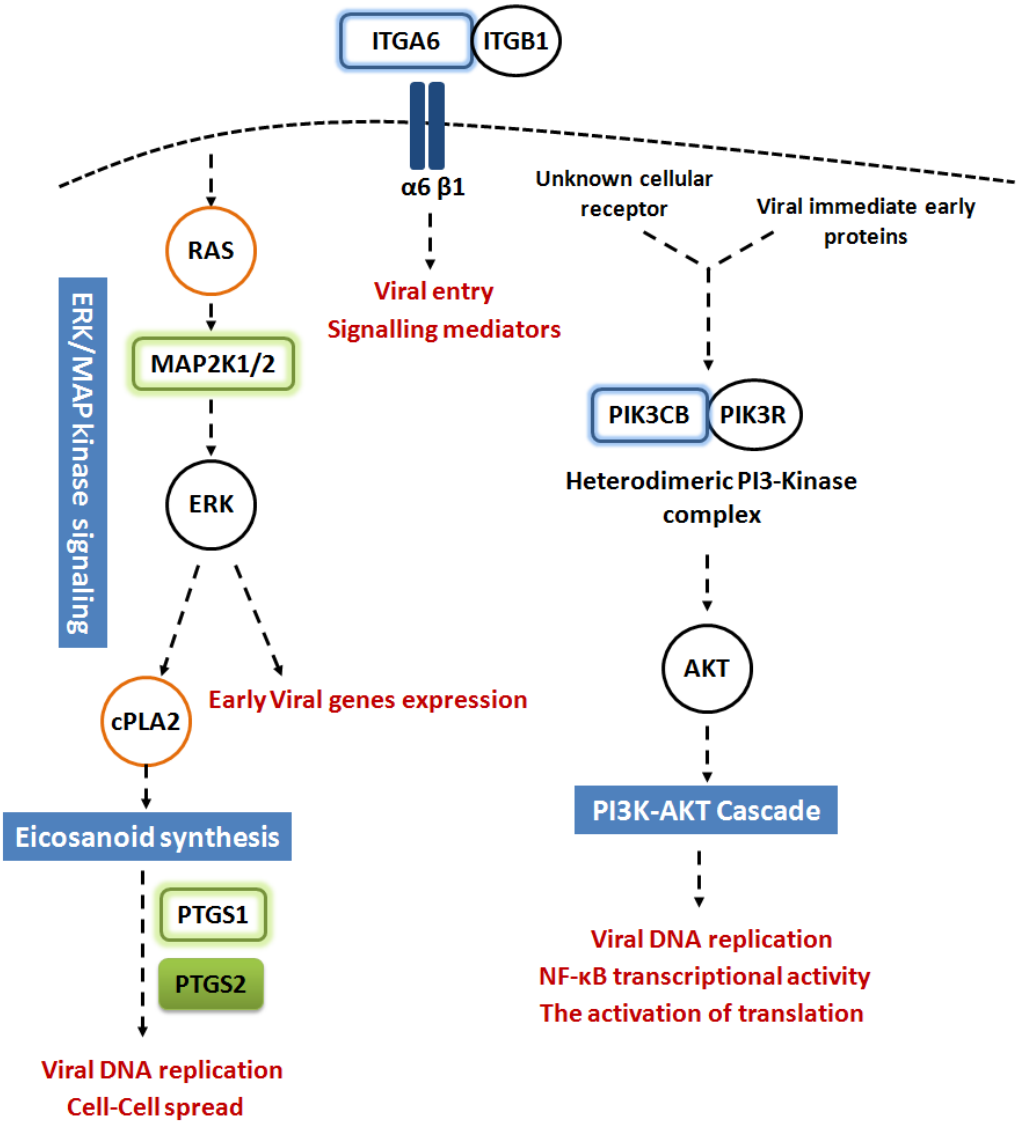

Figure 4.5: A graphical representation for miR-199-3p regulated signaling pathways in context of CMV infection. Predicted conserved and non-conserved targets between human and mouse are shown in blue and green boxes, respectively. Validated non-conserved miR-199-3p target is denoted by shaded green box. Genes which were found to be regulated by miR-199 although no miR-199 sites in their 3′UTRs were predicted are denoted by orange circles.

4.2.9 Network analysis for the potential targets of miR-199a-3p

As discussed in section 4.2.6, 30 putative targets of miR-199-3p have been identified in this study. In addition, based on IPA analysis, several pathways including PI3K-AKT, ERK-MAP kinase, IGF, and prostaglandin signaling are regulated by this miRNA. It was therefore decided to examine whether the 30 targets of miR-199-3p are directly or indirectly associated with the regulated pathways. The 30 conserved potential target genes of miR-199-3p were uploaded into IPA to explore the molecular relationships between the targets and AKT, ERK, IGF, and PTGS, which are the core components in the PI3K-AKT, ERK-MAP kinase, IGF and prostaglandin signaling pathways. 9 putative targets were shown to have a regulatory role in the activation of AKT, while 5 regulated ERK (Figure 4.6). Only PRDX6 was linked with prostaglandin production and the other two targets (PIK3CB and YWHAE) appeared to be involved in insulin-like growth factors (IGF). On the basis of these results, several miR-199-3p target genes appear to be associated with PI3K-AKT and ERK-MAP kinase.

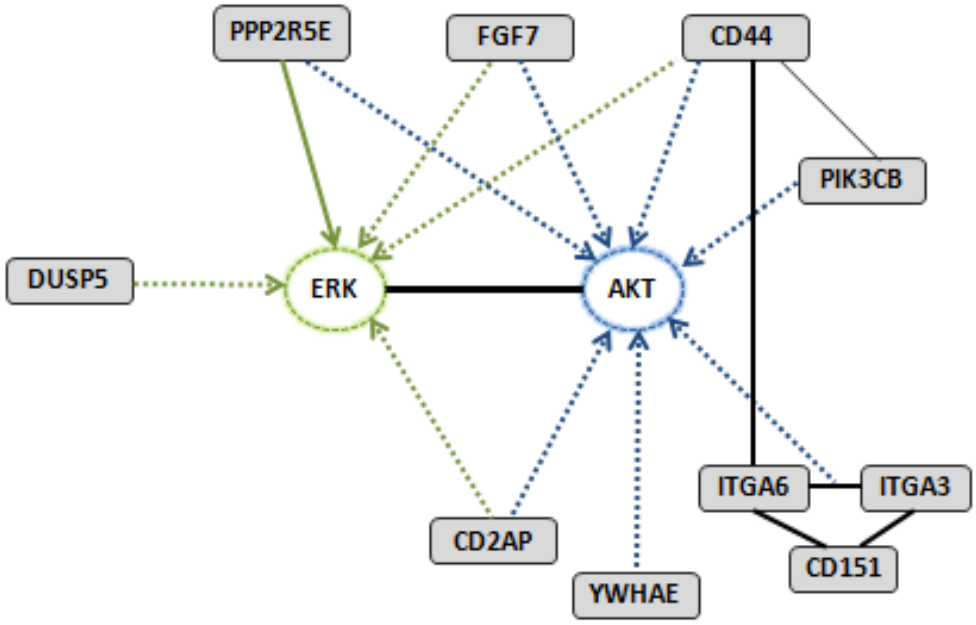

Figure 4.6: A sub-network of a network analysis preformed in IPA using a list of 30 conserved putative targets of miR-199-3p. The interactions between AKT and miR-199-3p potential targets are shown in blue arrows while ERK1/2 and miR-199-3p targets interactions are linked with green arrows, Dash lines denote indirect interactions and solid ones represent direct relationships.

4.2.10 AKT phosphorylation but not ERK1/2 phosphorylation is modulated in miR-199-3p transfected cells

ERK1/2 and AKT signaling are signaling pathways identified in the miR-199-3p dataset, however, ERK1/2 and AKT genes was not found to have sites that match the miR-199-3p seed. Rather, ERK1/2 and AKT interact with a number of miR-199-3p target genes and it was thus hypothesised that miR-199-3p regulates the activities, rather than expression levels, of ERK1/2 and/or AKT proteins through potential target(s) of miR-199-3p that are upstream of either and both ERK1/2 and AKT. In order to determine whether miR-199-3p has an effect on AKT and/or ERK1/2 activation, the phosphorylation of AKT at Ser473 and ERK1/2 at Thr-202 and Tyr-204 were examined in cells transfected with miR-199-3p as these are the main phosphorylation sites in both AKT and ERK1/2. MRC-5 cells were cultured for 48 hours; untreated or transfected with RISC-free siRNA, miR-199-3p mimic or inhibitor. Cell lysates were then harvested and subjected to western blot analysis. As can be seen in Figure 4.7, a small but reproducible reduction in independent experiments was evident in the phosphorylation of Ser473 and Thr308 in AKT but not at Thr-202 and Tyr-204 in ERK1/2 in cells transfected with miR-199-3p mimic when compared to the untreated or control transfected samples. No effect was observed on the phosphorylation of AKT or ERK in cells transfected with miR-199-3p inhibitor.

Based on these results, the IPA identification of AKT regulation but not ERK1/2 was confirmed by examining the down-regulation of phosphorylated (Ser473 and Thr308) in AKT. It appears the activation level of AKT, at least as far as can be indicated by the serine and theronine phosphorylation, is indeed regulated by miR-199-3p.

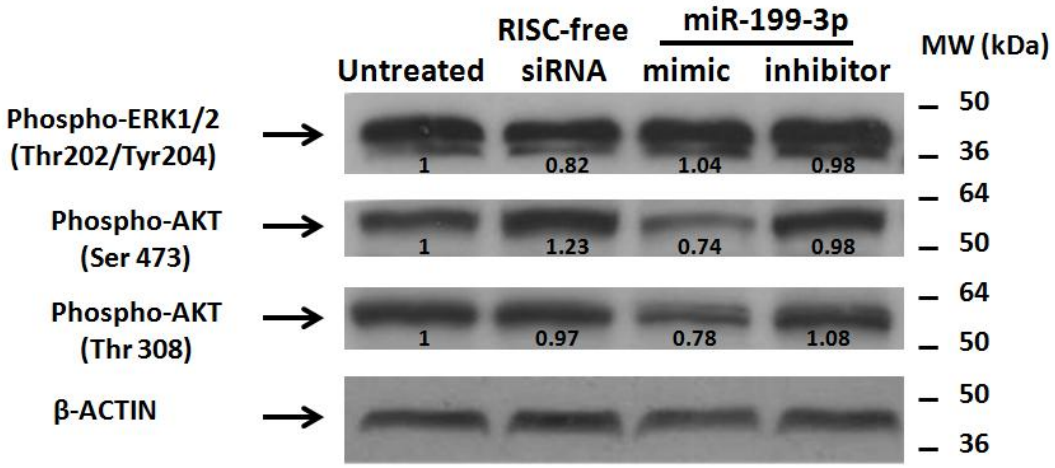

Figure 4.7: miR-199-3p regulates the phosphorylation of AKT but not ERK1/2. Western blot showing a reduction in the phosphorylation of AKT at serine 473 (Ser473) and theronine (Thr 308) residues and no change in ERK1/2 phosphorylation at theronine (Thr202) and tyrosine (Tyr204) residues. MRC-5 cells were untreated or transfected with control RISC-free siRNA, miR-199-3p mimic, or miR-199-3p inhibitor for 48 hours. 20µg of protein was loaded per lane and membrane was immunoblotted with primary antibodies against either phospho-AKT (ser473), phospho-AKT (Thr308), Phospho-ERK1/2 (Thr202/Tyr204), and β-ACTIN. Blots were then quantified by densitometry and normalized to the corresponding β-ACTIN. The untreated was set as 1 and values for other treatments were expressed relative to the untreated value.

4.2.11 Hypothesised model for the regulation of AKT signaling by miR-199-3p

The goal in this chapter was to develop a model for how miR-199-3p exerts its antiviral function. Based on the results described above (4.2.7 to 4.2.10), it appears that miR-199-3p targets upstream regulator(s) of AKT phosphorylation and subsequently inhibits its activation and downstream functions, which could be hypothesized as resulting in the antiviral effects of miR-199-3p against CMV. The IPA's sub-network shown in Figure 4.6 suggested the presence of 9 upstream interactions between potential or validated miR-199-3p targets and AKT. CD44 and 5 other potential targets of miR-199-3p, PIK3CB, ITGA3, ITGA6, CD151, and FGF7 were included in the hypothesised model (see Figure 4.8).

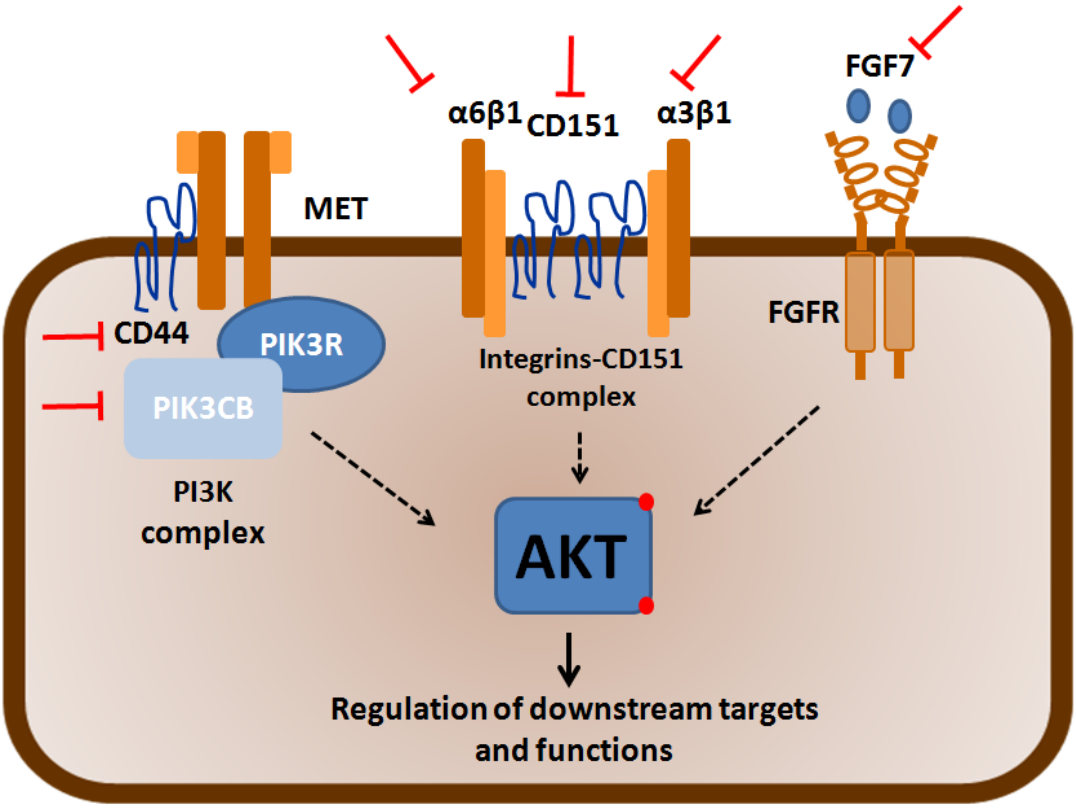

Figure 4.8: Suggested model for miR-199-3p regulation of AKT activation. PIK3CB is an isoform of PI3-Kinase complex, the critical regulator of AKT phosphoregulation. CD44, CD151 and intergrins are adhesion molecules known to induce the activation of PI3-kinase and AKT. Fibroblast growth factor-7 (FGF-7) can bind to it receptor and trigger PI3K-AKT cascades. Red arrows indicate miR-199-3p targets.

4.2.12 Initial validation of miR-199-3p targets from the microarray analysis, PIK3CB, ITGA3, ITGA6, CD151, and FGF7.

PIK3CB, ITGA3, ITGA6, CD151, and FGF7 were found to be regulated by miR-199-3p in the microarray analysis shown in section 4.2.4 and at least one conserved miR-199-3p binding site was found in their 3′-untranslated regions (3′UTR). In order to validate the microarray data, the expression levels of these putative targets were measured using qRT-PCR analysis. As miR-199-3p has antiviral function against MCMV and HCMV infections, it was hypothesised that the targets of miR-199-3p are likely to be conserved in both mouse and human cells. Therefore, mouse NIH-3T3 and human MRC-5 cell lines were mock-transfected or transfected with miR-199-3p mimic or inhibitor. Controls included cells transfected with RISC-free siRNA, *C. elegans* mimic, or *C. elegans* inhibitor. Indeed the expression of the 5 candidate targets was unaffected in cells transfected with negative controls, RISC-free siRNA, *C. elegans* mimic, or *C. elegans* inhibitor in both NIH-3T3 and MRC-5 cell lines. By comparison the expression of all five candidate targets was upregulated with miR-199-3p inhibitor treatment. Up regulation was significant in NIH-3T3 cells, however, in MRC-5 increases were not significantly different from controls. In the presence of miR-199-3p mimic all candidate targets showed a significant decrease in expression in MRC-5 and NIH-3T3, except mouse ITGA6 which was decreased but not significantly. 18S rRNA was included as a negative control and did not show any significant change in the presence of miR-199-3p mimic or inhibitor in comparison to transfected controls or untreated cells (Figure 4.9f). In mouse cells, the expression levels of PIK3CB, ITGA3, CD151 and FGF7 mRNAs were significantly down-regulated by miR-199-3p mimic and upregulated by miR-199-3p inhibitor (Figure 4.9a,b,c,e). For ITGA6, upregulation was only found in cells transfected with miR-199-3p inhibitor, while no significant change was noted upon mimic transfection (Figure 4.9d). In human cells PIK3CB, ITGA3, ITGA6, CD151, and FGF7 mRNAs were reduced in cells transfected with miR-199-3p mimic and no obvious regulation occurred in miR-199-3p inhibitor transfected cells (Figure 4.9a,b,c,d,e).

To conclude, the results from the initial experiment to validate the microarray data suggest that miR-199-3p regulates PIK3CB, ITGA3, ITGA6, CD151, and FGF7 in human and mouse cells.

A

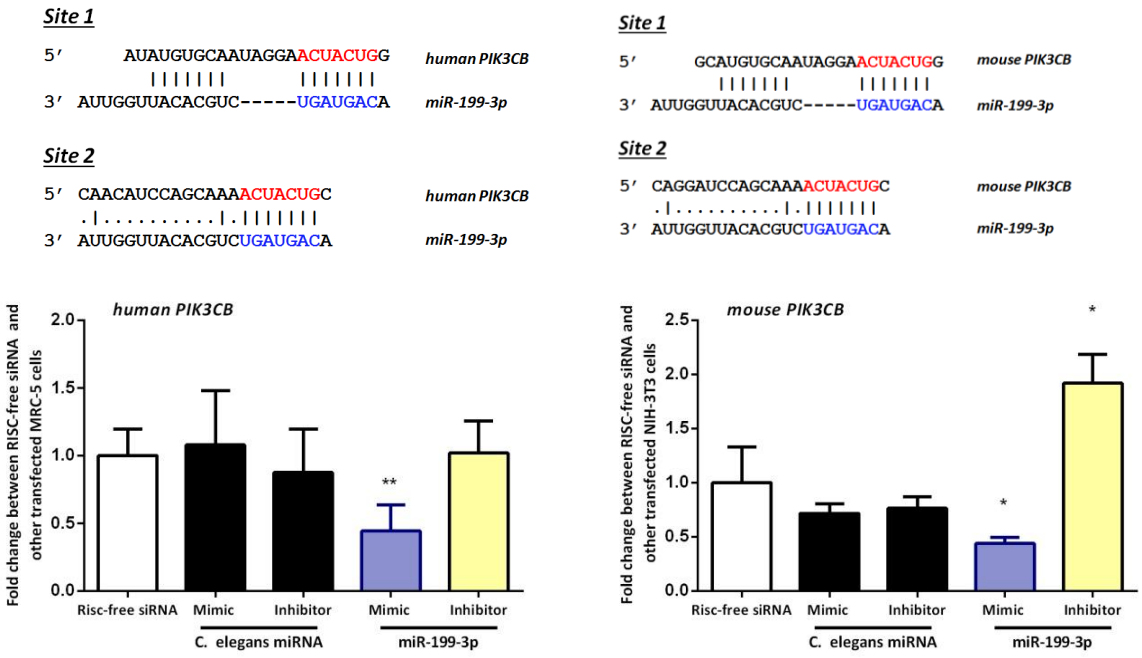

B

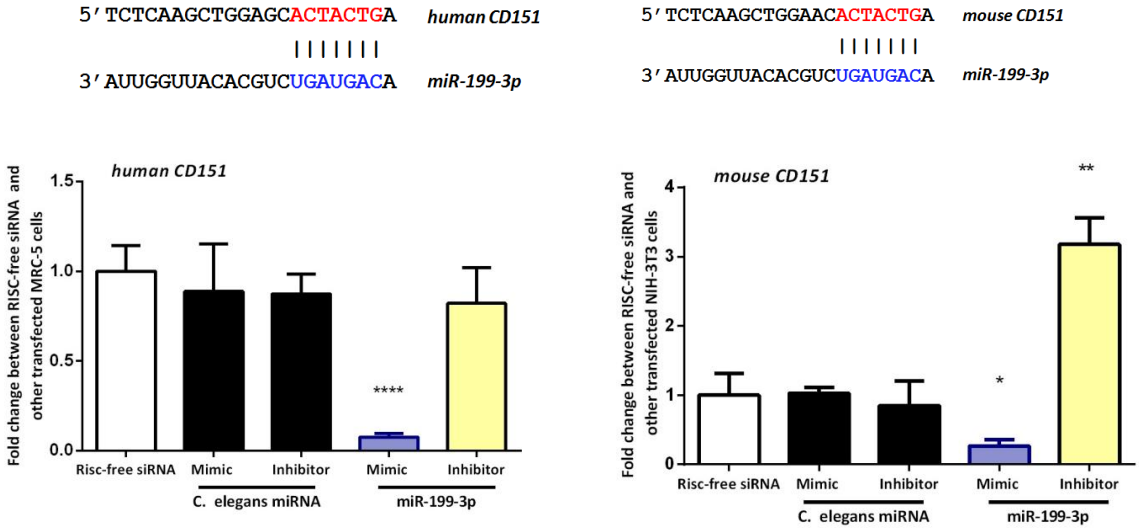

C

5′ GACTCGGGACCAATACTACTGA *human ITGA3*

3′ AUUGGUUACACGUCUGAUGACA *miR-199-3p*

5′ GACTCGGGACCGATACTACTGA *mouse ITGA3*

3′ AUUGGUUACACGUCUGAUGACA *miR-199-3p*

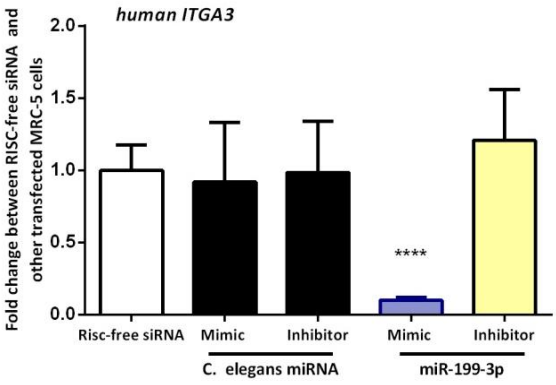

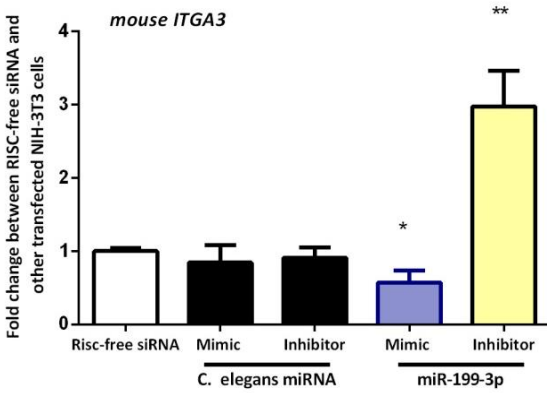

D

5′ ATATTCCAAACTGAACTACTTG *human ITGA6*

3′ AUUGGUUACACGUCUGAUGACA *miR-199-3p*

5′ ATATTCCAAACTGAACTACTTG *mouse ITGA6*

3′ AUUGGUUACACGUCUGAUGACA *miR-199-3p*

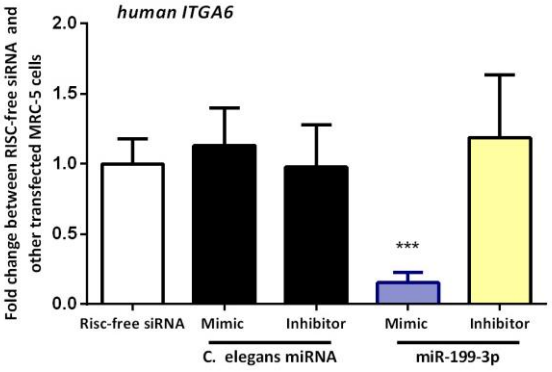

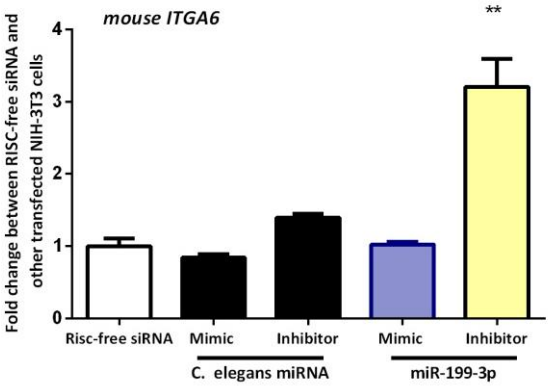

E

5′ AAGAAAGGCUGGAAAACUACUGA *human FGF7*

3′ AUUGGUUACACGUCUGAUGACA *miR-199-3p*

5′ AAGAAAGGCUGGAAAACUACUGA *mouse FGF7*

3′ AUUGGUUACACGUCUGAUGACA *miR-199-3p*

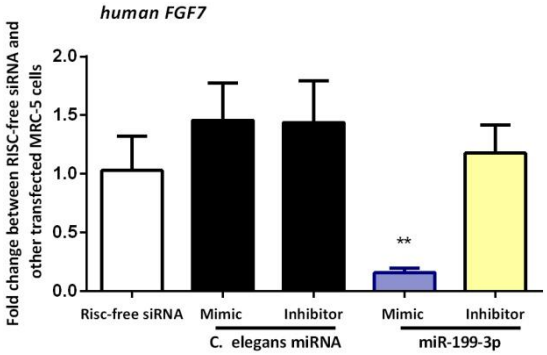

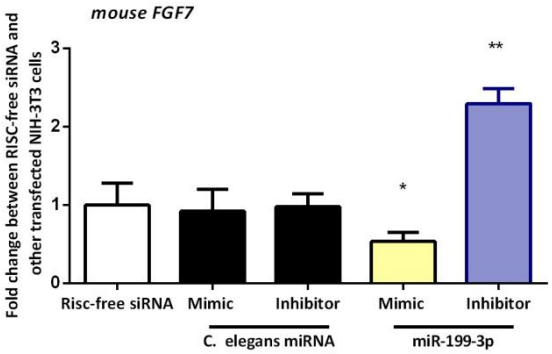

F

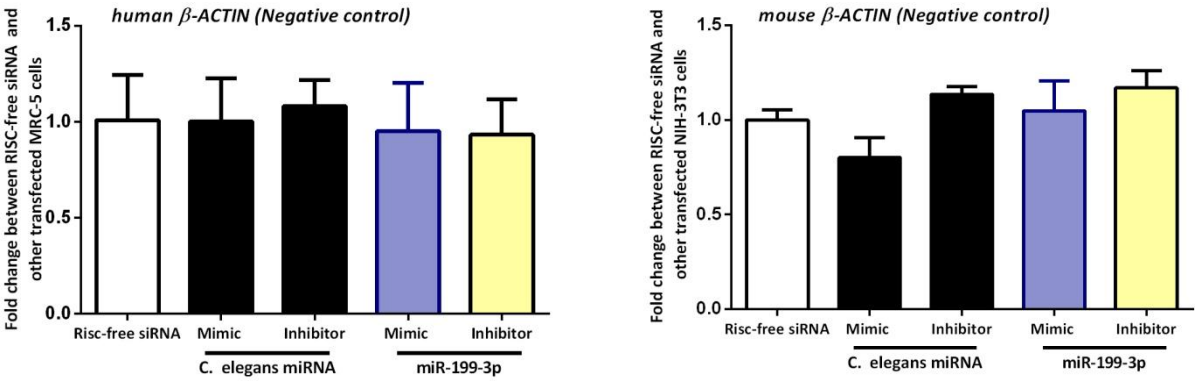

Figure 4.9: qRT-PCR validation of predicted mRNA targets of miR-199-3p. NIH-3T3 and MRC-5 cells were transfected with 25nM of each RISC-free siRNA, *C. elegans* mimic, *C. elegans* inhibitor, miR-199-3p mimic or miR-199-3p inhibitor for 48 hours. The expression levels of PIK3CB (A), CD151 (B), ITGA3 (C), ITGA6 (D), FGF7 (E) were quantified by qRT-PCR and normalised to GAPDH level. β-ACTIN (F) was included as a negative control. Data presented are the mean fold change ± S.D (n=4). and are representative of three independent experiments.*$p < 0.05$, **$p < 0.01$, ***$p < 0.001$, and ****$P<0.0001$ compared to RISC-free siRNA transfected cells as determined by two-tailed Student's *t* test.

4.3 Discussion

A key objective of this study was to identify the genes regulated by miR-199-3p that might contribute to its antiviral properties. Target prediction is an important step in understanding the functional regulation of miR-199-3p and its consequent antiviral properties. Given that the antiviral role of miR-199-3p has been observed in three distinct herpes viruses (CMV, HSV-1 and MHV-68) and also against SFV (Santhakumar et al., 2010), the antiviral role of miR-199-3p is expected to be caused by regulation of host genes by this miRNA instead of direct interaction with the virus. Despite this, it is difficult to exclude the existence of miR-199-3p-virus interactions, indeed two different studies have shown direct effects of miR-199-3p on hepatitis B virus transcripts (HBsAg and HBeAg) and on the 5′UTR of the hepatitis C virus genome (Zhang et al. 2010; Murakami et al. 2009). While this direct regulation of viral genes by miR-199-3p has a negative impact on HBV and HCV replication, the existence of cellular targets of miR-199-3p might also support its antiviral properties in these infections.

4.3.1 Experimental and computational identification of miR-199-3p targets

Two methods were employed for the purpose of identifying the cellular targets of miR-199-3p. The first of these was the use of gene expression profiles comparing miR-199-3p overexpression or inhibition experiments. The other method was computational analysis of the miR-199-3p seed complement sequences in the 3′ untranslated regions of the regulated genes. However, there are several caveats to consider in this approach. First, the microarray experiment does not identify miRNA targets that are only regulated at the translational level, however, miRNAs can regulate on average 100-200 mRNA targets (Krek et al. 2005; Lim et al. 2005). Secondly, microarray analysis is unable to discriminate direct targets from those genes that are secondarily regulated by the direct targets. To address this, the target prediction program (TargetScan 5.0) was used to identify direct targets on the basis of miR-199-3p target sites in the 3′UTR. Thirdly the prediction program (TargetScan 5.0) predicts false positive targets besides being unable to predict non-canonical miRNA-target interactions such as bulge and centred sites (Shin et al. 2010; Chi et

al. 2012). A recent transcriptome-wide study of cellular targets for miR-155 has shown that miRNA-mRNA interactions can occur both canonically (perfect seed match) and non-canonically (without perfect match). Loeb et al. (2012) suggests that both types of interactions are important to ultimately confer a bigger picture as to how miR-155 regulates overall gene expression.

4.3.2 Functional and pathway analysis of miR-199-3p regulated genes

The next step was to gain insight into the biology of differentially regulated genes by miR-199-3p, which was identified in the microarray analysis. IPA functional analysis identified several host pathways that are required if not essential for CMV replication and infection process, such as prostaglandin production, ERK/MAPK and PI3K/AKT signaling (Figure 4.5 and Table 4.3). The enrichment for ERK/MAP kinase and prostaglandin synthesis is consistent with previous reports that have shown that miR-199-3p targets MET and its downstream effector ERK2 (Kim et al. 2008). miR-199-3p has also been found to target PTGS2 (COX-2), which is the key enzyme in prostaglandin biosynthesis (Chakrabarty et al. 2007). In addition to the 3 altered cancer canonical pathways in miR-199-3p dataset, the most significant functions including proliferation, apoptosis and movement (Table 4.6) suggest a link between this miRNA and cancer. Consistent with these results, the regulation of miR-199a-3p expression has been reported in several cancers (Table 1.5). miR-199-3p expression has also been found to reduce or enhance the survival and proliferation as well as the motility and invasion of tumour cells (Table 4.1).

There are two main possibilities that could explain the dual function of miR-199-3p. First, as the gene expression profile is not identical between different cells, the targets of miR-199-3p can differ from one cell type to another, with the result that miR-199-3p manifests different or opposing functions in the different cell types. Second, an individual gene may have opposing functions in different or same cell types, which suggests that the role of miR-199-3p can change based on the target role in this cell type or at specific stage in the life of a cell. For example CD44, a direct target of miR-199-3p, is implicated in both tumor progression and suppression of breast cancers (Reviewed in Louderbough and Schroeder 2011). As the observed antiviral effect of miR-199-3p was found in both human and mouse infections, it

seems more likely that targets of relevance will be those conserved between the two species. Therefore, non-conserved targets were excluded. However, it is also possible that the non-conserved targets could contribute to the outcome of miR-199-3p on viral infection or that miR-199-3p could exert its antiviral function in HCMV and MCMV infections through different sets of non-conserved targets.

In an attempt to better understand the role of the 30 conserved targets, the IPA network analysis revealed that 9 of these targets are indirectly connected with AKT and 5 of the targets are linked to ERK (Figure 4.6). While the pathway and network analysis showed regulation of AKT and ERK by miR-199-3p, neither AKT nor ERK expression are altered in the miR-199-3p dataset and neither has a seed site for miR-199-3p in its 3′UTR. It was therefore of interest to examine whether miR-199-3p disrupts the activity of either of these genes, rather than their expression levels. This may be important for understanding the role of miR-199-3p in infection, as both of these proteins have been previously shown to be essential for HCMV gene expression and infection (Johnson et al. 2001a; 2001b; Yu and Alwine 2002).

4.3.3 miR-199-3p negatively regulates the activation of AKT

Overexpression or inhibition of miR-199-3p in human fibroblasts had no observed effect on the regulation of ERK1/2 phosphorylation, which is contradictory to the previous reported data by Kim and colleagues. They reported that the overexpression of miR-199-3p caused a down-regulation of ERK2 protein in non-starved A549 cells (human lung adenocarcinoma epithelial cell line), however, this effect was extremely subtle on starved A549 cells. The authors concluded that serum starvation may potentially affect the level of ERK2 down-regulation. Additionally, the mechanism by which miR-199-3p affects ERK2 protein level was not elucidated (Kim et al. 2008). However, miR-199a-3p overexpression did result in a significant reduction in the expression of phosphorylated serine and theronine in AKT. The inhibition of miR-199-3p activity in human MRC-5 cell lines did not promote the activation of AKT, which may be due to unsuccessful inhibition of miR-199-3p or to the low endogenous levels of miR-199-3p in this cell line The finding here that miR-199-3p regulates AKT signaling led to the search for candidate targets of miR-199-3p to understand how miR-199-3p regulates AKT. It is important to note that the upstream

components activating AKT signaling during HCMV infection have yet to be elucidated. However, 6 targets of miR-199-3p were chosen from the dataset for further validation and investigation based on the results of network analysis, which linked them to AKT function.

4.3.4 Validation of PIK3CB, ITGA3, ITGA6, CD151, and FGF7 as targets of *miR-199-3p*

PIK3CB is a member of the Phosphatidyl-3-kinases (PI3K), which are primarily involved in the regulation of AKT activation. It also harbours two conserved potential binding sites for miR-199-3p in its 3′UTR, making it one of the most promising candidates for regulation of AKT signaling.

CD151 has been reported to form a functional complex with some integrin subunits, such as ITGA3 and ITGA6. These integrins and CD151 are all predicted to be targets of miR-199-3p and each contains one conserved site in their 3′UTRs for this miRNA. The integrin α3β1 complex regulates cell-cell adhesion, cytoskeleton organisation and the production of matrix metalloproteinase 2 (MMP-2) (Shigeta et al. 2003; Chattopadhyay et al. 2003; Sugiura and Berditchevski 1999). CD151 has also been shown to determine the molecular distribution of integrin α6 on the cell membrane, which affects morphological and functional aspects of cells, such as migration, invasion and adhesion signaling (Yang et al. 2008). The involvement of CD151, integrin α3 and integrin α6 in HGF-MET signaling has been shown to reduce AKT phosphorylation in cells in which either CD151, integrin α3 or integrin α6 were knocked down (Klosek et al. 2009). Importantly, several studies have reported various viruses exploiting integrins for the purpose of mediating their attachment, internalisation and/or to trigger signaling cascades in host cells that are required for infection (Stewart and Nemerow 2007). HCMV gB glycoprotein, which is required for viral attachment and entry into the host cells, contains a dis-integrin sequence that is conserved in β and γ-herpes viruses but not α-herpes viruses. Several cellular integrins, αvβ1, α6β1 and αvβ3, were reported to facilitate HCMV entry and signaling (Wang et al. 2005; Feire et al. 2004). HSV-1 entry is associated with αvβ3 while human herpes virus-8 (HHV-8) requires α3β1 (Parry et al. 2005; Akula et al.

2002). The decision was therefore made that the integrins and CD151 complex would be included for further validation in this work.

The adhesion molecule CD44 has been found to be upregulated in fibroblasts infected with HCMV and a direct target of miR-199-3p (Ito et al. 1995; Henry et al. 2010). CD44 has also been reported to promote the proliferation, survival and migration through the activation of PI3K and AKT in colon carcinoma cells (Park et al., 2011; Subramaniam et al. 2007).

FGF7, also known as keratinocyte growth factor (KGF), the production of which is restricted to fibroblasts and epithelial cells, has broad biological functions including proliferation and survival through activation of the PI3-Kinase/AKT signaling pathway (Bao et al. 2005; Zhang et al. 2010; Chang et al. 2009). However, no investigations have studied the expression or role of FGF7 in HCMV or other herpes viral infections.

qRT-PCR was used for the initial experimental validation of the response of PIK3CB, ITGA3, ITGA6, CD151, and FGF7 genes to manipulation of miR-199-3p. In mouse NIH-3T3 transfected with miR-199-3p inhibitor, the PIK3CB, ITGA3, ITGA6, CD151 and FGF7 transcripts were all up-regulated, whereas in the cells transfected with miR-199-3p mimic, PIK3CB, ITGA3 and CD151 mRNAs were all down-regulated. Human MRC-5 transfected with miR-199-3p mimic showed a pronounced reduction in transcript for each candidate (PIK3CB, ITGA3, ITGA6, CD151 and FGF7). Unlike with the miR-199-3p mimic, no reverse effect was found in terms of the expression of these target transcripts in MRC-5 transfected with miR-199-3p inhibitor. As discussed previously, endogenous expression of miR-199-3p may be low in MRC-5 or this miRNA may not be inhibited successfully (Figure 4.9). In support of this, the antiviral effect of miR-199-3p mimic in HCMV infected MRC-5 was extremely pronounced, whereas the proviral impact of miR-199-3p inhibitor in infected MRC-5 was very subtle (Santhakumar et al. 2010). However, this validation does not distinguish between the direct and indirect targets of miR-199-3p.

In conclusion, the work in this chapter aimed to characterise the effect of miR-199-3p disregulation on cellular pathways and to identify target genes of miR-199-3p that could be linked to a role in CMV infection in fibroblasts. The genome-wide expression analysis demonstrated a large number of regulated genes (198 gene) that contains 30 direct genes with at least one conserved target site for miR-199-3p. This single host-encoded miRNA regulates multiple pathways required and/or activated by CMV, including PI3K/AKT and ERK/MAPK signaling and prostaglandin synthesis. Evidence was also provided that shows AKT phosphorylation is down-regulated by the overexpression of miR-199-3p in human fibroblasts. The regulation of AKT activation occurred indirectly, therefore, CD44 and the 5 other conserved predicted targets of miR-199-3p previously linked with the regulation of AKT activation were chosen for further analysis. The initial validation for PIK3CB, ITGA3, ITGA6, CD151 and FGF7 show that these targets were regulated at the transcriptional levels in NIH-3T3 and MRC-5 cells transfected with either miR-199-3p mimic or inhibitor. In the next chapter, data from a more in depth investigation of AKT activation during the HCMV infection in MRC-5 cells is presented. New questions will be asked in an attempt to discern whether these genes are direct targets of miR-199-3p and whether their regulation influences HCMV growth specifically through AKT activation.

5 The Antiviral Properties of miR-199-3p May Be Associated with Suppression of AKT Phosphorylation

5.1 Introduction

5.1.1 The phosphoinositide 3-kinase (PI3K)/ protein kinase B (PKB/AKT) pathway

PI3K-AKT is a signaling pathway that mediates a broad range of cellular functions in response to extracellular signals. PI3Ks are lipid kinases composed of two subunits, one regulatory and one catalytic subunit. The regulatory subunits include five isoforms, three alternative splicing of the PIK3R1 gene yields three isoforms (p85α, p55α, p50α), PIK3R2 (p85β), and PIK3R3 (p55γ) and three isoforms of catalytic subunits, PIK3CA (p110 α), PIK3CB (p110β), and PIK3CD (p110δ) (Figure 5.1). The regulatory subunits are associated with recruitment and stabilisation of the catalytic subunit to avert its rapid degradation. The PI3k (p110) catalytic subunit primarily phosphorylates constitutive phosphatidylinositol-4,5-bisphosphate (PIP2) on the plasma membrane to produce the major product phosphatidylinositol 3,4,5-triphosphate (PIP3), which recruits protein kinase B (PKB/AKT). Upon recruitment to the plasma membrane AKT is phosphorylated at two critical residues, threonine 308 (Thr308) and serine (Ser473) to fully activate its kinase activity. 3'-phosphoinositide-dependent protein kinase 1 (PDK1) phosphorylates AKT at Thr308, whereas mTORC2 complex phosphorylates AKT at Ser473. The phosphorylated AKT then translocates from the plasma membrane to other cell compartments to phosphorylate its numerous downstream targets that regulate several cellular processes including cell survival, proliferation, protein synthesis, glucose metabolism, and others (Reviewed in Hennessy et al. 2005; Vanhaesebroeck et al. 2012).

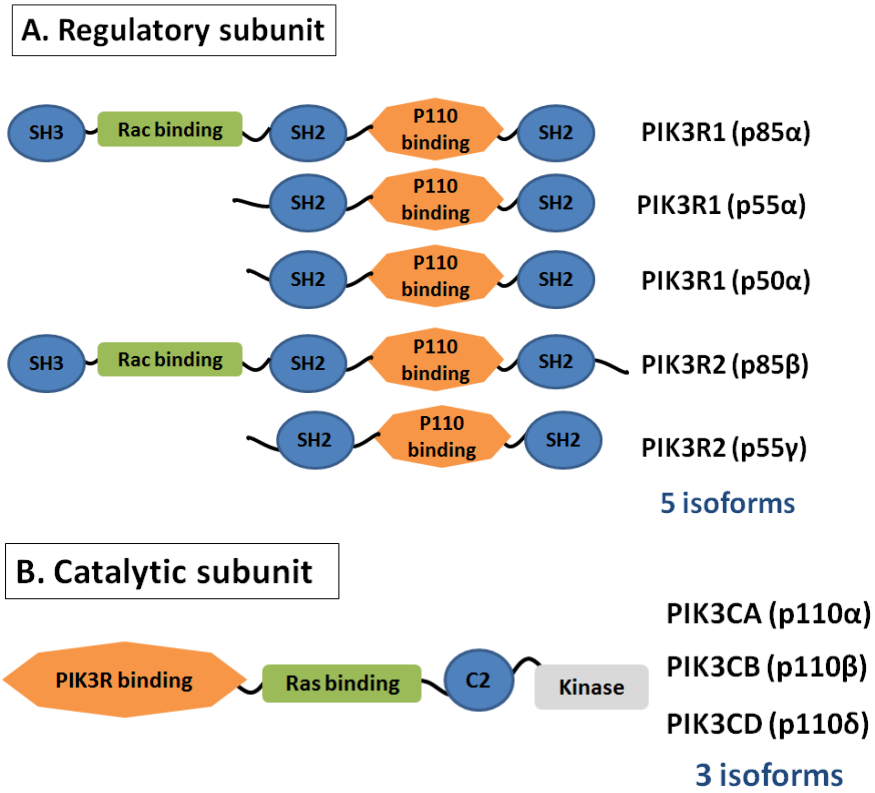

Figure 5.1: Schematic diagram of the structure of catalytic and regulatory subunits of the phosphatidylinositol 3-kinase (PI3K). (A) Each regulatory isoform contains two highly conserved SRC Homology 2 (SH2) domains that mediate binding to phosphotyrosine residues and one p110-binding domain. The longer isoforms PIK3R1 (p85α) and PIK3R2 (p85β) possess two additional domains in the N-terminal region: one SRC homology 3 (SH3) domain and RAC-binding domain, which can interact to members of the Rac and CDC42 GTPases. p85α, p55α, and p50α are alternative protein products of a single gene (PIK3R1). (B) Each catalytic subunit contains a Ras-associating domain and a C2 domain (Calcium binding motif) in addition to the kinase domain and another to interact with the regulatory subunit (PIK3R binding domain).

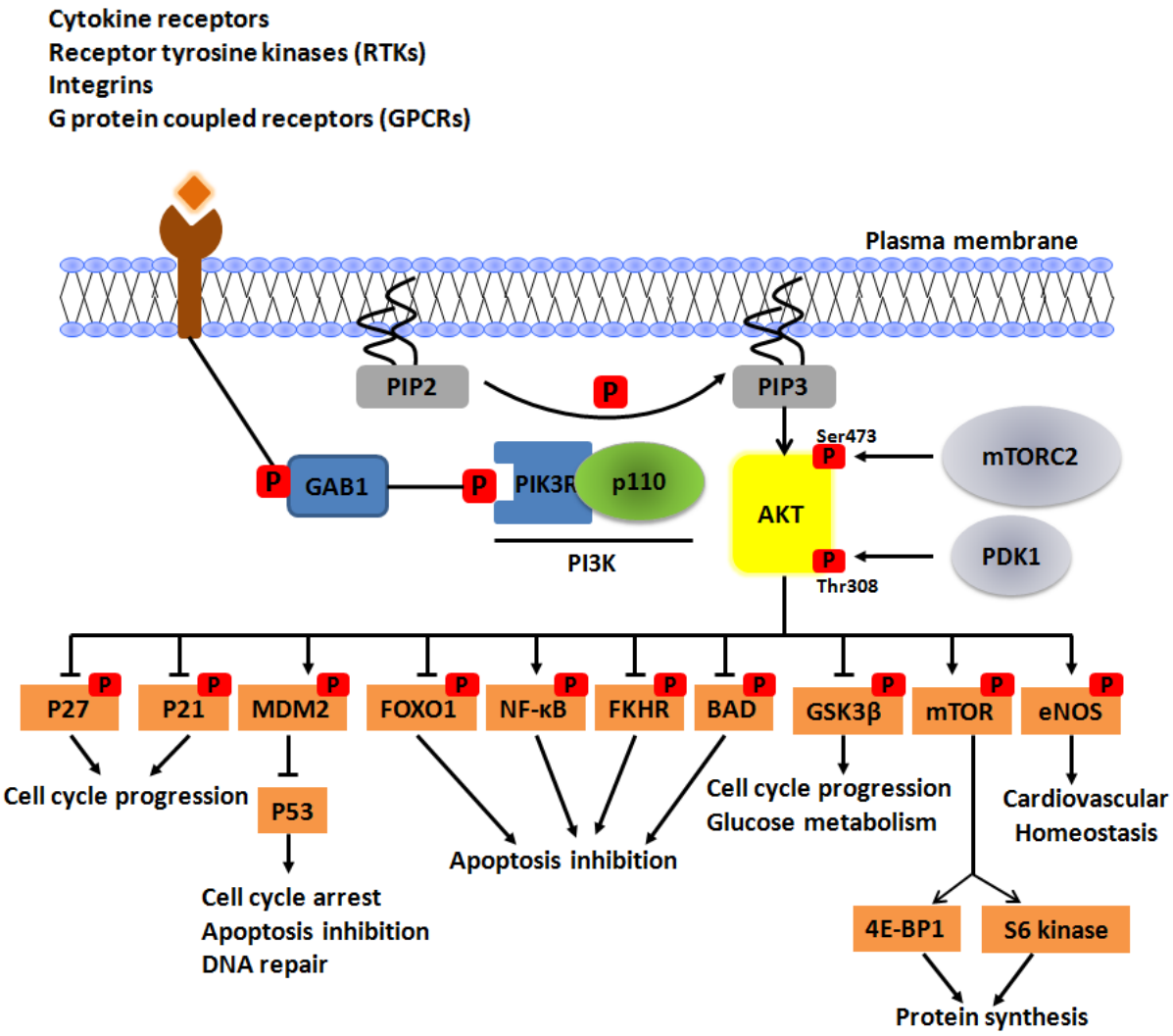

Figure 5.2: Schematic diagram of the phosphatidylinositol 3-kinase (PI3K)/AKT signaling pathway. Activation of growth factor receptor tyrosine kinases leads to the recruitment of the regulatory subunit (PIK3R) directly or indirectly through an adaptor. This recruitment results in activation of the catalytic subunit (p110) and then phosphorylation of phosphatidylinositol-4,5-biphosphate (PIP2) to generate the second messenger phosphatidylinositol-3,4,5-triphosphate (PIP3). PIP3 recruits AKT kinase and results in consequent double phosphorylation of AKT. Once phosphorylated, Akt mediates the activation and inhibition of several targets involved in apoptosis, growth, metabolism, translation and cycle cycle through various mechanisms.

5.1.2 The contribution of PI3K-AKT signaling in viral infection

Activation of PI3k-AKT modulates critical cellular processes involved in viral infection: 1) PI3K-AKT signaling regulates the cytoskeleton remodelling, thereby assisting the endocytosis and trafficking of viruses into the nucleus; 2) it is required for viral gene expression and replication of a small number of viruses; 3) it supports cell survival, which aids efficient virus replication and propagation. This also allows for long-term persistence of virus in host cells; 4) the oncogenic viruses induce PI3K-AKT, which promotes tumour growth, angiogensis, and cellular migration; and 5) it enhances glucose uptake and overall metabolism. In spite of several viruses depending on PI3K-AKT activation for efficient infection, PI3K-AKT is also involved in the antiviral immune response in host cells. PI3K has reported to activate some transcription factors, like IRF3 and IRF7, leading to the expression of interferon-associated genes (Reviewed in Ji and Liu 2008).

5.1.3 Regulation of PI3K-AKT cascades in viral infection

Several viruses are known to up-regulate PI3K-AKT signaling during infection through viral elements. For example, PI3K-AKT cascades are induced by the HBx protein of HBV, the major immediate early protein (MIEP) of HCMV, the NS5A protein of HCV (Street et al. 2005; Guo et al. 2007), the NS1 protein of H1N1 (Hale et al. 2006; Shin et al. 2007), and the K1 protein of KSHV (Tomlinson and Damania 2004). Other viruses possess more than one viral protein that can activate the PI3K-AKT pathway including EBV (Portis and Longnecker 2004; Mei et al. 2007), HIV-1 (Deregibus et al. 2002; Linnemann et al. 2002), Human papillomavirus-16 (HPV16) (Menges et al. 2006; Kim et al. 2006; Spangle and Münger 2010), respiratory syncytical virus (RSV) (Bitko et al. 2007), and simian virus 40 (SV40) (Yuan et al. 2002; Yu and Alwine 2008). In contrast, there are a limited number of cases in which viral proteins suppress AKT signaling, but an example includes the VP1 protein in foot-and-mouth disease virus (FMDV) infection (Peng et al. 2004). It must be noted, however, that the activation of PI3K-AKT signal is differently regulated in various stages of the same infection. For example, HCV transiently stimulates the maximal activation of AKT during the early stage of infection and becomes undetectable at 24 and 48 hours post infection. This is to facilitate the viral entry into the host cells (Liu et al. 2012). HCMV infection contributes to the development of cardiovascular

diseases, including atherosclerosis (Söderberg-Nauclér 2006). HCMV promotes an important event in atherosclerosis, which is the reduction in endothelial nitric oxide synthase (eNOS) phosphorylation and activation in human aortic endothelial cells. This is likely to occur through inhibiting eNOS upstream signaling, AKT phosphorylation (Shen et al. 2006).

5.1.4 HCMV activates PI3K-AKT signaling during infection

HCMV infection induces phosphorylation of AKT at the Ser473 residue in a PI3K-dependent manner (Johnson et al. 2001; Yu and Alwine 2002). The activation of AKT is mediated via at least two mechanisms. Firstly, through transient induction, following HCMV binding to host cell receptors (Johnson et al. 2001b), though the actual cellular receptors used to enter the host cells and trigger PI3K-AKT are controversial (Isaacson et al. 2007). Second, persistent activation is a consequence of the expression of HCMV proteins (Johnson et al. 2001b; Yu and Alwine 2002; Kudchodkar et al. 2006), as experiments showed that transfection of either IE1 or IE2 promoted the activation of AKT (Yu and Alwine 2002). The activation of phosphorylated AKT results in the phosphorylation of its downstream targets the eukaryotic initiation factor-4E binding protein (4E-BP), ribosomal S6 Kinase (S6K), and transcription factor NF-κB (Johnson et al. 2001b; Kudchodkar et al. 2004). The inhibition of PI3-kinase activity using the inhibitor LY294002 impedes the expression of viral genes IE1 and IE2 and subsequent DNA replication. In contrast, treatment with LY294002 inhibitor in the presence of PIP3 rescues activation of AKT and the expression of viral proteins IE1 or IE2 (Johnson et al. 2001b). These results indicate that PI3K-AKT activation is an integral part of expression of the viral major IE proteins and viral DNA replication (Figure 5.3).

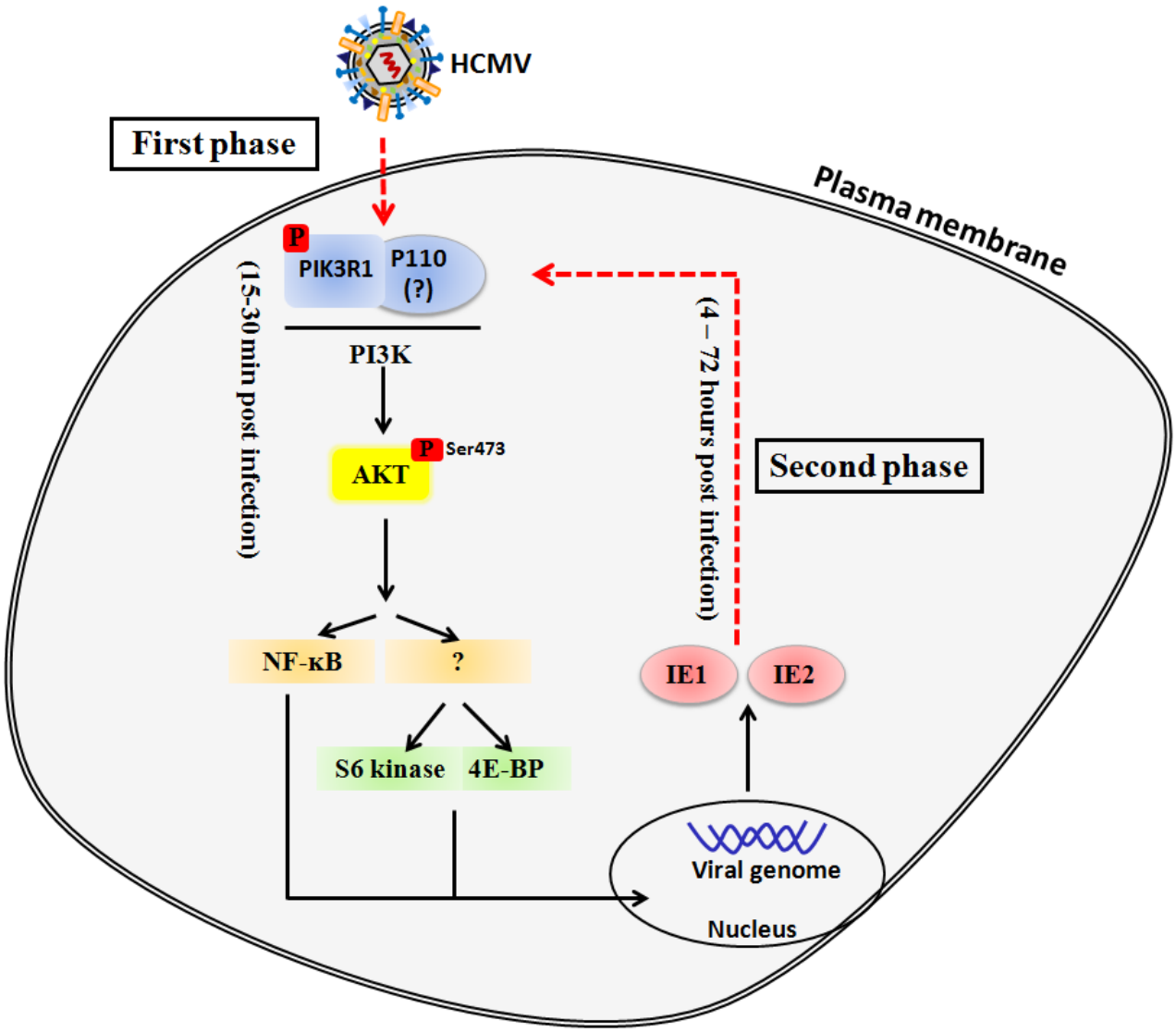

Figure 5.3: phosphatidylinositol 3-kinase (PI3K)/AKT signaling pathway in HCMV-infected cells.

5.1.5 Rational for studying the role of miR-199-3p in targeting PI3K/AKT signalling in HCMV infection

Given that PI3K-AKT activation is required for HCMV infection and that miR-199-3p negatively influences the phosphorylation of AKT (Figure 4.7), it was hypothesised that the antiviral role of miR-199-3p occurs through a molecular mechanism involving the regulation of PI3K-AKT signaling cascades. In particular, several predicted targets of miR-199-3p can mediate PI3K-AKT activation including not only the catalytic subunit PIK3CB, which forms the heterodimeric kinase PI3K, but also cellular receptors such as ITGA3, ITGA6, integrin-associated CD151, and CD44. In addition, the broad roles of PI3K-AKT in various aspects of viral infection may provide an explanation of the broad antiviral properties of miR-199-3p.

5.1.6 Aims

The objective of the work presented in this chapter is to validate targets of miR-199-3p that are associated with PI3K-AKT signaling. The correlation between the down-regulation of miR-199-3p and its targets during HCMV infection was further studied. Moreover, the functional small interfering RNA (siRNA)-mediated knockdown of the targets of miR-199-3p was used to investigate whether these targets can contribute to the regulation of viral infection.

5.2 Results

5.2.1 The experimental validation of predicated miR-199-3p targets in NIH-3T3 cells

As described in chapter 4, a microarray experiment was conducted to identify the cellular genes and biological pathways that are regulated by miR-199-3p. AKT signalling was identified in the IPA database as a significant regulated pathway in the miR-199-3p dataset and this was experimentally validated (see Figure 4.7). Based on the IPA database, eight of the miR-199-3p predicted targets (PPP2R5E, WYHAE, CD2AP, PIK3CB, ITGA3, ITGA6, CD151, and FGF7) as well as the validated miR-199-3p target, CD44, are linked to AKT regulation. Based on the literature, the most relevant targets for PI3K-AKT signalling, PIK3CB, ITGA3, ITGA6, and CD151, were chosen for further validation. In order to examine PIK3CB, ITGA3, ITGA6, and CD151 in more detail, qRT-PCR analysis was carried out on these gene transcripts using RNA extracted from cells that were transfected with miR-199-3p mimic or inhibitor. The data showed a decrease in the levels of target mRNAs in human and mouse cells transfected with miR-199-3p mimic and an increase in mouse cells transfected with the inhibitor. However, these experiments did not examine whether the regulation was through direct interaction between miR-199-3p and the targets, versus secondary effects from miR-199-3p regulation of other genes.

For this reason, a luciferase reporter assay was used to investigate the functional link between miR-199-3p and the 3′UTRs of the murine PIK3CB (~1.3 Kb), ITGA3 (~1.1Kb), ITGA6 (~0.9 Kb), and CD151 (~0.8 Kb) genes containing the predicted binding sites for miR-199-3p were cloned downstream of the *Renilla* luciferase gene of the psiCHECK-2 vector (Refer to Appendix 7 for results of sequence alignment). The cloning of PIK3CB and CD151 3′UTRs was performed by MSc student Laura Kelly under the supervision of Nouf Laqtom. To create a positive control, a miR-199-3p sensor containing a perfectly complementary mature miR-199-3p sequence was constructed. The expression vector (psiCHECK-2) also includes a second reporter gene, firefly luciferase, which serves as an internal control for transfection efficiency and variation in cell count.

Next, co-transfection experiments were carried out to measure the ability of miR-199-3p to regulate the expression of the luciferase gene bearing the 3′UTR of each target, NIH-3T3 cells were left untreated or transfected with either: psiCHECK-2 (empty vector); psiCHECK-2-miR-199-3p sensor; psiCHECK-2-PIK3CB 3′UTR; psiCHECK-2-ITGA3 3′UTR; psiCHECK-2-ITGA6 3′UTR; psiCHECK-2-CD151 3′UTR along with miR-199-3p mimic, inhibitor, or RISC-free siRNA. As before, C. *elegans* mimic, C. *elegans* inhibitor or RISC-free siRNA were included as controls. psiCHECK-2 harbouring a single target 3′UTR were also transfected alone to measure the effect of the endogenous population of miRNAs on the regulation of luciferase expression. Cells were lysed 48 hours post-transfection and measurements were taken of the expression of firefly and *Renilla* luciferases.

5.2.1.1 miRNAs does not interfere with the expression of Renilla luciferase from the psiCHECK-2 (empty vector)

The psiCHECK-2 (empty vector) was transfected in all experiments to measure the non-specific effect of the co-transfected RISC-free siRNA, mimics or inhibitors of *C. elegans* miRNA and miR-199-3p on the regulation of luciferase expression. The luciferase expression of psiCHECK-2 (empty vector), which has no inserted 3′UTR downstream of its *Renilla* sequence, showed no significant differences in the ratio of *Renilla* to firefly luciferase activity when co-transfected with either *C. elegans* mimic, *C. elegans* inhibitor, miR-199-3p mimic, miR-199-3p inhibitor, or RISC-free siRNA (Figure 5.4, 5.6, 5.7, 5.8a). This suggests that there is no non-specific effect on luciferase expression associated with the co-transfection of mimics or inhibitors.

5.2.1.2 Functional validation of miR-199-3p sensor

A significant inhibition ~30 fold was observed in the ratio of luciferase activity of psiCHECK-miR-199-3p sensor (positive control) in cells transfected with psiCHECK-miR-199-3p sensor alone. This inhibition most likely occurs as a result of regulation by endogenous miR-199-3p in NIH-3T3 cells (figure 5.5). Moreover, the co-transfection of psiCHECK-miR-199-3p sensor with miR-199-3p mimic results in a greater than 90-fold reduction in the ratio of luciferase activity (Figure 5.4a), in comparison to the co-transfection with miR-199-3p inhibitor, which led to ~500 fold upregulation in luciferase expression relative to the control *C. elegans* inhibitor

(Figure 5.4b). This shows that the miR-199-3p sensor plasmid serves as a control for miR-199-3p activity in the luciferase activity. The psiCHECK-2 (empty vector) and psiCHECK-miR-199-3p sensor (positive control) were included in all experiments to identify experimental non-specific effects and support the functionality of miR-199-3p activity.

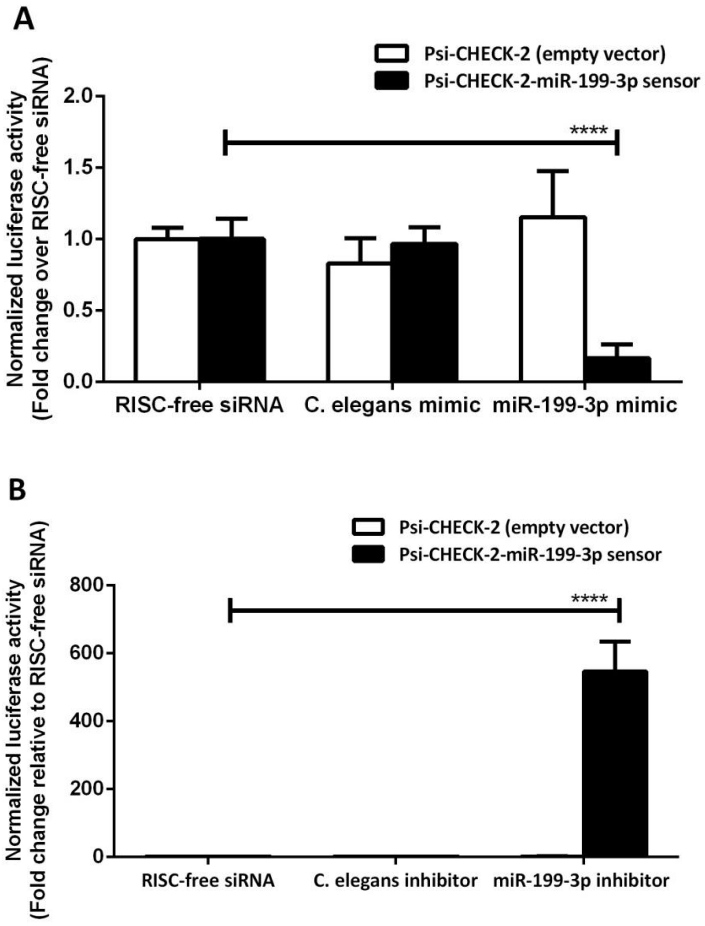

Figure 5.4: Validation of psiCHECK-2-miR-199-3p sensor. Luciferase reporter plasmids, either psiCHECK-2 or psiCHECK-2-miR-199-3p sensor were co-transfected into NIH-3T3 cells with either RISC-free siRNA or mimic (A) or inhibitor (B) for both *C. elegans* miRNA (Cel-miR-67) and miR-199-3p. Cells were lysed and luciferase expression was measured at 48 hours post transfection. The low background luciferase activity of the untreated cells was subtracted from the luciferase activity of transfected cells. The luciferase activity of *Renilla* were normalised to second firefly control luciferase activity to correct the variations in transfection efficiency and cell count. Data presented are the mean fold change ± S.D. (n=4) of the ratio between *Renilla* luciferase and firefly control luciferase activities and are representative of three independent experiments. ****P<0.0001 compared to RISC-free siRNA transfected cells as determined by unpaired Student's *t* test.

5.2.1.3 *Endogenous miRNAs regulate the Renilla luciferase expression harbouring the 3'UTR of PIK3CB, ITGA3, ITGA6, or CD151 mRNAs*

The ratio of *Renilla* to firefly luciferase activity of cells transfected psiCHECK-2-miR-199-3p, psiCHECK-2-PIK3CB 3′UTR, psiCHECK-2-ITGA6 3′UTR, psiCHECK-2-ITGA3 3′UTR, or psiCHECK-2-CD151 3′UTR alone was reduced in comparison to psiCHECK-2 transfected cells (Figure 5.5). This reduction likely indicates that the endogenously expressed miRNA is capable of regulating that 3′UTR that cloned downstream of the *Renilla* gene.

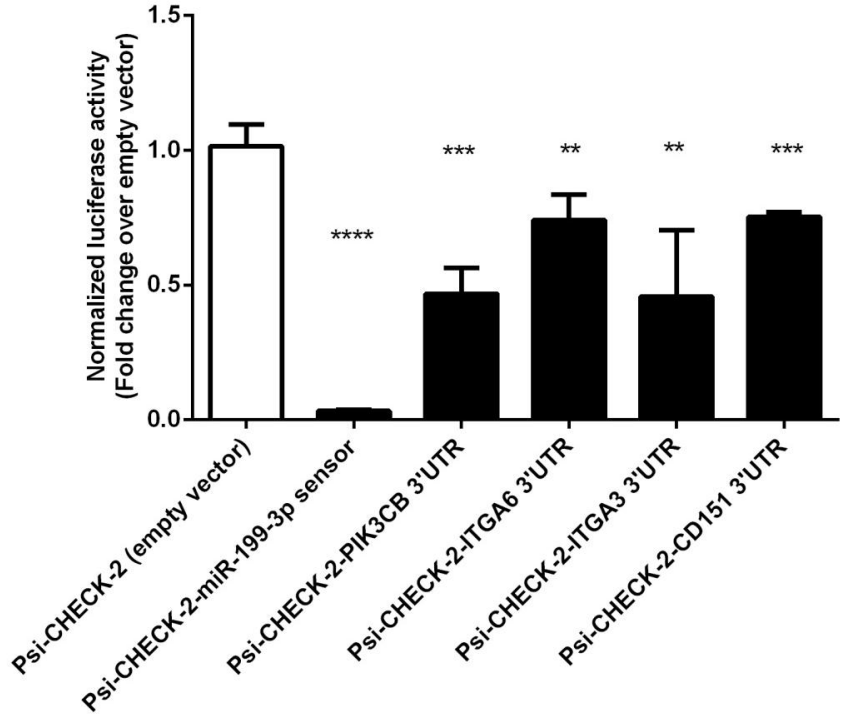

Figure 5.5: The influence of endogenous miRNAs on the *Renilla* luciferase expression containing target 3'UTRs. Luciferase reporter plasmids, either psiCHECK-2 (empty vector), psiCHECK-2-miR-199-3p sensor, psiCHECK-2-PIK3CB 3′UTR, psiCHECK-2-ITGA6 3′UTR, psiCHECK-2-ITGA3 3′UTR, or psiCHECK-2 CD151 3′UTR were transfected into NIH-3T3 cells. Cells were lysed and luciferase expression was measured at 48 hours post transfection. The low background luciferase activity of the untreated cells was subtracted from the luciferase activity of transfected cells. The luciferase activity of *Renilla* were normalised to second firefly control luciferase activity to correct the variations in transfection efficiency and cell count. Data presented are the mean fold change ± S.D. (n=4) of the ratio between *Renilla* luciferase and firefly control luciferase activities and are representative of three independent experiments. **P<0.01, ***P<0.001, and ****P<0.0001 compared to psiCHECK-2 (empty vector) transfected cells as determined by unpaired Student's *t* test.

5.2.1.4 ITGA3 and CD151 are direct targets of miR-199-3p

The luciferase experiment was then carried out to examine the functional relationship between miR-199-3p levels and the *Renilla* luciferase gene harbouring the 3′UTR of either ITGA3 or CD151 mRNAs. In cells transfected with psiCHECK-2-CD151 3′UTR or psiCHECK-2-ITGA3 3′UTR in the presence of miR-199a-3p mimic, a decrease in the luciferase ratios was observed (2.5 fold and 1.7 fold, respectively) (Figure 5.6a,b). Whereas in the presence of miR-199-3p inhibitor, a significant increases (2.8 fold and 1.5 fold) in the luciferase ratios were observed (Figure 5.6a,b). As expected, the luciferase ratios of psiCHECK-2-CD151 3′UTR and psiCHECK-2-ITGA3 3′UTR were unchanged in cells co-transfected with either the *C. elegans* mimics or inhibitors or RISC-free siRNA (Figure 5.6a,b). The results obtained strongly suggest ITGA3 and CD151 are directly regulated by miR-199-3p through their 3′UTRs.

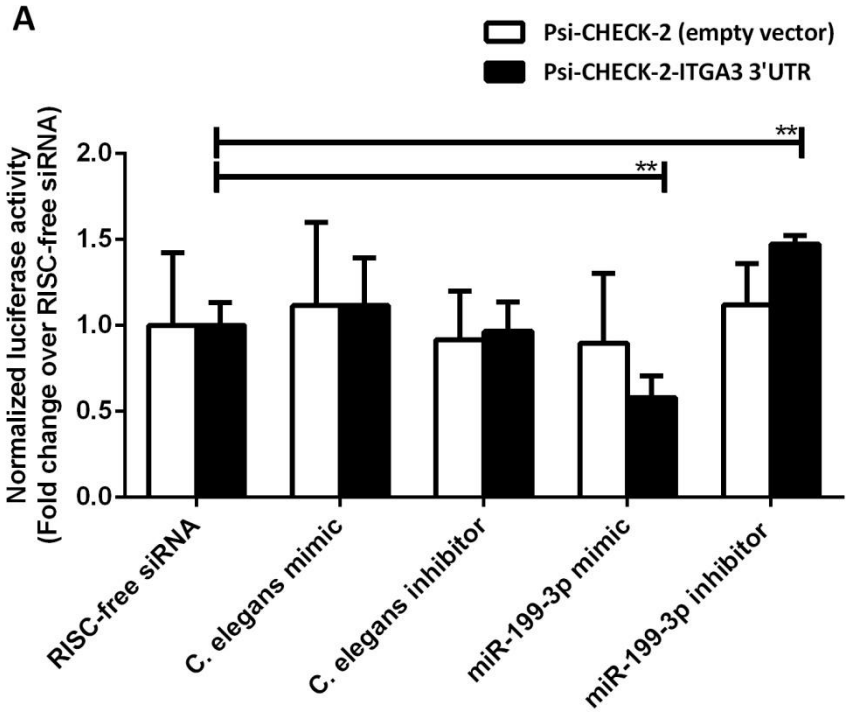

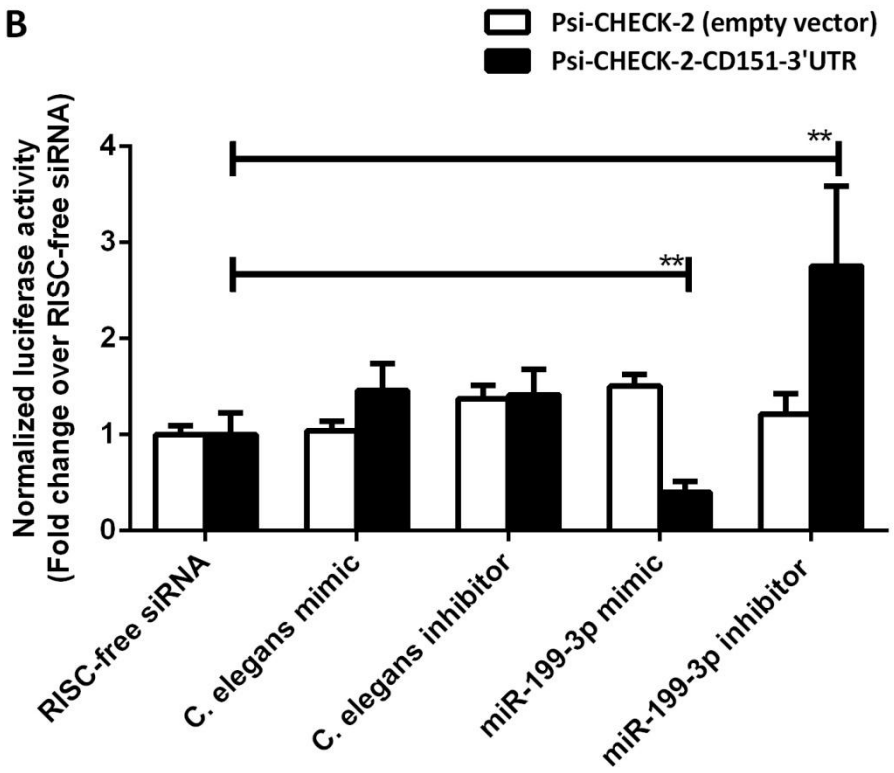

Figure 5.6: ITGA3 and CD151 are direct target of miR-199-3p. Luciferase reporter plasmids, either psiCHECK-2-ITGA3 3′UTR (A) or psiCHECK-2-CD151 3′UTR (B) were co-transfected into NIH-3T3 cells with either RISC-free siRNA or mimic or inhibitor for both *C. elegans* miRNA (Cel-miR-67) and miR-199-3p. Cells were lysed and luciferase expression was measured at 48 hours post transfection. The low background luciferase activity of the untreated cells was subtracted from the luciferase activity of transfected cells. The luciferase of *Renilla* were normalised to second firefly control luciferase activity to correct the variations in transfection efficiency and cell count. Data presented are the mean fold change ± S.D. (n=4) of the ratio between *Renilla* luciferase and firefly control luciferase activities and are representative of three independent experiments. **P<0.01 compared to RISC-free siRNA transfected cells as determined by unpaired Student's *t* test.

5.2.1.5 miR-199-3p does not regulate ITGA6 through its 3'UTR

The same experiments were preformed with the *Renilla* gene construct containing the ITGA6 3′UTR in the presence of either miR-199-3p mimic or inhibitor. However, there was no significant change in the luciferase ratios in the presence of miR-199-3p mimic or inhibitor compared to RISC-free siRNA (Figure 5.7). The transfection of control *C. elegans* mimic or inhibitor was also found to have no discernible effect on the luciferase expression of psiCHECK-2-ITGA6 3′UTR relative to RISC-free siRNA. The results presented here indicate that the ITGA6 3′UTR is not involved in the regulation of ITGA6 by miR-199-3p, at least in murine cells.

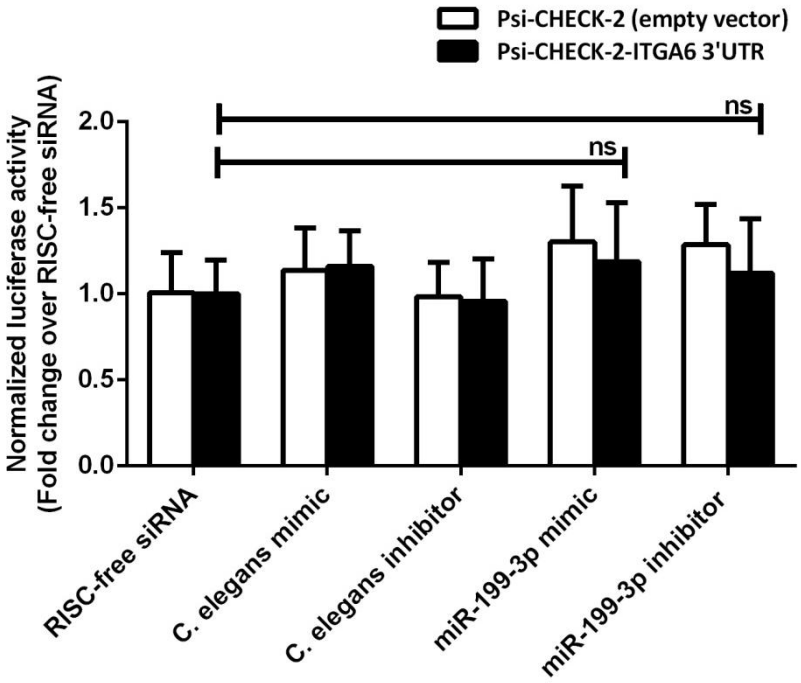

Figure 5.7: miR-199-3p does not regulate murine ITGA6 through its 3′ UTR. Luciferase reporter plasmid, psiCHECK-2-ITGA6 was co-transfected into NIH-3T3 cells with either RISC-free siRNA or mimic or inhibitor for both *C. elegans* miRNA (Cel-miR-67) and miR-199-3p. Cells were lysed and luciferase expression was measured at 48 hours post transfection. The low background luciferase activity of the untreated cells was subtracted from the luciferase activity of transfected cells. The luciferase of *Renilla* were normalised to second firefly control luciferase activity to correct the variations in transfection efficiency and cell count. Data presented are the mean fold change ± S.D. (n=4) of the ratio between *Renilla* luciferase and firefly control luciferase activities and are representative of three independent experiments. ns (for non-significance) compared to RISC-free siRNA transfected cells as determined by unpaired Student's *t* test.

5.2.1.6 *miR-199-3p targets PIK3CB 3′UTR through two functional binding sites*

PIK3CB 3′UTR containing two conserved binding sites for miR-199-3p was also examined in the presence of miR-199-3p mimic or inhibitor. miR-199-3p resulted in a significant reduction of ~2.2 fold in the luciferase ratios of psiCHECK-2-PIK3CB 3′UTR construct compared to the luciferase level in cells transfected with control RISC-free siRNA. In cell co-transfected with miR-199-3p inhibitor, there was an increase in the luciferase ratios by ~3.7 fold relative to RISC-free siRNA (Figure 5.8a). No effect was observed on the luciferase expression in cells co-transfected with either *C. elegans* mimic or inhibitor. These results suggest that PIK3CB is directly regulated by miR-199-3p through its 3′UTR.

To further test whether the direct effect of miR-199-3p on the PIK3CB 3′UTR reporter construct occurred through the predicted binding sites, a 3 base-pair mutation in the seed sequence match was introduced in one or both miR-199-3p binding sites in the PIK3CB 3′UTR, resulting in three mutant constructs: psiCHECK-2-MUT1-PIK3CB 3′UTR, psiCHECK-2-MUT2-PIK3CB 3′UTR, and psiCHECK-2-MUT1/2-PIK3CB 3′UTR (Figure 5.8b). The mutations in the miR-199-3p binding sites were in nucleotides predicted to pair at nucleotides 2-4 in miR-199-3p (within the seed site).

The reporter containing a mutation in the first site (1097nt at the PIK3CB 3′UTR) resulted in a 1.4 fold decrease in luciferase ratios in cells co-transfected with miR-199-3p mimic, whereas the second mutant site (1139nt at the PIK3CB 3′UTR) resulted in a 2 fold decrease. In contrast, the luciferase expression in the cells co-transfected with the miR-199-3p inhibitor showed an approximate increase of 1.7 fold in the first mutant and 2 fold in the second mutant (Figure 5.8c).

Remarkably, the double mutant construct resulted in no significant difference in luciferase expression when cells were co-transfected with miR-199-3p mimic or inhibitor as compared to the luciferase expression in RISC-free control transfected cells. Therefore, we conclude that the single mutation only attenuates the effect of miR-199-3p on PIK3CB, while the mutation of both miR-199-3p sites was able to completely abolish the effect. These results indicate that miR-199-3p targets PIK3CB

3′UTR directly, through two functional binding sites. In conclusion, these results demonstrated that miR-199-3p has a combinatorial effect to suppress the expression of PIK3CB as the double mutations in the two target sites rather than the individual mutation eliminated the repression from miR-199-3p.

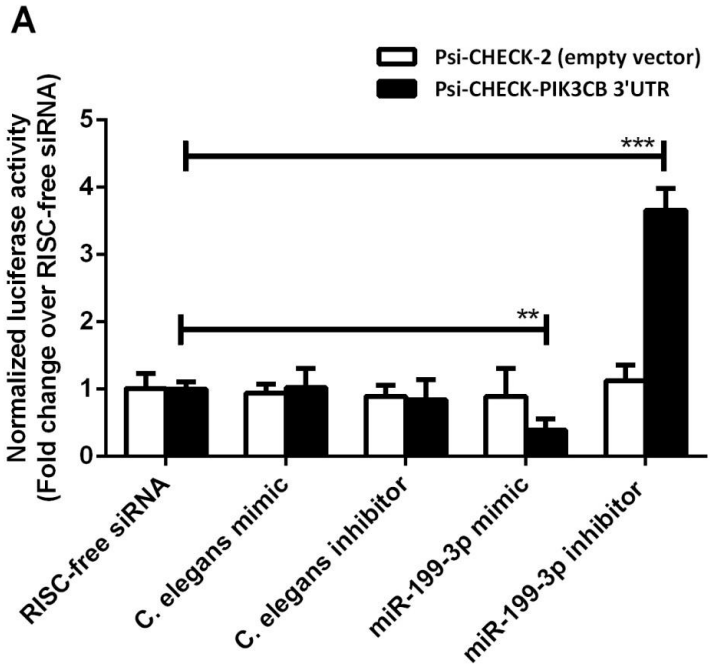

B

First binding site at of PIK3CB at 1097 nt

```
5'  ....GCAUGUGCAAUAGGAACUACUGG     Wild type PIK3CB 3'UTR
           |||||||       |||||||
3'  AUUGGUUACACGUC-----UGAUGACA     miR-199-3p
           |||||||       |||***|
5'  AUUGGUUACACGUC-----UGAUGACA     Mutant PIK3CB 3'UTR
```

Second binding site at of PIK3CB at 1139 nt

```
5′  CAGGAUCCAGCAAAACUACUGC          Wild type PIK3CB 3'UTR
    .|..........|.|||||||
3′  AUUGGUUACACGUCUGAUGACA          miR-199-3p
    .|..........|.|||***|
5′  CAGGAUCCAGCAAAACUTGAGC          Mutant PIK3CB 3'UTR
```

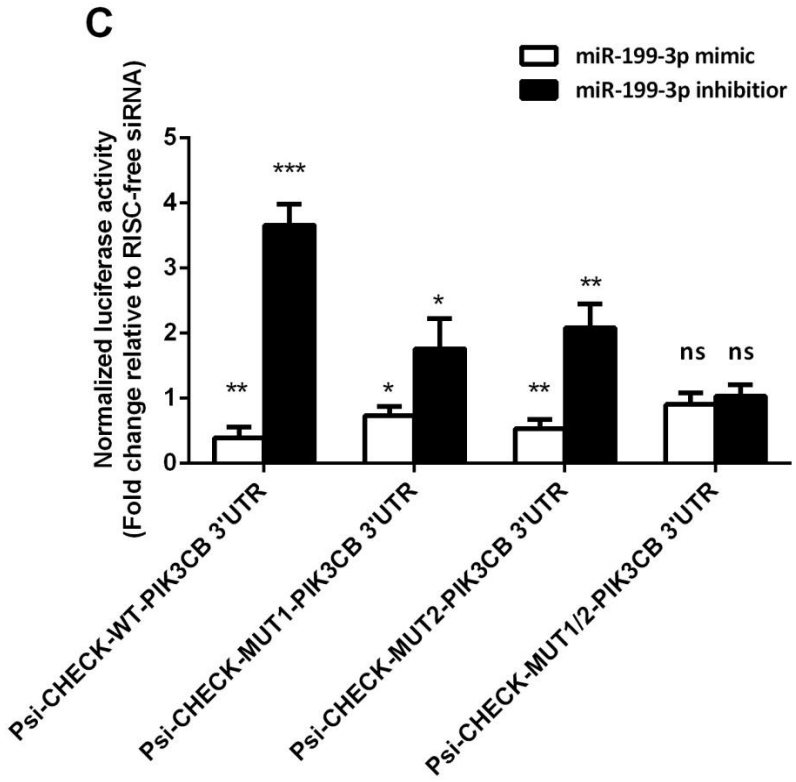

Figure 5.8: PIK3CB is a direct target of miR-199-3p through two binding sites in its 3′UTR. (A) Luciferase reporter plasmid, psiCHECK-2-PIK3CB 3′UTR was co-transfected into NIH-3T3 cells with either RISC-free siRNA or mimic or inhibitor for both *C. elegans* miRNA (Cel-miR-67) and miR-199-3p. Cells were lysed and luciferase expression was measured at 48 hours post transfection. The low background luciferase activity of the untreated cells was subtracted from the luciferase activity of transfected cells. The luciferase of *Renilla* were normalised to second firefly control luciferase activity to correct the variations in transfection efficiency and cell count. Data presented are the mean fold change ± S.D. (n=4) of the ratio between *Renilla* luciferase and firefly control luciferase activities and are representative of three independent experiments. **P<0.01 and ***P<0.001 compared to RISC-free siRNA transfected cells as determined by unpaired Student's *t* test. (B) Schematic diagram representing the location and mutation of the putative miR-199-3p binding sites within the 3′UTR of PIK3CB mRNA. Mutated regions are shown in A1097/1139T, C1098/1140G, and T1099/1141A in PIK3CB 3′UTR. Red-colored nucleotides indicate the seed match in the PIK3CB 3′UTR and starts (*) represent the sites of the point mutation. (C) Luciferase reporter plasmid, psiCHECK-2-PIK3CB 3′UTR, psiCHECK-2-MUT1-PIK3CB 3′UTR, psiCHECK-2-MUT2-PIK3CB 3′UTR, or psiCHECK-2-MUT1/2-PIK3CB 3′UTR was co-transfected into NIH-3T3 cells with either RISC-free siRNA or mimic or inhibitor for miR-199-3p. Cells were lysed and luciferase expression was measured as I in A. Data presented are the mean fold change ± S.D. (n=4) of the ratio between Renilla luciferase and firefly control luciferase activities and are representative of three independent experiments. ns (for non-significance), *P<0.05, **P<0.01 and ***P<0.001 compared to RISC-free siRNA transfected cells as determined by unpaired Student's *t* test.

5.2.2 PIK3CB and ITGA6 are regulated by miR-199-3p at the protein level

Although the luciferase reporter assay evidence that the gene is indeed regulated by the miRNA, there are caveats of using this assay: 1) the luciferase reporter is dependent on the region selected for cloning from the target gene; 2) the *Renilla* and firefly luciferase genes are controlled by different promoters within the psi-CHECK-2 construct. Theoretically, the transcriptional activity of any of these promoters can be affected by overexpression or inhibition of miRNA 3) the overlap in the emission spectra ranges can cause bleed-through of the firefly into *Renilla* during the sequential measurements. In order to further examine miR-199-3p regulation of its targets, the expression of human PIK3CB and ITGA6 protein was examined in fibroblast cell lines, namely MRC-5 and HEFs. The human cells were selected because human antibodies were available.

MRC-5 and HEFs were either untreated or transfected with RISC-free siRNA, miR-199-3p mimic or inhibitor. Cell lysates were subsequently collected at 48 hours post transfection, for quantification of the protein levels by Western analysis.

As can be seen in Figure 5.9, the protein levels of PIK3CB and ITGA6 were lower in those cells transfected with miR-199-3p in comparison to the level in untreated cells or cells transfected with RISC-free siRNA. This was seen in both HEF and MRC-5 cells. As is consistent with the qRT-PCR data presented in the previous chapter (Figure 4.9a,d), no significant upregulation was found in PIK3CB and ITGA6 levels in miR-199-3p inhibitor transfected MRC-5 cells. Commercial antibody for ITGA3 was not available and CD151 was not suitable for Western blots as it generates strong and multiple nonspecific bands.

In conclusion, miR-199-3p was found to regulate the expression of *Renilla* reporter gene bearing the 3′UTR of ITGA3 or CD151, suggesting that these genes are direct targets of this miRNA. No difference in reporter gene expression was observed when it contained the 3′UTR sequence of ITGA6 under the same conditions. This is despite the fact that qRT-PCR and Western blot analysis showed down-regulation of mRNA and the protein levels of ITGA6 in response to miR-199-3p mimic. Therefore, it seems to be the case that ITGA6 is regulated by miR-199-3p but

perhaps not through its 3′UTR. All the data strongly suggest that PIK3CB is a direct target of miR-199-3p through two sites of interaction.

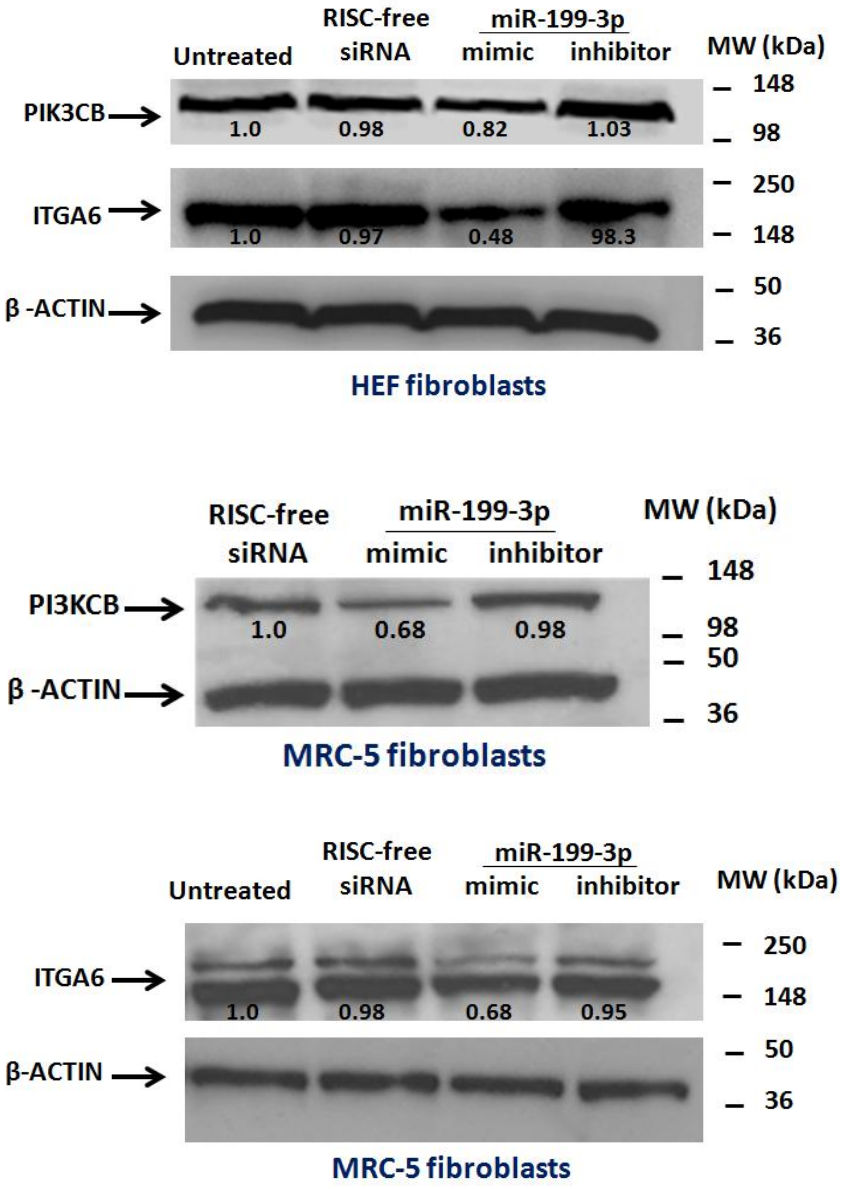

Figure 5.9: miR-199-3p regulates PIK3CB and ITGA6 protein levels in HEF and MRC-5 cell lines. MRC-5 and HEFs were either untreated or transfected with RISC-free siRNA, miR-199-3p mimic or inhibitor. Cell lysates were then harvested at 48 hours after transfection. 25µg of cell lysates was loaded per lane and membrane was immunoblotted with primary antibodies against PIK3CB, ITGA6, or β-ACTIN as a loading control. Blots were then quantified by densitometry and normalized to the corresponding β-ACTIN. For the upper and lower panels, the untreated was set as 1 whereas the RISC-free was 1 for the middle panel. Other values were expressed relative to the untreated value (the upper and lower panels) or RISC-free siRNA (the middle panel).

5.2.3 Regulation of miR-199-3p targets in HCMV infection

The expression of miR-199-3p is down-regulated during both HCMV and MCMV infections (Chapter 3) and several of its cellular targets have been identified (Chapter 4) and validated (Chapter 5). However, an important question is whether the down-regulation of miR-199-3p during infection actually influences the target genes under physiological conditions (rather than transfection with synthetic reagents). The hypothesis is that miR-199-3p targets are up-regulated following infection, to correlate with miR199 down-regulation (which occurs between 24 to 72 hpi). In order to examine this hypothesis, it was necessary to first serum starve MRC-5 fibroblast cells before infection. Serum starvation is a common procedure that eliminates growth factors and hormones in culture media in order to reduce cell signalling to basal levels. This culture condition was used when investigating AKT signalling (below) and in all experiments where reproducibly, uniform culture conditions were necessary. Following serum starvation, MRC-5 cells were then mock infected or infected with HCMV at MOI of 5. Total RNA and cell lysates were harvested from infected cells at the following times, 30min, 2, 4, 8, 12, 24, 36, 48, and 72 hpi.

Total RNA was analysed using qRT-PCR and Northern blot and cell lysates were analysed by Western blot. The qRT-PCR detected expression levels of miR-199-3p and target mRNAs were normalised to U6 snRNA and GAPDH mRNA, respectively. U6 snRNA and GAPDH were found to maintain a stable expression level during the infection.

As described previously in this thesis (Result 3.2.9), mature miR-199-3p levels decrease at 24 hpi and this is maintained until 72 hpi during HCMV infection. In the experiment presented here, PIK3CB mRNA was found to increase by ~8 fold at 24 hpi and ~30 fold at 72 hpi (Figure 5.10a). Similarly, ITGA6 increased ~14 fold at 24 hpi and reached ~25 fold at 72 hpi compared with control cells (Figure 5.10b). ITGA3 was also up-regulated, with a ~2 to 3 fold increase in its mRNA level observed at 24 and 48 hpi (Figure 5.10c). The upregulation of ITGA3 was less pronounced than that observed for PIK3CB and ITGA6, but still significantly

increased as compared to controls. By contrast, the level of CD151 mRNA gradually reduced at 24 and 72 hpi by ~2 to 4 fold respectively (Figure 5.10d). In addition to this, CD44, a validated target of miR-199-3p (Henry et al., 2010), was found to have a ~5 fold induction in the expression of its mRNA within 30 min of HCMV infection, with a peak of ~6 fold at 2 hours, after which it began to decrease leading to ~8 fold decrease in mRNA level at 24 and 72 hpi, respectively (Figure 5.10e).

Northern blot results verified the down-regulation of miR-199-3p expression within 24 hpi under these experimental conditions (Figure 5.11a). Western blot analysis was also used to confirm the up-regulation of PIK3CB and ITGA6 at the protein level in infected cells at 24 to 72 hpi. These results show that the increase in the mRNA levels of the target genes, PIK3CB and of ITGA6 is indeed reflected in their protein levels in HCMV infection. CD44 protein expression was also found to correlate with its mRNA level, showing a rapid up-regulation during the first 8 hours of HCMV infection and a decrease from 24 hours onward (Figure 5.11b). As mentioned above, the other proteins have not been included in this Western blot analysis due to unavailability of suitable antibodies.

In conclusion, an inverse correlation was identified between the expression of miR-199-3p and several of its targets (PIK3CB, ITGA6 and ITGA3) during infection. Therefore, it is possible that the suppressive effect of HCMV infection on miR-199-3p expression directly contributes to the upregulated expression levels of these targets, PIK3CB, ITGA6 and ITGA3. However, additional factors, such as transcriptional regulation could also contribute to their up-regulation during infection. The expression of CD44 and CD151 transcripts did not show an inverse correlation with miR-199-3p expression, and rather these genes were down-regulated during infection.

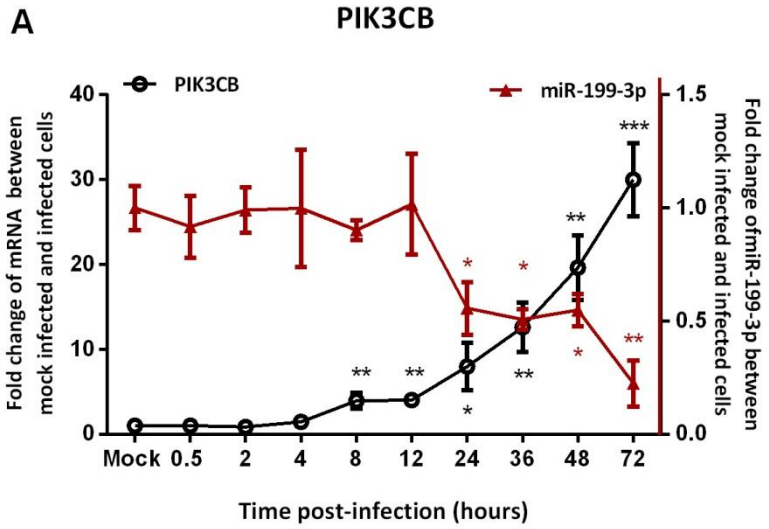
A
PIK3CB
PIK3CB
miR-199-3p
Fold change of mRNA between mock infected and infected cells
Fold change ofmiR-199-3p between mock infected and infected cells
Mock 0.5 2 4 8 12 24 36 48 72
Time post-infection (hours)

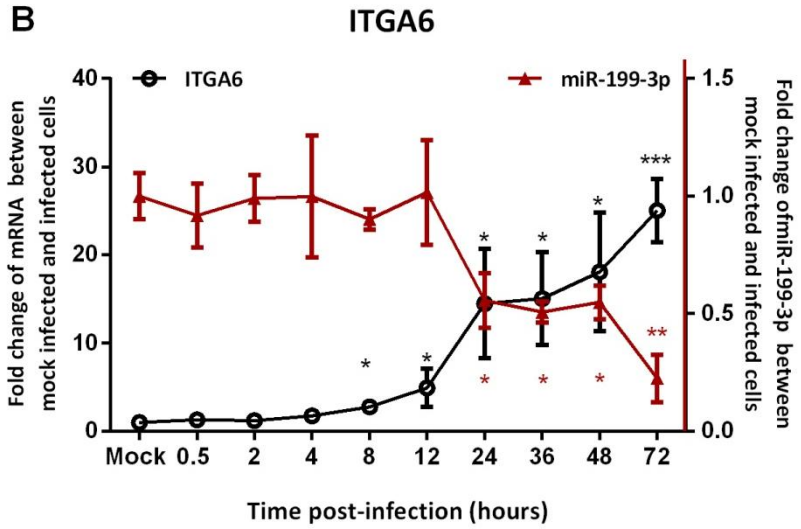
B
ITGA6
ITGA6
miR-199-3p
Fold change of mRNA between mock infected and infected cells
Fold change ofmiR-199-3p between mock infected and infected cells
Mock 0.5 2 4 8 12 24 36 48 72
Time post-infection (hours)

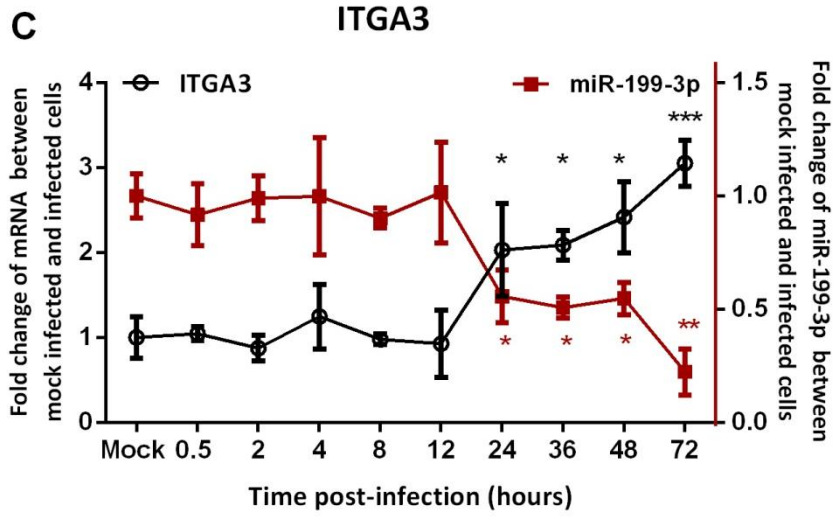
C
ITGA3
ITGA3
miR-199-3p
Fold change of mRNA between mock infected and infected cells
Fold change of miR-199-3p between mock infected and infected cells
Mock 0.5 2 4 8 12 24 36 48 72
Time post-infection (hours)

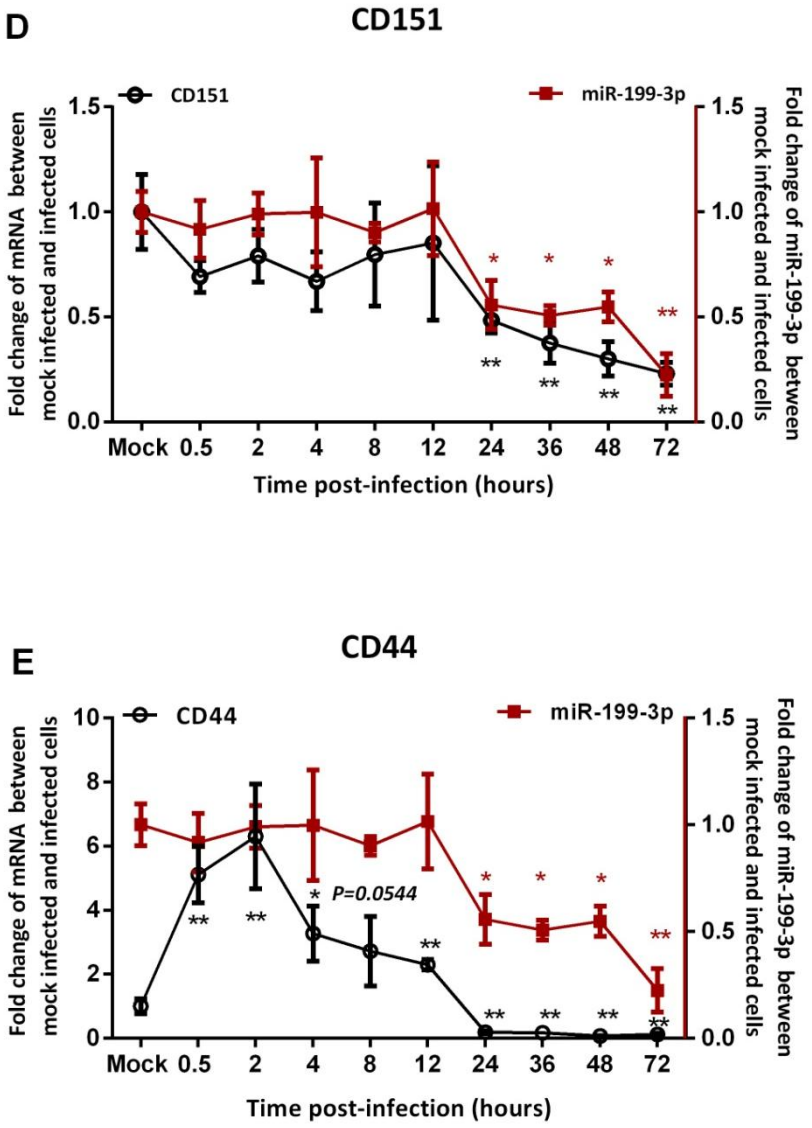

Figure 5.10: The expression kinetics of miR-199-3p and its target mRNAs, PIK3CB, ITGA6, ITGA3, CD151, and CD44 during HCMV infection. MRC-5 cells were serum starved for 48 hours and either mock infected or infected with HCMV at an MOI=5 for the indicated times. The expression level of miR-199-3p and its target mRNAs were quantified by qRT-PCR. The first was normalised to miR-16 and the later to GAPDH mRNA. Mock infected cells from the different time points (0hr, 24hr and 48hr) were averaged and compared to infected cells at each time point. Data presented are the mean fold change ± S.D. of two independent experiments in triplicates (n=6). *P<0.05 compared to mock infected cells as determined by a repeated measures one-way ANOVA with Sidak's post-test for multiple comparisons.

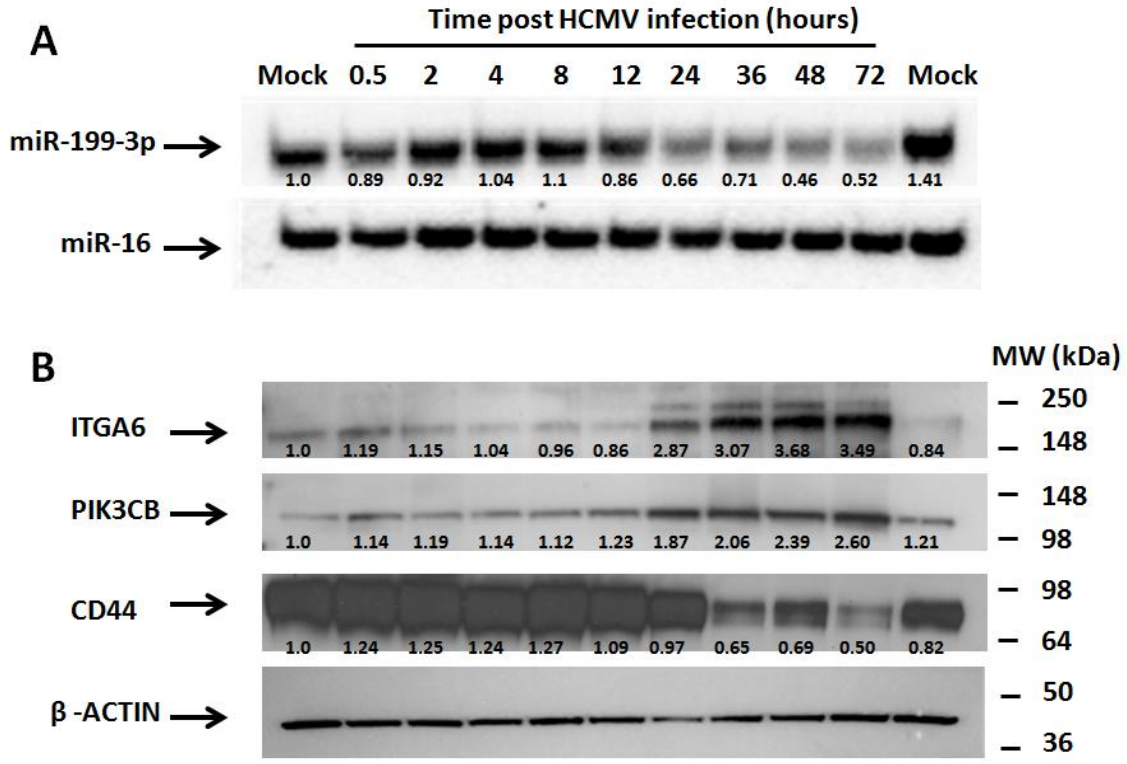

Figure 5.11: The expression of miR-199-3p and its target protein, PIK3CB, ITGA6, and CD44 during HCMV infection. MRC-5 cells were serum starved for 48 hours and either mock infected or infected with HCMV at an MOI=5 for the indicated times. (A) Northern blot analysis of miR-199-3p during HCMV infection. Total RNA was harvested from MRC-5 cells mock infected or infected as described above. 7µg of total RNA was loaded per lane and membrane was hybridised with 32P-labeled probes. miR-16 probe was used as a loading control (lower panel), followed by densitometric analysis. The densitometric value for the mock infected was set as 1 and values for other time points post infection were expressed relative to the mock value. (B) Western blot showing the protein expression of PIK3CB, ITGA6 and CD44 during HCMV infection. Whole cell lysates were harvested from MRC-5 cells mock infected or infected as described above. 20µg of cell lysates was loaded per lane and membrane was immunoblotted with primary antibodies against PIK3CB, ITGA6, CD44 or β-ACTIN as a loading control. Blots were then quantified by densitometry and normalized to the corresponding β-ACTIN. The mock infected was set as 1 and values for other time points were expressed relative to this mock infected value.

5.2.4 AKT is activated in HCMV infected MRC-5 fibroblasts

The detailed kinetics of the phosphorylation of AKT have been studied previously in human embryonic lung fibroblast cells (HELs) infected with HCMV. A biphasic activation was observed; a rapid phosphorylation of AKT appeared at 15-30 min, which was then followed by a sustained phosphorylation that continued to increase from 4 to 48 hours post HCMV infection (Johnson et al. 2001b). In the study presented here, it was found that miR-199-3p regulates AKT phosphorylation. Based on IPA computational analysis (Chapter 4), AKT is linked to several miR-199-3p targets including PIK3CB, ITGA6, ITGA3, CD151, and CD44.

The aim in this section was therefore to analyse AKT activation during HCMV infection of MRC-5 cells and to determine if this could result from the regulation of its targets. For maximal kinase activation AKT can be phosphorylated at two sites, at threonine 308 (Thr308) and serine 473 (Ser473) residues, both phosphorylation sites were examined.

As can be seen in Figure 5.12, both Ser473 and Thr308 sites of AKT were highly phosphorylated within 30 min and up to 2 hpi. Levels of phosphorylation at both sites returned to the basal level at 4 hpi and were undetectable thereafter. This shows a rapid AKT phosphorylation during the first two hours of HCMV infection of MRC-5 fibroblasts and down-regulation of phosphorylation afterwards. However, these results of AKT phosphorylation in HCMV infected MRC-5 were not consistent with the kinetics shown in HCMV infected HELs by Johnson and colleagues (Johnson et al. 2001b), where increasing phosphoryation was observed at later time points.

According to these results, AKT phosphorylation in HCMV infected MRC-5 fibroblasts did not correlate with miR-199-3p expression, which decreased from 24 hpi. The increase in AKT phosphorylation at 2 hours preceded miR-199-3p down-regulation during infection, which indicates that miR-199-3p is unlikely to be involved in AKT phosphorylation under these conditions.

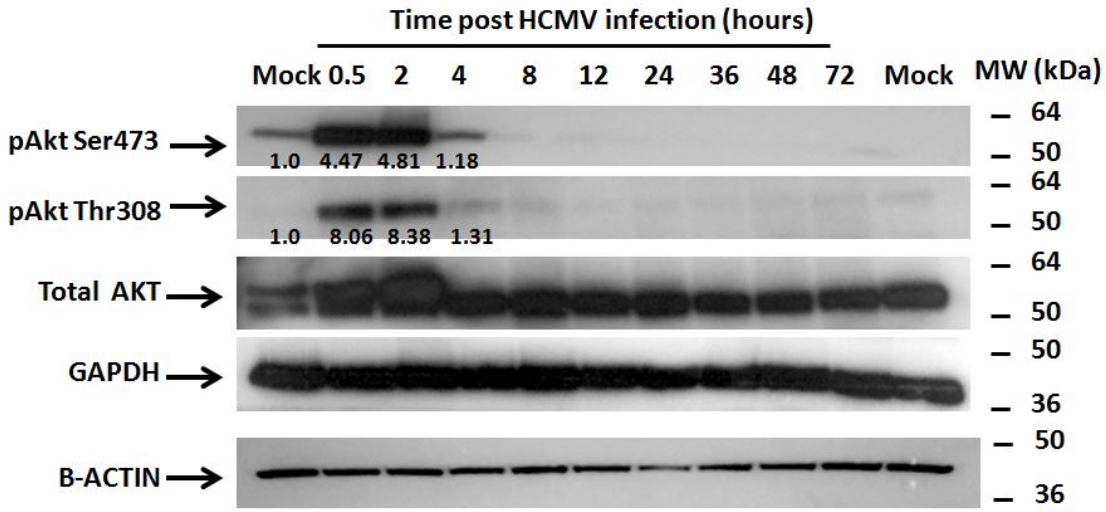

Figure 5.12: The kinetics of AKT phosphorylation during HCMV infection. MRC-5 cells were serum starved for 48 hours and then either mock infected or infected with HCMV at an MOI=5 for the indicated times. 20µg of cell lysates was loaded per lane and membrane was immunoblotted with primary antibodies against the phosphorylated-Ser473 and phosphorylated-Thr308, total AKT, β-ACTIN, or GAPDH as a loading control. Blots were then quantified by densitometry and normalized to the corresponding GAPDH. The mock infected was set as 1 and values for other time points were expressed relative to this mock infected value.

5.2.5 Over-expression of miR-199-3p reduces AKT phosphorylation at early time points post infection

The results in section 4.2.10 demonstrate that the expression of miR-199-3p has a negative effect on AKT phosphorylation at both phosphorylation sites, Ser473 and Thr308. It was thus hypothesised that the pre-transfection of miR-199-3p into cells would reduce the level of HCMV induced AKT phosphorylation at 30 min and 2 hpi.

To examine this hypothesis, AKT phosphorylation was assessed in cells transfected with miR-199-3p and subsequently infected with HCMV for 30 min and 2 hours. In more details, MRC-5 cells were untreated or transfected with control RISC-free siRNA or miR-199-3p mimic for 24 hours. Cells were then serum starved for a further 24 hours and either mock infected or infected with HCMV at MOI of 5. Cell lysates were harvested at 30 min and 2 hpi and subjected to Western blotting.

As can be seen in Figure 5.13, the overexpression of miR-199-3p reduced the phosphorylation at the Ser473 site while the level of total AKT is comparable between the conditions. The results suggest that miR-199-3p reduces the phosphorylation of AKT without affecting the translational regulation of AKT itself, suggesting that this is mediated by miR-199-3p targets that involved in regulation of AKT phosphorylation such as PI3KCB.

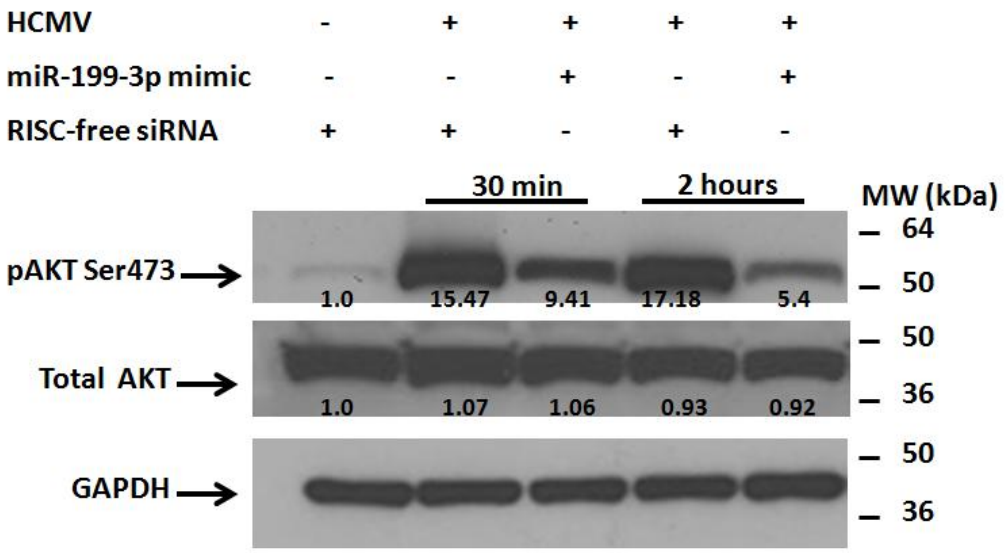

Figure 5.13: The AKT phosphorylation following HCMV infection is repressed by miR-199-3. MRC-5 cells were transfected with miR-199-3p or control RISC-free siRNA for 24 hours prior to serum-starvation. 24 hours following the starvation, cells were either mock infected or infected with HCMV at an MOI=5 for the indicated times. 20µg of cell lysates was loaded per lane and membrane was immunoblotted with primary antibodies against the phosphorylated-Ser473, total AKT, or GAPDH as a loading control. Blots were then quantified by densitometry and normalized to the corresponding GAPDH. The mock infected was set as 1 and values for other time points were expressed relative to this mock infected value.

5.2.6 The rapid activation of AKT is PI3K dependent and may required for HCMV infected MRC-5 fibroblasts

It has previously been shown that inhibition of AKT phosphorylation suppress HCMV replication (Johnson et al. 2001b). In the previous section (5.2.5), it was demonstrated that the HCMV infection of cells transfected with miR-199-3p reduces the phosphorylation levels of AKT. It was therefore hypothesised that this effect is responsible for antiviral activity of miR-199-3p.

Cells were seeded for 24 hours and then treated with LY294002, a specific inhibitor of PI3-Kinase for 30 min prior to HCMV infection. LY294002 is an ATP-competitor that targets the active ATP binding site of PI3K kinase. It should be noted that the PI3-Kinase inhibitor, LY294002, can inhibit the phosphorylation of AKT as well as other PI3K-related enzymes such as the DNA-dependent protein kinase (DNA-PK and ATM) (Rosenzweig et al. 1997; Izzard et al. 1999). Control cells were treated with DMSO as LY294002 is prepared in DMSO. Ly294002 can be used at a concentration of 50μM according to the manufacturer's instructions (Cell Signalling Technology). However, this concentration caused a marked reduction in the viability of cultured cells after 24 hours. Therefore, two other concentrations of Ly294002, 10 and 25μM, were examined for their effects on cell viability and PI3K activity. The treatment with 25μM of Ly294002 does not lead to cellular death and has a stronger inhibitory effect on PI3K activity and AKT phosphorylation in the MRC-5 cell line than 10μM of Ly294002 (data not shown). To assess viral growth, LY294002-treated and DMSO-treated control cells were infected at MOI of 0.5 with HCMV that expresses GFP under control of the UL127 promoter or were mock infected (HCMV-GFP). Viral growth was assessed by measuring the GFP signal twice/day from 0 to 156 hours (Day 7 of infection) using Varioskan Flash Multimode Reader (excitation wave length of 485 nm and emission of 520 nm).

A significant reduction was observed in viral growth in LY294002-treated cells in comparison to the control DMSO-treated or mock infected cells. The reduction was more pronounced in cells treated with 25μM LY294002 than in 10μM LY294002-treated cells (Figure 5.14).

In conclusion, the viral growth of HCMV was suppressed by LY294002 in a dose-dependent manner, which is likely due to the inhibition of AKT phosphorylation. This, in turn suggests that PI3K-AKT signalling has important at the early stage of HCMV life cycle.

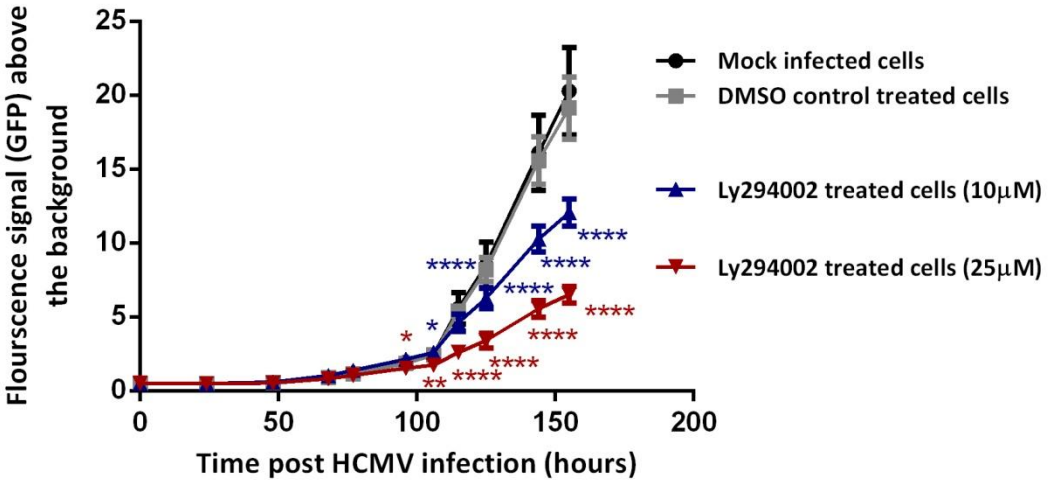

Figure 5.14: Blocking AKT phosphorylation in MRC-5 cells results in reduced viral growth. MRC-5 cells were either untreated or treated with DMSO, 10μM and 25μM Ly294002. After 30 min of treatment, MRC-5 were then mock infected or infected with HCMV-GFP at an MOI= 0.5. The growth curve of GFP virus in infected untreated or treated MRC-5 cells with control DMSO or Ly294002. The fluorescent signal of mock infected cells is considered as a background. Data presented are the mean normalized fluorescence ± S.D. (n=3) and are representative of 3 independent experiments. *P<0.05, **P<0.01, and ****P<0.0001 compared to DMSO treated and infected cells as determined by a repeated measures two-way ANOVA with Sidak's post-test for multiple comparisons.

5.2.7 miR-199-3p targets, PIK3CB, ITGA6, and ITGA3 may not be associated with the antiviral properties of miR-199-3p in HCMV infection

The data presented here show that miR-199-3p regulates the phosphorylation of AKT, and that inhibition of this phosphorylation reduces viral growth, likely because AKT is required early in the life cycle. However, these results do not address the functional significance of the natural down-regulation of miR-199-3p during infection, which occurs at 24 hpi. It is not clear if this influence AKT phospho-regulation, since this was not observed *in vitro* (Fig. 5.12).

The data presented in section 5.2.3 shows that cellular genes PIK3CB, ITGA6 and ITGA3 are up-regulated when miR-199-3p is down-regulated from 24 to 72 hpi. A hypothesis, therefore, is that the down-regulation of miR-199-3p during HCMV infection contributes to the upregulation of these genes and that these genes have a direct role in promoting viral growth. It should be noted that while the induced expression of PIK3CB, ITGA6 and ITGA3 occurs concomitant with miR-199-3p suppression in HCMV infection, this alone is insufficient evidence to conclude that miR-199-3p is alone responsible for their up-regulation or that these targets can be associated with the antiviral function of miR-199-3p. Experiments were therefore designed to investigate whether these targets of miR-199-3p play a role in HCMV infection.

5.2.7.1 The functional significance of PIK3CB, ITGA6 and ITGA3 in HCMV infection

In this section the question whether PIK3CB, ITGA6, and ITGA3 play a role in HCMV infection was examined. Therefore, HCMV viral growth was monitored in cells in which PIK3CB, ITGA6, and ITGA3 were knocked down by siRNA. Since these genes are up-regulated during infection, their silencing should be an effective strategy to examine whether or not they are necessary to the viral growth.

MRC-5 cells were transfected with control RISC-free siRNA, a specific target siRNAs for ITGA6 or ITGA3, or two different siRNAs for PIK3CB for 48 and 72 hours. Total RNA was then isolated in order to test whether the siRNAs were effective in gene silencing by measuring the mRNA levels using qRT-PCR. Cell

lysates were also harvested to check protein levels using available antibodies. Relative to cells transfected with control RISC-free siRNA, the knockdown observed for each gene at 48 and 72 hours post transfection was: PIK3CB 1 (5.5 and 12-fold) ; PIK3CB 2 (11 and 7-fold); ITGA6 (9.5 and 13.5-fold); and ITGA3 (4 and 5.5-fold) (Figure 5.15a). The protein levels of PIK3CB were also examined following the knock down and showed more than 50% decrease using either siRNA (Figure 5.15b).

MRC-5 cells were either untreated or transfected for 48 hours with RISC-free siRNA, *C. elegans* mimic, miR-199-3p mimic, e-GFP siRNA, ITGA6, ITGA3, or two different siRNAs for PIK3CB. Following transfection, cells were mock infected or infected with HCMV-GFP at MOI of 0.5. Viral growth was then monitored in transfected cells infected cells by measuring GFP expression over a 6 day time course of infection. In parallel, the cell viability was measured prior to infection. All transfected cells showed a viability value of >90% (Figure 5.16).

Viral growth was similar in untreated cells or cells transfected with the control *C. elegans* mimic (Figure 5.17). This demonstrates that the transfection procedure did not affect viral growth. The viral growth in cells transfected with RISC-free siRNA was attenuated in comparison to untreated and control mimic, implicating non-specific effects of RISC-free siRNA (Figure 5.17). However, this was statistically significance only at day 7. An siRNA directed at the viral GFP gene expression (e-GFP siRNA) serve as a control for transfection efficiency, however, it was able to decrease the expression of GFP-protein from the HCMV-GFP by ~2.3 fold at 96 hpi, ~5 fold at 120 hpi and ~2 fold at 168 hpi (Figure 5.17). Cells transfected with miR-199-3p mimic showed a ~1.7 fold, ~3 fold, and ~1.4 fold decrease in the fluorescence signal at 96, 120, and 168 hpi respectively, indicating that miR-199-3p had a negative effect on viral growth. It is therefore possible to conclude that the transfection procedure was successful and that miR-199-3p has antiviral properties as expected (Figure 5.17).

The growth rate of HCMV-GFP was also evaluated in cells in which the expression of ITGA6, ITGA3, and PIK3CB genes was knocked down. No significant difference was observed in the growth rate of HCMV-GFP in MRC-5 cells transfected with

ITGA6 siRNA relative to the control RISC-free transfected cells or untreated cells over the chosen time course (Figure 5.18a). The knock down of ITGA3 and PIK3CB resulted in an increase in the fluorescence signal observed relative to the GFP signal emitted by infected RISC-free transfected cells at day 6 and 7, whereas no significant change was detected in the growth of HCMV-GFP in those cells compared to untreated cells (Figure 5.18a,b).

As the silencing of gene expression can be incomplete (not 100% efficient) for most proteins, a small amount of expression of these proteins can still be sufficient to exert their potential functions. Therefore, an experimental complementation of other approaches (i.e. the pharmacological inhibition, stable knock down or knock out animal or cell line) can support and provide more rigorous conclusions. It has been recently described the pharmacological inhibition of the kinase activity of PIK3CB with the new drug TGX-221 (Jackson et al. 2005), it was therefore decided to use this approach to further evaluate the involvement of the PIK3CB kinase function in HCMV infection. It should be noted that PIK3CB siRNA is able to affect the kinase dependent and independent function of PIK3CB, whereas the drug TGX-221 selectively blocks the kinase function of PIK3CB.

Cells were either untreated or treated with 50 nM TGX-221 or control DMSO for 2 hours prior to infection. The concentrations to be used in order to block the kinase activity of PIK3CB are in a range of 5-50 nM according to the manufacturer's instructions (Cayman Chemical). These concentrations do not affect the kinase activity of other PI3K isoforms, i.e. PIK3CA and PIK3CD. In addition, 50 nM does not result in a significant change in the proliferation or survival of cultured cells (data not shown). As a positive control, cells were treated for 2 hours with 25µM Ly294002, which has an antiviral effect (as shown in Figure 5.14). Treated cells were then infected with HCMV-GFP at MOI of 0.5 and the viral growth monitored based on its fluorescent signal. No change in viral growth was observed in TGX-221 treated cells in comparison to control DMSO treated cells or the untreated cells over the time course of the HCMV infection (Figure 5.19). In contrast, a significant inhibition in viral growth was seen in Ly294002 treated cells (Figure 5.19).

Overall, the negative control, RISC-free siRNA causes nonspecific effects on viral growth or its GFP expression compared to untreated cells or *C. elegans* mimic transfected cells, therefore the results from siRNA experiments can be hard to interpret. The knock down of PIK3CB and ITGA3 showed proviral effects relative to control RISC-free transfected cells but no significant effect was observed relative to untreated cells. Moreover, the knock down of ITGA6 has no effect on the viral growth when compared to that in untreated or control RISC-free transfected cells. Comparative analysis of PIK3CB knock down experiments was performed using pharmacological inhibitor TGX-221 to examine the role of kinase-dependent functions of PIK3CB in HCMV infection. Specific blockade of PIK3CB kinase function did not influence viral growth. It may therefore be the case that the antiviral function of miR-199-3p is not associated with any of these target genes.

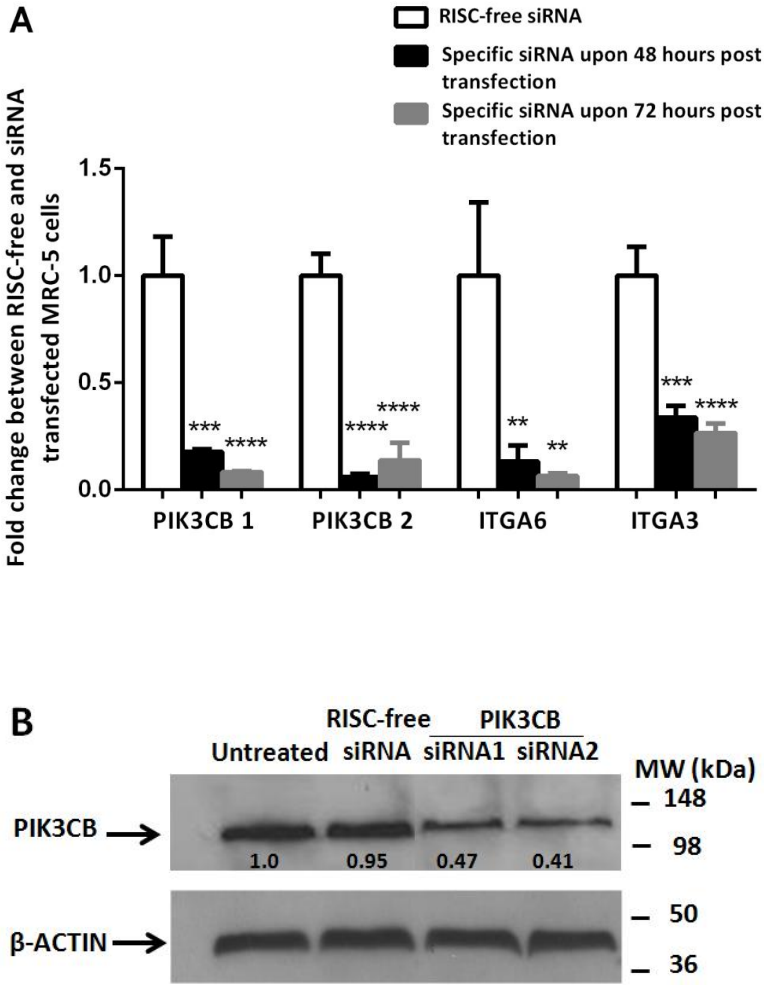

Figure 5.15: The Knock down of PIK3CB, ITGA6, and ITGA3 using siRNAs. A) Reduction in the mRNA levels of PIK3CB, ITGA6, and ITGA3 in cells transfected for 48 and 72 hours with siRNAs directed against each gene. The expression levels of target genes were quantified by qRT-PCR and normalised to GAPDH and compared to cells transfected with RISC-free siRNA. Data presented are the mean fold change ± S.D. (n=3) and are representative of two independent experiments. **P<0.01, ***P<0.001, and ****P<0.0001 compared to RISC-free siRNA transfected cells as determined by unpaired Student's *t* test. B) Western blot showing reduction in PIK3CB protein in cells transfected with either PIK3CB siRNAs. MRC-5 cells were untreated or transfected with either RISC-free or PIK3CB siRNAs for 48 hours. 20µg of cell lysates was loaded per lane and membrane was immunoblotted with primary antibodies against the PIK3CB or β-ACTIN as a loading control. Blots were then quantified by densitometry and normalized to the corresponding β-ACTIN. The untreated was set as 1 and values for transfected cells were expressed relative to the untreated value.

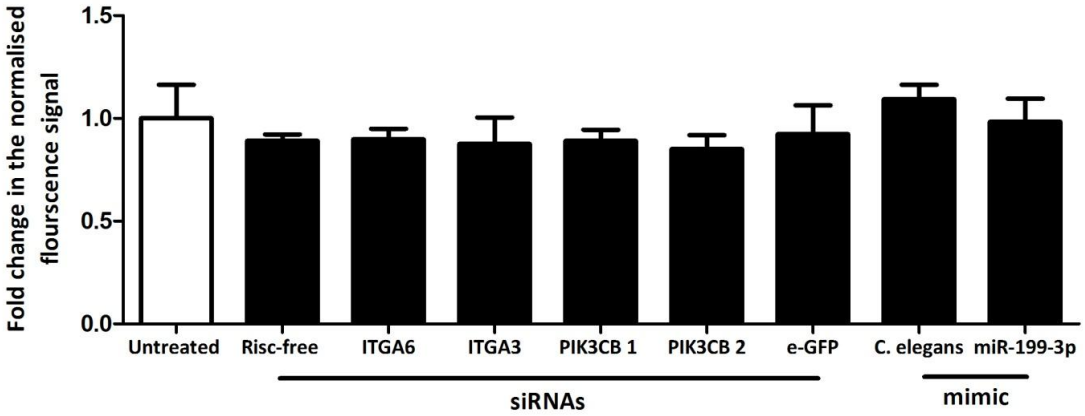

Figure 5.16: Effects of PIK3CB, ITGA6, and ITGA3 knockdown on cell viability. The measurement of cell viability was performed using cell titer blue assay. The background fluorescence of the culture medium was subtracted from the fluorescence values of the cells. The values above the background were compared to untreated samples. Data presented are the mean fold change ± S.D. (n=4) of one representative experiment (out of two independent experiments).

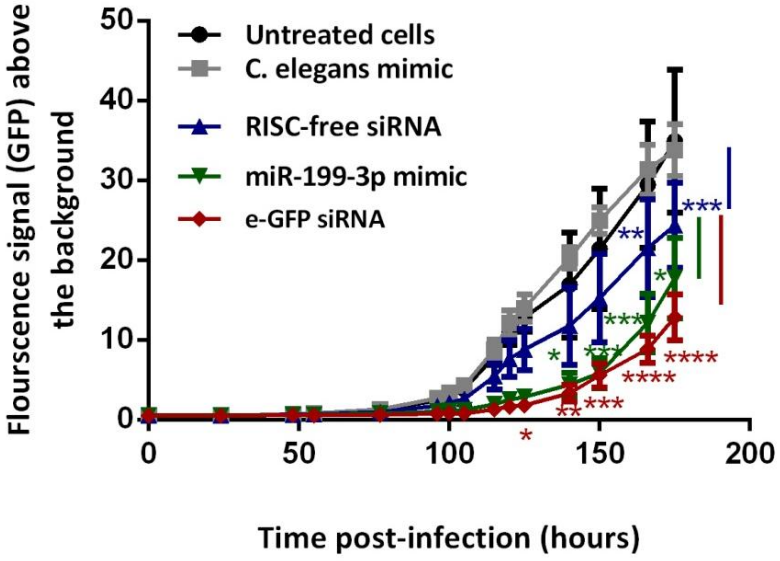

Figure 5.17: HCMV-GFP growth curve in MRC-5 cells transfected with miR-199-3p, *C. elegans* mimic, control RISC-free and e-GFP siRNA. Transfected cells were infected with HCMV-GFP at MOI=0.5. The graph displays growth curves of HCMV-GFP, which was monitored over 168 hours post infection. The fluorescent signal of mock infected cells is considered as a background. Data presented are the mean normalized fluorescence ± S.D. (n=3) and are representative of 3 independent experiments. *P<0.05, **P<0.01, ***P<0.001 and ****P<0.0001 compared to RISC-free transfected and infected cells or untreated infected cells as determined by a repeated measures two-way ANOVA with Sidak's post-test for multiple comparisons.

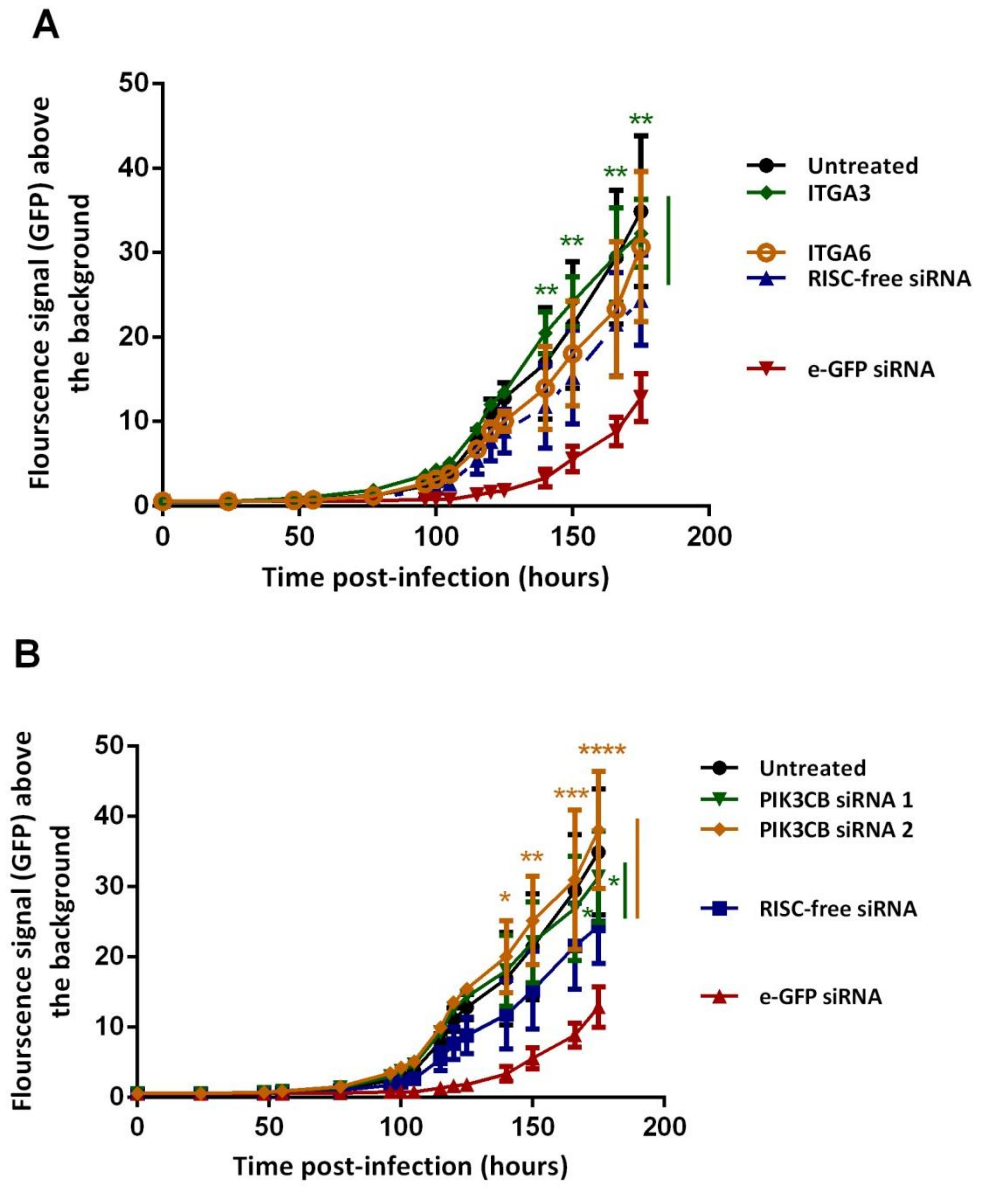

Figure 5.18: Growth curves of HCMV-GFP in transfected MRC-5 cells with controls and target siRNAs. HCMV-GFP growth curves in cells in which ITGA6, ITGA3 (A) or PIK3CB (B) were knocked down in MRC-5 cells. Transfected cells were mock infected or infected with HCMV-GFP at MOI=0.5. The graph displays growth curves of HCMV-GFP, which was monitored over 168 hours post infection. The fluorescent signal of mock infected cells is considered as a background. Data presented are the mean normalized fluorescence ± S.D. (n=3) and are representative of three independent experiments. **P<0.01 compared to RISC-free transfected and infected cells as determined by a repeated measures two-way ANOVA with Sidak's post-test for multiple comparisons.

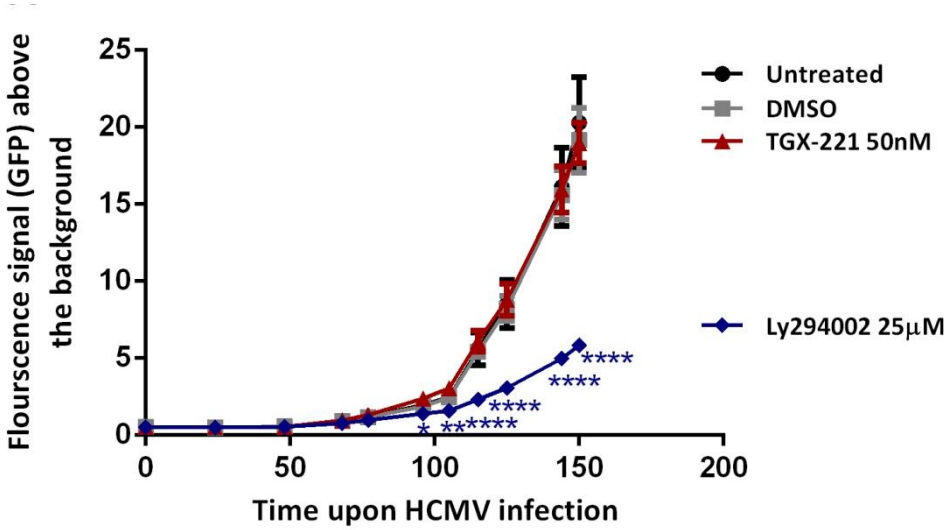

Figure 5.19: HCMV-GFP growth curves of MRC-5 cells treated with TGX-221. HCMV-GFP growth curves in cells untreated or treated with 50nM TGX-221, or 25µM Ly294002. Untreated and treated cells were infected with HCMV-GFP at MOIO=0.5. The graph displays growth curves of HCMV-GFP, which was monitored over 168 hours post infection. The fluorescent signal of mock infected cells is considered as a background. Data presented are the mean normalized fluorescence ± S.D. (n=3) and are representative of three independent experiments. *P<0.05, **P<0.01, and ****P<0.0001 compared to DMSO treated and infected cells as determined by a repeated measures two-way ANOVA with Sidak's post-test for multiple comparisons.

5.3 Discussion

miRNAs have an important role in regulating intracellular signaling cascades, which ultimately result in modification of diverse cell functions. As mentioned in the previous chapter, miR-199-3p was found to modulate PI3K-AKT signalling based on the reduced level of phosphorylation of AKT at key sites in cells transfected with miR-199-3p mimic. In addition to this, in silico analysis using IPA and TargetScan 5.0 software suggest a number of targets of miR-199-3p that are associated with the regulation of AKT, such as PIK3CB, ITGA6, ITGA3, CD151, and CD44. Of these six targets, only CD44 has been previously shown to be a direct target of miR-199-3p (Henry et al., 2010). Given the above findings, the role of miR-199-3p in regulating AKT and targets of miR-199-3p linked to AKT were selected for the further functional studies presented in this chapter.

5.3.1 The validation of miR-199-3p targets using a luciferase reporter system and Western blot analysis.

To date, the most specific method for validating miRNA target sites is based on reporter assays where the 3′UTR with target site is cloned downstream of a luciferase gene. The luminescence should be altered in the event that the target sequence is regulated by miRNA and this can be tested with mutation of target site. In addition, an inhibition of luminescence can be observed through the introduction of a regulatory miRNA mimic or induction of luminescence is seen when the endogenous level of this regulatory miRNA is knocked down. Importantly, the reporter has an internal control for transfection efficiency and cell count. A caveat to using miRNA overexpression in this assay is that the miRNA could be at non-physiological concentrations and therefore have non-physiological interactions. Here, it was shown that miR-199-3p targets ITGA3 and CD151 through binding to their 3′UTRs, as well as targeting PIK3CB through two conserved sequences within the PIK3CB 3′UTR (Figure 5.8). The only candidate target of miR-199-3p that did not respond to either the overexpression or inhibition of miR-199-3p was ITGA6, though ITGA6 mRNA and protein were down-regulated by miR-199-3p mimic in human cells (Figure 4.9 and 5.9). However, changes in expression level does not prove a direct interaction with miRNA, therefore it is possible that ITGA6 might be an indirect target of

miR-199-3p. There are a number of other possible explanations for why ITGA6 is regulated by miR-199-3p but not validated as a direct target with luciferase assay: 1) there could be a non-canonical binding site(s) for miR-199-3p within ITGA6 5'UTR or ORF (Ørom et al. 2008; Stark et al. 2007) (only the 3′UTR is examined in the above luciferase assay); and 2) it is possible that the mouse and human 3′UTRs of ITGA6 respond differently to miR-199-3p (this experiment used mouse 3′UTR). The mouse and human ITGA6 3′UTRs are 75% conserved, including a conserved miR-199-3p binding site. But it is possible that the mouse and human 3′UTRs have different RNA structural features, which could interfere with target-site accessibility and the mRNA:miRNA interaction.

5.3.2 The inverse correlation between miR-199-3p and its targets for during infection

It was hypothesised that the reduction of miR-199-3p in CMV infection at 24 to 72 hours resulted in, or contributed to, the upregulation of target genes, and this is expected to be beneficial to the virus. Therefore, the correlation between the miRNA and target mRNAs was examined in the context of infection. Upon HCMV infection, PIK3CB and ITGA6 were induced at the mRNA and protein levels while ITGA3 showed less pronounced upregulation. As it is generally believed that miRNAs exert subtle effects on their target genes, additional mechanisms may be involved in regulating these genes during infection, which could work in concert with miR-199-3p.

With regards to CD151 and CD44, these targets were markedly down-regulated when miR-199-3p was repressed during HCMV infection. While this does not exclude the possibility that these genes are regulated by miR-199-3p, it seems less likely that their regulation by miR-199-3p would have a large effect on their levels during infection. On this basis, these two genes were not analysed further in this study.

5.3.3 Regulation of AKT phosphorylation in cells upon HCMV infection

The main hypothesis addressed in this chapter is whether the viral modulation of miR-199-3p altered AKT phosphorylation during HCMV infection. In order to

answer that question, the kinetics of AKT phosphorylation were examined in MRC-5 fibroblasts. Surprisingly, phosphorylated AKT, a protein kinase crucial for the regulation of a range of cellular functions, was completely dephosphorylated at 4 hpi. However, it was strongly phosphorylated within 30 min and 2 hpi, potentially indicating that AKT signalling is required during the first stages of infection, such as viral entry, internalisation and trafficking into the nucleus. Johnson and colleagues (2010b) showed that HCMV infection leads to the phosphorylation of AKT at the serine residue in a PI3K dependent manner at 30 min and then from 4 to 48 hpi. This phosphorylation and activation of AKT required for the expression of immediate early genes (IE1 and IE2) and early genes such as UL44 and UL84, which are involved in the initiation of viral DNA replication (Johnson et al. 2001b). It is not clear why the AKT phosphorylation was not observed at late time points as was published (Johnson et al. 2001b). One possible explanation is that it results from the use of two different laboratory strains. Johnson (2001b) used human cytomegalovirus strain Towne while this study uses the AD169 strain. It should be noted that Towne and AD169 share approximately 90% of their nucleotide sequences (Pritchett 1980). Another possibility is that a mutation occurred during the laboratory passage, such as deletion or rearrangement of viral DNA sequence (Cha et al. 1996). It is also important to mention the use of different cell lines, although both MRC-5 and HELs are fibroblasts. However, according to the data presented here, the phosphorylation of AKT, which happens at 30 min to 2 hpi is not caused by the down-regulation of miR-199-3p, which happens at 24 to 72 hpi. As the experimental procedure used to elucidate the role of miR-199-3p in HCMV infection was based on the transfection of miR-199-3p mimic prior to infection, the miR-199-3p mimic could exert a negative regulation of AKT phosphorylation during the first two hours of infection. In other words, the transfection of miR-199-3p creates a cellular environment that is less conducive to early stages of infection. The pharmacological inhibition of AKT phosphorylation using PI3K inhibitor (LY294002) showed that AKT appears to be required for HCMV infection and therefore, the reduced AKT phosphorylation in miR-199-3p transfected cells could lead to antiviral effect. As LY294002 can also block other PI3K-related enzymes, a further experiment is needed to confirm the role of AKT protein during HCMV infection using more specific methods to inactivate

AKT (i.e. cells expressing dominant negative forms of AKT (kinase dead) and/or PI3K). However the natural function of miR-199-3p in regulating PI3K-AKT signalling at later times post infection remains unclear.

5.3.4 PIK3CB, ITGA6, and ITGA3 do not appear to be involved in the antiviral function of miR-199-3p

As the expression levels of PIK3CB, ITGA6, and ITGA3 are correlated with the down-regulation of miR-199-3p during HCMV infection, it was decided to examine their functional properties during infection. In order to investigate the functional role of PIK3CB, ITGA6 and ITGA3 genes in HCMV infection, it was decided to use the knock down of ITGA6, ITGA3, and PIK3CB as well as the pharmacological inhibition of PIK3CB kinase function. As PIK3CB can function as a protein kinase or independent of its kinase activity, the use of siRNA would therefore affect both functions, whereas TGX-221 selectively blocks the kinase function of PIK3CB (Jia et al., 2008). Neither PIK3CB siRNAs nor TGX-221 negatively impacted the growth of HCMV-GFP reporter virus. It is important to note that as the knock down of PIK3CB at the protein level was incomplete, the remaining level expressed after knock down may enough for its function during the infection. However further studies are required in order to properly determine the function of PIK3CB through utilisation of more efficient method of silencing. It is also important to mention that there is two isoforms of PI3K catalytic subunits, PIK3CA and PIK3CB, which have functional redundancy as well as the distinct roles inside cells (Foukas et al. 2006; Bi et al. 2002; Chaussade et al. 2007). It is possible that functional loss of PIK3CB could be compensated for by the expression of PIK3CA in this cell type. In regard to ITGA6 and ITGA3, either these do not influence or the partial knock down was insufficient to see an effect. Feire and collegues used integrin blocking antibodies to identify different α and β subunits of integrin receptors that are engaged in the entry pathway of HCMV into NHDF fibroblasts. Important roles were revealed for integrin subunits α2, α6, αV, β1 and β3 in supporting virus entry, however, this is not the case for α3. It has been suggested that HCMV apparently engages multiple integrin subunits to perform redundant functions (Feire et al. 2004). Consequently, the knock down of α6 may not inhibit viral infection. HCMV is also known to have a broad

tissue tropism, suggesting that either HCMV exploits a combination of viral envelope glycoproteins (Isaacson and Compton 2009; Mach et al. 2000; Kinzler and Compton 2005; Britt 1984) and cellular receptors to infect a range of different cells or that a universal cellular receptor mediates the interaction between the different host cells and viral envelope protein(s). The research question posed for this thesis 'to identify the targets of miR-199-3p that are responsible for its antiviral properties' still needs further examination. However, this is exceptionally challenging largely due to the fact that individual miRNAs can target multiple cellular and viral genes.

In conclusion, the first evidence has been provided to show that PIK3CB, CD151, ITGA3 are direct targets of miR-199-3p through their 3′UTRs. ITGA6 is also regulated by miR-199-3p, although it remains unclear whether this involves a direct interaction with the miRNA. It has also been indentified that PIK3CB, ITGA6, and ITGA3 are up-regulated by HCMV at 24 to 72 hours post infection, in concert with the viral repression of miR-199-3p, however, this does not appear to be the case for CD151, or CD44. While the silencing of these target genes PIK3CB, ITGA3 or ITGA6 does not appear to influence viral growth, these results are still insufficient to conclude that these genes are not associated with the antiviral role of miR-199-3p. However, further experiments should be conducted in order to elucidate their roles during HCMV infection. This study has shown for the first time that miR-199-3p induces the impairment of AKT phosphorylation in HCMV infected fibroblasts. In addition, the phosphoregulation of AKT was demonstrated to occur in early infection (2 hours) while the viral down-regulation of miR-199-3p later in infection (24- 72 hours) is therefore after AKT phosphorylation that occurs in the first two hours. Finally, the down-regulation of AKT phosphorylation as result of the pre-transfection of miR-199-3p seems to have a negative effect on viral infection. The antiviral role of reducing AKT phosphorylation requires more specific experiments for confirmation.

6 Discussion

6.1 Rational and objectives of the study

Besides HCMV infection is a significant cause of fatal and childhood developmental abnormalities such as neurologic sequelae and deafness, and also establishes a latent infection accompanied by an inherent risk of reactivation and corresponding risk of life-threatening diseases, as is in the case of immunocompromised hosts, particularly in transplant recipients and AIDS patients. In the United States *The Committee to Study Priorities for Vaccine Development for the 21st Century* has ranked HCMV as one of the top priorities for vaccine research in an attempt to prevent the prenatal infection and other complications encountered by immunocompromised patients (Stratton et al. 2001). Therefore, the development of a vaccine or reliable anti-virals for the prevention of the initial infection, super-infection or HCMV recurrences is of critical importance. A greater understanding of 'HCMV Biology and Pathology' at the molecular, cellular and systemic levels is essential for this. A new class of molecules small non-coding RNA (miRNAs), are now appreciated to play important roles in virus-host interactions since the discovery of a host miR-122, which is capable of modulating the replication of HCV (Jopling et al. 2005).

The functional significance of miRNAs in the context of viral infections is supported by a number of key findings in the last nine years: 1) certain viruses, including members of *Herpesviridae*, encode miRNAs indicating the significance of this mode of gene regulation to the viral life cycle; 2) certain host-encoded miRNAs have positive or negative effects in acute, latent and reactivated phases of infections, either in a direct or indirect manner; 3) host miRNAs play a role in the regulation of antiviral immune responses, as well as in the maintenance of basic cellular functions, such as proliferation, apoptosis, and metabolism; and 4) viruses have evolved numerous strategies for the manipulation of the expression of host-encoded miRNAs. The significance of miRNAs as therapeutic targets is now widely recognised. For example, miR-122 antagonists were administered to chimpanzees chronically infected with HCV, which led to a significant decrease in HCV RNA in serum (Lanford et al. 2010). miR-122 antagonists are currently being assessed in Phase II

clinical trials. In addition, a few miRNAs are in pre-clinical developmental stages, such as miR-34 and let-7 mimics. These have been shown to prevent tumour growth in mouse models for lung and prostate cancer (Wiggins et al. 2010; Liu et al. 2011) and the latter also in lung cancer mouse model (Trang et al. 2010).

The expression levels of cellular miRNAs has been characterised in MCMV and HCMV infection and initial insights into the functional role of these miRNAs have been reported (Wang et al. 2008; Santhakumar et al. 2010). Santhakumar and colleagues showed the broad antiviral properties of miR-199-3p in DNA viruses corresponding to three subfamilies of *Herpesviridae (α, β, γ-Herpesviruses)* including HCMV, MCMV, HSV-1 and MHV-68 and also SFV, a positive-stranded RNA virus of *Togaviridae*. Despite the fact that *Herpesviridae* and *Togaviridae* are not evolutionarily conserved, it is possible that these viruses use similar host proteins or signalling cascades to support their infections. A deeper understanding of the antiviral functional of miR-199-3p may define valuable targets for HCMV therapies and/or other viruses. In addition, while a significant inhibition of this antiviral miRNA occurs at 24 hours of HCMV infection, the mechanism of this inhibition had not been previously defined. This project examined the mechanisms by which miR-199a-3p is down-regulated in HCMV infection, and examined possible targets of the miRNA that could mediate its antiviral function.

The main objectives of this study were to:

1. Identify the level of regulation by which miR-199-3p expression is reduced upon infection with CMV.
2. Determine the functional role of miR-199-3p in the modulation of cellular signalling pathways in the context of CMV infections.
3. Validate the target genes of miR-199-3p that are responsible for its antiviral properties.

6.2 Overview of Thesis Results' Chapters

Chapter 3: Regulation of miR-199a/214 cluster expression in CMV infection

Chapter 3 examines three core objectives regarding the down-regulation of miR-199-3p expression in MCMV and HCMV infections. The first of these objectives examined whether CMV regulates miR-199-3p biogenesis at the transcriptional or post-transcriptional level. As described, miR-199-3p comes from a cluster, the other members in this cluster, including miR-199-5p and miR-214 were also down-regulated during infection, suggesting that regulation of the the primary transcript could occur. Therefore, the level of the pri-miR-199a/214 transcript encoding miR-199a-3p, miR-199a-5p, and miR-214 was assessed in a time course of infection. This revealed that in both MCMV and HCMV infections, the pri-miR-199a/214 transcript is downregulated by 4 hpi. As this down-regulation of the primary transcript could result from a change in promoter activity, the activation of the miR-199a/214 promoter was measured during MCMV infection. The infection is able to suppress the promoter activity by 4 hpi, which is consistent with the down-regulation of pri-miR-199a/214 transcript in infected cells at 4 hours.

The second objective was to determine the transcriptional factor(s) involved in the regulation of miR-199a/214 cluster during infection. A bioinformatic approach coupled with a functional characterisation of the promoter sequence was employed in order to determine the sequences critical to miR-199a/214 promoter function and to identify those transcription factors with binding sites within this critical sequence. The minimal promoter sequence was identified, which spans 696nt, and the sequence spanning -421 to -273 was shown to play the most critical contribution to the promoter activity based on 5′ deletion constructs of the miR-199a/214 promoter.

This sequence contains conserved sites for several transcription factors, including SRF and ELK-1. Both of these transcription factors were shown to be important for the basal activation of miR-199/214 promoter and subsequent their expression levels. However, it is now known that SRF is a transcription factor critical for the regulation of miR-199a/214 expression in smooth or cardiac muscles. However, it remains

unclear whether this regulation is based on a direct interaction with miR-199a/214 promoter or an indirect result of SRF binding to another gene (Park et al. 2011; Zhang et al. 2011). As for ELK-1, no work has been conducted yet to examine whether this transcription factor regulates miR-199a/214 promoter either directly or indirectly.

In addition, their regulation needs to be examined during CMV infection. Another transcription factor, TWIST-1 was examined as it has been reported that the expression of the primary transcript of miR-199a/214 and its mature cluster is regulated by TWIST-1 suggesting that regulation occurs at the transcriptional level (Lee et al. 2009). It was found that TWIST-1 protein is down-regulated in MCMV infection by 48 hours and this also occurs in HCMV infection, but at an earlier time point of 24 hours. However, the timing of the down-regulation of TWIST-1 protein does not correlate with the down-regulation of the primary transcript, which occurs by 4 hpi. Therefore, the change in TWIST-1 levels during infection does not contribute to the early down-regulation of the pri-miR-199a/214 transcript. It is possible that this protein may still play a role as in other systems, TWIST-1 can be regulated at the post-translational level, which could potentially interfere with its functional properties (Vichalkovski et al. 2010; Firulli and Conway 2008; Firulli et al. 2008). Therefore, further examination of the phosphoregulation of TWIST-1 in infected cells may be worthwhile to find out whether it plays any role in the down-regulation of miR-199a/214 expression.

The third objective was to examine whether viral gene expression is required for the transcriptional down-regulation of miR-199a/214 cluster. Therefore, the IE3 deletion mutant MCMVdie3 was examined in comparison to wild type MCMV regarding its capacity to regulate the promoter activity as well as the expression of the primary transcript and mature members of miR-199a/214 cluster.

It was showed in cells infected with MCMVdie3, the level of pri-miR-199a/214 transcript is not down-regulated by 4 hpi and only slightly by 24 hpi. In contrast infection of cells expressing IE3, the NIH-3T3-BAM25 with MCMVdie3 was able to complement the expression defects of IE3 in the mutant virus and partially rescue the

phenotype towards the wild-type MCMV phenotype, which suggests that the expression of the IE3 gene is essential in the regulation of miR-199a/214 by MCMV infection. Based on all the results in this chapter, it is concluded that the down-regulation of miR-199-5p, miR-199-3p and miR-214 is primarily controlled at the transcriptional level in both MCMV and HCMV infections. This down-modulation may involve TWIST-1 and other transcription factors during CMV infections. The expression of the viral gene IE3 is crucial for the transcriptional down-regulation of miR-199a/214 by MCMV.

Chapter 4: A proposed model for the antiviral function of miR-199-3p in MCMV infection

This chapter focused on building a model for the possible functions of miR-199-3p during infection. One of the important mechanisms of miRNA functional regulation is the induction of mRNA degradation. For this reason, an mRNA microarray study was conducted to identify mRNAs regulated in response to over-expression or inhibition of miR-199-3p. In an attempt to distinguish the direct targets of miR-199-3p from all the regulated mRNAs, computational target prediction software (TargetScan 5.0) was used to identify direct target sites of miR-199-3p within the 3'UTR of each individual mRNA. In addition to the mRNA expression profile, pathway analysis of miR-199-3p regulated genes was also carried out. This showed that miR-199-3p modulates multiple pathways required for and/or induced in CMV infection, including PI3K-AKT and ERK-MAPK signaling, and prostaglandin production.

These results suggest that miR-199-3p may regulate PI3K-AKT signalling. Consequently, the phosphoregulation of AKT, which has been reported to be required for the productive infection of HCMV, was examined in response to miR-199-3p over-expression or inhibition. The suppression of AKT phosphorylation was demonstrated at Ser473 and Thr308 in cells transfected with miR-199-3pmimic. This would be expected to disrupt the AKT signalling cascade, with a resultant negative effect on viral infection. Nine potential targets of miR-199-3p are associated with AKT. Four targets were validated using qRT-PCR analysis and selected for further

studies, PIK3CB, ITGA6, ITGA3, and CD151. CD44, a validated target of miR-199-3p, was also included to examine its regulation in infected cells.

Chapter 5: The antiviral properties of miR-199-3p may associated with suppressed AKT phosphorylation

The aim in Chapter 5 was to validate the target genes of miR-199-3p and to examine which of these are responsible for the observed antiviral function of miR-199-3p. Three questions were pursued: 1) Are PIK3CB, ITGA6, ITGA3, and CD151, which are associated with AKT, direct targets of miR-199-3p; 2) Is the expression of these target genes and the phosphorylation of AKT enhanced when miR-199-3p is down-regulated during HCMV infection; 3) Do the expression of these targets and AKT phosphorylation influence viral growth?

The work reported in Chapter 5 provides evidence that PIK3CB, ITGA3, and CD151 are novel direct targets of miR-199-3p. In addition, the site-directed mutagenesis of the PIK3CB 3'UTR revealed that miR-199-3p regulates PIK3CB by interacting with two sites in its 3′UTR. While ITGA6 expression (mRNA and protein) is regulated in cells transfected with miR-199-3p mimic, the luciferase reporter harbouring the ITGA6 3'UTR was not affected by miR-199-3p transfection. Therefore, ITGA6 appears to be regulated by miR-199-3p but not through a target site in its 3'UTR. The effect of HCMV infection on endogenous PIK3CB, ITGA6, ITGA3, CD151, and CD44 expression was investigated. Only the levels of PIK3CB, ITGA6, and ITGA3 increased in HCMV infection, from 24 hours onward, correlating with the decrease in miR-199-3p. The phosphorylation of AKT was induced at the initiation of infection and disappeared after 4 hours, demonstrating that miR-199-3p inhibition at 24, 48, 72 hours of HCMV infection does not increase the level of phosphorylated AKT, as it was found to be completely dephosphorylated at these times. These observations suggest that the inhibition of miR-199-3p at 24, 48 and 72 hours post HCMV infection contributes to the upregulation of its targets, namely PIK3CB, ITGA6 and ITGA3. However, it is not clear whether these targets contribute to the antiviral properties of miR-199-3p. Therefore, the functional significance of PIK3CB, ITGA6, and ITGA3 was evaluated during viral infection based on siRNA

knock-down. The results suggested that ITGA6 and ITGA3 do not have negative influence the growth of HCMV. In addition, combined approaches demonstrated that neither the pharmacologic inhibition of PIK3CB kinase activity nor its knock-down had any inhibitory effect on viral growth. Although the above experiments do not explain the physiological function of miR-199-3p down-regulation during infection, it was still of interest to explain its antiviral properties.

Overexpression of miR-199-3p mimic prevented the complete phosphorylation of AKT during the early stage of HCMV infection (2 hours). The pharmacological inhibition of AKT phosphorylation with Ly294002 (PI3-Kinase inhibitor) was also found to reduce the growth of HCMV. This suggests that the transfection of miR-199-3p into cells affects the phosphorylation of AKT, which may explain at least in part its antiviral properties. Because LY294002 is not exclusively selective for AKT but all PI3K-related enzymes, more experiments are required. However, the direct target(s) of miR-199-3p mediating the phosphorylation step of AKT remain to be determined. The functional importance of phosphorylated AKT within the first two hours of infection also remains unknown.

6.3 Conclusion

The dysregulation of miRNAs in infection and disease necessitates an improved understanding of the transcriptional and post-transcriptional mechanisms controlling these miRNAs. Previous reports have shown that miRNAs are often transcribed from RNA polymerase II promoters, which are also responsible for the transcription of cellular mRNAs (Bortolin-Cavaillé et al. 2009; Lee et al. 2004). This allows for a similar set of molecular and computational tools to be applied in the study of miRNAs promoters. In this thesis, an initial characterisation of the promoter sequence of miR-199a/214 was carried out, which also included the identification of the transcription start site, the minimal promoter sequence needed for basal transcriptional activation, and several putative transcription factor binding sites within the promoter. The search for transcription factor binding sites resulted in identification of a serum response element (SRE) that contains SRF and ETS sites. It will be important to examine whether these transcription factors are recruited to the promoter by making use of the point mutations in the core sequences recognized by

the transcription factors, ELK-1 and/or SRF, such a mutation can affect the binding of these transcription factors and subsequently, the promoter activity. In addition to that, the interaction between transcription factors and the promoter sequence should be validated.

The results obtained so far suggest a requirement for ELK-1 and SRF in the basal expression of the pri-miR-199a/214 transcript, however, the relative contribution of these transcription factors to the suppression of expression upon infection is not clear. An important consideration in this context is that both the expression and activity (e.g. phosphorylation and dimerisation) of these transcription factors could be regulated by the virus. The promoter results presented in this thesis are based on studies of the murine promoter, which is highly conserved in sequence (89%) to the promoter in human. This indicates that a similar mechanism of transcriptional regulation may occur in both mouse and human, however, these results should be confirmed in the human cells.

Continued investigation of the transcriptional mechanism controlling the expression of miR-199a/214 may lead to the development of a novel approach to manipulate the expression of this cluster in infections or diseases in which the miR-199a/214 levels are disregulated. The attenuated, inactivated or non-productive virus is generally used to evaluate the requirement of *de novo* viral proteins (e.g. those not tegument proteins) in a cellular process. The UV-radiation of the virus particles is an efficient method for damaging viral DNA, meaning that the virus is incapable of gene expression and DNA replication. Several studies have used UV-radiation with MCMV to create UV-irradiated virus particles (Budt et al. 2009; Bale et al. 1985; Wang and Chen 2009; Wiebusch et al. 2008). In the work presented in this thesis, the use of MCMVdie3, which has a deletion mutation disrupting the product of the IE3 gene, was a preferred approach rather than using UV-radiation of MCMV. The use of MCMVdie3 overcomes certain technical difficulties regarding the use of UV-irradiated MCMV, such as the variation between UV-irradiated batches. MCMVdie3 is able to expresses IE1 and IE2 at attenuated levels and is unable to produce IE3 and those genes downstream of it. An advantage of using MCMVdie3 as a tool is that the IE3 protein can be restored when grown in NIH-3T3-Bam25 cells.

The experimental results from infection with the mutant virus suggest that the down-regulation of the primary transcript of miR-199a/214 at 4 hours is dependent on viral *de novo* expression, of most likely IE3 and/or early viral proteins, which are expressed during these hours. Therefore, IE1, IE2, tegument proteins, and the cellular proteins regulated during viral entry are not sufficient to down-regulate the pri-miR-199a/214 transcript since these proteins present in both MCMVdie3 and MCMV infections. The decrease in miR-199-3p at 24 hours may influence various aspects of the viral life cycle, such as the expression of late viral genes, viral assembly, egress from infected cells, and/or cell-cell spread or disregulated cellular processes required for virus and/or host cell survival, cell cycle, and/or metabolism. Since the transcriptional regulation of miR-199a/214 cluster occurs in both MCMV and HCMV infections, and that there is high degree of conservation between MCMV IE3 and HCMV IE2, it seems likely that the regulation also requires IE2 in HCMV.

One of the most challenging aims in the miRNA field is to understand how an miRNA exerts its functional properties in a particular cell, given the large number of potential targets. Therefore, understanding the biological role of miR-199-3p in HCMV infection requires the identification of all its host cell or viral gene targets. Given that miR-199-3p is inhibited at 24, 48, and 72 hpi, it is expected that the miR-199-3p targets that contribute to its function would be upregulated at these times.

In the context of this thesis, there are three limitations that need to be acknowledged and addressed: first, it is assumed that that the functional consequences of miR-199-3p relate to the targeting of host genes, rather than direct interactions with viral transcripts. Therefore, the viral targets of miR-199-3p were excluded based on the observation that the antiviral functions of miR-199-3p extended to evolutionary unrelated viruses such as herpesviruses and SFV. Indeed, the direct regulation by miR-199-3p of the HBV and HCV genes, which belong to unrelated groups of DNA and RNA viruses, suggest that miRNA-virus interaction could occur. It is not impossible that both host and viral targets of miR-199-3p influence HCMV and MCMV infections. More importantly, the role of miR-199-3p in HBV and HCV infections supports the argument that miR-199-3p is broad antiviral miRNA acting against several DNA and RNA enveloped viruses. Second, it is assumed all effects

will be detected at transcriptional level, therefore, microarray was used to produce a large and unbiased dataset that identified differences between transfected and control cells, the observations are also made at the transcriptional level, which can be misleading as it does not necessarily reflect protein level. This method therefore, fails to identify target genes that are regulated primarily at the translational level or to distinguish between genes that are direct and genes that are regulated indirectly. A high-throughput technique (AGO2-CRAC) is now available to the group, which is based on the precipitation of miRNA and its target mRNA within the RISC complexes, the effectors of which are Argonaute (Ago) proteins (Libri et al. 2012). This approach would improve the overall scope of this study by determining the direct targets through indication of the interaction sites between the miRNA and its target mRNA, even for those targets with unpredicted and non-canonical binding sites. It is likely that this would make the interpretation of the antiviral function of miR-199-3p less challenging, although still relatively complex as an miRNA can target hundreds of genes, with each gene being implicated in distinct cellular functions and subsequently having a range of effects upon viral infection. This suggests that the list of miR-199-3p target genes may include antiviral, proviral, and neutral targets, however, the net influence on the infection is antiviral. Importantly, the elucidation of an miRNA function appears to be more complicated than limiting it to one or two targets, which seems to be the case in the majority of published studies.

A third assumption was that miR-199-3p targets multiple components of a pathway to effectively modulate its signalling cascade to interfere with the viral life cycle. The results of pathway analysis suggest that miR-199-3p modulates several pathways, ERK-MAPK, PI3K-AKT signalling and prostaglandin synthesis, which are all associated with viral gene expression, DNA replication, and spread of HCMV infection. Given that an miRNA can regulate numerous targets (several hundred targets) simultaneously, miR-199-3p might regulate several genes within a particular signalling pathway leading to pronounced modulation in its signalling cascades. This miRNA could also subtlety influence several biological pathways simultaneously. This thesis investigated the phosphoregulation of two signalling proteins, ERK and AKT in response to miR-199-3p over-expression and found a suppression of AKT

phosphorylation but not ERK by miR-199-3p. The hypothesis was therefore, that miR-199-3p reduces the phosphoregulation of AKT and the subsequent activation of its cascade, and this inhibits HCMV infection.

A major concern in functional studies of miR-199-3p is that inhibition of its endogenous level does not result in a significant increase in the level of expression of targets or a high level of phosphorylated AKT. The qRT-PCR data showed successful inhibition of the endogenous level of miR-199-3p in MRC-5 and HEF cells (2.5-fold and 3.5-fold). It is important to note that the observed modest level of miRNA inhibition as shown by qRT-PCR could be due to the technical caveat. miRNA inhibitors are designed to act through irreversible interactions with their target miRNA forming antimiR:miR heteroduplexes without causing miRNA degradation. This creates a problem when levels of miRNA are quantified by qRT-PCR. During the initial denaturation step of reverse transcription antimiR:miR duplexs dissociate and now single stranded miRNAs can be polyadenylated and quantified by PCR which will result in an underestimated level of inhibition. Taken together, due to the possible technical caveat, these results should be taken with caution. Indeed, the degree of miR-199-3p inhibition in cells transfected with the inhibitor is comparable to its level in cells infected with HCMV. Therefore, more evidence is required to demonstrate that the decrease in miR-199-3p during HCMV infection significantly contribute to the upregulation of its targets.

HCMV infection leads to rapid increase in AKT phosphorylation at both Ser473 and Thr308 residues within 30 min to 2 hours, followed by dephosphorylation at the same residues between 4 and 72 hours. This increased phosphorylation during the initial 2 hpi does not correlate with the down-regulation of miR-199-3p, which occurs between 24 and 72 hpi. Although the ideal scenario is to observe an increase in AKT phosphorylation when miR-199-3p is downregulated, it is essential to keep in mind that AKT is a central protein to several cellular processes and therefore, expected to be regulated through a highly complex network of genes. It is important to note that these experiments were conducted using high MOI (5 PFU per cell), which typically result in a single round of viral replication. It might be at low MOIs (0.01 to 1 PFU per cell), which result in multiple rounds of viral infection and re-

infection, phosphorylated AKT is present at the initiation of each round of infection and here the viral down-regulation of miR-199-3p would assist the re-infection step through enhancing the level of phosphorylated AKT in infected cells.

Despite the expression of PIK3CB, ITGA6 and ITGA3 correlating with miR-199-3p expression during infection, no antiviral effect was shown in the knock down studies. The HCMV-GFP virus was used in these studies to measure the growth of the virus following the transfection with siRNA or TGX-221. Although GFP expression is correlated with viral growth, there is a possibility that the treatment affected the GFP signal and not viral growth. Therefore, plaque assay based growth curves should be conducted to confirm the results.

It is especially noteworthy that, despite being derived from the same primary transcript, miR-199-3p and miR-214 are reported to exert opposite effects on AKT regulation. It has been reported that miR-214 up-regulates phosphorylated AKT through targeting of phosphatase and tensin homolog (PTEN), which acts as the main negative regulator of the PI3-kinase (Yang et al. 2008). miR-199-3p down-regulates the level of phosphorylated AKT by targeting of PIK3CB or unknown targets and therefore this cluster could balance levels of AKT phosphorylation within the cells. However, it is even more complex as these miRNAs probably function in concert with other genes to result in a pronounced effect on AKT phosphoregulation.

Further investigation of both miR-199-3p and its target PI3K-AKT signalling pathway is required to improve our understanding of the underlying mechanism by which miR-199-3p regulates this signalling pathway. It is not a surprise that the broad antiviral properties of miR-199-3p are consistent with the important role of PI3K-AKT cascades in a wide range of viral infections. Therefore, the role of miR-199-3p in regulating AKT could likely be extended to other virus-host interactions. Finally, the role of miR-199-3p in regulating this central pathway may form the basis for future treatments for several viral infections and cancers.

6.4 Significance of the thesis

It is evident that cellular miRNAs are an important part of viral–host interactions, and viruses have evolved mechanisms to regulate miRNA expression and subsequently their activities to control cellular processes and/or the viral life cycle. To date, rather little is known about the mechanisms by which miRNAs are regulated during viral infection. Here it was shown that all mature members of miR-199a/214 cluster, miR-199-3p, miR-199-5p and miR-214 are down-regulated with a similar kinetics in both MCMV and HCMV infections. This down-regulation occurs at the transcriptional level and requires viral gene products. This thesis also provides insight into the role of miR-199-3p during infection. The central model that was examined is whether miR-199-3p down-regulates host signalling pathways required for HCMV life cycle, which would explain its antiviral activity. By employing a strategy that integrates molecular, biochemical and bioinformatic approaches, it was identified that miR-199-3p regulates the PI3K-AKT signalling pathway by reducing AKT phosphorylation. Several targets of miR-199-3p including PIK3CB, ITGA6, ITGA3 and CD151 were validated which are known to be associated with AKT phosphorylation. Consistent with these results, published targets of miR-199-3p include CD44, MET and mTOR, all of which are known to activate AKT signalling cascades. It is important to examine whether these targets are regulated by miR-199-3p to modulate AKT phosphorylation and its subsequent functions. AKT is a central protein involved in several cancers and viral infections and this work may further the understanding of why miR-199-3p has anti-oncogenic functions and broad antiviral properties.

6.5 Future considerations

The findings from this study suggest a number of potentially important avenues for future investigation, specifically with regards to obtaining a better understanding of the mechanisms involved in the regulation of miR-199-3p and the targets that mediate antiviral properties.

1. **Is miR-199-3p implicated the innate immune response against viral infection?**
2. **At which stage does miR-199-3p interfere with the viral life cycle?**
3. **What is the mechanism for the transcriptional down-modulation of miR-199a and miR-214 during CMV infection?**
    - Is IE3 directly involved in the regulation of miR-199a/214 transcription?
    - Is TWIST-1 activity involved in the early regulation of miR-199a/214 transcription, and if so, is it by a viral mechanism?
    - Are SRF and ELK-1 involved in the transcriptional regulation of miR-199a/214 during infection?
    - What is the DNA methylation status of the miR-199a/214 promoter upon infection?
    - Can miR-199a and miR-214 be transcriptionally regulated independently of one another?
4. **Which targets of miR-199-3p mediate its effect on AKT phosphorylation?**
5. **Does miR-199-3p target viral transcripts in addition to the cellular targets?**
6. **Are these target transcripts responsible for miR-199-3p antiviral properties?**

7 Appendices

- **Appendix 1**

	Genomatix ID	Start	End	Length	CAGE Analysis
Promoter Region	**GXP_803705**	**164147254**	**164147949**	**696bp**	
Primary transcript 1	**NR_002870**	**164147754**	**164155681**	**7928bp**	
Transcription start site	**TSR_605431**	**164147794**	**164147794**	**1bp**	**2 CAGE**
Transcription start site	**TSR_605432**	**164147843**	**164147844**	**2bp**	**2 CAGE**
Primary transcript 2	**ENSMUST00000104989**	**164147849**	**164148319**	**471bp**	
Transcription start site	**TSR_605433**	**164148035**	**164148047**	**13bp**	**18 CAGE**
Promoter Region	**GXP_250851**	**164148458**	**164149069**	**612bp**	
Primary transcript 1	**AK020051**	**164148958**	**164149850**	**893 bp**	
Primary transcript 2	**AK134411**	**164148964**	**164150370**	**1407bp**	
Primary transcript 3	**AK053654**	**164148969**	**164152904**	**3936bp**	
Transcription start site	**TSR_605434**	**164148958**	**164148969**	**12 bp**	**3 CAGE**

Transcription start site	**TSR_605435**	**164149138**	**164149169**	**32 bp**	**2 CAGE**
Promoter Region	**GXP_406132**	**164149427**	**164150340**	**914 bp**	
Primary transcript 1	**AK164873**	**164149927**	**164153141**	**3215bp**	
Primary transcript 2	**ENSMUST00000104988**	**164150240**	**164150371**	**132bp**	
Transcription start site	**TSR_605436**	**164149927**	**164149927**	**1bp**	**1 CAGE**
Promoter Region	**GXP_250853**	**164151246**	**164151846**	**601 bp**	
Primary transcript 1	**AK051872**	**164151746**	**164154539**	**2794bp**	
Transcription start site	**TSR_605437**	**164151273**	**164151273**	**1bp**	**2 CAGE**
Transcription start site	**TSR_605438**	**164151746**	**164151746**	**1bp**	**1 CAGE**
Transcription start site	**TSR_605439**	**164153693**	**164153727**	**35bp**	**6 CAGE**

Appendix 1: Multiple putative promoters in the mouse DNM3os gene were extracted from Genomatix promoter database using Gene2promoter program. This prediction is based on an optimised length of genomic sequences spanning 500 nucleotides (nt) upstream and 100 nt downstream of the candidate start sites of each transcript. Each promoter region was given an ID starting with 'GXP'. In addition to its genomic location, length, and the transcripts that potentially can be expressed from each promoter. Similarly, some of the information about the transcript is listed like the accession ID, the genomic location, and length. The transcriptional start regions (TSR), which are supported by experimental evidence from the sequencing of full-length cDNA clones and 5' CAGE tags count is the most crucial parameter of promoter predictions. However, if the distance between the TSSs are within or less than 40 nt, these TSSs were grouped together and considered as a unique TSR.

- **Appendix 2**

	Genomatix ID	*Start*	*End*	*Length*	*CAGE Analysis*
Promoter Region	**GXP_3181847**	**172113834**	**172114434**	**601bp**	
Primary transcript 1	**ENSG00000230630**	**172113934**	**172109461**	**4474bp**	
Transcription start site	**TSR_244844**	**172113918**	**172113933**	**13bp**	**5 CAGE**
Transcription start site	**TSR_244843**	**172113763**	**172113763**	**1bp**	**2 CAGE**
Transcription start site	**TSR_244842**	**172113693**	**172113693**	**1bp**	**6 CAGE**
Promoter Region	**GXP_180810**	**172109629**	**172110229**	**601bp**	
Primary transcript 1	**AK021543**	**172108192**	**172109729**	**1538bp**	
Transcription start site	**TSR_244841**	**172109729**	**172109729**	**1bp**	**1 CAGE**

Appendix 2: Two promoters in the human DNM3os gene was predicted using Gene2promoter (Genomatix).

- **Appendix 3**

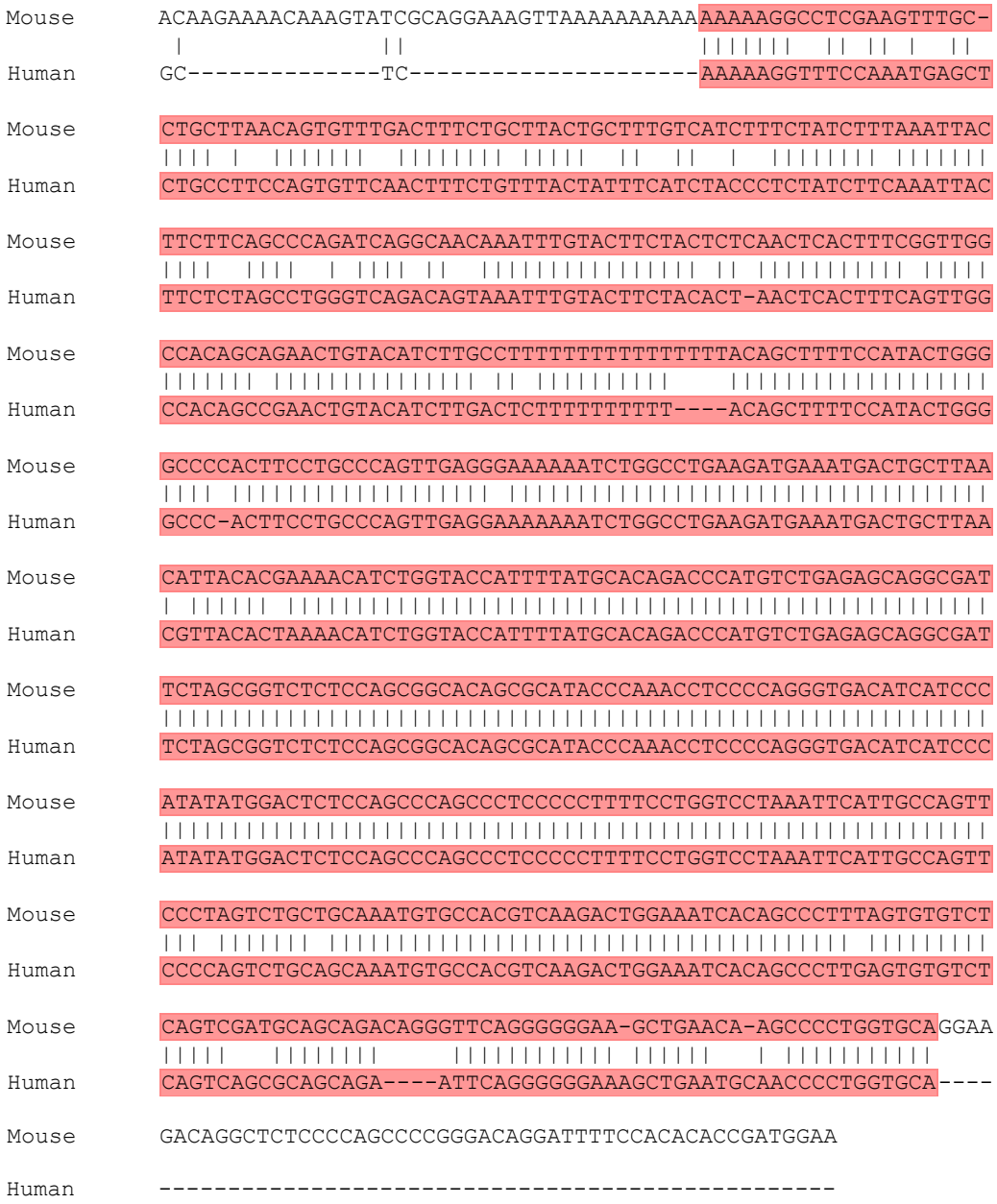

Appendix 3: sequence alignment of miR-199a/214 promoter showing 89.7% conservation among the mouse and human.

- **Appendix 4**

Family	Matrix	Opt. threshold	Start pos.	End pos.	Strand	Matrix sim.	Core sim.	Sequence
V$BARB	V$BARBIE.01	0.88	2	16	+	0.886	1	aaagAAAGgggggag
V$ZF02	V$ZNF219.01	0.91	2	24	-	0.925	1	agttggggctCCCCcctttcttt
V$ZF02	V$ZBP89.01	0.93	5	27	-	0.942	1	ataagttggggctCCCCcctttc
V$PLAG	V$PLAG1.02	0.97	7	29	+	1	1	aaGGGGggagccccaacttatct
V$NFKB	V$NFKAPPAB50.01	0.83	9	23	+	0.944	1	gggGGGAgccccaac
V$MZF1	V$MZF1.01	0.99	9	19	+	0.996	1	ggGGGGagccc
V$RXRF	V$PXR_RXR.01	0.8	15	39	-	0.902	1	tagtgaGGTCagataagttggggct
V$RORA	V$REV-ERBA.01	0.88	20	42	-	0.891	1	ccttagtgagGTCAgataagttg
V$GATA	V$GATA1.03	0.95	20	32	-	0.992	1	gtcaGATAagttg
V$FKHD	V$ILF1.01	0.98	50	66	+	0.989	1	tacaagaaAACAaagta
V$LEFF	V$LEF1.01	0.86	53	69	+	0.877	1	aagaaaaCAAAgtatcg
V$SORY	V$SOX4.01	0.91	54	78	+	0.952	1	agaaaACAAagtatcgcaggaaagt
V$HEAT	V$HSF1.01	0.84	60	84	+	0.879	0.952	caaagtatcgcaGGAAagttaaaaa
V$ARID	V$JARID2.01	0.89	62	82	-	0.893	0.9	tttaacTTTCctgcgatactt
V$BTBF	V$KAISO.01	0.92	66	76	-	0.996	1	tttcCTGCgat

Family	Matrix	Opt. threshold	Start pos.	End pos.	Strand	Matrix sim.	Core sim.	Sequence
V$NFAT	V$NFAT5.02	0.87	69	87	+	0.872	1	gcaGGAAagttaaaaaaaa
V$MYT1	V$MYT1L.01	0.92	72	84	+	0.967	1	ggaaAGTTaaaaa
V$MYT1	V$MYT1.02	0.88	99	111	+	0.885	1	tcgAAGTttgcct
V$SORY	V$SOX2.01	0.92	128	152	-	0.924	1	agatgACAAagcagtaagcagaaag
V$AP1R	V$TCF11MAFG.01	0.81	135	155	-	0.924	1	gaaagaTGACaaagcagtaag
V$EVI1	V$EVI1.07	0.9	142	158	-	0.962	1	atagaAAGAtgacaaag
V$MEF2	V$SL1.01	0.84	148	170	+	0.898	1	catctttCTATctttaaattact
V$GATA	V$GATA2.02	0.9	151	163	-	0.918	1	taaaGATAgaaag
V$HOXF	V$HOXC6.01	0.85	155	173	-	0.863	1	agaagtAATTtaaagatag
V$LHXF	V$LHX3.02	0.82	159	181	-	0.856	1	tgggctgaagaagTAATttaaag
V$PCBE	V$PREB.01	0.86	179	193	+	0.911	1	ccagaTCAGgcaaca
V$CART	V$ISX.01	0.85	183	203	-	0.882	1	agtacaAATTtgttgcctgat
V$CART	V$ISX.01	0.85	188	208	+	0.875	1	gcaacaAATTtgtacttctac
V$RUSH	V$SMARCA3.02	0.98	197	207	+	0.994	1	ttgtACTTcta
V$IRFF	V$ISGF3G.01	0.82	213	233	-	0.877	1	gtggccaaccGAAAgtgagtt
V$PLZF	V$PLZF.01	0.86	234	248	-	0.927	1	atgTACAgttctgct
V$FKHD	V$HNF3B.03	0.87	261	277	-	0.896	1	aagctgTAAAaaaaaaa

Family	Matrix	Opt. threshold	Start pos.	End pos.	Strand	Matrix sim.	Core sim.	Sequence
V$NFAT	V$NFAT5.02	0.87	266	284	-	0.872	1	tatGGAAaagctgtaaaaa
V$OCT1	V$OCT1.04	0.8	272	286	-	0.852	1	agTATGgaaaagctg
V$SrfF	V$Srf.04	0.86	275	293	-	0.866	1	gggccccagTATGgaaaag
V$SrfF	V$Srf.02	0.84	276	294	+	0.852	1	ttttcCATActggggcccc
V$HOMF	V$HMX3.01	0.89	288	306	-	0.898	1	tgggcaggAAGTggggccc
V$ETSF	V$ETS1.01	0.92	288	308	-	1	1	actgggcaGGAAgtggggccc
V$STAT	V$STAT.01	0.87	304	322	+	0.905	1	ccagttgagGGAAaaaatc
V$NFAT	V$NFAT5.01	0.83	310	328	+	0.892	1	gagGGAAaaaatctggcct
V$CIZF	V$NMP4.01	0.97	313	323	+	0.99	1	ggAAAAaatct
V$EVI1	V$MEL1.03	0.95	325	341	+	0.973	1	gcctgaaGATGaaatga
V$TCFF	V$TCF11.01	1	336	342	-	1	1	GTCAttt
V$HAND	V$TAL1BETAE47.01	0.87	355	375	-	0.946	1	atggtacCAGAtgttttcgtg
V$GREF	V$PRE.01	0.84	357	375	-	0.852	1	atggtaccagaTGTTttcg
V$MYOD	V$TCFE2A.02	0.94	358	374	-	0.981	1	tggtaccaGATGttttc
V$RP58	V$RP58.01	0.84	359	371	+	0.962	1	aaaaCATCtggta
O$VTBP	O$VTATA.02	0.89	368	384	-	0.904	1	gtgcaTAAAatggtacc
V$RUSH	V$SMARCA3.01	0.96	370	380	+	0.961	1	taCCATtttat

Family	Matrix	Opt. threshold	Start pos.	End pos.	Strand	Matrix sim.	Core sim.	Sequence
V$ABDB	V$HOXA9.02	0.85	371	387	-	0.853	1	tctgtgcaTAAAatggt
V$STEM	V$OCT3_4.02	0.88	371	389	-	0.928	1	ggtctgtGCATaaaatggt
V$PARF	V$DBP.01	0.84	372	388	+	0.864	1	ccattTTATgcacagac
V$OCT1	V$POU3F3.01	0.81	373	387	-	0.907	1	tctgtGCATaaaatg
V$RBP2	V$PLU1_JARID1B.01	0.96	381	389	+	0.972	1	GCACagacc
V$RBP2	V$PLU1_JARID1B.01	0.96	429	437	+	1	1	GCACagcgc
V$ZF02	V$ZNF300.01	0.99	437	459	+	0.994	1	catacccaaacctCCCCagggtg
V$RREB	V$RREB1.01	0.8	440	454	+	0.928	1	aCCCAaacctcccca
V$GLIF	V$ZIC2.01	0.89	443	457	+	0.933	1	caaacctCCCCaggg
V$NOLF	V$EBF1.01	0.88	443	465	+	0.977	1	caaaccTCCCcagggtgacatca
V$ZF05	V$ZFP410.01	0.84	460	474	-	0.941	1	tatatgGGATgatgt
V$YY1F	V$YY1.02	0.94	463	483	+	0.945	1	tcatcCCATatatggactctc
V$SrfF	V$Srf.04	0.86	463	481	-	0.993	1	gagtccataTATGggatga
V$SrfF	V$Srf.04	0.86	464	482	+	0.99	1	catcccataTATGgactct
V$RUSH	V$SMARCA3.01	0.96	466	476	+	0.985	1	tcCCATatatg
V$PLAG	V$PLAG1.02	0.97	480	502	-	1	1	aaGGGGgagggctgggctggaga
V$ZF02	V$ZBP89.01	0.93	483	505	+	0.974	1	ccagcccagccctCCCCcttttc

Family	Matrix	Opt. threshold	Start pos.	End pos.	Strand	Matrix sim.	Core sim.	Sequence
V$ZF02	V$ZNF219.01	0.91	486	508	+	0.921	1	gcccagccctCCCCcttttcctg
V$EGRF	V$CKROX.01	0.88	488	504	-	0.96	1	aaaaggGGGAgggctgg
V$ZF07	V$ZNF263.01	0.92	489	503	+	0.944	1	cagccCTCCcccttt
V$KLFS	V$GKLF.01	0.86	492	508	-	0.867	1	caggaaaaggggggAGGG
V$BARB	V$BARBIE.01	0.88	493	507	-	0.925	1	aggaAAAGggggagg
V$STAT	V$Stat3.02	0.94	499	517	+	0.962	1	ccttTTCCtggtcctaaat
V$SORY	V$HMGA.01	0.88	505	529	-	0.886	1	aactggcaatgAATTtaggaccagg
V$ABDB	V$HOXB9.01	0.88	505	521	+	0.946	1	cctggtccTAAAttcat
V$NF1F	V$NF1.04	0.87	537	557	+	0.883	1	ctgctgcaaatgtGCCAcgtc
V$CREB	V$ATF6.02	0.85	544	564	-	0.992	1	cagtcttGACGtggcacattt
V$E4FF	V$E4F.01	0.82	547	559	-	0.904	1	ttgACGTggcaca
V$HIFF	V$HRE.01	0.91	547	563	-	0.917	1	agtcttgaCGTGgcaca
V$CREB	V$CREB.02	0.89	547	567	-	0.919	1	ttccagtctTGACgtggcaca
V$SMAD	V$SMAD4.01	0.94	555	565	-	0.941	1	ccaGTCTtgac
V$GFI1	V$GFI1.01	0.96	564	578	+	0.99	1	ggaAATCacagccct
O$INRE	O$DINR.01	0.94	587	597	+	0.975	1	tcTCAGtcgat
V$KLFS	V$EKLF.01	0.89	598	614	+	0.941	1	gcagcagacaGGGTtca

Family	Matrix	Opt. threshold	Start pos.	End pos.	Strand	Matrix sim.	Core sim.	Sequence
V$ZF02	V$ZBTB7.01	0.9	608	630	-	0.935	1	tgttcagcttcCCCCctgaaccc
V$ETSF	V$SPI1.02	0.96	611	631	+	0.961	1	ttcaggggGGAAgctgaacaa
V$PLAG	V$PLAG1.02	0.97	613	635	+	1	1	caGGGGggaagctgaacaagccc
V$MZF1	V$MZF1.01	0.99	615	625	+	0.996	1	ggGGGGaagct
V$ETSF	V$ETV1.02	0.96	636	656	+	0.989	1	ctggtgcaGGAAgacaggctc
V$ZF02	V$ZNF300.01	0.99	645	667	+	0.994	1	gaagacaggctctCCCCagcccc
V$CP2F	V$CP2.01	0.9	647	665	-	0.92	1	ggCTGGggagagcctgtct
V$KLFS	V$KKLF.01	0.91	650	666	-	0.932	1	gggctGGGGagagcctg
V$SP1F	V$SP1.01	0.88	655	671	-	0.896	1	tcccgGGGCtggggaga
V$NFAT	V$NFAT5.02	0.87	667	685	-	0.932	1	tgtGGAAaatcctgtcccg
V$NFAT	V$NFAT.01	0.95	669	687	-	0.96	1	tgtgtGGAAaatcctgtcc
V$NFKB	V$NFKAPPAB65.01	0.87	671	685	+	0.969	1	acaggattTTCCaca

Appendix 4: MatInspector prediction of binding sites in the mouse pri-miR-199a/214 promoter. The factors are listed with the sequence of their DNA site (consensus sequence are highlighted in uppercase). The score cut-off was set to ≥0.85 and ≥0.9 for matrix and core similarities, respectively. Also, we have just selected the conserved sites between mouse and human. The 'V$' prefixes to each family or matrix indicates its name based on the vertebrate library. Yellow rows highlight the transcription factors confer the highest transcriptional activity to the miR-199a/214 promoter (-421 to -272).

- **Appendix 5**

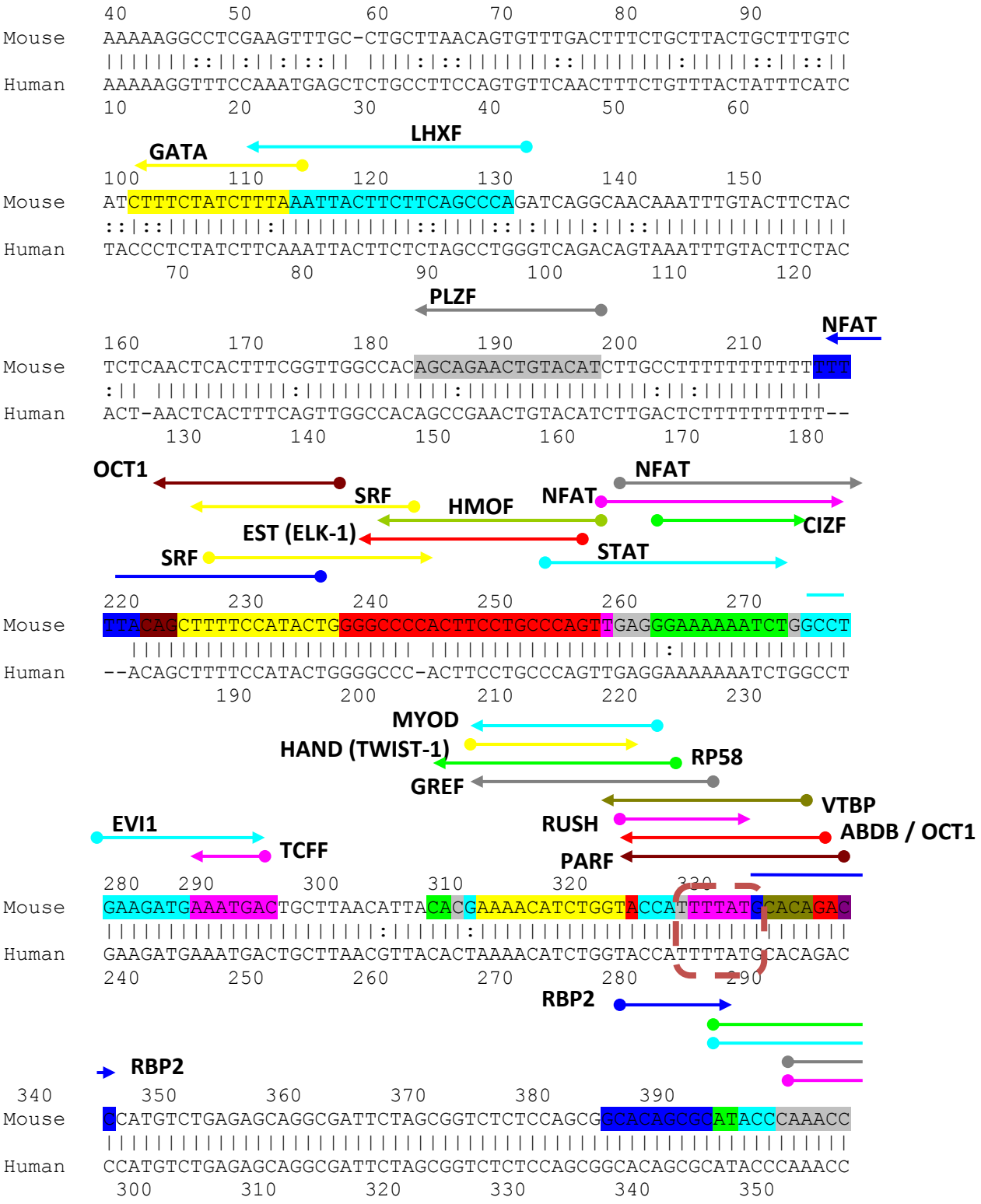
LHXF
GATA
PLZF
NFAT
OCT1
SRF
HMOF
NFAT
NFAT
CIZF
EST (ELK-1)
STAT
SRF
MYOD
HAND (TWIST-1)
RP58
GREF
VTBP
EVI1
RUSH
ABDB / OCT1
TCFF
PARF
RBP2
RBP2

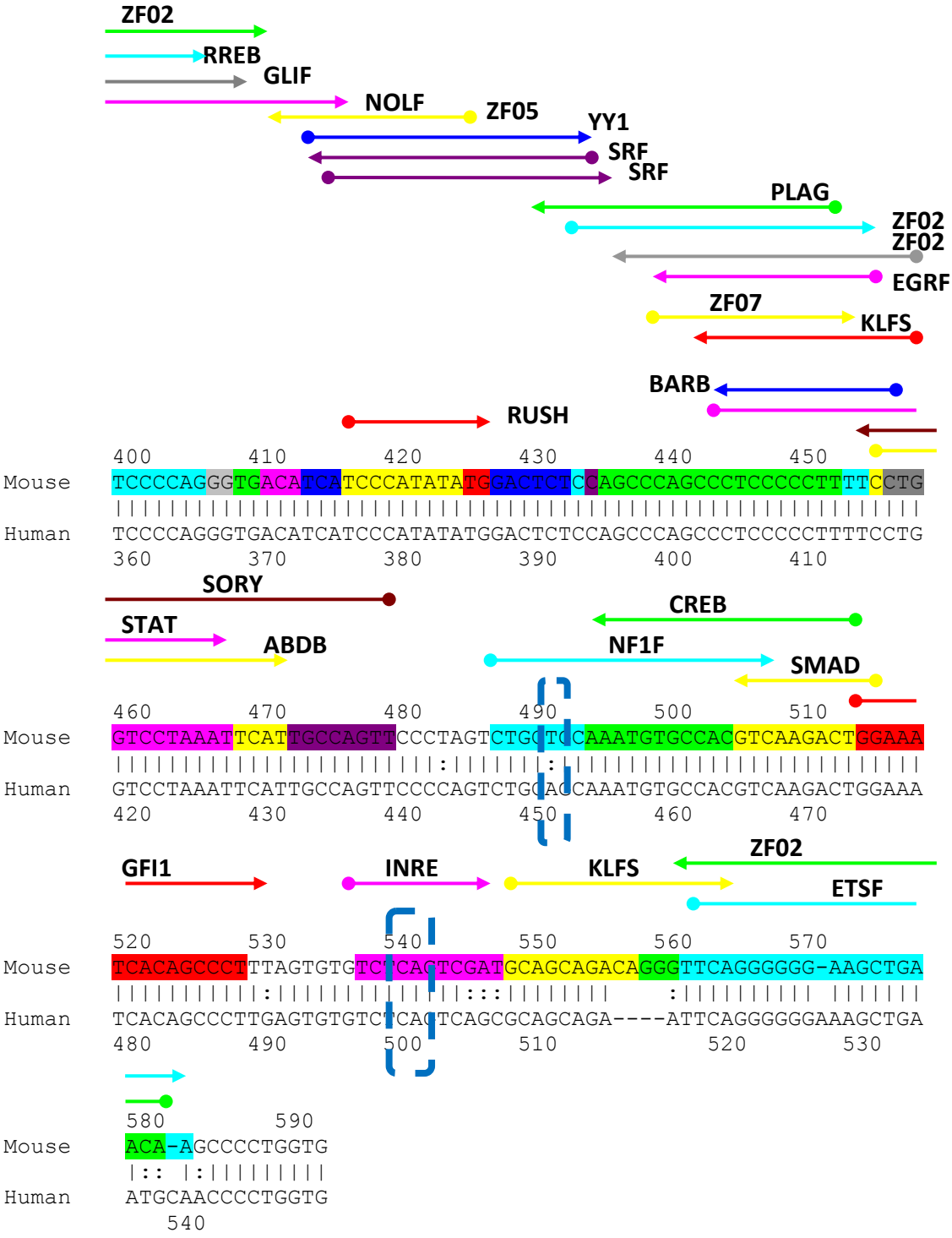

Appendix 5: Evolutionary conserved binding sites in the genomic sequence of mouse and human pri-miR-199a/214 promoters. MatInspector (Genomatix) were used to find the conserved putative binding elements in the promoter sequences and aligned with human promoter. The putative sites are marked with arrows above the DNA sequence. Also, these arrows point out the orientation and extension of the binding site. The used threshold for this prediction is 0.9 and 0.85 for core and matrix similarities. Potential TATA Box is marked with red-dashed box. Predicted transcription start sites (TSS) are in blue-dashed boxes.

- **Appendix 6**

Gene Symbol	Ref Seq	Fold-Change	FDR adjusted P value
1700029F09RIK	BC119032	-1.47796	1.3447E-07
2810407C02RIK	NM_001040396	-1.76231	1.47747E-08
AHCY	NM_016661	-1.55303	5.06164E-08
AK4	NM_001177602	-1.68752	3.43908E-06
AKR1B3	NM_009658	-1.77502	1.72508E-06
ALDH3A1	NM_007436	-1.54204	8.46094E-06
ALG14	NM_024178	-1.74012	6.07156E-06
ALG3	NM_145939	-1.44439	6.11195E-05
ANGPTL4	NM_020581	-2.04532	3.14155E-06
ANK	NM_020332	-1.74956	8.85795E-09
ANKRD1	NM_013468	-1.53286	1.81714E-08
ANKRD13C	NM_001013806	-1.95331	3.60477E-07
ARRDC3	NM_001042591	-1.47001	0.000130958
BNC1	NM_007562	-1.49495	6.83697E-05
BNIP3	NM_009760	-1.75893	2.99076E-06
CAPG	NM_007599	-1.42639	2.46402E-05
CASP3	NM_009810	-1.40022	1.93699E-06
CCL2	NM_011333	-2.17358	2.66214E-08
CCL7	NM_013654	-2.2755	8.63116E-07
CCND1	NM_007631	-1.61118	0.000455877
CCNT1	NM_009833	-1.50185	0.000302526
CCNYL1	NM_001097644	-1.78677	1.49543E-06
CD151	NM_009842	-4.93796	1.5166E-12
CD2AP	NM_009847	-1.41062	0.000172628
CD44	NM_009851	-1.73196	1.10317E-06
CD55	NM_010016	-1.89187	0.00021562
CDR2	NM_007672	-1.44745	1.40685E-06
CEP55	NM_001164362	-1.52857	5.31744E-05
CHI3L1	NM_007695	-1.4358	0.00107833
CNIH4	NM_030131	-1.45704	0.000682372
CNOT7	NM_011135	-1.40966	0.000332731

Gene Symbol	Ref Seq	Fold-Change	FDR adjusted P value
COBLL1	NM_177025	-1.41866	0.00108778
COQ10B	NM_001039710	-1.41411	0.00020181
CP	NM_001042611	-1.49695	8.86904E-05
CPT1A	NM_013495	-1.4613	2.32189E-06
CTGF	NM_010217	-1.51907	0.00037741
CTHRC1	NM_026778	-1.4659	7.21627E-06
CXCL5	NM_009141	-1.9934	2.24749E-06
CYB5B	NM_025558	-1.74762	2.3446E-08
CYCS	NM_007808	-1.43036	1.23779E-05
CYR61	NM_010516	-1.56317	0.000108099
D030056L22RIK	BC020125	-1.67767	2.09558E-07
D10WSU102E	NM_026579	-1.42705	0.000507577
D17H6S56E-5	L78788	-1.49655	2.39057E-07
DDAH1	NM_026993	-2.0222	3.03164E-07
DHFR	NM_010049	-1.44426	0.000597181
DKK3	NM_015814	-1.4254	1.10523E-06
DOK1	NM_010070	-1.45078	1.25039E-06
DUSP1	NM_013642	-1.42706	3.5206E-07
DUSP14	NM_019819	-1.41831	0.00000381
DUSP5	NM_001085390	-1.74983	9.59739E-07
DUSP6	NM_026268	-1.97079	1.3818E-06
EEF1E1	NM_025380	-1.41432	0.000730955
EIF2B2	NM_145445	-1.51639	9.95125E-06
EIF4E	NM_007917	-1.43021	8.60235E-08
ENPP1	NM_008813	-1.54937	9.57035E-08
ENPP3	NM_134005	-1.6313	1.15791E-07
EPHA2	NM_010139	-1.61001	5.30671E-07
EPS8	NM_007945	-1.41415	9.41879E-08
ERCC1	NM_007948	-1.51737	5.30065E-05
EREG	NM_007950	-2.14346	9.30926E-06
ERRFI1	NM_133753	-2.42044	2.03407E-09
ETV1	NM_007960	-1.64897	1.30665E-05
F2R	NM_010169	-1.46289	1.21663E-05

Gene Symbol	Ref Seq	Fold-Change	FDR adjusted P value
FAM198B	NM_133187	-1.40142	0.00343189
FAM60A	NM_019643	-1.49705	2.0233E-06
FGF7	NM_008008	-1.9612	9.32754E-08
FHL2	NM_010212	-1.46813	0.00160295
FIGNL1	NM_001163359	-1.40162	3.56903E-05
FKTN	NM_139309	-1.43223	1.30538E-05
FOSL1	NM_010235	-2.15032	1.96678E-06
FTH1	NM_010239	-1.60975	4.83762E-10
G3BP2	NM_011816	-1.66335	2.92499E-06
GALNT7	NM_144731	-1.65901	0.000287219
GBE1	NM_028803	-1.73676	1.31869E-06
GEMIN6	NM_026053	-1.41288	7.41889E-05
GJA1	NM_010288	-1.44478	0.000483414
GM6644	NR_028277	-1.80654	1.15911E-06
GNPTAB	NM_001004164	-1.4336	1.76738E-06
GPR149	NM_177346	-1.41348	0.000122706
GREM2	NM_011825	-1.40238	0.000112603
GRIK2	NM_010349	-1.93807	9.50799E-07
GSTO1	NM_010362	-1.73911	7.37015E-06
GSTO2	NM_026619	-1.74605	6.66188E-07
HAS2	NM_008216	-1.46653	0.00041128
HAUS5	NM_027999	-1.51584	7.25432E-05
HBEGF	NM_010415	-1.58978	0.00013898
HGF	NM_010427	-1.46838	0.000264262
HMGA1	NM_016660	-1.64585	2.66952E-05
HMGA2	NM_010441	-1.64278	1.49216E-05
HPRT	NM_013556	-1.40571	7.97293E-06
HRSP12	NM_008287	-1.59351	4.79526E-08
HSPA1A	NM_010479	-1.74463	7.06982E-06
HYOU1	NM_021395	-1.47716	0.00157838
IL1RL1	NM_001025602	-1.91541	9.03198E-07
IL4RA	NM_001008700	-1.51981	2.56941E-06
ITGA3	NM_013565	-2.63318	2.0554E-08

Gene Symbol	Ref Seq	Fold-Change	FDR adjusted P value
ITGA6	NM_008397	-1.55628	5.25789E-06
LBH	NM_029999	-1.54208	6.9417E-06
LCLAT1	NM_001081071	-1.45479	0.000195678
LMAN2	NM_025828	-1.4407	0.000133464
LPCAT3	NM_145130	-1.54999	9.6278E-07
LRP8	NR_033496	-1.47575	0.000183082
LY6A	NM_010738	-1.48547	0.000123839
MAK16	NM_026453	-1.42345	0.000353268
MAPRE1	NM_007896	-1.53249	8.96014E-08
MARCKSL1	NM_010807	-1.57792	4.41005E-05
MMD	NM_026178	-1.61318	7.28023E-07
MRPL20	NM_025570	-1.4062	3.71448E-05
MSLN	NM_018857	-1.50677	2.12621E-05
MSN	NM_010833	-1.40196	0.00119516
MT2	NM_008630	-1.42366	0.000991689
NAA25	NM_172722	-1.68734	0.000376675
NACC1	NM_025788	-2.02042	1.39208E-05
NDUFB7	NM_025843	-1.70403	1.4164E-07
NET1	NM_019671	-1.67756	3.03659E-06
NHP2	NM_026631	-1.42995	1.01108E-05
NIPAL1	NM_001081205	-1.50835	3.74801E-07
NQO1	NM_008706	-2.00114	7.04287E-05
NR4A1	NM_010444	-2.48262	6.30722E-07
NRN1	NM_153529	-1.76588	3.87547E-06
NUTF2	NM_026532	-1.50356	0.00012034
NXT2	NM_172782	-1.43783	6.23117E-05
OAF	NM_178644	-1.52895	7.73761E-06
ORC2	NM_008765	-1.42209	2.25477E-07
OSTM1	NM_172416	-1.49617	5.28874E-06
OTUD6B	NM_152812	-1.98159	3.68495E-06
PDCL	NM_026176	-1.42818	2.17703E-05
PFKL	NM_008826	-1.78819	6.47225E-07
PGD	NM_001081274	-1.41145	1.29755E-06

Gene Symbol	Ref Seq	Fold-Change	FDR adjusted P value
PHLDA1	NM_009344	-1.48313	0.000284529
PIK3CB	NM_029094	-1.64019	6.97561E-05
PLA2G4A	NM_008869	-1.44995	3.11538E-05
PLA2G7	NM_013737	-1.43543	1.08871E-05
PLAU	NM_008873	-1.45949	1.53577E-05
PLAUR	NM_011113	-1.56884	0.000234949
PLEKHA3	NM_031256	-1.56756	4.37545E-07
POLR1B	NM_009086	-1.40511	0.000445411
PON2	NM_183308	-1.85379	7.09827E-08
PPP1R14B	NM_008889	-1.44446	0.00016005
PPP2R5E	NM_012024	-1.47601	4.89489E-05
PRDX6	NM_007453	-1.69073	5.37588E-07
PRL2C3	NM_011118	-3.44125	7.63928E-10
PRL2C5	NM_181852	-7.19066	8.99114E-09
PSMD10	NM_016883	-1.76691	5.77087E-10
PTCD3	NM_027275	-1.45642	3.87367E-05
PTGFR	NM_008966	-1.52193	1.39221E-05
PTGS1	NM_008969	-1.79867	1.29275E-07
PTGS2	NM_011198	-3.1678	5.65403E-06
PTPMT1	NM_025576	-1.4751	2.90195E-05
RAMP3	NM_019511	-1.43461	2.23778E-05
RANGRF	NM_021329	-1.44513	0.00374417
RGS2	NM_009061	-1.47057	8.91837E-08
RRAS2	NM_025846	-1.51847	1.28891E-07
RRM2	NM_009104	-1.50732	7.94797E-05
SC5D	NM_172769	-1.42257	7.29202E-07
SCAMP1	NM_029153	-1.43732	2.09414E-06
SDCCAG1	NM_025441	-1.42925	0.000290392
SDPR	NM_138741	-1.49042	0.000343916
SERPINE1	NM_008871	-1.98196	0.000208534
SERTAD4	NM_198247	-1.80483	1.84171E-05
SFRP1	NM_013834	-1.574	0.000681926
SGK1	NM_001161845	-1.69265	6.98813E-08

Gene Symbol	Ref Seq	Fold-Change	FDR adjusted P value
SLC16A13	NM_172371	-1.55871	7.64107E-06
SLC25A13	NM_015829	-1.7932	1.14786E-07
SLC39A10	NM_172653	-1.54462	0.000116719
SLCO2A1	NM_033314	-1.70031	1.16237E-05
SOCS6	NM_018821	-1.4052	3.49774E-06
SPON2	NM_133903	-3.24746	4.2321E-08
SPP1	NM_009263	-2.89187	1.4871E-09
SYNGR2	NM_009304	-1.41049	7.79583E-06
TDG	NM_011561	-1.41238	6.85761E-07
TES	NM_207176	-1.87482	1.58087E-06
TFB2M	NM_008249	-1.45678	2.47201E-06
TFRC	NM_011638	-2.40897	1.12668E-05
THBS1	NM_011580	-2.07816	6.4052E-08
THY1	NM_009382	-1.70035	9.52816E-05
TIMM8A1	NM_013898	-1.51935	1.34026E-05
TIMP1	NM_001044384	-1.53957	0.000105795
TIPIN	NM_025372	-1.4483	1.2446E-06
TK1	NM_009387	-1.44598	8.20347E-05
TMEM30A	NM_133718	-1.62202	8.7512E-06
TMSB4X	NM_021278	-1.53573	0.000225598
TNC	NM_011607	-2.71629	4.81097E-06
TNFRSF12A	NM_013749	-1.57746	3.39357E-06
TNFRSF23	NM_024290	-1.61242	2.9723E-06
TPBG	NM_011627	-1.4517	4.48576E-06
TRIB2	NM_144551	-1.44386	7.24317E-06
TWF1	NM_008971	-1.40188	2.49236E-06
UACA	NM_028283	-1.58546	1.50851E-08
UBE2F	NM_026454	-1.46197	4.16773E-05
UCHL5	NM_019562	-1.45458	1.38511E-05
VAMP3	NM_009498	-2.10972	2.25175E-09
VDR	NM_009504	-1.50419	0.000777416
WDR3	NM_175552	-1.42053	0.000815868
WISP2	NM_016873	-1.52514	3.83123E-05

Gene Symbol	Ref Seq	Fold-Change	FDR adjusted P value
YRDC	NM_153566	-1.40902	5.53707E-05
YWHAE	NM_009536	-1.48485	1.20663E-09

Appendix 6: According to Affymetrix microarray analysis of genes regulated by miR-199-3p mimic versus inhibitor.

- **Appendix 7**

PIK3CB 3′UTR

```
CGTCCGCCCTACTCTGCCGCACTTGCCTGTTCGTTTCCTTTCCATTTTGCACTTGCACTATTGAACATGACCCTGCCAGA
||||||||||||||||||||||||||||||||||||||||||||||||||||||||||||||||||||||||||||||||
CGTCCGCCCTACTCTGCCGCACTTGCCTGTTCGTTTCCTTTCCATTTTGCACTTGCACTATTGAACATGACCCTGCCAGA

AATGCAAAGGGAATGAAATCCTGAAGCTCAGAGTGAAGTTCAAACCACGGCGTCCCGCAGAGCCTAGTCTGAACCACCCC
||||||||||||||||||||||||||||||||||||||||||||||||||||||||||||||||||||||||||||||||
AATGCAAAGGGAATGAAATCCTGAAGCTCAGAGTGAAGTTCAAACCACGGCGTCCCGCAGAGCCTAGTCTGAACCACCCC

ATGCCCACCCTGTGTTCCCGAGCGCTTCCAGGACTCATCGTGAGCAGCAGCATGGAGGCCCCTTCCTGCTGACCTTGCAC
||||||||||||||||||||||||||||||||||||||||||||||||||||||||||||||||||||||||||||||||
ATGCCCACCCTGTGTTCCCGAGCGCTTCCAGGACTCATCGTGAGCAGCAGCATGGAGGCCCCTTCCTGCTGACCTTGCAC

GCGAGGGATGCTACTAGGGACTGCTGGGGATCTTTTCTTTCTTTCCTTCAGTATTTGGTACTTTACCAGAGAGGTGTACA
||||||||||||||||||||||||||||||||||||||||||||||||||||||||||||||||||||||||||||||||
GCGAGGGATGCTACTAGGGACTGCTGGGGATCTTTTCTTTCTTTCCTTCAGTATTTGGTACTTTACCAGAGAGGTGTACA

TACTTCTTTTCAGTGTTGTGACCAAGTGCTGCGACTCAGCCAACAACTTACCACATTCGGGGCTGGGAGCTGTTCTAAGA
||||||||||||||||||||||||||||||||||||||||||||||||||||||||||||||||||||||||||||||||
TACTTCTTTTCAGTGTTGTGACCAAGTGCTGCGACTCAGCCAACAACTTACCACATTCGGGGCTGGGAGCTGTTCTAAGA

AAGGGACCTCCCTCTCCTTTTTAAATTGGTGAGCCACAAATTACATTGATTATGTTGAACTTATTATTCTTCAAAGAAAA
||||||||||||||||||||||||||||||||||||||||||||||||||||||||||||||||||||||||||||||||
AAGGGACCTCCCTCTCCTTTTTAAATTGGTGAGCCACAAATTACATTGATTATGTTGAACTTATTATTCTTCAAAGAAAA

TATTTTAAACCTGTGAAAACTCACTAATTTTGTTAATATTTATCATGATGGCATCATTTCAGCCAGACTCGCTGAGAATC
||||||||||||||||||||||||||||||||||||||||||||||||||||||||||||||||||||||||||||||||
TATTTTAAACCTGTGAAAACTCACTAATTTTGTTAATATTTATCATGATGGCATCATTTCAGCCAGACTCGCTGAGAATC

TATTGGTGGGGCAAATATAATATATATATAATATATATATATATATATGCTGCATATATATTTATAAAATTTCTAGTGGG
||||||||||||||||||||||||||||||||||||||||||||||||||||||||||||||||||||||||||||||||
TATTGGTGGGGCAAATATAATATATATATAATATATATATATATATGCTGCATATATATTTATAAAATTTCTAGTGGG

AGTTCTATATAAAAAGATGTTTCTTTGGTATTCTTCAGCCTGTGTTTTCAAGTTTTACAGAAGCAGAGCTTTTCCCTAAG
||||||||||||||||||||||||||||||||||||||||||||||||||||||||||||||||||||||||||||||||
AGTTCTATATAAAAAGATGTTTCTTTGGTATTCTTCAGCCTGTGTTTTCAAGTTTTACAGAAGCAGAGCTTTTCCCTAAG

TTCCTCTTCGGTTCACTGTAGATCCAGTTCTTCCAGCCGCTTCAGCACTGAGGCGCCATGAATGCGGTTTCTCTGTGTAG
||||||||||||||||||||||||||||||||||||||||||||||||||||||||||||||||||||||||||||||||
TTCCTCTTCGGTTCACTGTAGATCCAGTTCTTCCAGCCGCTTCAGCACTGAGGCGCCATGAATGCGGTTTCTCTGTGTAG

CTCTGAGAGTTCGTTTCATAGAACACAACACTTGAGCAGATGCATCCAAGGAGGCGAGCAAATGAAAAGGAATCTATTTA
||||||||||||||||||||||||||||||||||||||||||||||||||||||||||||||||||||||||||||||||
CTCTGAGAGTTCGTTTCATAGAACACAACACTTGAGCAGATGCATCCAAGGAGGCGAGCAAATGAAAAGGAATCTATTTA

TGGAATAAACTCGAAACCTAAATTTCAGTATTTTAGTAATATGCCAGCTGTTCTTAATGTATTTATTAAAATGTATAACA
||||||||||||||||||||||||||||||||||||||||||||||||||||||||||||||||||||||||||||||||
TGGAATAAACTCGAAACCTAAATTTCAGTATTTTAGTAATATGCCAGCTGTTCTTAATGTATTTATTAAAATGTATAACA

ATGTGATTTTTCAATGGTATTAGTTCAAATTGACGTGGATTCATGCCACATGGAAATCTTTAATTTATTTGTTGAGGTAC
||||||||||||||||||||||||||||||||||||||||||||||||||||||||||||||||||||||||||||||||
ATGTGATTTTTCAATGGTATTAGTTCAAATTGACGTGGATTCATGCCACATGGAAATCTTTAATTTATTTGTTGAGGTAC

CATATAGCCAGGGTGCTAGGTGATGAGTGGTGTTAGCATGTGCAATAGGAACTACTGGTTTGCTGTGTAAATGGATGTCA
||||||||||||||||||||||||||||||||||||||||||||||||||||||||||||||||||||||||||||||||
CATATAGCCAGGGTGCTAGGTGATGAGTGGTGTTAGCATGTGCAATAGGAACTACTGGTTTGCTGTGTAAATGGATGTCA

GGATCCAGCAAAACTACTGCTTTCTTCTCCAAAGACATGTGGGAGCCTTCAATCCTCAGTGGCATGGGAAACAGCTGAGT
||||||||||||||||||||||||||||||||||||||||||||||||||||||||||||||||||||||||||||||||
GGATCCAGCAAAACTACTGCTTTCTTCTCCAAAGACATGTGGGAGCCTTCAATCCTCAGTGGCATGGGAAACAGCTGAGT
```

```
ACTTGCCCCGTGACTTCAGTTTTCTATAGGAATTTTATTAAAGAGTGTTTAATTTTGTTGTCCTTCTTAATGTTCTCAGT
||||||||||||||||||||||||||||||||||||||||||||||||||||||||||||||||||||||||||||||||
ACTTGCCCCGTGACTTCAGTTTTCTATAGGAATTTTATTAAAGAGTGTTTAATTTTGTTGTCCTTCTTAATGTTCTCAGT

CAAATAAATGGGTGGTTTCATCTGTTTGGGG
||||||||||||||||||||||||||||||
CAAATAAATGGGTGGTTTCATCTGTTTGGGG
```

CD151 3′UTR

```
GAACACTACTGACCACGATGATGTCAGGCCGGGCGGCCAGCCTTGCACTACTGACCACGATGATGCCAGGCTGGGCGGCC
||||||||||||||||||||||||||||||||||||||||||||||||||||||||||||||||||||||||||||||||
GAACACTACTGACCACGATGATGTCAGGCCGGGCGGCCAGCCTTGCACTACTGACCACGATGATGCCAGGCTGGGCGGCC

AGCCTTGCACTATGTCCCAGCCCCACTACTGAACACTACTGACTTAGACTGCTGACTGCCAGAGGTAGCTACCCTCATGC
||||||||||||||||||||||||||||||||||||||||||||||||||||||||||||||||||||||||||||||||
AGCCTTGCACTATGTCCCAGCCCCACTACTGAACACTACTGACTTAGACTGCTGACTGCCAGAGGTAGCTACCCTCATGC

CATCGCCATGACCCCCCCTGGCATGCCACCTCAGGGGCATGCACCTTCAAGTGCCTTTCACTGCACACCAAAGTCCCAAA
||||||||||||||||||||||||||||||||||||||||||||||||||||||||||||||||||||||||||||||||
CATCGCCATGACCCCCCCTGGCATGCCACCTCAGGGGCATGCACCTTCAAGTGCCTTTCACTGCACACCAAAGTCCCAAA

GCTCGAAGCAGCGTACTTGCCCCAGCATTAAGAAGGGGGGGGGGGGTGGGGGGTTCAAATGCCAGTGTTGGGCTAGGCCT
||||||||||||||||||||||||||||||||||||||||||||||||||||||||||||||||||||||||||||||||
GCTCGAAGCAGCGTACTTGCCCCAGCATTAAGAAGGGGGGGGGGGGTGGGGGGTTCAAATGCCAGTGTTGGGCTAGGCCT

GGCTAGTAGAATAGGGTTTAGATTATTTGACAGAAGTGCCTCTTATGCAGACTGCTTCCCTTTGGGTAGCTGTGATCTGC
||||||||||||||||||||||||||||||||||||||||||||||||||||||||||||||||||||||||||||||||
GGCTAGTAGAATAGGGTTTAGATTATTTGACAGAAGTGCCTCTTATGCAGACTGCTTCCCTTTGGGTAGCTGTGATCTGC

AGTAAGTCTGGGGAGAACCTGAGTACACCACTACACGTTGGGTAAAAGCAGGTGGGGCCTTTCTGGTTGGATTAGGCACC
||||||||||||||||||||||||||||||||||||||||||||||||||||||||||||||||||||||||||||||||
AGTAAGTCTGGGGAGAACCTGAGTACACCACTACACGTTGGGTAAAAGCAGGTGGGGCCTTTCTGGTTGGATTAGGCACC

CTTCATGCCTGCTACCAGGAACTCTCAGATCTGCTTGCCCCAAACAAATGGTGTAAGCTGAGGGAAACTCCAACCCCACA
||||||||||||||||||||||||||||||||||||||||||||||||||||||||||||||||||||||||||||||||
CTTCATGCCTGCTACCAGGAACTCTCAGATCTGCTTGCCCCAAACAAATGGTGTAAGCTGAGGGAAACTCCAACCCCACA

CTTGATGCTCTGTCCTCTCCACACAGGCCTCTTGCTCCTAACAGCTCAGCCCTGGCCTTTTCTCACTACTGATAGCATCA
||||||||||||||||||||||||||||||||||||||||||||||||||||||||||||||||||||||||||||||||
CTTGATGCTCTGTCCTCTCCACACAGGCCTCTTGCTCCTAACAGCTCAGCCCTGGCCTTTTCTCACTACTGATAGCATCA

TGTAAATGCTCCATGTTCCTGTACACTGTCTCCTTTTGGAGCATCTCTGAATGGAGCATGGCTGTTTTCATCTCACTGCT
||||||||||||||||||||||||||||||||||||||||||||||||||||||||||||||||||||||||||||||||
TGTAAATGCTCCATGTTCCTGTACACTGTCTCCTTTTGGAGCATCTCTGAATGGAGCATGGCTGTTTTCATCTCACTGCT

GTATTCCAGATGCTGCCCACAAATGCTCCTGCTATGTAACAGGTGCTCAATAAATGTAAATGTATAAGCACTCG
||||||||||||||||||||||||||||||||||||||||||||||||||||||||||||||||||||||||||
GTATTCCAGATGCTGCCCACAAATGCTCCTGCTATGTAACAGGTGCTCAATAAATGTAAATGTATAAGCACTCG
```

ITGA3 3′UTR

TCCCCGACAAACCTTCCGGCGCTCCCTTCCTTCCTATTTATCATAAATTATGACTCCGACAGTCCAAAGGGGGCCACGCC
||||||||||||||||||||||||||||||||||||||||||||||||||||||||||||||||||||||||||||||||
TCCCCGACAAACCTTCCGGCGCTCCCTTCCTTCCTATTTATCATAAATTATGACTCCGACAGTCCAAAGGGGGCCACGCC

CTTGGCTGGCACCAGCAGGCTCAGGCATCTATCCCTCTTCAGTGCAGGCATGTTTTCTGGGGCCCTGGAATCTCCTTCAA
||||||||||||||||||||||||||||||||||||||||||||||||||||||||||||||||||||||||||||||||
CTTGGCTGGCACCAGCAGGCTCAGGCATCTATCCCTCTTCAGTGCAGGCATGTTTTCTGGGGCCCTGGAATCTCCTTCAA

GACCTTGCAATGCTGAGCCCAGCACAGCCCTTGCACAGTGGACACACACACAGGGCCTACTGCTAATGGCCTGCTCTGAT
||||||||||||||||||||||||||||||||||||||||||||||||||||||||||||||||||||||||||||||||
GACCTTGCAATGCTGAGCCCAGCACAGCCCTTGCACAGTGGACACACACACAGGGCCTACTGCTAATGGCCTGCTCTGAT

ATATCATGGAGGGTGCCGTATCCAAGTCTCTGTCTGTGCCAAAACCAAGCCAAAGCGCCTCTACTGGGAGACAGGAGGAA
||||||||||||||||||||||||||||||||||||||||||||||||||||||||||||||||||||||||||||||||
ATATCATGGAGGGTGCCGTATCCAAGTCTCTGTCTGTGCCAAAACCAAGCCAAAGCGCCTCTACTGGGAGACAGGAGGAA

AAGGTCCCTGATGTGGGGACACGGCTCCTCCACACTGAATCCCCCTTGAGCCATTGTCAATGGATGGAGTTTACTGTCCA
||||||||||||||||||||||||||||||||||||||||||||||||||||||||||||||||||||||||||||||||
AAGGTCCCTGATGTGGGGACACGGCTCCTCCACACTGAATCCCCCTTGAGCCATTGTCAATGGATGGAGTTTACTGTCCA

GAATAAAACTACTGATGCGGAGGAGACAGTCAGGCTCAGCTGCAATTCCTGCCAGGCACTGGAGCGCAGGGCTACACTAA
||||||||||||||||||||||||||||||||||||||||||||||||||||||||||||||||||||||||||||||||
GAATAAAACTACTGATGCGGAGGAGACAGTCAGGCTCAGCTGCAATTCCTGCCAGGCACTGGAGCGCAGGGCTACACTAA

AGGCTACCCAGGGGATGTTCTTACGACCTGCGTGCTCAGACGCAAGAGCAATGAACTAGAAAGCAGGTCGCCGGAATGGG
||||||||||||||||||||||||||||||||||||||||||||||||||||||||||||||||||||||||||||||||
AGGCTACCCAGGGGATGTTCTTACGACCTGCGTGCTCAGACGCAAGAGCAATGAACTAGAAAGCAGGTCGCCGGAATGGG

CTTTATGGGTGCATCTCTAAAATCGTGGCTACAGAGAGAGCTGGCAAGAAACGCAGCCCGAAGGAACAAAGAGAGACCGT
||||||||||||||||||||||||||||||||||||||||||||||||||||||||||||||||||||||||||||||||
CTTTATGGGTGCATCTCTAAAATCGTGGCTACAGAGAGAGCTGGCAAGAAACGCAGCCCGAAGGAACAAAGAGAGACCGT

GGGCAGCCTGGACGCACACACTGTGCTGGGACTGACCTGGAGCATGGCGGCATCCTTCAGAGAGCAGGGTCCTGGCGCAG
||||||||||||||||||||||||||||||||||||||||||||||||||||||||||||||||||||||||||||||||
GGGCAGCCTGGACGCACACACTGTGCTGGGACTGACCTGGAGCATGGCGGCATCCTTCAGAGAGCAGGGTCCTGGCGCAG

CAGACATTGGTAGGATGAAGAGGAGAGACTTCTGATCCATCCTGACCACCTCAGCCTGGGCAAGGCCTGGAGATCCCCAC
||||||||||||||||||||||||||||||||||||||||||||||||||||||||||||||||||||||||||||||||
CAGACATTGGTAGGATGAAGAGGAGAGACTTCTGATCCATCCTGACCACCTCAGCCTGGGCAAGGCCTGGAGATCCCCAC

GAGACCACGTGGGGTGTGATACTTGAATGTAGCATGGCAGGGGAGGGCCCAGCCCCTGCCCCAGTTGGCCAGACTTAACT
||||||||||||||||||||||||||||||||||||||||||||||||||||||||||||||||||||||||||||||||
GAGACCACGTGGGGTGTGATACTTGAATGTAGCATGGCAGGGGAGGGCCCAGCCCCTGCCCCAGTTGGCCAGACTTAACT

CTGCTCCCTTGACCACAGAGATGAGATTCTGAGCTGCCTGTGGCTTTCTTCCCCTCCCCCAGGGGCTGCATCCCCATTCT
||||||||||||||||||||||||||||||||||||||||||||||||||||||||||||||||||||||||||||||||
CTGCTCCCTTGACCACAGAGATGAGATTCTGAGCTGCCTGTGGCTTTCTTCCCCTCCCCCAGGGGCTGCATCCCCATTCT

AGCAGTGGAGGCTGATTTCCCAGGTCCTCTCCCCATCCCGGTCCACAGGCAGGCCCACTCCCCAGCTCTGTCCCCTCCAC
||||||||||||||||||||||||||||||||||||||||||||||||||||||||||||||||||||||||||||||||
AGCAGTGGAGGCTGATTTCCCAGGTCCTCTCCCCATCCCGGTCCACAGGCAGGCCCACTCCCCAGCTCTGTCCCCTCCAC

CCCACGGTACTATAACAACTTCCCCGATCCTGTGCCTTCTTTGT
|||||||||||||||||||||||||||||||||||||||||||
CCCACGGTACTATAACAACTTCCCCGATCCTGTGCCTTCTTTGT

ITGA6 3′UTR

```
CTTTAAGCGCTCTAGGTACGATGACAGCATTCCCCGATACCATGCGGTGCGGATCCGGAAAGAAGAGCGAGAGATCAAAG
||||||||||||||||||||||||||||||||||||||||||||||||||||||||||||||||||||||||||||||||
CTTTAAGCGCTCTAGGTACGATGACAGCATTCCCCGATACCATGCGGTGCGGATCCGGAAAGAAGAGCGAGAGATCAAAG

ATGAGAAACACATGGATAACCTCGAAAAAAAACAGTGGATCACCAAGTGGAATGAAAACGAAAGTTACTCATAGAGAGGA
||||||||||||||||||||||||||||||||||||||||||||||||||||||||||||||||||||||||||||||||
ATGAGAAACACATGGATAACCTCGAAAAAAAACAGTGGATCACCAAGTGGAATGAAAACGAAAGTTACTCATAGAGAGGA

GGGCACAGGAAAGAACACCTCACACTACCCAAAGCCCCCCCTTATTTTTTCCAGCTCAGAAATTCAGGTGGCTTCAAAGC
||||||||||||||||||||||||||||||||||||||||||||||||||||||||||||||||||||||||||||||||
GGGCACAGGAAAGAACACCTCACACTACCCAAAGCCCCCCCTTATTTTTTCCAGCTCAGAAATTCAGGTGGCTTCAAAGC

CTGCTCAGCTCCCCCATATATGATTTCAGACTGACGACACCCAGTATGGACCTACAGTTTCAACTGTGGATATTGTTACA
||||||||||||||||||||||||||||||||||||||||||||||||||||||||||||||||||||||||||||||||
CTGCTCAGCTCCCCCATATATGATTTCAGACTGACGACACCCAGTATGGACCTACAGTTTCAACTGTGGATATTGTTACA

CCTAAGGCTCCTGTTTTGCACAGCCAAATTTAAGACTGGTAGAGTGGATTTTTCTTTAACTGCCTTAATTTAACTTTCCG
||||||||||||||||||||||||||||||||||||||||||||||||||||||||||||||||||||||||||||||||
CCTAAGGCTCCTGTTTTGCACAGCCAAATTTAAGACTGGTAGAGTGGATTTTTCTTTAACTGCCTTAATTTAACTTTCCG

GATTGCCTTTGTTTTTGACGTGGCTGACTTCCACACGCTGGGGCAGGGCCTGCCCATCTGCACTGCTGGGATGCTCTCCC
||||||||||||||||||||||||||||||||||||||||||||||||||||||||||||||||||||||||||||||||
GATTGCCTTTGTTTTTGACGTGGCTGACTTCCACACGCTGGGGCAGGGCCTGCCCATCTGCACTGCTGGGATGCTCTCCC

CCAGGTCACCTGTGCTAACAGAGTGGCTATCCCAGCCTGCTCCCACAAGCATTCTTCTCATAAGATTGACCTTGGCTCAA
||||||||||||||||||||||||||||||||||||||||||||||||||||||||||||||||||||||||||||||||
CCAGGTCACCTGTGCTAACAGAGTGGCTATCCCAGCCTGCTCCCACAAGCATTCTTCTCATAAGATTGACCTTGGCTCAA

GACTGCCAATGGATAGCTGTGCCTCTGGTGAAAGTTCTGTCTTAAATGTGCAATAGAAGGTGATGTTACCCTTTGGCCTT
||||||||||||||||||||||||||||||||||||||||||||||||||||||||||||||||||||||||||||||||
GACTGCCAATGGATAGCTGTGCCTCTGGTGAAAGTTCTGTCTTAAATGTGCAATAGAAGGTGATGTTACCCTTTGGCCTT

CTTTCTCCATCTCCTAGAAGTGAGGACCCTTGCTGACGCCAAATGCACACAGGTTCCCGTCTCCCTTGTCACTAAAGCAC
||||||||||||||||||||||||||||||||||||||||||||||||||||||||||||||||||||||||||||||||
CTTTCTCCATCTCCTAGAAGTGAGGACCCTTGCTGACGCCAAATGCACACAGGTTCCCGTCTCCCTTGTCACTAAAGCAC

AGGGTCGACAGACTTGAATGCTAGTTACATTTGTTTGTATATGATATTTATTTTTTTCTTCAAGCCATCTTGCTGTTGAC
||||||||||||||||||||||||||||||||||||||||||||||||||||||||||||||||||||||||||||||||
AGGGTCGACAGACTTGAATGCTAGTTACATTTGTTTGTATATGATATTTATTTTTTTCTTCAAGCCATCTTGCTGTTGAC

TAATAGGCCAAAGATGCTTCTGGGTGGTTTAAGCAATGAGAATGAGAACCTGGGAGGTCTTGTTGTTGTTG
||||||||||||||||||||||||||||||||||||||||||||||||||||||||||||||||||||||||||
TAATAGGCCAAAGATGCTTCTGGGTGGTTTAAGCAATGAGAATGAGAACCTGGGAGGTCTTGTTGTTGTTG
```

Appendix 7: Sequence alignment between Sanger sequencing reads of cloned 3′UTRs to reference sequences (from NCBI) using BioEdit software.

8 Bibliography

Abate, D.A., Watanabe, S. and Mocarski, E.S., 2004. Major human cytomegalovirus structural protein pp65 (ppUL83) prevents interferon response factor 3 activation in the interferon response. *J Virol*, 78(20):10995–1006.

Abrahante, J.E. et al., 2003. The Caenorhabditis elegans hunchback-like gene lin-57/hbl-1 controls developmental time and is regulated by microRNAs. *Dev Cell*, 4(5): 625–37.

Adler, B. and Sinzger, C., 2009. Endothelial cells in human cytomegalovirus infection: one host cell out of many or a crucial target for virus spread? *Thromb Haemost*, 102(6): 1057–63.

Ahlqvist, J. and Mocarski, E., 2011. Cytomegalovirus UL103 controls virion and dense body egress. *J Virol*, 85(10):5125–35.

Ahluwalia, J.K. et al., 2008. Human cellular microRNA hsa-miR-29a interferes with viral nef protein expression and HIV-1 replication. *Retrovirology*, 5:117.

Akhtar, N. and Haqqi, T.M., 2012. MicroRNA-199a* regulates the expression of cyclooxygenase-2 in human chondrocytes. *Ann Rheum Dis*, 71(6):1073–80.

Akter, P., 2003. Two novel spliced genes in human cytomegalovirus. *J Gen Virol*, 84(pt 5):1117–22.

Akula, S.M. et al., 2002. Integrin alpha3beta1 (CD49c/29) is a cellular receptor for kaposi's sarcoma-associated herpesvirus (KSHV/HHV-8) entry into the target cells. *Cell*, 108(3):407–19.

Alanen, A. et al., 2005. Seroprevalence, incidence of prenatal infections and reliability of maternal history of varicella zoster virus, cytomegalovirus, herpes simplex virus and parvovirus B19 infection in South-Western Finland. *BJOG* , 112(1):50–6.

Alba, M.M. et al., 2001. Genomewide function conservation and phylogeny in the herpesviridae. *Genome Res*, 11(1):43–54.

Andersson, M.G. et al., 2005. Suppression of RNA interference by adenovirus virus-associated RNA. *J Virol*, 79(15):9556–65.

Angulo, A., Ghazal, P. and Messerle, M., 2000. The major immediate-early gene ie3 of mouse cytomegalovirus is essential for viral growth. *J Virol*, 74(23):11129–36.

Angulo, A. et al., 2000. Identification of a boundary domain adjacent to the potent human cytomegalovirus enhancer that represses transcription of the divergent UL127 Promoter. *J Virol*, 74(6):2826–39.

Aoyagi, M., Gaspar, M. and Shenk, T.E., 2010. Human cytomegalovirus UL69 protein facilitates translation by associating with the mRNA cap-binding complex and excluding 4EBP1. *Proc Natl Acad Sci U S A*, 107(6):2640–5.

Arlt, H. et al., 1994. Identification of binding sites for the 86-kilodalton IE2 protein of human cytomegalovirus within an IE2-responsive viral early promoter. *J Virol*, 68(7):4117–25.

AuCoin, D.P. et al., 2006. Betaherpesvirus-conserved cytomegalovirus tegument protein ppUL32 (pp150) controls cytoplasmic events during virion maturation. *J Virol*, 80(16): 8199–210.

Bader, A.G. et al., 2011. Developing therapeutic microRNAs for cancer. *Gene Ther*, 18(12):1121–6.

Baek, D. et al., 2008. The impact of microRNAs on protein output. *Nature*, 455(7209):64–71.

Bale, J.F., O'Neil, M.E. and Greiner, T., 1985. The interaction of murine cytomegalovirus with murine neutrophils: effect on migratory and phagocytic activities. *J Leukoc Biol*, 38(6):723–34.

Bao, S. et al., 2005. Keratinocyte growth factor induces Akt kinase activity and inhibits Fas-mediated apoptosis in A549 lung epithelial cells. *Am J Physiol Lung Cell Mol Physiol.* 288(1):L36–42.

Bartel, D.P., 2004. microRNAs: genomics, biogenesis, mechanism, and function. *Cell*, 116(2):281–97.

Bartel, D.P. and Chen, C.Z., 2004. Micromanagers of gene expression: the potentially widespread influence of metazoan microRNAs. *Nat Rev Genet*, 5(5):396–400.

Bartonicek, N. and Enright, A.J., 2010. SylArray: a web server for automated detection of miRNA effects from expression data. *Bioinformatics*, 26(22):2900–1.

Baskerville, S. and Bartel, D.P., 2005. Microarray profiling of microRNAs reveals frequent coexpression with neighboring miRNAs and host genes. *RNA*, 11(3):241–7.

Bazzini, A.A., Lee, M.T. and Giraldez, A.J., 2012. Ribosome profiling shows that miR-430 reduces translation before causing mRNA decay in zebrafish. *Science*, 336(6078):233–7.

Beaudet-Miller, M. et al., 1996. Virus-specific interaction between the human cytomegalovirus major capsid protein and the C terminus of the assembly protein precursor. *J Virol*, 70(11):8081–8.

Bechtel, J.T. and Shenk, T., 2002. Human cytomegalovirus UL47 tegument protein functions after entry and before immediate-early gene expression. *J Virol*, 76(3):1043–50.

Behm-Ansmant, I. et al., 2006. mRNA degradation by miRNAs and GW182 requires both CCR4:NOT deadenylase and DCP1:DCP2 decapping complexes. *Genes Dev*, 20(14):1885–98.

Beitzinger, M. et al., 2007. Identification of human microRNA targets from isolated argonaute protein complexes. *RNA Biol*, 4(2):76–84.

Béthune, J., Artus-Revel, C.G. and Filipowicz, W., 2012. Kinetic analysis reveals successive steps leading to miRNA-mediated silencing in mammalian cells. *EMBO Rep*, 13(8):716–23.

Bi, L. et al., 2002. Early embryonic lethality in mice deficient in the p110beta catalytic subunit of PI3-kinase. *Mamm Genome*, 13(3):169–72.

Bitko, V. et al., 2007. Nonstructural proteins of respiratory syncytial virus suppress premature apoptosis by an NF-kappaB-dependent, interferon-independent mechanism and facilitate virus growth. *J Virol*, 81(4):1786–95.

Bodaghi, B. et al., 1999. Entry of human cytomegalovirus into retinal pigment epithelial and endothelial cells by endocytosis. *Invest Ophthalmol Vis Sci*, 40(11):2598–607.

Bogner, E., Radsak, K. and Stinski, M.F., 1998. The gene product of human cytomegalovirus open reading frame UL56 binds the pac motif and has specific nuclease activity. *J Virol*, 72(3):2259–64.

Bohnsack, M.T., 2004. Exportin 5 is a RanGTP-dependent dsRNA-binding protein that mediates nuclear export of pre-miRNAs. *RNA*, 10(2):185–91.

Bonin, L.R. and McDougall, J.K., 1997. Human cytomegalovirus IE2 86-kilodalton protein binds p53 but does not abrogate G1 checkpoint function. *J Virol*, 71(8):5861–70.

Borchert, G.M., Lanier, W. and Davidson, B.L., 2006. RNA polymerase III transcribes human microRNAs. *Nat struct Mol Biol*, 13(12):1097–101.

Borst, E.M. et al., 1999. Cloning of the human cytomegalovirus (HCMV) genome as an infectious bacterial artificial chromosome in Escherichia coli: a new approach for construction of HCMV mutants. *J Virol*, 73(10):8320–9.

Borst, E.M. and Messerle, M., 2005. Analysis of human cytomegalovirus oriLyt sequence requirements in the context of the viral genome. *J Virol*, 79(6):3615–26.

Bortolin-Cavaillé, M.L. et al., 2009. C19MC microRNAs are processed from introns of large Pol-II, non-protein-coding transcripts. *Nucleic Acids Res*, 37(10):3464–73.

Boyle, K.A. and Compton, T., 1998. Receptor-binding properties of a soluble form of human cytomegalovirus glycoprotein B. *J Virol*, 72(3):1826–33.

Boyle, K.A., Pietropaolo, R.L. and Compton, T., 1999. Engagement of the cellular receptor for glycoprotein B of human cytomegalovirus activates the interferon-responsive pathway. *Mol Cell Biol*, 19(5):3607–13.

Bradley, A.J. et al., 2009. High-throughput sequence analysis of variants of human cytomegalovirus strains Towne and AD169. *J Gen Virol*, 90(Pt 10):2375–80.

Braun, J.E. et al., 2011. GW182 proteins directly recruit cytoplasmic deadenylase complexes to miRNA targets. *Mol Cell*, 44(1):120–33.

Brennan, D.C., 2001. Cytomegalovirus in renal transplantation. *J Am Soc Nephrol*, 12(4):848–55.

Brennecke, J. et al., 2003. Bantam encodes a developmentally regulated microRNA that controls cell proliferation and regulates the proapoptotic gene hid in Drosophila. *Cell*, 113(1):25–36.

Brenner, B. et al., 2011. microRNAs as a potential prognostic factor in gastric cancer. *World J Gastroenterology*, 17(35):3976–85.

Britt, W.J, 1984. Neutralizing antibodies detect a disulfide-linked glycoprotein complex within the envelope of human cytomegalovirus. *Virology*, 135(2):369–78.

Brocchieri, L. et al., 2005. Predicting coding potential from genome sequence: application to betaherpesviruses infecting rats and mice. *J Virol*, 79(12):7570–96.

Broderick, J.A. and Zamore, P.D., 2011. microRNA therapeutics. *Gene Ther*, 18(12):1104–10.

Browne, E.P. and Shenk, T., 2003. Human cytomegalovirus UL83-coded pp65 virion protein inhibits antiviral gene expression in infected cells. *Proc Natl Acad Sci U S A.*, 100(20):11439–44.

Bryant, L.A. et al., 2000. The human cytomegalovirus 86-kilodalton major immediate-early protein interacts physically and functionally with histone acetyltransferase P/CAF. *J Virol*, 74(16):7230–7.

Budt, M. et al., 2009. Specific inhibition of the PKR-mediated antiviral response by the murine cytomegalovirus proteins m142 and m143. *J Virol*, 83(3):1260–70.

Buendia, B., Courvalin, J.C. and Collas, P., 2001. Dynamics of the nuclear envelope at mitosis and during apoptosis. *Cell Mol Life Sci*, 58(12-13):1781–9.

Butcher, S.J. et al., 1998. Structure of the human cytomegalovirus B capsid by electron cryomicroscopy and image reconstruction. *J Struct Biol*, 124(1):70–6.

Cai, X., Hagedorn, C.H. and Cullen, B.R., 2004. Human microRNAs are processed from capped, polyadenylated transcripts that can also function as mRNAs. *RNA*, 10(12):1957–66.

Cantrell, S.R. and Bresnahan, W.A., 2006. Human cytomegalovirus (HCMV) UL82 gene product (pp71) relieves hDaxx-mediated repression of HCMV replication. *J Virol*, 80(12):6188–91.

Cantrell, S.R. and Bresnahan, W.A., 2005. Interaction between the human cytomegalovirus UL82 gene product (pp71) and hDaxx regulates immediate-early gene expression and viral replication. *J Virol*, 79(12):7792–802.

Caposio, P. et al., 2010. The Elk-1 and serum response factor binding sites in the major immediate-early promoter of human cytomegalovirus are required for efficient viral replication in quiescent cells and compensate for inactivation of the NF-kappaB sites in proliferating cells. *J Virol*, 84(9):4481–93.

Carninci, P. et al., 2005. The transcriptional landscape of the mammalian genome. *Science*, 309(5740):1559–63.

Cartharius, K. et al., 2005. MatInspector and beyond: promoter analysis based on transcription factor binding sites. *Bioinformatics*, 21(13):2933–42.

Caswell, R. et al., 1993. The human cytomegalovirus 86K immediate early (IE) 2 protein requires the basic region of the TATA-box binding protein (TBP) for binding, and interacts with TBP and transcription factor TFIIB via regions of IE2 required for transcriptional regulation. *J Gen Virol*, 74 (Pt 12):2691–8.

Cepeda, V., Esteban, M. and Fraile-Ramos, A., 2010. Human cytomegalovirus final envelopment on membranes containing both trans-Golgi network and endosomal markers. *Cell Microbiol*, 12(3):386–404.

Cha, T.A. et al., 1996. Human cytomegalovirus clinical isolates carry at least 19 genes not found in laboratory strains. *J Virol*, 70(1):78–83.

Chakrabarty, A. et al., 2007. microRNA regulation of cyclooxygenase-2 during embryo implantation. *Proc Natl Acad Sci U S A*, 104(38):15144–9.

Chan, Y.J. et al., 1996. Synergistic interactions between overlapping binding sites for the serum response factor and ELK-1 proteins mediate both basal enhancement and phorbol ester responsiveness of primate cytomegalovirus major immediate-early promoters in monocyte and T-lympho. *J Virol*, 70(12):8590–605.

Chang, H.L. et al., 2009. Keratinocyte growth factor (KGF) regulates estrogen receptor-alpha (ER-alpha) expression and cell apoptosis via phosphatidylinositol 3-kinase (PI3K)/Akt pathway in human breast cancer cells. *Anticancer Res*, 29(8):3195–205.

Chattopadhyay, N. et al., 2003. alpha3beta1 integrin-CD151, a component of the cadherin-catenin complex, regulates PTPmu expression and cell-cell adhesion. *Journal Cell Biol*, 163(6):1351–62.

Chaussade, C. et al., 2007. Evidence for functional redundancy of class IA PI3K isoforms in insulin signalling. *Biochem J*, 404(3):449–58.

Chee, M. et al., 1990. Analysis of the protein coding content of the sequence of human cytomegalovirus strain AD169. *Curr Top Microbiol Immunol*, 154:125–69.

Cheloufi, S. et al., 2010. A dicer-independent miRNA biogenesis pathway that requires Ago catalysis. *Nature*, 465(7298):584–9.

Chen, D.H. et al., 1999. Three-dimensional visualization of tegument/capsid interactions in the intact human cytomegalovirus. *Virology*, 260(1):10–6.

Chen, Y. et al., 2011. A liver-specific microRNA binds to a highly conserved RNA sequence of hepatitis B virus and negatively regulates viral gene expression and replication. *FASEB J*, 25(12):4511–21.

Chendrimada, T.P. et al., 2010. TRBP recruits the Dicer complex to Ago2 for microRNA processing and gene silencing. *Nature*, 436(7051):740–4.

Cheng, W. et al., 2012. microRNA-199a targets CD44 to suppress the tumorigenicity and multidrug resistance of ovarian cancer-initiating cells. *FEBS J*, 279(11):2047–59.

Cheung, H.H. et al., 2011. Methylation of an intronic region regulates miR-199a in testicular tumor malignancy. *Oncogene*, 30(31):3404–15.

Chi, S.W. et al., 2009. Argonaute HITS-CLIP decodes microRNA-mRNA interaction maps. *Nature*, 460(7254):479–86.

Chi, S.W., Hannon, G.J. and Darnell, R.B., 2012. An alternative mode of microRNA target recognition. *Nat Struct Mol Biol*, 19(3):321–7.

Child, S.J. et al., 2004. Evasion of Cellular Antiviral Responses by Human Cytomegalovirus TRS1 and IRS1. *J Virol*, 78(1):197–205.

Chung, C.H. et al., 2011. Glioma-associated oncogene family zinc finger 1 expression and metastasis in patients with head and neck squamous cell carcinoma treated with radiation therapy (RTOG 9003). *J Clin Oncol*, 29(10):1326–34.

Cifuentes, D. et al., 2011. A novel miRNA processing pathway independent of Dicer requires Argonaute2 catalytic activity. *Science*, 328(5986):1694–8.

Coller, K.E. et al., 2007. The capsid and tegument of the alphaherpesviruses are linked by an interaction between the UL25 and VP1/2 proteins. *J Virol*, 81(21):11790–7.

Compton, T., Nepomuceno, R.R. and Nowlin, D.M., 1992. Human cytomegalovirus penetrates host cells by pH-independent fusion at the cell surface. *Virology*, 191(1):387–95.

Compton, T., Nowlin, D.M. and Cooper, N.R., 1993. Initiation of human cytomegalovirus infection requires initial interaction with cell surface heparan sulfate. *Virology*, 193(2):834–41.

Cougot, N., Babajko, S. and Séraphin, B., 2004. Cytoplasmic foci are sites of mRNA decay in human cells. *J Cell Biol*, 165(1):31–40.

Cullen, B.R., 2011. Viruses and microRNAs : RISCy interactions with serious consequences. *Genes Dev*, 25(18):1881–94.

Cunningham, C. et al., 2010. Sequences of complete human cytomegalovirus genomes from infected cell cultures and clinical specimens. *J Gen Virol*, 91(Pt 3):605–15.

Dahiya, N. et al., 2008. microRNA expression and identification of putative miRNA targets in ovarian cancer. *PloS one*, 3(6):e2436.

Das, S. and Pellett, P.E., 2007. Members of the HCMV US12 family of predicted heptaspanning membrane proteins have unique intracellular distributions, including association with the cytoplasmic virion assembly complex. *Virology*, 361(2):263–73.

Das, S. and Pellett, P.E., 2011. Spatial relationships between markers for secretory and endosomal machinery in human cytomegalovirus-infected cells versus those in uninfected cells. *J Virol*, 85(12):5864–79.

Das, S., Vasanji, A. and Pellett, P.E., 2007. Three-dimensional structure of the human cytomegalovirus cytoplasmic virion assembly complex includes a reoriented secretory apparatus. *J Virol*, 81(21):11861–9.

Davison, A.J., 2003. Homology between the human cytomegalovirus RL11 gene family and human adenovirus E3 genes. *J Gen Virol*, 84(3):657–63.

Davison, A.J, 1993. Origins of the herpesviruses. In *Abstr. Int. Herpesvirus Meet.* p.p. S–27.

Davison A. J., 2007. Overview of classification. In Arvin A., Campadelli-Fiume G. Mocarski E. Moore P. S. Roizman B. Whitley R. and Yamanishi K. (eds.) Human Herpesviruses; Cambridge University Press. Cambridge. Chapter 1.

Denli, A.M. et al., 2004. Processing of primary microRNAs by the Microprocessor complex. *Nature*, 432(7014):231–5.

Deregibus, M.C. et al., 2002. HIV-1-Tat protein activates phosphatidylinositol 3-kinase/AKT-dependent survival pathways in Kaposi's sarcoma cells. *J Biol Chem*, 277(28):25195–202.

Derfoul, A. et al., 2011. Decreased microRNA-214 levels in breast cancer cells coincides with increased cell proliferation, invasion and accumulation of the Polycomb Ezh2 methyltransferase. *Carcinogenesis*, 32(11):1607–14.

Didiano, D. and Hobert, O., 2006. Perfect seed pairing is not a generally reliable predictor for miRNA-target interactions. *Nat Struct Mol Biol*, 13(9):849–51.

Ding, X. and Grosshans, H., 2009. Repression of C. elegans microRNA targets at the initiation level of translation requires GW182 proteins. *EMBO J*, 28(3):213–22.

Dittmer, A. and Bogner, E., 2005. Analysis of the quaternary structure of the putative HCMV portal protein PUL104. *Biochemistry*, 44(2):759–65.

Djuranovic, S., Nahvi, A. and Green, R., 2012. miRNA-mediated gene silencing by translational repression followed by mRNA deadenylation and decay. *Science*, 336(6078):237–40.

Doench, J.G., Petersen, C.P. and Sharp, P.A., 2003. siRNAs can function as miRNAs. *Genes Dev*, 17(4): 438–42.

Doench, J.G. and Sharp, P.A., 2004. Specificity of microRNA target selection in translational repression. *Genes Dev*, 18(5):504–11.

Dolan, A., 2004. Genetic content of wild-type human cytomegalovirus. *J Gen Virol*, 85(5):1301–12.

Duan, Q. et al., 2012. ER stress negatively modulates the expression of the miR-199a/214 cluster to regulates tumor survival and progression in human hepatocellular cancer. *PloS One*, 7(2):e31518.

Duan, Z. et al., 2011. microRNA-199a-3p is downregulated in human osteosarcoma and regulates cell proliferation and migration. *Mol Cancer Ther*, 10(8):1337–45.

Dunn, W. et al., 2003. Functional profiling of a human cytomegalovirus genome. *Proc Natl Acad Sci U S A*, 100(24):14223–8.

Duursma, A.M. et al., 2008. miR-148 targets human DNMT3b protein coding region. *RNA*, 14(5):872–7

Easow, G., Teleman, A.A. and Cohen, S.M., 2007. Isolation of microRNA targets by miRNP immunopurification. *RNA*, 13(8):1198–204.

Eulalio, A. et al., 2012. Functional screening identifies miRNAs inducing cardiac regeneration. *Nature*, 492(7429):376–81.

Fabian, M.R. et al., 2009. Mammalian miRNA RISC recruits CAF1 and PABP to affect PABP-dependent deadenylation. *Mol Cell*, 35(6):868–80.

Fabian, M.R. et al., 2011. miRNA-mediated deadenylation is orchestrated by GW182 through two conserved motifs that interact with CCR4 – NOT. *Nat Struct Mol Biol.*, 18(11):1211–7.

Fang, Z. and Rajewsky, N., 2011. The impact of miRNA target sites in coding sequences and in 3′UTRs. *PloS One*, 6(3):e18067

Feire, A.L., Koss, H. and Compton, T., 2004. Cellular integrins function as entry receptors for human cytomegalovirus via a highly conserved disintegrin-like domain. *Proc Natl Acad Sci U S A*, 101(43):15470–5.

Firulli, A.B. and Conway, S.J., 2008. Phosphoregulation of Twist1 provides a mechanism of cell fate control. *Cur Med Chem*, 15(25):2641–7.

Firulli, B.A. et al., 2008. Altered Twist1 and Hand2 dimerization is associated with Saethre-Chotzen syndrome and limb abnormalities. *Nat Genet*, 37(4):373–81.

Fornari, F. et al., 2010. miR-199a-3p regulates mTOR and c-Met to influence the doxorubicin sensitivity of human hepatocarcinoma cells. *Cancer Res*, 70(12):5184–93.

Fortunato, E.A. et al., 1997. Identification of domains within the human cytomegalovirus major immediate-early 86-kilodalton protein and the retinoblastoma protein required for physical and functional interaction with each other. *J Virol*, 71(11):8176–85.

Fortunato, E.A. and Spector, D.H., 1999. Regulation of human cytomegalovirus gene expression. *Adv Virus Res*, 54:61–128.

Foukas, L.C. et al., 2006. Critical role for the p110alpha phosphoinositide-3-OH kinase in growth and metabolic regulation. *Nature*, 441(7091):366–70.

Friedman, R.C. et al., 2009. Most mammalian mRNAs are conserved targets of microRNAs. *Genome Res*, 19(1):92–105.

Gawn, J.M. and Greaves, R.F., 2002. Absence of IE1 p72 Protein Function during Low-Multiplicity Infection by Human Cytomegalovirus Results in a Broad Block to Viral Delayed-Early Gene Expression. *J Virol*, 76(9):4441–55.

Gibson, W., Baxter, M.K. and Clopper, K.S., 1996. Cytomegalovirus "missing" capsid protein identified as heat-aggregable product of human cytomegalovirus UL46. *J Virol*, 70(11):7454–61.

Gibson, W. and Roizman, B., 1972. Proteins specified by herpes simplex virus: VIII. Characterization and composition of multiple capsid forms of subtypes 1 and 2. *J Virol*, 10(5):1044–52.

Gicklhorn, D., 2003. Differential effects of glycoprotein B epitope-specific antibodies on human cytomegalovirus-induced cell-cell fusion. *J Gen Virol*, 84(Pt 7):1859–62.

Giugni, T.D. et al., 1996. Neutralization of human cytomegalovirus by human CD13-specific antibodies. *J infect Dis*, 173(5):1062–71.

Greaves, R.F. and Mocarski, E.S., 1998. Defective growth correlates with reduced accumulation of a viral DNA replication protein after low-multiplicity infection by a human cytomegalovirus ie1 mutant. *J Virol*, 72(1):366–79.

Greco, D. et al., 2011. Human papillomavirus 16 E5 modulates the expression of host microRNAs. *PloS one*, 6(7):e21646.

Gregory, R.I. et al., 2005. Human RISC couples microRNA biogenesis and posttranscriptional gene silencing. *Cell*, 123(4):631–40.

Gregory, R.I. et al., 2004. The Microprocessor complex mediates the genesis of microRNAs. *Nature*, 432(7014):235–40.

Griffiths-Jones, S., 2004. The microRNA Registry. *Nucleic Acids Res*, 32 (Database issue):D109–11.

Grimson, A. et al., 2007. microRNA targeting specificity in mammals: determinants beyond seed pairing. *Mol Cell*, 27(1):91–105.

Gu, S. et al., 2009. Biological basis for restriction of microRNA targets to the 3′ untranslated region in mammalian mRNAs. *Nat Struct Mol Biol*, 16(2):144–50.

Guo, H. et al., 2007. Regulation of hepatitis B virus replication by the phosphatidylinositol 3-kinase-akt signal transduction pathway. *J Virol*, 81(18):10072–80.

Haase, A.D. et al., 2005. TRBP, a regulator of cellular PKR and HIV-1 virus expression, interacts with Dicer and functions in RNA silencing. *EMBO Rep*, 6(10):961–7.

Haghikia, A. et al., 2011. Signal transducer and activator of transcription 3-mediated regulation of miR-199a-5p links cardiomyocyte and endothelial cell function in the heart: a key role for ubiquitin-conjugating enzymes. *Eur Heart J*, 32(10):1287–97.

Hahn, G. et al., 2004. Human cytomegalovirus UL131-128 genes are indispensable for virus growth in endothelial cells and virus transfer to leukocytes. *J Virol*, 78(18):10023–33.

Hale, B.G. et al., 2006. Influenza A virus NS1 protein binds p85beta and activates phosphatidylinositol-3-kinase signaling. *Proc Natl Acad Sci U S A*, 103(38):14194–9.

Hall, T.A., 1999. *BioEdit*: a user-friendly biological *sequence alignment editor* and analysis program for Windows 95/98/NT. *Nucleic acid symposium series*, 41:95-98.

Hamilton, J.D. and Seaworth, B.J., 1985. Transmission of latent cytomegalovirus in a murine kidney tissue transplantation model. *Transplantation*. 39(3):290–6.

Han, J. et al., 2004. The Drosha–DGCR8 complex in primary microRNA processing. Genes Dev, 18(24): 3016–27.

Hannachi, N. et al., 2011. [Seroprevalence of rubella virus, varicella zoster virus, cytomegalovirus and parvovirus B19 among pregnant women in the Sousse region, Tunisia]. Bull Soc Pathol Exot, 104(1):62–7.

Hannenhalli, S. et al., 1995. Genome sequence comparison and scenarios for gene rearrangements: a test case. *Genomics*, 30(2):299–311.

Hayhurst, G.P. et al., 1995. CCAAT box-dependent activation of the TATA-less human DNA polymerase alpha promoter by the human cytomegalovirus 72-kilodalton major immediate-early protein. *J Virol*, 69(1):182–8.

He, J. et al., 2010. miRNA-mediated functional changes through co-regulating function related genes. *PloS one*, 5(10):e13558.

He, J. et al., 2012. Reactive oxygen species regulate ERBB2 and ERBB3 expression via miR-199a/125b and DNA methylation. *EMBO Rep*, 13(12):1116–22.

Hendrickson, D.G. et al., 2008. Systematic identification of mRNAs recruited to argonaute 2 by specific microRNAs and corresponding changes in transcript abundance. *PloS one*, 3(5):e2126.

Henke, J.I. et al., 2008. microRNA-122 stimulates translation of hepatitis C virus RNA. *EMBO J*, 27(24):3300–10.

Hennessy, B.T. et al., 2005. Exploiting the PI3K/AKT pathway for cancer drug discovery. *Nat Rev Drug discov*, 4(12):988–1004.

Henry, J.C. et al., 2010. miR-199a-3p targets CD44 and reduces proliferation of CD44 positive hepatocellular carcinoma cell lines. *Biochem Biophys Res Commun.*, 403(1):120–5.

Hensel, G. et al., 1995. Nuclear localization of the human cytomegalovirus tegument protein pp150 (ppUL32). *Journal Gen Virol*, 76 (Pt 7):1591–601.

Hinshaw, J.E., 2000. Dynamin and its role in membrane fission. *Annu Rev Cell Dev Biol*, 16:483–519.

Ho, B.C. et al., 2011. Enterovirus-induced miR-141 contributes to shutoff of host protein translation by targeting the translation initiation factor eIF4E. *Cell Host Microbe*, 9(1):58–69.

Ho, M., 2008. The history of cytomegalovirus and its diseases. *Med microbiol and immunol*, 197(2):65–73.

Hobom, U. et al., 2000. Fast screening procedures for random transposon libraries of cloned herpesvirus genomes: mutational analysis of human cytomegalovirus envelope glycoprotein genes. *J Virol*, 74(17):7720–9.

Hofmann, H. et al., 2002. Functional Interaction between the pp71 Protein of Human Cytomegalovirus and the PML-Interacting Protein Human Daxx. *J Virol*, 76(11):5769–83.

Holzenburg, A., Dittmer, A. and Bogner, E., 2009. Assembly of monomeric human cytomegalovirus pUL104 into portal structures. *J Gen Virol*, 90(Pt 10):2381–5.

Hou, J. et al., 2011. Identification of miRNomes in human liver and hepatocellular carcinoma reveals miR-199a/b-3p as therapeutic target for hepatocellular carcinoma. *Cancer cell*, 19(2):232–43.

Huang, J.C. et al., 2007. Using expression profiling data to identify human microRNA targets. *Nat. Methods*, 4(12):1045–9.

Huang, J. et al., 2007. Cellular microRNAs contribute to HIV-1 latency in resting primary CD4+ T lymphocytes. *Nat Med*, 13(10):1241–7.

Huang, Y.S. et al., 2008. Microarray analysis of microRNA expression in hepatocellular carcinoma and non-tumorous tissues without viral hepatitis. *J Gastroenterol Hepatol*, 23(1):87–94.

Hudson, J., 1979. The murine cytomegalovirus as a model for the study of viral pathogenesis and persistent infections. *Arch Virol*, 62(1):1–29.

Huh, Y.H. et al., 2008. Binding STAT2 by the acidic domain of human cytomegalovirus IE1 promotes viral growth and is negatively regulated by SUMO. *J Virology*, 82(21): 10444–54.

Hume, A.J. et al., 2008. Phosphorylation of retinoblastoma protein by viral protein with cyclin-dependent kinase function. *Science*, 320(5877):797–9.

Hwang, E.S. et al., 2009. Human cytomegalovirus IE1-72 protein interacts with p53 and inhibits p53-dependent transactivation by a mechanism different from that of IE2-86 protein. *J Virol*, 83(23):12388–98.

Hwang, J.S. and Bogner, E., 2002. ATPase activity of the terminase subunit pUL56 of human cytomegalovirus. *Journal Biol Chem*, 277(9):6943–8.

Ichimi, T. et al., 2009. Identification of novel microRNA targets based on microRNA signatures in bladder cancer. *Int J Cancer*,125(2):345–52.

Indran, S.V., Ballestas, M.E. and Britt, W.J., 2010. Bicaudal D1-dependent trafficking of human cytomegalovirus tegument protein pp150 in virus-infected cells. *J Virol*, 84(7):3162–77.

Indran, S.V. and Britt, W.J., 2011. A role for the small GTPase Rab6 in assembly of human cytomegalovirus. *J Virol*, 85(10):5213–9.

Iorio, M.V. et al., 2007. MicroRNA signatures in human ovarian cancer. *Cancer Res*, 67(18):8699–707.

Irie, S. et al., 2002. An Endoplasmic Reticulum Protein, p180, Is Highly Expressed in Human Cytomegalovirus-Permissive Cells and Interacts with the Tegument Protein Encoded by UL48. *J Virol*, 76(5):2350–62.

Isaacson, M.K. and Compton, T., 2009. Human cytomegalovirus glycoprotein B is required for virus entry and cell-to-cell spread but not for virion attachment, assembly, or egress. *J Virol*, 83(8):3891–903.

Isaacson, M.K., Feire, A.L. and Compton, T., 2007. Epidermal growth factor receptor is not required for human cytomegalovirus entry or signaling. *J Virol*, 81(12):6241–7.

Ito, M. et al., 1995. Increased expression of adhesion molecules (CD54, CD29 and CD44) on fibroblasts infected with cytomegalovirus. *Microbiol Immunol.*, 39(2):129–33.

Iwamoto, G.K. et al., 1990. Modulation of interleukin 1 beta Gene expression by the immediate early genes of human cytomegalovirus. *J Clin Invest*, 85(6):1853–7.

Izzard, R.A., Jackson, S.P. and Smith, G.C., 1999. Competitive and noncompetitive inhibition of the DNA-dependent protein kinase competitive and noncompetitive inhibition of the DNA-dependent protein kinase 1. *Cancer Res*, 59(11):2581–6.

Jackson, S.P. et al., 2005. PI3-kinase p110beta: a new target for antithrombotic therapy. *Nat Med*, 11(5):507–14.

Ji, W.T. and Liu, H.J., 2008. PI3K-Akt signaling and viral infection. *Recent Pat Biotechnol*, 2(3):218–26.

Jia, S. et al., 2008. Kinase-dependent and -independent functions of the p110β phosphoinositide-3-kinase in cell growth, metabolic regulation and oncogenic transformation. *Nature*, 454(7205):776–9.

John, B. et al., 2004. Human MicroRNA Targets. *PLoS Biol.* 2(11):e363.

Johnson, R.A. et al., 2001a. The role of MKK1/2 kinase activity in human cytomegalovirus infection. *J Gen Virol*, 82(Pt 3):493–7.

Johnson, R.A. et al., 2001b. Human Cytomegalovirus Up-Regulates the Phosphatidylinositol 3-Kinase (PI3-K) Pathway: Inhibition of PI3-K Activity Inhibits Viral Replication and Virus-Induced Signaling. *J Virol*,75(13):6022–32.

Jones, L. et al., 2006. Assessment of the relationship between pre-chip and post-chip quality measures for Affymetrix GeneChip expression data. *BMC bioinformatics*, 7:211.

Jopling, C.L. et al., 2005. Modulation of hepatitis C virus RNA abundance by a liver-specific microRNA. *Science*, 309(5740):1577–81.

Jordan, M.C., Shanley, J.D. and Stevens, J.G., 1978. Immunosuppression reactivates and disseminates latent murine cytomegalovirus. *IARC Sci Publ*, (24 Pt 2):769–74.

Jordan, S. et al., 2011. Virus progeny of murine cytomegalovirus bacterial artificial chromosome pSM3fr show reduced growth in salivary Glands due to a fixed mutation of MCK-2. *J Virol*, 85(19):10346–53.

Kalejta, R.F., 2008. Tegument proteins of human cytomegalovirus. *Microbiol Mol Biol Rev*, 72(2):249–65.

Kalejta, R.F. and Shenk, T., 2002. Proteasome-dependent, ubiquitin-independent degradation of the Rb family of tumor suppressors by the human cytomegalovirus pp71 protein. *Proc Natl Acad Sci U S A*, 100(6):3263-8.

Kalejta, R.F. and Shenk, T., 2003. The Human Cytomegalovirus UL82 Gene Product (pp71) Accelerates Progression through the G1 Phase of the Cell Cycle. *J Virol*, 77(6):3451–9.

Karginov, F.V. et al., 2007. A biochemical approach to identifying microRNA targets. *Proc Natl Acad Sci U S A*,, 104(49):19291–6.

Kari, B. and Gehrz, R., 1992. A human cytomegalovirus glycoprotein complex designated gC-II is a major heparin-binding component of the envelope. *J Virol*, 66(3):1761–4.

Karlin, S., Mocarski, E.S. and Schachtel, G.A., 1994. Molecular Evolution of Herpesviruses: Genomic and Protein Sequence Comparisons. *J Virol*, 68(3):1886–902.

Kawaji, H. et al., 2006. CAGE Basic/Analysis Databases: the CAGE resource for comprehensive promoter analysis. *Nucleic acids research*, 34 (Database issue):D632–6.

Kawasaki, H. and Taira, K., 2004. MicroRNA-196 inhibits HOXB8 expression in myeloid differentiation of HL60 cells. *Nucleic acids symposium series (2004)*, (48):211–2.

Keay, S. and Baldwin, B., 1991. Anti-idiotype antibodies that mimic gp86 of human cytomegalovirus inhibit viral fusion but not attachment. *J Virol*, 65(9): 5124–8.

Keay, S. and Baldwin, B., 1992. The human fibroblast receptor for gp86 of human cytomegalovirus is a phosphorylated glycoprotein. *J Virol*, 66(8):4834–8.

Kehlenbach, R.H. et al., 1999. A role for RanBP1 in the release of CRM1 from the nuclear pore complex in a terminal step of nuclear export. *J Cell Biol*, 145(4):645–57.

Keil, G. M., Ebeling-Keil, A., and Koszinowski, U. H. (1987). Immediate-early genes of murine cytomegalovirus: location, transcripts, and translation products. *J Virol*, 61(2), 526–33.

Kertesz, M. et al., 2007. The role of site accessibility in microRNA target recognition. *Nat Genet*, 39(10):1278-84.

Khvorova, A., Reynolds, A. and Jayasena, S.D., 2003. Functional siRNAs and miRNAs exhibit strand bias. *Cell*, 115(2):209–16.

Kilpatrick, B.A. and Huang, E.S., 1977. Human cytomegalovirus genome: partial denaturation map and organization of genome sequences. *J Virol*, 24(1):261–76.

Kim, S.H. et al., 2006. Human papillomavirus 16 E5 up-regulates the expression of vascular endothelial growth factor through the activation of epidermal growth factor receptor, MEK/ ERK1,2 and PI3K/Akt. *Cell Mol Life Sci*, 63(7-8):930–8.

Kim, S. et al., 2008. microRNA miR-199a* regulates the MET proto-oncogene and the downstream extracellular signal-regulated kinase 2 (ERK2). *J Biol Chem*, 283(26):18158–66.

Kincaid, R.P. and Sullivan, C.S., 2012. Virus-Encoded microRNAs : An Overview and a Look to the Future. *PLoS pathog*, 8(12):e1003018.

Kinzler, E.R. and Compton, T., 2005. Characterization of Human Cytomegalovirus Glycoprotein-Induced Cell-Cell Fusion. *J Virol*, 79(12):7827–37.

Kiriakidou, M. et al., 2004. A combined computational-experimental approach predicts human microRNA targets. *Genes Dev*, 18(10):1165–78.

Kline, J.N. et al., 1994. Regulation of expression of the IL-1 receptor antagonist (IL-1ra) gene by products of the human cytomegalovirus immediate early genes. *J Immunol*, 152(5):2351–7.

Kloosterman, W.P. et al., 2004. Substrate requirements for let-7 function in the developing zebrafish embryo. *Nucleic Acids Res*, 32(21):6284–91.

Klosek, S.K. et al., 2009. CD151 regulates HGF-stimulated morphogenesis of human breast cancer cells. *Biochemic Biophys Res commun*, 379(4):1097–100.

Klupp, B.G. et al., 2002. Pseudorabies virus UL36 tegument protein physically interacts with the UL37 protein. *J Virol*, 76(6):3065–71.

Koh, K. et al., 2009. Human cytomegalovirus infection downregulates the expression of glial fibrillary acidic protein in human glioblastoma U373MG cells: identification of viral genes and protein domains involved. *J Gen Virol*, 90(Pt 4):954–62.

Kozomara, A. and Griffiths-Jones, S., 2011. miRBase: integrating microRNA annotation and deep-sequencing data. *Nucleic Acids Res*, 39 (Database issue):D152–7.

Krauss, S. et al., 2009. Physical requirements and functional consequences of complex formation between the cytomegalovirus IE1 protein and human STAT2. *J Virol*, 83(24):12854–70.

Krmpotic, A. et al., 2003. Pathogenesis of murine cytomegalovirus infection. *Microbes Infect*, 5(13):1263–77.

Kudchodkar, S.B. et al., 2006. Human cytomegalovirus infection alters the substrate specificities and rapamycin sensitivities of raptor- and rictor-containing complexes. *Proc Natl Acad Sci U S A*, 103(38):14182–7.

Kudchodkar, S.B. et al., 2004. Human cytomegalovirus infection induces rapamycin-insensitive phosphorylation of downstream effectors of mTOR kinase. *J Virol*, 78(20):11030–9.

Lacaze, P. et al., 2011. Temporal profiling of the coding and noncoding murine cytomegalovirus transcriptomes. *J Virol*, 85(12):6065–76.

Lagos, D. et al., 2010. miR-132 regulates antiviral innate immunity through suppression of the p300 transcriptional co-activator. *Nat Cell Biol*, 12(5):513–9.

Lall, S. et al., 2006. A Genome-wide map of conserved microrna targets in C . elegans. *Curr Biol*, 16(5):460–71.

Land, S.C. and Tee, A.R., 2007. Hypoxia-inducible factor 1alpha is regulated by the mammalian target of rapamycin (mTOR) via an mTOR signaling motif. *J Biol Chem*, 282(28):20534–43.

Landthaler, M., Yalcin, A. and Tuschl, T., 2004. The human DiGeorge syndrome critical region gene 8 and its D . melanogaster homolog are required for miRNA biogenesis. *Curr Biol*, 14(23):2162–7.

Lanford, R.E. et al., 2010. Therapeutic silencing of microRNA-122 in primates with chronic hepatitis C virus infection. *Science*, 327(5962):198–201.

Lang, D. et al., 1995. Functional interaction between the human cytomegalovirus 86-kilodalton IE2 protein and the cellular transcription factor CREB. *J Virol*, 69(10):6030–7.

Laqtom, N.N. and Buck, A.H., 2011. microRNA manipulation as a host-targeted antiviral therapeutic strategy. *European pharmaceutical Rev*, 16(6):52–55.

Lee, K. et al., 2005. Downregulation of GFAP, TSP-1, and p53 in human glioblastoma cell line, U373MG, by IE1 protein from human cytomegalovirus. *Glia*, 51(1):1–12.

Lee, R.C., Feinbaum, R.L. and Ambros, V., 1993. The C. elegans heterochronic gene lin-4 encodes small RNAs with antisense complementarity to lin-14. *Cell*, 75(5):843–54.

Lee, Y. et al., 2004. MicroRNA genes are transcribed by RNA polymerase II. *EMBO J*, 23(20):4051–60.

Lee, Y. et al., 2002. MicroRNA maturation: stepwise processing and subcellular localization. *EMBO J*, 21(17):4663–70.

Lee, Y. et al., 2003. The nuclear RNase III Drosha initiates microRNA processing. *Nature*, 425(6956):415–9

Lee, Y. et al., 2006. The role of PACT in the RNA silencing pathway. *The EMBO journal*, 25(3):522–32.

Lee, Y.B. et al., 2009. Twist-1 regulates the miR-199a/214 cluster during development. *Nucleic Acids Res*, 37(1):123–8.

Lewis, B.P., Burge, C.B. and Bartel, D.P., 2005. Conserved seed pairing , often flanked by adenosines , indicates that thousands of human genes are microrna targets we predict regulatory targets of vertebrate microRNAs. *Cell*, 120:15–20.

Liang, Y. et al., 2007. Characterization of microRNA expression profiles in normal human tissues. *BMC Genomics*, 8:166.

Libri, V. et al., 2012. Murine cytomegalovirus encodes a miR-27 inhibitor disguised as a target. *Proc Natl Acad Sci U S A*, 109(1):279–84.

Lim, L.P. et al., 2005. Microarray analysis shows that some microRNAs downregulate large numbers of target mRNAs. *Nature*, 433(7027):769–73.

Lin, E.A. et al., 2009. miR-199a, a bone morphogenic protein 2-responsive MicroRNA, regulates chondrogenesis via direct targeting to Smad1. *J Biol Chem*, 284(17):11326–35.

Lin, S. et al., 2003. The C. elegans hunchback homolog hbl-1, controls temporal patterning and is a probable microRNA target. *Dev Cell*, 4(5):639–50.

Lingel, A. et al., 2003. Structure and nucleic-acid binding of the Drosophila Argonaute 2 PAZ domain. *Nature*, 426(6965):465–9.

Linnemann, T. et al., 2002. Interaction between Nef and phosphatidylinositol-3-kinase leads to activation of p21-activated kinase and increased production of HIV. *Virology*, 294(2):246–55.

Lischka, P. et al., 2006. The UL69 transactivator protein of human cytomegalovirus interacts with DEXD / H-Box RNA helicase UAP56 to promote cytoplasmic accumulation of unspliced RNA. *Mol Cell Biol*, 26(5):1631–43.

Liu, B. and Stinski, M.F., 1992. Human cytomegalovirus contains a tegument protein that enhances transcription from promoters with upstream ATF and AP-1 cis-acting elements. *J Virol*, 66(7):4434–44.

Liu, J. et al., 2004. Argonaute2 is the catalytic engine of mammalian RNAi. *Science*, 305(5689):1437–41.

Liu, Zhe et al., 2012. Transient Activation of the PI3K-AKT Pathway by HCV to Enhance Viral Entry. *J Biol Chem*, 287(50):41922-30.

Loeb, G.B. et al., 2012. Transcriptome-wide miR-155 binding map reveals widespread noncanonical microRNA targeting. *Mol Cell*, 48(5):760–70.

Loebel, D.A. et al., 2005. A conserved noncoding intronic transcript at the mouse Dnm3 locus. *Genomics*, 85(6):782–9.

Louderbough, J.M. and Schroeder, J.A., 2011. Understanding the dual nature of CD44 in breast cancer progression. *Mol Cancer Res*, 9(12):1573–86.

Lukac, D.M. et al., 1997. TAF-like functions of human cytomegalovirus immediate-early proteins. *J Virol*, 71(10):7227–39.

Lukac, D.M., Manuppello, J.R. and Alwine, J.C., 1994. Transcriptional activation by the human cytomegalovirus immediate-early proteins: requirements for simple promoter structures and interactions with multiple components of the transcription complex. *J Virol*, 68(8):5184–93.

Lund, E. et al., 2004. Nuclear export of microRNA precursors. *Science*, 303(5654):95–8.

Lurain, N.S. and Chou, S., 2010. Antiviral drug resistance of human cytomegalovirus. *Clin Microbiol Rev*, 23(4):689–712.

Luxton, G.W et al., 2005. Targeting of herpesvirus capsid transport in axons is coupled to association with specific sets of tegument proteins. *Proc Natl Acad Sci U S A*, 102(16):5832–7.

Lytle, J.R., Yario, T.A. and Steitz, J.A., 2007. Target mRNAs are repressed as efficiently by microRNA-binding sites in the 5’ UTR as in the 3' UTR. *Proc Natl Acad Sci U S A*, 104(23):9667–72.

Ma, J.B., Ye, K. and Patel, D.J., 2004. Structural basis for overhang-specific small interfering RNA recognition by the PAZ domain. *Nature*, 429(6989):318–22.

MacCormac, L.P. and Grundy, J.E., 1999. Two clinical isolates and the Toledo strain of cytomegalovirus contain endothelial cell tropic variants that are not present in the AD169, Towne, or Davis strains. *J Med Virol*, 57(3):298–307.

Mach, M et al., 2000. Complex Formation by Human Cytomegalovirus Glycoproteins M (gpUL100) and N (gpUL73). *J Virol*, 74(24), 11881-92.

MacRae, I.J. et al., 2008. In vitro reconstitution of the human RISC-loading complex. *Proc Natl Acad Sci U S A*, 105(2):512–7.

MacRae, I.J. and Doudna, J.A., 2007. Ribonuclease revisited: structural insights into ribonuclease III family enzymes. *Curr Opi Struct Biol*, 17(1):138–45.

Mahoss, C.J. et al., 1994. A Specific Inhibitor of Phosphatidylinositol 3-Kinase, 2-(4-morpholinyl)-8-phenyl-4H-1-benzopyran-4-one (LY294002). *J Biol Chem*, 269(7):5241–8.

Maniataki, E. and Mourelatos, Z., 2005. A human, ATP-independent, RISC assembly machine fueled by pre-miRNA. *Genes Dev*, 19(24):2979–90.

Manning, B. and Cantley, L., 2007. AKT/PKB Signalling: Navigating Downstream. *Cell*, 129(7):1261–74.

Marchini, A., Liu, H. and Zhu, H., 2001. Human cytomegalovirus with IE-2 (UL122) deleted fails to express early lytic genes. *J Virol*, 75(4):1870–8.

Marcinowski, L. et al., 2012. Degradation of cellular mir-27 by a novel, highly abundant viral transcript is important for efficient virus replication in vivo. *PLoS pathog*, 8(2):e1002510.

Margolis, M.J. et al., 1995. Interaction of the 72-kilodalton human cytomegalovirus IE1 gene product with E2F1 coincides with E2F-dependent activation of dihydrofolate reductase transcription. *J Virol*, 69(12):7759–67.

Marshall, E.E. et al., 2009. Essential role for either TRS1 or IRS1 in human cytomegalovirus replication. *J Virol*, 83(9):4112–20.

Martinez, I. et al., 2008. Human papillomavirus type 16 reduces the expression of microRNA-218 in cervical carcinoma cells. *Oncogene*, 27(18):2575–82.

Mathonnet, G. et al., 2007. MicroRNA inhibition of translation initiation in vitro by targeting the cap-binding complex eIF4F. *Science*, 317(5845):1764–7.

Maul, G.G. and Negorev, D., 2008. Differences between mouse and human cytomegalovirus interactions with their respective hosts at immediate early times of the replication cycle. *Med Microbiol Immunol*, 197(2):241–9.

Mayo D.R., Armstrong J.A., and Ho M., 1977. Reactivation of murine cytomegalovirus by cyclophosphamide. *Nature*, 267(5613):721–3.

McGeoch, D.J. et al., 1995. Molecular phylogeny and evolutionary timescale for the family of mammalian herpesviruses. *J Mol Biol*, 247(3):443–58.

McVoy, M.A. and Adler, S.P., 1994. Human cytomegalovirus DNA replicates after early circularization by concatemer formation, and inversion occurs within the concatemer. *J Virol*, 68(2):1040–51.

Mei, Y. et al., 2007. Silencing of LMP1 induces cell cycle arrest and enhances chemosensitivity through inhibition of AKT signaling pathway in EBV-positive nasopharyngeal carcinoma cells. *Cell Cycle*, 6(11):1379–85.

Meister, G. et al., 2004. Human Argonaute2 mediates RNA cleavage targeted by miRNAs and siRNAs. *Mol Cell*, 15(2):185–97.

Menges, C.W. et al., 2006. Human papillomavirus type 16 E7 up-regulates AKT activity through the retinoblastoma protein. *Cancer Res*, 66(11):5555–9.

Messerle, M., Bühler, B., Keil, G.M., and Koszinowski, U.H. (1992). Structural organization, expression, and functional characterization of the murine cytomegalovirus immediate-early gene 3. *J Virol*, 66(1), 27–36.

Messerle, M. et al., 1997. Cloning and mutagenesis of a herpesvirus genome as an infectious bacterial artificial chromosome. *Proc Natl Acad Sci U S A*, 94(26):14759–63.

Messerle, M., Keil, G.M., and Koszinowski, U.H. (1991). Structure and expression of murine Structure and Expression of Murine Cytomegalovirus Immediate-Early Gene 2. *J Virol*, 65(3), 1638–43.

Mettenleiter, T.C., 2004. Budding events in herpesvirus morphogenesis. *Virus Res*, 106(2):167–80.

Mettenleiter, T.C., 2002. Minireview Herpesvirus Assembly and Egress. *J Virol*, 76(4):1537–47.

Mettenleiter, T.C., Klupp, B.G. and Granzow, H., 2006. Herpesvirus assembly: a tale of two membranes. *Curr Opi in Microbiol*, 9(4):423–9.

Mettenleiter, T.C., Klupp, B.G. and Granzow, H., 2009. Herpesvirus assembly: an update. *Virus Res*, 143(2), 222–34.

Mi, S. et al., 2007. MicroRNA expression signatures accurately discriminate acute lymphoblastic leukemia from acute myeloid leukemia. *Proc Natl Acad Sci U S A*, 104(50):19971–6.

Milbradt, J. et al., 2010. Novel mode of phosphorylation-triggered reorganization of the nuclear lamina during nuclear egress of human cytomegalovirus. *Journal Biol Chem*, 285(18):13979–89.

Mocarski, E.S., Jr. 2004. Immune escape and exploitation strategies of cytomegaloviruses: impact on and imitation of the major histocompatibility system. *Cell Microbiol*, 6(8):707–17.

Mocarski, E.S. et al., 1996. A deletion mutant in the human cytomegalovirus gene encoding IE1(491aa) is replication defective due to a failure in autoregulation. *Proc Natl Acad Sci U S A*, 93(21):11321–6.

Mocarski, E.S., Jr. and Kemble, G., 1996. Recombinant cytomegaloviruses for study of replication and pathogenesis. *Intervirology*, 39(5-6):320–30.

Molkentin, J.D. et al., 1998. A calcineurin-dependent transcriptional pathway for cardiac hypertrophy. *Cell*, 93(2):215–28.

Montague, M.G. and Iii, C.A., 2000. Gene content phylogeny of herpesviruses. *Proc Natl Acad Sci U S A*, 97(10):5334-9.

Monteys, A.M. et al., 2010. Structure and activity of putative intronic miRNA promoters. *RNA*, 16(3),495–505.

Moss, E.G., Lee, R.C. and Ambros, V., 1997. The cold shock domain protein LIN-28 controls developmental timing in C. elegans and is regulated by the lin-4 RNA. *Cell*, 88(5):637–46.

Murakami, Y. et al., 2006. Comprehensive analysis of microRNA expression patterns in hepatocellular carcinoma and non-tumorous tissues. *Oncogene*, 25(17):2537–45.

Murakami, Y. et al., 2009. Regulation of the hepatitis C virus genome replication by miR-199a. *J Hepatol*, 50(3):453–60.

Murayama, T. et al., 2000. The immediate early gene 1 product of human cytomegalovirus is sufficient for up-regulation of interleukin-8 gene expression. *Biochem Biophys Res commun*, 279(1):298–304.

Muriaux, D. et al., 2001. RNA is a structural element in retrovirus particles. *Proc Natl Acad Sci U S A*, 98(9):5246–51.

Murphy, E. et al., 2003. Coding potential of laboratory and clinical strains of human cytomegalovirus. *Proc Natl Acad Sci U S A*, 100(25):14976–81.

Nathans, R. et al., 2009. Cellular microRNA and P bodies modulate host-HIV-1 interactions. *Mol Cell*, 34(6):696–709.

Navarro, D. et al., 1993. Glycoprotein B of human cytomegalovirus promotes virion penetration into cells, transmission of infection from cell to cell, and fusion of infected cells. *Virology*, 197(1):143–58.

Nevels, M., Paulus, C. and Shenk, T., 2004. Human cytomegalovirus immediate-early 1 protein facilitates viral replication by antagonizing histone deacetylation. *Proc Natl Acad Sci U S A*, 101(49):17234–9.

Neyts, J. et al., 1992. Sulfated polymers inhibit the interaction of human cytomegalovirus with cell surface heparan sulfate. *Virology*, 189(1):48–58.

O'Connor, C. and Shenk, T., 2012. Human cytomegalovirus pUL78 G protein-coupled receptor homologue is required for timely cell entry in epithelial cells but not fibroblasts. *J Virology*, 86(21):11425–33.

Odland, J.Ø. et al., 2001. Seropositivity of cytomegalovirus, parvovirus and rubella in pregnant women and recurrent aborters in Leningrad County, Russia. *Acta obstetricia et gynecologica Scandinavica*, 80(11):1025–9.

Ogawa-goto, K. et al., 2007. p180 is involved in the interaction between the endoplasmic reticulum and microtubules through a novel microtubule-binding and bundling domain. *Mol Biol Cell*, 18(10):3741–51.

Oien, N.L. et al., 1997. Assembly of herpes simplex virus capsids using the human cytomegalovirus scaffold protein: critical role of the C terminus. *J Virology*, 71(2):1281–91.

Okada, C. et al., 2009. A high-resolution structure of the Pre-microRNA Nuclear Export Machinery. *Science*, 326(5957):1275-9.

Okamura, K. et al., 2007. The mirtron pathway generates microRNA-class regulatory RNAs in Drosophila. *Cell*, 130(1):89–100.

Ørom, U.A., Nielsen, F.C. and Lund, A.H., 2008. microRNA-10a binds the 5′UTR of ribosomal protein mRNAs and enhances their translation. *Mol Cell*, 30(4):460–71.

Othumpangat, S., Walton, C. and Piedimonte, G., 2012. microRNA-221 modulates RSV replication in human bronchial epithelium by targeting NGF expression. *PloS one*, 7(1):e30030.

Otsuka, M. et al., 2007. Hypersusceptibility to vesicular stomatitis virus infection in Dicer1-deficient mice is due to impaired miR24 and miR93 expression. *Immunity*, 27(1):123–34.

Otto, H. et al., 2001. Identification of tyrosine-phosphorylated proteins associated with the nuclear envelope. *FEBS*, 268(2):420–8.

Ouda, R. et al., 2011. RIG-I-inducible miR-23b inhibits infections by minor group rhinoviruses through down-regulation of the receptor VLDLR. *J Biol Chem*, 286(29), 26210–9.

Ouellet, D.L. et al., 2008. Identification of functional microRNAs released through asymmetrical processing of HIV-1 TAR element. *Nucleic Acids Res*, 36(7):2353–65.

Ozsolak, F. et al., 2008. Chromatin structure analyses identify miRNA promoters. *Genes Dev*, 22(22):3172–83.

Pante, N. and Kann, M., 2002. Nuclear Pore Complex Is Able to Transport Macromolecules with Diameters of about 39 nm. *Mol Cell Biol*, 13(2):425–34.

Park, C. et al., 2011. Serum response factor-dependent MicroRNAs regulate gastrointestinal smooth muscle cell phenotypes. *Gastroenterology*, 141(1):164–75.

Parry, C. et al., 2005. Herpes simplex virus type 1 glycoprotein H binds to alphavbeta3 integrins. *J Gen Virol*, 86(Pt 1):7–10.

Pasquinelli, A.E. et al., 2000. Conservation of the sequence and temporal expression of let-7 heterochronic regulatory RNA. *Nature*, 408(6808):86–9.

Patrone, M. et al., 2005. Human cytomegalovirus UL130 protein promotes endothelial cell infection through a producer cell modification of the virion. *J Virol*, 79(13):8361–73.

Paulus, C., Krauss, S. and Nevels, M., 2006. A human cytomegalovirus antagonist of type I IFN-dependent signal transducer and activator of transcription signaling. Proc Natl Acad Sci U S A, 103(10):3840–5.

Pedersen, I.M. et al., 2007. Interferon modulation of cellular microRNAs as an antiviral mechanism. *Nature*, 449(7164):919–22.

Peinado, H., Olmeda, D. and Cano, A., 2007. Snail, Zeb and bHLH factors in tumour progression: an alliance against the epithelial phenotype? *Nat Rev. Cancer*, 7(6):415–28.

Peng, J.M., Liang, S.M. and Liang, C.M., 2004. VP1 of foot-and-mouth disease virus induces apoptosis via the Akt signaling pathway. *J Biol Chem*, 279(50):52168–74.

Peng, R.Q. et al., 2012. MicroRNA-214 suppresses growth and invasiveness of cervical cancer cells by targeting UDP-N-acetyl-α-D-galactosamine:polypeptide N-acetylgalactosaminyltransferase 7. *J Biol Chem*, 287(17):14301–9.

Pepperl, S. et al., 2000. Dense bodies of human cytomegalovirus induce both humoral and cellular immune responses in the absence of viral gene expression dense bodies of human cytomegalovirus induce both humoral and cellular immune responses in the absence of viral gene expression. *J Virol*, 74(13):6132–46.

Peter, M. et al., 1990. In vitro disassembly of the nuclear lamina and M phase-specific phosphorylation of lamins by cdc2 kinase. *Cell*, 61(4):591–602.

Petersen, C.P. et al., 2006. Short RNAs repress translation after initiation in mammalian cells. *Mol Cell*, 21(4):533–42.

Pfeffer, S. et al., 2004a. Identification of virus-encoded microRNAs. *Science*, 304(5671):734–6.

Pietropaolo, R. and Compton, T., 1999. Interference with annexin II has no effect on entry of human cytomegalovirus into fibroblast cells. *J Gen Virol*, 80 (Pt 7):1807–16.

Pietropaolo, R.L. and Compton, T., 1997. Direct interaction between human cytomegalovirus glycoprotein B and cellular annexin II. *J Virol*, 71(12):9803–7.

Plafker, S.M. and Gibson, W., 1998. Cytomegalovirus assembly protein precursor and proteinase precursor contain two nuclear localization signals that mediate their own nuclear translocation and that of the major capsid protein. *J Virol*, 72(10):7722–32.

Poma, E.E. et al., 1996. The human cytomegalovirus IE1-72 protein interacts with the cellular p107 protein and relieves p107-mediated transcriptional repression of an E2F-responsive promoter. *J Virol*, 70(11):7867–77.

Poole, E. et al., 2011. Virally induced changes in cellular microRNAs maintain latency of human cytomegalovirus in CD34+ progenitors. *J Gen Virol*, 92(Pt 7):1539–49.

Portis, T. and Longnecker, R., 2004. Epstein-Barr virus (EBV) LMP2A mediates B-lymphocyte survival through constitutive activation of the Ras/PI3K/Akt pathway. *Oncogene*, 23(53):8619–28.

Potenza, N. et al., 2011. Human microRNA hsa-miR-125a-5p interferes with expression of hepatitis B virus surface antigen. *Nucleic Acids Res*, 39(12):5157–63.

Preston, C.M. and Nicholl, M.J., 2006. Role of the cellular protein hDaxx in human cytomegalovirus immediate-early gene expression. *J Gen Virol*, 87(Pt 5):1113–21.

Pritchett, R.F., 1980. DNA nucleotide sequence heterogeneity between the Towne and AD169 strains of cytomegalovirus. *J Virol*, 36(1):152–61.

Quandt, K. et al., 1995. MatInd and MatInspector: new fast and versatile tools for detection of consensus matches in nucleotide sequence data. *Nucleic Acids Res*, 23(23):4878–84.

Randall, G. et al., 2007. Cellular DNA repair cofactors affecting hepatitis C virus infection and replication. *Proc Natl Acad Sci U S A*, 104(31):12884–9.

Rawlinson, W.D., Farrell, H.E. and Barrell, B.G., 1996. Analysis of the complete DNA sequence of murine cytomegalovirus. *J Virol*, 70(12): 8833-49.

Raynor, C. et al., 1999. Annexin II enhances cytomegalovirus binding and fusion to phospholipid membranes. *Biochemistry*, 38(16):5089–95.

Reddehase, M.J. et al., 1994. The conditions of primary infection define the load of latent viral genome in organs and the risk of recurrent cytomegalovirus disease. *J Exp Med*, 179(1):185-93.

Reddehase, M.J. et al., 1985. Interstitial murine cytomegalovirus pneumonia after irradiation: characterization of cells that limit viral replication during established infection of the lungs. *J Virol*, 55(2):264–73.

Rehwinkel, J. et al., 2005. A crucial role for GW182 and the DCP1:DCP2 decapping complex in miRNA-mediated gene silencing. *RNA*, 11(11):1640–7.

Rixon, F.J. (1993). Structure and assembly of herpesviruses. *Semin Virol*, 4, 135– 44.

Roizman, B. et al., 1992. The family Herpesviridae: an update, 123(3-4):425-49.

Rosenzweig, K.E. et al., 1997. Radiosensitization of human tumor cells by the phosphatidylinositol3-kinase inhibitors wortmannin and LY294002 correlates with inhibition of DNA-dependent protein kinase and prolonged G2-M delay. *Clin Cancer Res*, 3(7):1149–56.

Rowe, W. et al., 1957. Cytopathogenic agent resembling human salivary gland virus recovered from tissue cultures of human adenoids. *Pro Soc Exp Biol Med*, 92:418–24.

Ruby, J.G., Stark, A., et al., 2007. Evolution, biogenesis, expression and target predictions of a substantially expanded set of Drosophila microRNAs. *Genome Res*,17(12):1850-64.

Ruby, J.G., Jan, C.H. and Bartel, D.P., 2007. Intronic microRNA precursors that bypass Drosha processing. *Nature*, 448(7149):83–6.

Ryckman, B.J. et al., 2006. Human cytomegalovirus entry into epithelial and endothelial cells depends on genes UL128 to UL150 and occurs by endocytosis and low-pH fusion. *J Virol*, 80(2):710–22.

Saffert, R.T. and Kalejta, R.F., 2006. Inactivating a cellular intrinsic immune defense mediated by daxx is the mechanism through which the human cytomegalovirus pp71 protein stimulates viral immediate-early gene expression. *J Virol*, 80(8):3863–71.

Sakurai, K. et al., 2011. microRNAs miR-199a-5p and -3p target the Brm subunit of SWI/SNF to generate a double-negative feedback loop in a variety of human cancers. *Cancer Res*, 71(5):1680–9.

Sanchez, V. et al., 2000. Accumulation of virion tegument and envelope proteins in a stable cytoplasmic compartment during human cytomegalovirus replication: characterization of a potential site of virus assembly. *J Virol*, 74(2): 975–86.

Sanders, R.L. et al., 2008. Development of cell lines that provide tightly controlled temporal translation of the human cytomegalovirus IE2 proteins for complementation and functional analyses of growth-impaired and nonviable IE2 mutant viruses. *J Virol*,, 82(14):7059–77.

Santhakumar, D. et al., 2010. Combined agonist-antagonist genome-wide functional screening identifies broadly active antiviral microRNAs. *Proc Natl Acad Sci U S A*, 107(31), 13830–5.

Sasaki, T. et al., 2003. Identification of eight members of the Argonaute family in the human genome*. *Genomics*, 82(3):323–30.

Scalzo, A.A. et al., 2007. The interplay between host and viral factors in shaping the outcome of cytomegalovirus infection. *Immunol Cell Biol*, 85(1):46–54.

Schauflinger, M. et al., 2011. The tegument protein UL71 of human cytomegalovirus is involved in late envelopment and affects multivesicular bodies. *J Virol*, 85(8):3821–32.

Scheffczik, H. et al., 2002. The terminase subunits pUL56 and pUL89 of human cytomegalovirus are DNA-metabolizing proteins with toroidal structure. *Nucleic Acids Res*, 30(7):1695–703.

Schierling, K. et al., 2004. Human cytomegalovirus tegument proteins ppUL82 (pp71) and ppUL35 interact and cooperatively activate the major immediate-early enhancer. *J Virol*, 78(17):9512–23.

Scholz, B., 2003. Identification of the ATP-binding site in the terminase subunit pUL56 of human cytomegalovirus. *Nucleic Acids Res*, 31(5):1426–33.

Schröer, J. and Shenk, T., 2008. Inhibition of cyclooxygenase activity blocks cell-to-cell spread of human cytomegalovirus. *Proc Natl Acad Sci U S A*, 105(49):19468–73.

Schwartz, R., Helmich, B. and Spector, D.H., 1996. CREB and CREB-binding proteins play an important role in the IE2 86-kilodalton protein-mediated transactivation of the human cytomegalovirus 2.2-kilobase RNA promoter. *J Virol*, 70(10):6955–66.

Schwarz, D.S. et al., 2003. Asymmetry in the assembly of the RNAi enzyme complex. *Cell*, 115(2):199–208.

Scott, H. et al., 2012. miR-3120 is a mirror microRNA that targets heat shock cognate protein 70 and auxilin messenger RNAs and regulates clathrin vesicle uncoating. *Journal Biol Chem*, 287(18):14726–33.

Scrivano, L. et al., 2011. HCMV spread and cell tropism are determined by distinct virus populations. *PLoS pathogens*, 7(1):e1001256.

Scully, A.L. et al., 1995. The human cytomegalovirus IE2 86-kilodalton protein interacts with an early gene promoter via site-specific DNA binding and protein-protein associations. *J Virol*, 69(10):6533–40.

Selbach, M. et al., 2008. Widespread changes in protein synthesis induced by microRNAs. *Nature*, 455(7209):58–63.

Seo, G.J., Chen, C.J. and Sullivan, C.S., 2009. Merkel cell polyomavirus encodes a microRNA with the ability to autoregulate viral gene expression. *Virology*, 383(2):183–7.

Seo, J.Y. and Britt, W.J., 2008. Multimerization of tegument protein pp28 within the assembly compartment is required for cytoplasmic envelopment of human cytomegalovirus. *J Virol*, 82(13):6272–87.

Shanley, J.D. et al., 1979. Pathogenesis of reactivated latent murine cytomegalovirus infection. *Am J Pathol*, 95(1):67–80.

Shatseva, T. et al., 2011. microRNA miR-199a-3p regulates cell proliferation and survival by targeting caveolin-2. *J Cell Sci*, 124(Pt 16): 2826–36.

Shen, Q. et al., 2010. Role of microRNA-199a-5p and discoidin domain receptor 1 in human hepatocellular carcinoma invasion. *Mol Cancer*, 9:227.

Shen, S. et al., 2007. DNA vaccines expressing glycoprotein complex II antigens gM and gN elicited neutralizing antibodies against multiple human cytomegalovirus (HCMV) isolates. *Vaccine*, 25(17):3319–27.

Shen, Y.H. et al., 2006. Human cytomegalovirus inhibits Akt-mediated eNOS activation through upregulating PTEN (phosphatase and tensin homolog deleted on chromosome 10). *Cardiovasc Res*, 69(2):502–11.

Sheth, U. and Parker, R., 2003. Decapping and decay of messenger RNA occur in cytoplasmic processing bodies. *Science*, 300(5620):805–8.

Shigehara, K. et al., 2011. Real-time PCR-based analysis of the human bile microRNAome identifies miR-9 as a potential diagnostic biomarker for biliary tract cancer. *PloS one*, 6(8):e23584.

Shigeta, M. et al., 2003. CD151 regulates epithelial cell-cell adhesion through PKC- and Cdc42-dependent actin cytoskeletal reorganization. *J Cell Biol*, 163(1):165–76.

Shimamura, M., Mach, M. and Britt, W.J., 2006. Human Cytomegalovirus Infection Elicits a Glycoprotein M (gM)/ gN-Specific Virus-Neutralizing Antibody Response. *J Virol*, 80(9):4591–600.

Shin, C. et al., 2010. Expanding the microRNA targeting code: functional sites with centered pairing. *Mol Cell*, 38(6):789–802.

Shin, Y.K. et al., 2007. Influenza A virus NS1 protein activates the phosphatidylinositol 3-kinase (PI3K)/Akt pathway by direct interaction with the p85 subunit of PI3K. *J Gen Virol*, 88(Pt 1):13–8.

Skaletskaya, A. et al., 2001. A cytomegalovirus-encoded inhibitor of apoptosis that suppresses caspase-8 activation. *Proc Natl Acad Sci U S A*, 98(14):7829–34.

Skalsky, R.L. and Cullen, B.R., 2010. Viruses, microRNAs, and host interactions. *Annu Rev Microbiol*, 64:123–41.

Slack, F.J. et al., 2000. The lin-41 RBCC gene acts in the C. elegans heterochronic pathway between the let-7 regulatory RNA and the LIN-29 transcription factor. *Mol Cell*, 5(4):659–69.

Smith, M., 1956. Propagation in tissue cultures of cytopathogenic virus from human salivary gland virus (SGV) disease. *Proc Soc Exp Biol Med*, 92:424–30.

Smith, M.S. et al., 2007. Roles of phosphatidylinositol 3-kinase and NF-kappaB in human cytomegalovirus-mediated monocyte diapedesis and adhesion: strategy for viral persistence. *J Virol*, 81(14):7683–94.

Söderberg, C. et al., 1993. CD13 (human aminopeptidase N) mediates human cytomegalovirus infection. *J Virol*, 67(11):6576–85.

Söderberg-Nauclér, C., 2006. Does cytomegalovirus play a causative role in the development of various inflammatory diseases and cancer? *J Intern Med*, 259(3):219–46.

Sommer, M.H., Scully, A.L. and Spector, D.H., 1994. Transactivation by the Human Cytomegalovirus IE2 86-Kilodalton Protein Requires a Domain That Binds to both the TATA Box-Binding Protein and the Retinoblastoma Protein. *J Virol*, 68(10):6223–31.

Song, G. et al., 2010. miR-199a regulates the tumor suppressor mitogen-activated protein kinase kinase kinase 11 in gastric cancer. *Biol pharm bull*, 33(11):1822–7.

Song, G. and Wang, Li, 2008. miR-433 and miR-127 arise from independent overlapping primary transcripts encoded by the miR-433-127 locus. *PloS one*, 3(10):e3574.

Song, J.J. et al., 2004. Crystal structure of Argonaute and its implications for RISC slicer activity. *Science*, 305(5689):1434–7.

Song, J.J. et al., 2003. The crystal structure of the Argonaute2 PAZ domain reveals an RNA binding motif in RNAi effector complexes. *Nat Struct Biol*, 10(12):1026–32.

Song, L. et al., 2010. Cellular microRNAs inhibit replication of the H1N1 influenza A virus in infected cells. *J virol*, 84(17):8849–60.

Song, Y.J. and Stinski, M.F., 2002. Effect of the human cytomegalovirus IE86 protein on expression of E2F-responsive genes: a DNA microarray analysis. Proc Natl Acad Sci U S A, 99(5):2836–41.

Soroceanu, L., Akhavan, A. and Cobbs, C.S., 2008. Platelet-derived growth factor-alpha receptor activation is required for human cytomegalovirus infection. *Nature*, 455(7211):391–5.

Spangle, J.M. and Münger, K., 2010. The human papillomavirus type 16 E6 oncoprotein activates mTORC1 signaling and increases protein synthesis. *J Virology*, 84(18):9398–407.

Speir, E. et al., 1996. Role of reactive oxygen intermediates in cytomegalovirus gene expression and in the response of human smooth muscle cells to viral infection. *Circ Res*, 79(6):1143-52.

Stark, A. et al., 2007. Discovery of functional elements in 12 Drosophila genomes using evolutionary signatures. *Nature*, 450(7167):219–32.

Stewart, P.L. and Nemerow, G.R., 2007. Cell integrins: commonly used receptors for diverse viral pathogens. *Trends in microbiol*, 15(11):500–7.

Stinski, M. et al., 1983. Organization and Expression of the Immediate Early Genes of. *J Virol*, 46(1):1–14.

Stråått, K. et al., 2009. Activation of telomerase by human cytomegalovirus. *J Natl Cancer Inst*, 101(7):488–97.

Street, A. et al., 2005. Hepatitis C Virus NS5A-Mediated Activation of Phosphoinositide 3-Kinase Results in Stabilization of Cellular β-Catenin and Stimulation of β-Catenin-Responsive Transcription. *J Virol*, 79(8):5006–16.

Su, C. et al., 2011. Ectopic expression of microRNA-155 enhances innate antiviral immunity against HBV infection in human hepatoma cells. *Virol J*, 8:354.

Su, S-F. et al., 2012. miR-30d, miR-181a and miR-199a-5p cooperatively suppress the endoplasmic reticulum chaperone and signaling regulator GRP78 in cancer. *Oncogene*.

Subramaniam, V. et al., 2007. CD44 regulates cell migration in human colon cancer cells via Lyn kinase and AKT phosphorylation. *Exp Mol Pathol*, 83(2):207–15.

Sugiura, T. and Berditchevski, F., 1999. Function of alpha3beta1-tetraspanin protein complexes in tumor cell invasion. Evidence for the role of the complexes in production of matrix metalloproteinase 2 (MMP-2). *J Cell Biol*, 146(6):1375–89.

Taft, R.J. et al., 2010. Non-coding RNAs : regulators of disease. *J pathol*, 220:126–139.

Taft, R.J., Pheasant, M. and Mattick, J.S., 2007. The relationship between non-protein-coding DNA and eukaryotic complexity. *BioEssays*, 29(3):288–99.

Tanaka-Taya, K. et al., 1996. Seroepidemiological study of human herpesvirus-6 and -7 in children of different ages and detection of these two viruses in throat swabs by polymerase chain reaction. *J Med Virol*, 48(1):88–94.

Tandon, R. and Mocarski, E.S., 2008. Control of cytoplasmic maturation events by cytomegalovirus tegument protein pp150. *J Virol*, 82(19):9433–44.

Tay, Y. et al., 2008. microRNAs to Nanog , Oct4 and Sox2 coding regions modulate embryonic stem cell differentiation. *Nature*, 455(7216):1124-8.

Terhune, S.S. and Shenk, T., 2004. RNAs Are packaged into human cytomegalovirus virions in proportion to their intracellular concentration. *J Virol*, 78(19):10390–8.

Theiler, R.N. and Compton, T., 2002. Distinct glycoprotein O complexes arise in a post-golgi compartment of cytomegalovirus-infected cells. *J Virol*, 76(6):2890–8.

Thoma, C. et al., 2006. Identification of the interaction domain of the small terminase subunit pUL89 with the large subunit pUL56 of human cytomegalovirus. *Biochemistry*, 45(29):8855–63.

Tomlinson, C.C. and Damania, B., 2004. The K1 Protein of Kaposi's sarcoma-associated herpesvirus Activates the Akt Signaling Pathway. *J Virol*, 78(4):1918–27.

Trang, P. et al., 2010. Regression of murine lung tumors by the let-7 microRNA. *Oncogene*, 29(11):1580–7.

Triboulet, R. et al., 2007. Suppression of microRNA-silencing pathway by HIV-1 during virus replication. *Science*, 315(5818):1579–82.

Van Dongen, S., Abreu-goodger, C. and Enright, A.J., 2009. Detecting microRNA binding and siRNA off-target effects from expression data. *Nat Methods*, 5(12):1023–5.

Van Rooij, E. et al., 2006. A signature pattern of stress-responsive microRNAs that can evoke cardiac hypertrophy and heart failure. *Proc Natl Acad Sci U S A*, 103(48):18255–60.

Vanhaesebroeck, B., Stephens, L. and Hawkins, P., 2012. PI3K signalling: the path to discovery and understanding. *Nat Rev. Mol Cell Biol*, 13(3):195–203.

Varnum, S.M. et al., 2004. Identification of proteins in human cytomegalovirus (HCMV) particles: the HCMV proteome. *J Virol*, 78(20):10960–6.

Vasudevan, S. and Steitz, J.A., 2007. AU-rich-element-mediated upregulation of translation by FXR1 and Argonaute 2. *Cell*, 128(6):1105–18.

Vasudevan, S., Tong, Y. and Steitz, J.A., 2007. Switching from repression to activation: microRNAs can up-regulate translation. *Science*, 318(5858):1931–4.

Vella, M.C. et al., 2004. The C. elegans microRNA let-7 binds to imperfect let-7 complementary sites from the lin-41 3′UTR. *Genes Dev*, 18(2):132–7.

Vichalkovski, A. et al., 2010. PKB/AKT phosphorylation of the transcription factor Twist-1 at Ser42 inhibits p53 activity in response to DNA damage. *Oncogene*, 29(24):3554–65.

Vischer, H.F., Leurs, R. and Smit, M.J., 2006. HCMV-encoded G-protein-coupled receptors as constitutively active modulators of cellular signaling networks. *Trends Pharmacol Sci*, 27(1):56–63.

Vittone, V. et al., 2005. Determination of Interactions between Tegument Proteins of Herpes Simplex Virus Type 1. *J Virol*, 79(15):9566–71.

Wagner, M. et al., 1999. Systematic excision of vector sequences from the BAC-cloned herpesvirus genome during virus reconstitution. *J Virol*, 73(8):7056-60

Wan, D. et al., 2013. Aberrant expression of miR-199a-3p and its clinical significance in colorectal cancers. *Med Oncol*, 30(1):378.

Wang, B., Yanez, A. and Novina, C.D., 2008. MicroRNA-repressed mRNAs contain 40S but not 60S components. *Proc Natl Acad Sci U S A*, 105(14):5343–8.

Wang, D. and Shenk, T., 2005. Human cytomegalovirus UL131 open reading frame is required for epithelial cell tropism. *J Virol*, 79(16):10330–8.

Wang, F.Z. et al., 2008. Human cytomegalovirus infection alters the expression of cellular microRNA species that affect its replication. *J Virol*, 82(18):9065–74.

Wang, L. et al., 2009. Entry mechanisms of the human cytomegalovirus (HCMV) into GM- and M-monocyte derived macrophages. *Life Sci*, 2(2004):2008–9.

Wang, P. et al., 2010. Inducible microRNA-155 feedback promotes type I IFN signaling in antiviral innate immunity by targeting suppressor of cytokine signaling 1. *J Immunol*, 185(10):6226–33.

Wang, S. and Aldovini, A., 2002. RNA incorporation is critical for retroviral particle integrity after cell membrane assembly of gag complexes. *J Virol*, 76(23):11853–65.

Wang, X. et al., 2012. miR-214 inhibits cell growth in hepatocellular carcinoma through suppression of β-catenin. *Biochem Biophys Res Commun*, 428(4):525–31.

Wang, X. et al., 2009. High-resolution human core-promoter prediction with CoreBoost_HM. *Genome Res*,19(2):266–75.

Wang, X. et al., 2005. Integrin alphavbeta3 is a coreceptor for human cytomegalovirus. *Nat Med*, 11(5):515–21.

Wang, X. and Chen, D.G., 2009. Recombinant murine cytomegalovirus vector activates human monocyte-derived dendritic cells in a NF-kappaB dependent pathway. *Mol Immunol*, 46(16):3462–5.

Wathen, M.W. and Stinski, M.F., 1982. Temporal patterns of human cytomegalovirus transcription: mapping the viral RNAs synthesized at immediate early, early, and late times after infection. *J Virol*, 41(2):462–77.

Welch, A.R. et al., 1991. A herpesvirus maturational proteinase, assemblin: identification of its gene, putative active site domain, and cleavage site. *Proc Natl Acad Sci U S A*, 88(23):10792–6.

Weller, T. et al., 1957. Isolation of intranuclear inclusion producing agents from infants with illnesses resembling cytomegalic inclusion disease. *Proc Soc Exp Biol Med*, 94(1):4–12.

Wiebusch, L. et al., 2008. Cell cycle-independent expression of immediate-early gene 3 results in G1 and G2 arrest in murine cytomegalovirus-infected cells. *J Virol*, 82(20):10188–98.

Wiggins, J.F. et al., 2010. Development of a lung cancer therapeutic based on the tumor suppressor microRNA-34. *Cancer Res*, 70(14):5923–30.

Wightman, B., Ha, I. and Ruvkun, G., 1993. Posttranscriptional regulation of the heterochronic gene lin-14 by lin-4 mediates temporal pattern formation in C. elegans. *Cell*, 75(5):855–62.

Williams, K.C. et al., 2012. The microRNA (miR)-199a/214 Cluster Mediates Opposing Effects of Progesterone and Estrogen on Uterine Contractility during Pregnancy and Labor. *Mol endocrinol*, 26(11):1857–67.

Winkler, M, Rice, S.A. and Stamminger, T., 1994. UL69 of human cytomegalovirus, an open reading frame with homology to ICP27 of herpes simplex virus, encodes a transactivator of gene expression. *J Virol*, 68(6):3943–54.

Wolfstein, A. et al., 2006. The inner tegument promotes herpes simplex virus capsid motility along microtubules in vitro. *Traffic*, 7(2):227–37.

Womack, A. and Shenk, T., 2010. Human cytomegalovirus tegument protein pUL71 is required for efficient virion egress. *MBio*, 1(5):e00282-10.

Wood, L.J. et al., 1997. Human cytomegalovirus capsid assembly protein precursor (pUL80.5) interacts with itself and with the major capsid protein (pUL86) through two different domains. *J Virol*, 71(1):179–90.

Woods, K., Thomson, J.M. and Hammond, S.M., 2007. Direct regulation of an oncogenic micro-RNA cluster by E2F transcription factors. *J Biol Chem*, 282(4):2130–4.

Wu, J., O'Neill, J. and Barbosa, M.S., 1998. Transcription factor Sp1 mediates cell-specifictrans-activation of the human cytomegalovirus DNA polymerase gene promoter by immediate-early protein IE86 in glioblastoma U373MG cells. *J Virol*, 72(1):236-44.

Wu, L. and Belasco, J.G., 2005. microRNA regulation of the mammalian lin-28 gene during neuronal differentiation of embryonal carcinoma cells. Mol Cell Biol, 25(21):9198-208.

Wu, Y.H. et al., 2011. The manipulation of microRNA-gene regulatory networks by KSHV induces endothelial cell motility. *Blood*, 118(10):2896-905.

Xia, H., Ooi, L.L. and Hui, K.M., 2012. miR-214 targets β-catenin pathway to suppress invasion, stem-like traits and recurrence of human hepatocellular carcinoma. *PloS one*, 7(9):e44206.

Yamashita, A. et al., 2005. Concerted action of poly(A) nucleases and decapping enzyme in mammalian mRNA turnover. *Nat Struct Mol Biol*, 12(12):1054–63.

Yan, K.S. et al., 2003. Structure and conserved RNA binding of the PAZ domain. *Nature*, 426(6965):468–74.

Yang, H. et al., 2008. microRNA expression profiling in human ovarian cancer: miR-214 induces cell survival and cisplatin resistance by targeting PTEN. *Cancer Res*, 68(2):425–33.

Yang, J.S. et al., 2010. Conserved vertebrate mir-451 provides a platform for Dicer-independent, Ago2-mediated microRNA biogenesis. *Proc Natl Acad Sci U S A*, 107(34):15163–8.

Yang, W. et al., 2006. Modulation of microRNA processing and expression through RNA editing by ADAR deaminases. *Nat Struct Mol Biol*, 13(1):13–21.

Yang, X.H. et al., 2008. CD151 accelerates breast cancer by regulating alpha 6 integrin function, signaling, and molecular organization. *Cancer Res*, 68(9):3204–13.

Yekta, S., Shih, I.H. and Bartel, D.P., 2004. MicroRNA-directed cleavage of HOXB8 mRNA. *Science*, 304(5670):594–6.

Yi, R. et al., 2003. Exportin-5 mediates the nuclear export of pre-microRNAs and short hairpin RNAs. *Genes Dev*, 17(24):3011–6.

Yin, G. et al., 2010. TWISTing stemness, inflammation and proliferation of epithelial ovarian cancer cells through MIR199A2/214. *Oncogene*, 29(24):3545–53.

Yu, D. et al., 2002. Construction of a self-excisable bacterial artificial chromosome containing the human cytomegalovirus genome and mutagenesis of the diploid TRL/IRL13 gene. *J Virol*, 76(5):2316–28.

Yu, D., Silva, M.C. and Shenk, T., 2003. Functional map of human cytomegalovirus AD169 defined by global mutational analysis. *Proc Natl Acad Sci U S A*, 100(21):12396–401.

Yu, X. et al., 2005. Dissecting human cytomegalovirus gene function and capsid maturation by ribozyme targeting and electron cryomicroscopy. *Proc Natl Acad Sci U S A*, 102(20):7103–8.

Yu, Y. and Alwine, J.C., 2002. Human cytomegalovirus major immediate-early proteins and simian virus 40 large T antigen can inhibit apoptosis through activation of the phosphatidylinositide 3'-OH kinase pathway and the cellular kinase Akt. *J Virol*, 76(8):3731–8.

Yu, Y. and Alwine, J.C., 2008. Interaction between simian virus 40 large T antigen and insulin receptor substrate 1 is disrupted by the K1 mutation, resulting in the loss of large T antigen-mediated phosphorylation of Akt. *J Virol*, 82(9):4521–6.

Yuan, H. et al., 2002. Simian virus 40 small tumor antigen activates AKT and telomerase and induces anchorage-independent growth of human epithelial cells. *J Virol*, 76(21):10685–91.

Yuan, Y.R. et al., 2005. Crystal structure of A. aeolicus argonaute, a site-specific DNA-guided endoribonuclease, provides insights into RISC-mediated mRNA cleavage. *Mol Cell*, 19(3):405–19.

Yurochko, A.D. et al., 1997. Induction of the transcription factor Sp1 during human cytomegalovirus infection mediates upregulation of the p65 and p105/p50 NF-kappaB promoters. *J Virol*, 71(6):4638–48.

Zeng, Y., 2003. Sequence requirements for micro RNA processing and function in human cells. *RNA*, 9(1):112–23.

Zeng, Y. et al., 2002. Both natural and designed microRNAs can inhibit the expression of cognate mrnas when expressed in human cells technique. *Mol Cell*, 9(6):1327–33.

Zeng, Y. and Cullen, B.R., 2005. Efficient processing of primary microRNA hairpins by Drosha requires flanking nonstructured RNA sequences. *Journal Biol Chem*, 280(30):27595–603.

Zeng, Y., Yi, R. and Cullen, B.R., 2005. Recognition and cleavage of primary microRNA precursors by the nuclear processing enzyme Drosha. *EMBO J*, 24(1):138–48.

Zhang, C.L. et al., 2002. Class II histone deacetylases act as signal-responsive repressors of cardiac hypertrophy. *Cell*, 110(4):479–88.

Zhang, G. et al., 2010. Suppression of hepatitis B virus replication by microRNA-199a-3p and microRNA-210. *Antiviral Res*, 88(2):169–75.

Zhang, H. et al., 2004. Single processing center models for human Dicer and bacterial RNase III. *Cell*, 118(1):57–68.

Zhang, L. et al., 2006. microRNAs exhibit high frequency genomic alterations in human cancer. *Proc Natl Acad Sci U S A*, 103(24):9136–41.

Zhang, T., Guan, H. and Yang, K., 2010. Keratinocyte growth factor promotes preadipocyte proliferation via an autocrine mechanism. *J Cell Biochem*, 109(4):737–46.

Zhang, X.J. et al., 2010. Dysregulation of miR-15a and miR-214 in human pancreatic cancer. *J Hematol Oncol*, 3:46.

Zhang, X. et al., 2011. Regulation of cardiac microRNAs by serum response factor. *J Biomed Sci*, 18(1):15.

Zhu, C. et al., 2011. PI3K/Akt and MAPK/ERK1/2 signaling pathways are involved in IGF-1-induced VEGF-C upregulation in breast cancer. *J Cancer Res Clin Oncol*, 137(11):1587–94.

Zhu, H. et al., 2002. Inhibition of cyclooxygenase 2 blocks human cytomegalovirus replication. *Proc Natl Acad Sci U S A*, 99(6):3932–7.

Zhu, Y, Huang, L. and Anders, D.G., 1998. Human cytomegalovirus oriLyt sequence requirements. *J Virol*, 72(6):4989–96.

Zielke, B. et al., 2011. Characterization of the betaherpesviral pUL69 protein family reveals binding of the cellular mRNA export factor UAP56 as a prerequisite for stimulation of nuclear mRNA export and for efficient viral replication. *J Virol*, 85(4):1804–19.

Zisoulis, D.G. et al., 2010. Comprehensive discovery of endogenous Argonaute binding sites in Caenorhabditis elegans. *Nat Struct Mol Biol*, 17(2):173–9.

9 Publications and Presentations

9.1 Publications

Peer reviewed manuscripts

- Santhakumar, D., Forster, T., **Laqtom, N.N.** et al., 2010. Combined agonist-antagonist genome-wide functional screening identifies broadly active antiviral microRNAs. *Proc Natl Acad Sci U S A*, 107(31):13830–5.
- **Laqtom, N.N.** and Buck, A.H., 2011. microRNA manipulation as a host-targeted antiviral therapeutic strategy. *European pharmaceutical review*, 16(6):52–5.
- Rückerl, D., Jenkins, S.J., **Laqtom, N.N.** et al., 2012. Induction of IL-4Rα-dependent microRNAs identifies PI3K/Akt signaling as essential for IL-4-driven murine macrophage proliferation *in vivo*. *Blood*, 120(11):2307-16.

Manuscript under preparation

- Inhibition of miR-199-3p expression by cytomegaloviruses regulates PI3K/AKT signaling in infected cells.

9.2 Oral Presentations

- **UK CMV conference. 2011. Nottingham, UK**

Laqtom N.N., Dicknson, P. and Buck, A.H. Expression and function of miR-199/214 cluster in cytomegalovirus infections.

- **Society for General Microbiology Autumn Conference. 2011. Haroggate, UK**

Laqtom N.N., Dicknson, P., Kelly, L. and Buck, A.H. The function and regulation of the miR-199/214 cluster in cytomegalovirus signalling pathways.

9.3 Poster presentations

- Edinburgh infectious diseases inaugural symposium" 2010. Edinburgh, UK. **Laqtom, N.N.,** Dicknson, P. and Buck A.H. Expression and function of miR-199a/214 cluster in cytomegalovirus infection.
- 7th Microsymposium on small RNAs. 2012. Basel, Switzerland.

Laqtom N.N., Dicknson, P., Kelly, L. and Buck, A.H. Expression and function of miR-199a/214 cluster in cytomegalovirus infection.

- 3rd International symposium on cancer, microRNAs, and other non-coding RNAs. 2012. London, UK.
  Laqtom N.N., Dicknson, P., Kelly, L. and Buck, A.H. Expression and function of miR-199a/214 cluster in cytomegalovirus infection.

- Biogenesis and turnover of small RNAs conference. 2013. Edinburgh, UK.
  Laqtom N.N., Dicknson, P., Kelly, L. and Buck, A.H. Expression and function of miR-199/214 cluster in cytomegalovirus infection.